

CIVIL ENGINEERING STUDIES
Transportation Engineering Series No. 137

UILU-ENG-2005-2003



ISSN-0197-9191

INVESTIGATION OF AGGREGATE SHAPE EFFECTS ON HOT MIX PERFORMANCE USING AN IMAGE ANALYSIS APPROACH

by

**Erol Tutumluer
Tongyan Pan
Samuel H. Carpenter**

**A final study report on the Transportation Pooled
Fund Study TPF-5 (023)**

**Prepared for
The Federal Highway Administration**

**DEPARTMENT OF CIVIL AND ENVIRONMENTAL ENGINEERING
UNIVERSITY OF ILLINOIS AT URBANA-CHAMPAIGN
URBANA, ILLINOIS**

February 2005

1. Report No.		2. Government Accession No.		3. Recipient's Catalog No.	
4. Title and Subtitle INVESTIGATION OF AGGREGATE SHAPE EFFECTS ON HOT MIX PERFORMANCE USING AN IMAGE ANALYSIS APPROACH				5. Report Date February 2005	
				6. Performing Organization Code	
				8. Performing Organization Report No. UILU-ENG-2005-2003	
7. Author(s) EROL TUTUMLUER, TONGYAN PAN, AND SAMUEL H. CARPENTER				10. Work Unit (TRAI5)	
9. Performing Organization Name and Address Department of Civil and Environmental Engineering Engineering Experiment Station University of Illinois at Urbana-Champaign Urbana, IL 61801-2352				11. Contract or Grant No. DTFH61-02-X-00029; TPF-5(023)	
				13. Type of Report and Period Covered Project Report	
				14. Sponsoring Agency Code	
12. Sponsoring Agency Name and Address Federal Highway Administration Illinois Division Office 3250 Executive Park Drive Springfield, IL 62703 Federal Highway Administration 400 7th Street, SW Washington, DC 20590				15. Supplementary Notes	
16. Abstract The objectives of this FHWA pooled fund research project included the measurement of imaging based volumetric and morphological indices of coarse aggregates and their correlations with laboratory and field performance results of asphalt concrete mixes as a wave of future in the development of asphalt pavement science and technology. The study partners were the National Center for Asphalt Technology (NCAT), state highway agencies of Alabama, Georgia, Indiana, Minnesota, Mississippi, Missouri, Montana, and South Carolina, and the FHWA Central Federal Lands and Highways Division. In Phase I of the study, the readily available image analysis device, University of Illinois Aggregate Image Analyzer (UIAIA), was used for validation and development of imaging based morphological indices, i.e., flat and elongated (F&E) ratio, angularity index (AI) and surface texture (ST) index, of the coarse aggregate used in the national NCAT Pavement Test Track rutting study and in typical asphalt mixes obtained from the pooled fund participating agencies. In Phase II, all UIAIA determined NCAT coarse aggregate shape indices indicated good correlations individually with the field rutting data from the NCAT Pavement Test Track with the ST index giving the best correlation and the AI giving the next best correlation. The UIAIA determined coarse aggregate shape indices were also correlated to the laboratory resilient modulus and permanent deformation test results of the participating agency specimens. For a total of 18 Superpave asphalt mix designs studied, the effects of the AI and ST indices on the hot mix asphalt resilient moduli and permanent deformations were especially significant from the test results when evaluated according to the below the restricted zone (BRZ) aggregate gradations. The resilient modulus test data, when grouped according to asphalt binder grade and/or stiffness, generally demonstrated a much better relationship with the coarse aggregate morphology. The increased stability and reduced permanent deformation or rutting potential trends of the most dense graded asphalt mixtures studied herein using the UIAIA approach were more favorably influenced primarily by the increased surface texture or roughness property of coarse aggregate particles.					
17. Key Words Coarse Aggregate, Hot Mix Asphalt, Performance, Imaging, Shape, Flat and Elongated, Gradation, Angularity, Surface Texture			18. Distribution Statement No restrictions. This document is available to the public through the National Information Service, Springfield, VA 22161		
19. Security Classif. (of this report) Unclassified		20. Security Classif. (of this page) Unclassified		21. No. of Pages	22. Price

ACKNOWLEDGMENTS

This pool funded-research project, TPF-5(023) on <http://www.pooledfund.org>, was initiated in 2002 at the University of Illinois at Urbana-Champaign with the lead agency support of the Illinois Division of the Federal Highway Administration (FHWA) in Springfield, Illinois. The authors would like to thank Mr. Pal Choudry, the project monitor from the FHWA Illinois Division, Mr. John D'Angelo, the project technical supervisor from the FHWA Turner-Fairbank Research Laboratory, and Mr. Charles Kotch, the contracting officer from the FHWA office in Washington, D.C. Dr. Eyad Masad of Texas A&M University also served as the project technical reviewer.

Our special thanks go to the study partners and sponsors including the National Center for Asphalt Technology (NCAT) in Auburn, Alabama, the state highway agencies of Alabama, Georgia, Indiana, Minnesota, Mississippi, Missouri, Montana, and South Carolina, and the Central Federal Lands and Highways Division.

TABLE OF CONTENTS

TECHNICAL REPORT DOCUMENTATION PAGE	
ACKNOWLEDGMENTS	i
TABLE OF CONTENTS	ii
LIST OF TABLES	iv
LIST OF FIGURES	vi
CHAPTER 1 INTRODUCTION	1
PERFORMANCE RELATED AGGREGATE PROPERTIES	1
STANDARD COARSE AGGREGATE TESTS AND SPECIFICATIONS	3
SIGNIFICANCE OF COARSE AGGREGATE SHAPE AND SIZE	5
ADVENT OF IMAGE ANALYSIS	8
STATEMENT OF THE POOLED FUND STUDY	10
OBJECTIVES AND SCOPE OF THE POOLED FUND STUDY	11
Phase I: Evaluation of the Shape and Size Properties and Validation of UIAIA	11
Phase II: Evaluation of Shape and Size Effects on Hot Mix Performance	12
REPORT OUTLINE	13
CHAPTER 2 UNIVERSITY OF ILLINOIS AGGREGATE IMAGE ANALYZER	16
NEED FOR 3-DIMENSIONAL IMAGE ANALYSIS	16
IMAGE ANALYSIS CONCEPTS	18
UNIVERSITY OF ILLINOIS AGGREGATE IMAGE ANALYZER (UIAIA)	19
COARSE AGGREGATE SIZE AND SHAPE INDICES IN UIAIA	23
Particle Size Determination	24
Particle Morphology Determination	28
<i>Flat and Elongated Ratio</i>	29
<i>Angularity Index (AI)</i>	30
<i>Surface Texture (ST) Index</i>	31
SUMMARY	34
CHAPTER 3 MATERIALS AND IMAGING BASED INDICES	35
MATERIAL ACQUISITION	35
IMAGING RESULTS OF NCAT AGGREGATES	41
Weight Computation	42
Gradation Analysis	42
Flat and Elongated Ratio	44
Angularity and Surface Texture	44
IMAGING RESULTS OF AGGREGATE FROM PARTICIPATING AGENCIES	48
Weight Computation	48
Gradation Analysis	50
Flat and Elongated Ratio	50
Angularity and Surface Texture	53
SUMMARY	60

CHAPTER 4 EFFECT OF COARSE AGGREGATE MORPHOLOGY ON RUTTING PERFORMANCE OF ASPHALT MIXES IN THE NCAT TEST TRACK	61
SIGNIFICANCE OF THE NCAT COARSE AGGREGATE STUDY	61
NCAT PAVEMENT TEST TRACK STUDY AND FIELD RESULTS	62
NCAT COARSE AGGREGATE SHAPE INDICES AND NORMALIZATION	64
RELATING COARSE AGGREGATE SHAPE INDICES TO NCAT TEST TRACK FIELD PERFORMANCE DATA	68
SUMMARY	74
CHAPTER 5 EFFECT OF COARSE AGGREGATE MORPHOLOGY ON PERMANENT DEFORMATION BEHAVIOR OF LABORATORY ASPHALT MIXES	76
EXPERIMENTAL DESIGN OF THE STUDY	77
PERMANENT DEFORMATION TESTING OF ASPHALT MIXES	79
Specimen Preparation and Testing	80
Permanent Deformation Results of the Asphalt Mixes	81
IMAGING INDICES OF COARSE AGGREGATE BLENDS IN ASPHALT MIXES	84
DATA ANALYSIS	85
Correlations of Coarse Aggregate Morphologies with the Primary Slope	86
Correlations of Coarse Aggregate F&E Ratio with HMA Stability and Aggregate Structure	86
Correlations of Coarse Aggregate Angularity with HMA Stability and Aggregate Structure	87
Correlations of Coarse Aggregate Texture with HMA Stability and Aggregate Structure	88
Possible Mechanism of Coarse Aggregate Morphologies Affecting HMA Stability and Aggregate Structure	91
SUMMARY	94
CHAPTER 6 EFFECT OF COARSE AGGREGATE MORPHOLOGY ON RESILIENT MODULUS OF ASPHALT MIXES	95
RESILIENT MODULUS AND STUDY GOALS	95
EXPERIMENTAL DESIGN OF THE STUDY	97
IMAGING INDICIAL RESULTS OF COARSE AGGREGATE	98
LABORATORY RESILIENT MODULUS TESTING	100
ANALYSIS OF THE RESULTS	103
SUMMARY	108
CHAPTER 7 SUMMARY AND CONCLUSIONS	110
RECOMMENDATIONS FOR FUTURE RESEARCH	116
REFERENCES	117
APPENDIX I IMAGING RESULTS OF THE POOLED FUND STUDY AGGREGATE SAMPLES	AI-1
APPENDIX II MIX DESIGNS USED IN THE LABORATORY TESTS	AII-1

LIST OF TABLES

Table 3-1 Aggregate Materials Received from the NCAT Pavement Test Track Field Evaluation Study	36
Table 3-2 Aggregates and Binders Received from the Participating Pooled Fund Partners	38
Table 3-2 Aggregates and Binders Received from the Participating Pooled Fund Partners (continued)	39
Table 3-2 Aggregates and Binders Received from the Participating Pooled Fund Partners (continued)	40
Table 3-3 UIAIA Imaging Based Weight Predictions for the NCAT Aggregate Samples	43
Table 3-4 UIAIA Flat and Elongated (F&E) Ratio Results for the NCAT Aggregate Samples	45
Table 3-5 UIAIA Imaging Based Angularity Indices (AI) of NCAT Aggregate Samples	46
Table 3-6 UIAIA Imaging Based Surface Texture (ST) Indices of NCAT Aggregate Samples	47
Table 3-7 UIAIA Imaging Based Weight Predictions for the Participating Agency Aggregate Samples	49
Table 3-7 UIAIA Imaging Based Weight Predictions for the Participating Agency Aggregate Samples (Continued)	50
Table 3-8 UIAIA Flat and Elongated (F&E) Ratio Results for the Participating Agency Aggregate	51
Table 3-8 UIAIA Flat and Elongated (F&E) Ratio Results for the Participating Agency Aggregate (Continued)	52
Table 3-9 UIAIA Imaging Based Angularity Index (AI) Results for Participating Agency Aggregate	53
Table 3-9 UIAIA Imaging Based Angularity Index (AI) Results for Participating Agency Aggregate (Continued)	54
Table 3-10 UIAIA Imaging Based Surface Texture (ST) Indices of the Participating Agency Aggregate	55
Table 3-10 UIAIA Imaging Based Surface Texture (ST) Indices of the Participating Agency Aggregate (Continued)	56
Table 3-11 Imaging Based Angularity and Surface Texture Indices of the Participating Agency Aggregate	58
Table 3-11 Imaging Based Angularity and Surface Texture Indices of the Participating Agency Aggregate (Continued)	59
Table 3-12 Typical Ranges of Angularity and Surface Texture Indices	59
Table 4-1 NCAT Test Track South and West Sections, Rutting Performances and Coarse Aggregate Used In Mix Designs	65
Table 4-2 NCAT Test Track North and East Sections, Rutting Performances and Coarse Aggregate Used In Mix Designs	66
Table 4-3 Imaging Based Indices Determined for Selected NCAT Coarse Aggregate Used In Mix Designs	67

Table 4-4 Weight Percentages of the UIAIA Processed Coarse Aggregate Used In the NCAT West Side Pavement Mix Designs	70
Table 4-5 Rut Depth Data Presented with Normalized Composite Shape Indices for Selected NCAT West Side Pavement Sections	71
Table 4-6. Results of the Statistical Analysis between Aggregate Shape Indices and NCAT Test Track Pavement Rut Depth Data	74
Table 5-1 Mix Designs and Permanent Deformation Results of the Laboratory Superpave HMA Specimens	79
Table 5-2 Imaging Based Composite Indices of the Coarse Aggregate Blends of the Asphalt Mix Designs	85
Table 5-3 Screening t-test for Regression Analysis	86
Table 6-1 Asphalt Mixes, Mix Properties, and Resilient Modulus Results	99
Table 6-2 Imaging Results of Composite AI and ST Indices for the 18 Asphalt Mixes Studied	101

LIST OF FIGURES

Figure 2-1 Three-dimensional Views of Two Regular Shaped Solids	17
Figure 2-2 Image Digitization	18
Figure 2-3 Schematic of the University of Illinois Aggregate Image Analyzer	20
Figure 2-4 Installation of Sensors for the UIAIA	22
Figure 2-5 Photograph Showing the University of Illinois Aggregate Image Analyzer	23
Figure 2-6 Three Orthogonal Views of a Particle Captured by the UIAIA	25
Figure 2-7 Acquiring Array Subsets for Images	27
Figure 2-8 Three Key Morphological Descriptors of Coarse Aggregate Particles	29
Figure 2-9 Illustration of the Longest and Shortest Perpendicular Dimensions	30
Figure 2-10 Illustration of An n-sided Polygon Approximating the Outline of a Particle	31
Figure 2-11 Change of an Aggregate Particle Surface Texture Before and After the Application of Optimum Cycles of Erosion and Dilation	33
Figure 3-1 UIAIA Imaging Based Particle Size Distributions for the Blacksburg 67 Sample	44
Figure 3-2 Imaging Based Angularity Index (AI) Repeatability Analysis of the Blacksburg 67 Sample	45
Figure 3-3 Imaging Based Surface Texture (ST) Repeatability Analysis of the Blacksburg 67 Sample	47
Figure 3-4 Imaging Based Particle Size Distributions for the FLHD-NM Aggregate Samples	51
Figure 3-5 Imaging Based Angularity Index (AI) Repeatability Analysis of the FLHD-NM 7/8-inch Rock	55
Figure 3-6 Imaging Based Surface Texture (ST) Repeatability Analysis of the FLHD-NM 7/8-inch Rock	57
Figure 3-7 Relationship between Coarse Aggregate Angularity (AI) and Surface Texture (ST) Indices	59
Figure 4-1 NCAT Pavement Test Track in Auburn, Alabama (courtesy of NCAT)	63
Figure 4-2 Section Assignment of the NCAT Pavement Test Track (courtesy of NCAT)	63
Figure 4-3 NCAT Test Track Pavement Rut Depth Data Correlated to Percent Coarse Aggregate with % F&E Ratios > 5:1	72
Figure 4-4 NCAT Test Track Pavement Rut Depth Data Correlated to Angularity Indices (AI) of Coarse Aggregate	72
Figure 4-5 NCAT Test Track Pavement Rut Depth Data Correlated to Surface Texture (ST) Indices of Coarse Aggregate	73
Figure 5-1 Schematic of Permanent Strain Accumulation in a Repeated Load Triaxial Test	82
Figure 5-2 Repeated Load Triaxial Setup Used in Permanent Deformation Testing of Asphalt Specimens at ATREL	83

Figure 5-3 Typical Ranges of Cumulative Permanent Strains with Number of Load Applications	83
Figure 5-4 Correlations between Log (FN) and Composite AI for the 18 Asphalt Mixes	88
Figure 5-5 Correlations between Secondary Slope (SS) and Composite AI for the 18 Asphalt Mixes	89
Figure 5-6 Correlations between Log (FN) and Composite ST index for the 18 Asphalt Mixes	90
Figure 5-7 Correlations between the Composite ST and the Secondary Slope (SS)	91
Figure 6-1 Resilient Modulus (MR) Test Device Utilized at the University of Illinois ATREL	101
Figure 6-2 The 1-Hz Haversine Load Waveform with 0.1-sec. Load Duration and 0.9-sec. Rest	102
Figure 6-3 Typical Recorder Output of the Resilient Modulus Test	102
Figure 6-4 Relationships between the Resilient Modulus and the AI and ST Indices	104
Figure 6-5 Resilient Moduli Grouped on the High Temperature of Superpave PG Grades	105
Figure 6-6 Effects of AI on Binder Stiffness-grouped Resilient Modulus	106
Figure 6-7 Effects of ST Index on Binder Stiffness-grouped Resilient Modulus	106
Figure 6-8 Effects of AI and ST Indices on Gradation-grouped Resilient Modulus	107
Figure 6-9 Effects of AI and ST Indices on Nominal Maximum Aggregate Size-grouped Modulus	108

CHAPTER 1

INTRODUCTION

Hot mix asphalt (HMA) or asphalt concrete (AC) contains two essential components, asphalt and aggregate materials. The asphalt works as a binder to hold together the aggregate particles, which forms the aggregate structure in the AC mixture. Having the largest particle size, coarse aggregate particles often form the skeleton of the aggregate structure and control transfer of the traffic and environmental loads to the underlying base, subbase and subgrade layers. Both the response and performance of the AC mix and eventually the HMA layer are directly affected by the basic material properties and composition of this aggregate skeleton, and accordingly, the AC mixtures are categorized as dense graded, coarse graded or stone mastic asphalt (SMA).

The low stiffness and instability of the AC mixtures and the excessive rutting that may be observed in HMA pavement surfaces are often attributed to the low performance, poor AC mixture designs primarily controlled by the asphalt binder and aggregate properties. Except for the fine mixes, the selection of coarse aggregate greatly influences the HMA behavior. Especially the physical shape and size properties of coarse aggregate particles and their effects on the strength and stability of HMA have been noted to contribute to the performances of the Strategic Highway Research Program (SHRP) superior performing asphalt pavement (Superpave) mix designs. Several Superpave research studies focused on linking the shape and size properties of coarse aggregate to mixture performances mainly relied on using manual standard tests in characterizing the shape properties. These shape effects, however, were not well understood due to the lack of accurate and repeatable measurements of the coarse aggregate morphology. More recently, research efforts have focused on developing new methodologies for objective and quantitative measurements of the important coarse aggregate shape properties, i.e., the form or flatness and elongation, angularity, and surface texture. This final report deals with making use of the recent advent of image analysis methods as a successful research application and potentially a practical mixture design tool in the investigation and understanding of aggregate shape effects on hot mix performance.

PERFORMANCE RELATED AGGREGATE PROPERTIES

Aggregate materials constitute the aggregate structure, the largest proportion by weight of asphalt concrete (AC) pavement surface courses. The significant role played by aggregate materials in the volumetric design

of hot mix asphalt inherently links aggregate properties to the strength, stability, and performance of AC pavement. Mechanical responses of HMA under traffic and environmental loads have been attributed to the properties of aggregate structure, asphalt content and stiffness, and their interactions (Anderson et al., 2002; Ahlrich, 1996). Research efforts have been made towards characterizing the fundamental properties of these component materials since long (Witczak et al., 2002). However, contrary to the well-studied properties of the AC bituminous material and its additives, properties of the aggregate structure are fairly complex and often technically categorized into three classes, i.e., source aggregate properties, consensus aggregate properties and aggregate gradation.

Source aggregate properties include the soundness, toughness of the aggregate, and the deleterious materials contained. These three properties of the source aggregate are determined using the Sodium or Magnesium Sulfate Soundness test (AASHTO T104 or ASTM C88), Los Angeles Abrasion test (AASHTO T96 or ASTM C131 or C535), and the Clay Lumps and Friable Particles test (AASHTO T112 or ASTM C142) respectively. Source aggregate properties closely relate to the quality of the mother rock and the producing quality control. Since quality of the mother rock can be easily determined nowadays, with rigorous quality control means, potential problems related to the source aggregate properties are usually prevented before the asphalt mixes are produced and therefore can be easily controlled in the AC mix design.

According to the SHRP, consensus properties of aggregate materials include the following items: coarse aggregate angularity; fine aggregate angularity; flat and elongated ratios of coarse aggregate particles; and clay content (McGennis et al., 1995). For coarse aggregate materials, coarse aggregate angularity is determined manually by counting the number of fractured faces. Superpave specifies a required percentage by weight of particles with crushed faces based on traffic level and the depth of the layer in the pavement (ASTM D5821). A proportional caliper is normally used to determine the flat and elongated ratio of aggregate particles to characterize the shape of the particles in a given sample (ASTM D4791). For fine aggregate materials, fine aggregate angularity is obtained from a simple test in which a sample of fine aggregate is poured into a small, calibrated cylinder by flowing through a standard funnel (ASTM C1252). The clay content is generally determined through sand equivalence test (ASTM D2419).

Aggregate materials are commonly divided into two domains based on their sizes, i.e. the coarse aggregate and the fine aggregate. According to the conventionally used mechanical sieve analysis as specified by ASTM D136, these two domains of aggregate materials refer to the portions of granular materials retained on and passing the 4.76 mm (No. 4) sieve in a sieve analysis respectively. To specify gradation for aggregates used in asphalt mixtures, Superpave uses a modification of an approach already known as the 0.45 power gradation chart to define a permissible gradation. The ordinate of the chart is percent passing. The abscissa is an arithmetic scale of sieve size in millimeters, raised to the 0.45 power. An important feature of this chart is the maximum density gradation, which plots as a straight line from

the maximum aggregate size through the origin. Sieve analysis results are also presented as a function of percentage weight passing on the 0.45 power gradation chart. Gradation of the aggregate structure is usually determined by using the sieve analysis according to ASTM D136.

As was specified by the Superpave volumetric design procedure, coarse aggregate materials occupy the highest proportion by weight (and volume) in the majority of HMA designs; with their bigger sizes, the coarse aggregate particles form the skeleton of the aggregate structure. Previous studies have shown that at the optimum binder content the strength and stability of asphalt mixes highly depends on the mechanical properties of the coarse aggregate (Kandhal and Cooley, 2001). To investigate the mechanism in which the aggregate structure resists the loads, research studies were conducted to link the critical properties of the component aggregate materials to the mechanical properties of the aggregate structure. Results of these studies proved that, of all the properties of the coarse aggregate materials, the physical shape properties significantly affect both the strength and stability of asphalt mixes (Kandhal and Cooley, 2001; Monismith, 1970; Barksdale et al., 1992). To design asphalt mixtures with long service lives, the aggregates must be then the proper gradation and shape. In general, it is preferable to have somewhat equal-dimensional and angular particles rather than flat, thin or elongated particles. Accordingly, to acquire an overall knowledge about the mechanism of coarse aggregate shape properties that affect the performance of AC, it is necessary to review the currently used standard specifications regarding the shape properties of the coarse aggregate materials, as well as the critical coarse aggregate shape properties that were linked to the performance of AC in previously conducted research studies.

STANDARD COARSE AGGREGATE TESTS AND SPECIFICATIONS

ASTM D4791 is the test procedure generally referenced for determination of the percentages of flat, elongated, or flat and elongated particles in coarse aggregate. The ASTM D4791 specifications aim at limiting percentages calculated by number or by weight of flat, elongated, or both flat and elongated particles in a given sample. The particles can be classified as 'flat', 'elongated', or 'flat and elongated' according to the undesirable ratios of width to thickness, length to width, or length to thickness, respectively. These dimensional ratios may be set at 2:1, 3:1, and 5:1 in the manual caliper shown in Figure 1-1 by adjusting the fixed position of a swinging arm so that the openings between the arms and the two fixed posts on both ends of the arm maintain a constant ratio (ASTM D4791).

The Superpave specifications characterize an aggregate particle only as 'flat and elongated' by comparing its length to its thickness or the maximum dimension to the minimum dimension (McGennis et al., 1995). Flat and elongated particles are undesirable since they have a tendency to break during construction and under traffic. If they do not break, they tend to produce mixtures with directionally

oriented material properties. Superpave allows no more than 10% by weight flat and elongated particles for the combined aggregate blend used in asphalt pavements having greater than 3 million equivalent single axle loads (ESALs) in the design life. The test is performed on the greater than 4.75 mm (+No. 4) aggregate and the flat and elongated particles are reported only as ‘percent by weight’ of particles having a ratio of over 5:1. Currently, the 5:1 ratio is used for Superpave requirements.

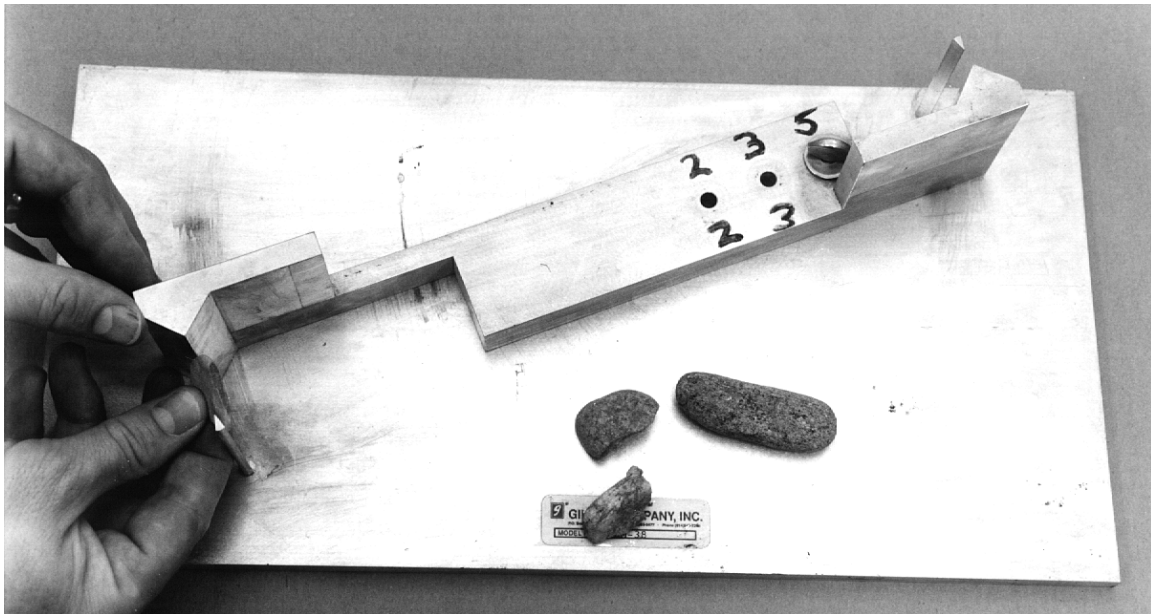


Figure 1-1 Proportional caliper device to measure flat and elongated particles
(Figure Courtesy FHWA: <http://www.fhwa.dot.gov/asphtech/>)

Coarse aggregate angularity is determined manually by counting the number of fractured faces (ASTM D5821). The amount or percentage of crushing (angularity) is important because it determines the level of internal shear resistance, which can be developed in the aggregate structure. Round, uncrushed aggregates tend to “roll” out from under traffic loads and therefore have a low rutting resistance. Superpave specifies a required ‘percentage by weight’ of crushed particles based on traffic level and the depth of the layer in the pavement (McGennis et al., 1995). The crushing requirements for low traffic volumes are low or none, regardless of depth. As traffic levels increase, so do the required percentages of particles with crushed faces. There is a higher level of crushing required for particles in the top 100 mm of the pavement because this is the region subjected to the highest shear due to traffic loads. Higher shear forces require a higher level of resistance to shear. There are currently no standard test methods for directly and objectively measuring coarse aggregate angularity and surface texture.

ASTM D3398-00, Standard Test Method for Index of Aggregate Particle Shape and Texture has been also adopted as the standard test to obtain an indirect measure of particle shape, angularity, and surface texture. In addition, the Uncompacted Air Voids Tests, ASTM C 1252-98 and AASHTO TP56, are also used to measure in an indirect manner the particle shape, angularity, and surface texture. Similar to AASHTO TP56, the particle index test (ASTM D3398-00) provides a combined shape-texture characterization. This test requires that an aggregate sample be divided up into specific size fraction. Each size fraction is placed into a container in three layers. This is done twice; the first time, each layer is compacted with 10 blows of a tamping rod, and the second time, each layer is compacted with 50 blows of a tamping rod. The particle index is computed as follows:

$$I_a = 1.25V_{10} - 0.25V_{50} - 32.0 \quad (1-1)$$

where:

I_a = Particle Index for a given size fraction;

V_{10} = Voids in the aggregate when compacted using 10 blows per layer;

V_{50} = Voids in the aggregate when compacted using 50 blows per layer.

The overall sample particle index is computed as a weighted average of the individual size fraction particle indexes based on the size fraction weights. Aggregates composed of rounded, smooth particles may have a low particle index of around 6 or 7, while aggregates composed of angular, rough particles may have a high particle index of between 15 and 20 or more.

Current standard tests do not fully explore the characteristics of aggregates and often provide an average value and but not a distribution of shape properties. Hence, there is an over emphasis on superior aggregate characteristics. Some tests are rather very time consuming, such as the ASTM D4791, and often subjective or operator dependent. The particle index and uncompacted void tests (ASTM D3398-00 and AASHTO TP56) give results for the combined shape, angularity, and texture properties. There is not a single standard test to adequately define and quantitatively determine the aggregate surface texture property. Further, there are contradictory findings in the literature on the influence of shape on performance.

SIGNIFICANCE OF COARSE AGGREGATE SHAPE AND SIZE

Past research efforts correlated aggregate physical and structural layer properties to pavement performance. A study undertaken by Monismith (Monismith, 1970) concluded that aggregate shape and

surface texture characteristics had an influence on the fatigue and stiffness characteristics of asphalt mixtures. Rough textured and densely graded materials could be compacted better and hence provided better stability in the mix due to higher stiffness. Laboratory studies based on the Marshall mix design procedure suggested that the use of crushed gravel over natural gravel significantly improved the stability of the hot mix asphalt (Benson, 1970). Further, it was also concluded that the use of crushed stone instead of gravel could increase the stability of the mix by as much as 45 percent (Benson, 1970).

Several studies in the last decade have also linked coarse aggregate size and shape properties to pavement performance. Yeggoni et al. (1994) noted a significant effect of aggregate size, shape and surface texture on the rutting resistance of asphalt concrete and underlying layers. Barksdale et al. (1992) indicated that using a coarser asphalt mix was found to reduce rutting in the base, asphalt binder, and surface courses by approximately 23, 14, and 13%, respectively; the exact percentage reduction depending upon the aggregate source. The benefits of reduced rutting were, however, offset by a decrease in fatigue life by 22, 11, and 28 percentage points, respectively. Targeting a good balance between fatigue life and rutting could therefore be an effective approach to choose the optimum coarseness of the mix.

Aggregate shape properties have also been found to influence Portland cement concrete (PCC) strength properties. Mixes containing angular particles produced higher strength and modulus values compared to PCC samples with gravel (Choubane et al., 1996). It is however interesting to note that this is somewhat in contradiction with the traditional recommendation to use rounded gravel with minimal surface areas for reduced paste requirement to cover the particle completely (Mindess and Young, 1981). The use of angular particles in PCC mixes would however increase the unit cost of the mix due to crushing costs and increased paste requirements.

In the base courses while compaction is important from a shear resistance and strength point of view, the shape, size and texture of coarse aggregates are also important in providing stability (National Stone Association, 1991). Field tests of conventional asphalt pavement sections with two different base thicknesses and three different base gradations showed that crushed-stone bases gave excellent stability because of a uniform, high degree of density and little or no segregation (Barksdale, 1984). Rounded river gravel with smooth surfaces was found to be twice as susceptible to rutting compared to crushed stones (Barksdale and Itani, 1989).

In light of all the above research efforts, the importance of adopting specifications to control the size and shape properties of aggregates cannot be over stated. Pioneering work in this regard by Huang (1962 and 1967) suggested the use of the particle index parameter to evaluate the combined effect of particle shape and surface texture. This test method has been accepted as the standard test method for index of aggregate particle shape and texture (ASTM D3398) as discussed in the previous section. The

particle index for a given aggregate sample is a weighted average of the weights of individual sizes. Subsequent work by Boutlier (1967) and McLeod and Davidson (1981) showed that a fairly good relationship existed between the particle index and Marshall Stability of HMA mixtures. The particle index test parameter was found to bear a high correlation with the percent crushed particles or crushed face count (Ahlrich, 1996; Kandhal and Cooley, 2001). Samples with higher percentages of crushed particles also possessed higher particle index.

Flat and elongated (F&E) ratio is another shape index that is used to check if particles have undesirable shapes that might negatively affect mechanical properties of the asphalt mixture. The standardized ASTM D4791 test for flat, elongated, or flat and elongated particles, was adapted from the original U.S. Corps of Engineers Method CRD-C 119 test, and is performed on particles retained on the No. 4 sieve. Puzinauskas (1964) showed that AC samples displayed a fair amount of anisotropic properties with the presence of flat particles. However, the effects of particle alignment became less pronounced as the size of the particles was reduced. Subsequent test results (Li and Kett, 1967) verified that the strength of asphalt mixes was adversely affected when they contained coarse aggregate particles with a length to width ratios greater than 3. Inclusion of more than 30-40% of particles with length to width ratios greater than 3:1 caused undesirable mix properties.

From constant strain fatigue tests it was concluded that the use of “slabby-shaped” particles resulted in shorter fatigue life relative to the use of rounded particles (Maupin, 1970). However, the conclusions by Livneh and Greenstein (1972) contradicted most findings in this regard. From laboratory tests of open graded and dense graded samples, they recommended that flaky aggregates could be used in producing asphaltic mixtures in the same manner as conventional aggregates from an engineering viewpoint. It is important to note that in this study, asphaltic samples with flaky aggregates still produced 15-20% lower stability than samples with cubical aggregates.

After Superpave adopted the ASTM D4791 test procedure for coarse aggregates used in asphalt concrete, there have been mixed opinions about using a controlled amount of particles with greater than 3:1 flat and elongated ratio rather than the existing 10% limit on percentage weight of particles bearing a F&E ratio of greater than 5:1. The need to comply with these stringent shape requirements was investigated through performance evaluation tests conducted on HMA mixes prepared with varying the percentages of 3:1 and 5:1 ratio flat and elongated particles (Buchanan, 2000; Vavrik et al., 2000). The types of aggregates used in the study by Buchanan (2000) were limestone and granite. On the other hand, Vavrik et al. (2000) used gravel and dolomite aggregates in their study. Both research efforts concluded that F&E particles affect the rutting susceptibility and volumetric properties of compacted HMA mixes. Buchanan (2000) also recommended that the hardness of the aggregate sample had to be accounted for in

establishing the limiting percentage of 3:1 F&E particles (i.e. not just one requirement for all aggregate types).

Kandhal and Parker (1998) summarized the various test procedures for aggregates currently practiced and presented a review of various research efforts that verify the effectiveness of these tests to correlate coarse aggregate shape and size with asphalt mixture strength properties. They recommended that an accelerated loading facility test would enable an evaluation of pavement performance under varying aggregate particle angularity, shape and surface texture parameters. To isolate the effects of coarse aggregate shape and size properties on the permanent deformation and fatigue characteristics of AC pavements, the fine aggregate content and gradation would need to be similar in all AC mixes studied.

Review of the currently adopted standard specifications regarding the coarse aggregate shape properties and the previously performed research studies show that while there is a general understanding of the influence of aggregate shape properties on the performance of HMA mixtures, the specifics have been somewhat elusive because the current methods used to characterize particle shape and surface texture are imprecise and cannot be applied across the broad range of aggregate materials without ambiguity. There are currently no standard test methods for directly and objectively measuring aggregate shape, angularity, and surface texture. The qualitative indirect methods now used by the paving industry are also quite tedious and laborious. Accordingly, along with a need to develop an objective and accurate measure to describe the particle shape of an aggregate, there is also a need to develop rapid and automated methods for determining aggregate properties.

ADVENT OF IMAGE ANALYSIS

Dependent on the most important sensory inputs to the human perceptual system, vision aided intelligent tools for improving production efficiency draws most of the attention in human's efforts to explore the unknown world. Engineers have investigated ways to make these machines capable of accurate interpretation of image inputs. The last few decades have seen a considerable increase in the new methods designed to increase the visual sensory capabilities of computers, also known as "image analysis." Image analysis finds wide applications in several fields, for example, medicine, astronomy, map data processing and aerial image analysis, digital and optical techniques for fingerprint analysis, three-dimensional reconstruction methods and analysis for robot navigation (Kasturi and Trivedi, 1990) and in recent years, in civil engineering.

Application of image analysis in the different fields of civil engineering can be tracked back to the 1980s in the pavement distress data collection (Cable and Marks, 1990), investigation of soil and rock properties (Raschke, 1998; Glaser and Haud, 1998), and microstructure of asphalt concrete (Yue et al.,

1995; Masad et al., 1998; Masad et al., 1999) and Portland Cement Concrete (Bentz and Garboczi, 1996). Image analysis techniques have also been combined with other tools such as finite element analysis (Kose et al., 2000) and artificial intelligence techniques (Chang et al., 2000). A hybrid model was developed based on image analysis and neural network modeling to provide reliable, consistent and objective quality assessment of steel bridge coating corrosion and further, to determine the extent of rehabilitation required (Chang et al., 2000). Research in fine aggregate shape analysis is also being actively pursued (Wilson et al., 1997; Masad et al., 2001).

As an application of the imaging technology, imaging based morphology analysis has been pursued for almost a decade now to quantify the shape, angularity and texture of coarse aggregate particles. Automated video imaging systems with varying levels of capabilities for determining critical coarse aggregate shape and size properties have been developed across the country. Contrary to the conventional standard manual tests, image analysis techniques provide a direct and objective measurement of the aggregate particle shape in a rapid and automated way. This can allow personnel more time for other duties. An image analysis database formed through such testing can assist in creating asphalt mix designs with longer service lives.

The use of a video imaging system primarily involves acquiring the image of the particles to be evaluated and then “processing” it with the use of an image analyzer system. A computer algorithm analyzes the image to estimate the desired information: dimensions and size of aggregate, shape, texture, angularity and gradation depending upon the capabilities of the image analysis algorithm used. Among the basic concepts that have been used for pattern recognition and shape characterization are the fractal dimension analysis (Yeggoni et al., 1994; Fan and Yashima, 1993; Li et al., 1993; Ribble et al., 1992), Hough Transforms to characterize shape and angularity (Wilson and Klotz, 1996; Wilson et al., 1997), 2-D to 3-D reconstruction models based on stereology or geometric probability (Maerz et al., 1996; Maerz, 1998), and measurement of particle dimensions and aspect ratios, (Laboratories Central Des Ponts et Chaussees, 1995; Weingart and Prowell, 1999; Prowell and Weingart, 1999; Brzezicki and Kasperkiewicz, 1999).

Several image analysis systems are currently available commercially or as prototype research devices to perform aggregate shape and size determination. The capabilities of these systems vary in terms of hardware used, analysis methods employed, degree of sophistication, and parameters computed. The concepts and capabilities of some of these systems were recently evaluated by Tutumluer et al. (2000). An ongoing research project sponsored by the National Cooperative Highway Research Program (NCHRP), NCHRP 4-30A, is presently studying test methods, including direct measurement methods such as imaging, for characterizing aggregate shape, texture and angularity by considering in the

evaluations such essential factors as the repeatability, reproducibility, operational characteristics, field applicability, practicality, labor requirements, ease of use, and cost.

STATEMENT OF THE POOLED FUND STUDY

The performance-based specifications require consensus property tests to be conducted for selecting good quality coarse and fine aggregates for asphalt mixture design. For coarse aggregate, which is the focus of this study, the specifications are with regard to the tests for aggregate gradation using sieve analysis as per ASTM C136, flat and elongated particles as per ASTM D4791, aggregate angularity as per ASTM D5821, and indirect aggregate shape property measurement for surface texture as per ASTM D 3398-00. Image analysis systems as alternatives for automation of these tests have already demonstrated obvious improved speed and efficiency especially when dealing with several different aggregate samples from different sources or quarries. A precise, fast, cost effective and locally usable test, e.g. video imaging, was needed to describe particle shape and size distribution characteristics to quantify the influence of particle shape, angularity, and surface texture on HMA performance.

The University of Illinois Aggregate Image Analyzer (UIAIA), recently developed and currently being evaluated by the NCHRP 4-30A project as a promising image analysis device, was utilized to provide a fast, objective, and automated means to describe particle shape and size distribution characteristics for quantifying the influence of particle shape, angularity, and surface texture on HMA performance. UIAIA showed high accuracy in the preliminary validation tests when Illinois DOT coarse aggregate samples were precisely and reliably quantified for shape, angularity, texture, and gradation properties from video imaging (Tutumluer et al., 2000). Among the presently available video image analysis systems, excluding x-ray computer tomography (CT) systems (Wang et al., 2001; Masad et al., 2002; Garboczi et al., 2004), UIAIA is the only system that can compute 3-D properties, such as the volume, of aggregate particles by the use of the three orthogonally captured camera views and quantify all four shape and size properties, i.e., F&E ratio, angularity, surface texture, and gradation, of coarse aggregates in a fast and automated way. Owing to the merits presented above, the UIAIA system can possibly replace four of the standard coarse aggregate shape test procedures, i.e., ASTM D 4791, ASTM D5821, ASTM D3398, AASHTO TP56. Future development of a production type device based on the UIAIA and its routine use in the State DOT material testing laboratories is anticipated to provide a significant cost savings to be realized in materials testing.

To evaluate the prospected application of the UIAIA system as targeted, the pooled fund study, research project DTFH61-02-X-00029: “Investigation of Aggregate Shape Effects on Hot Mix Performance Using an Image Analysis Approach,” was initiated by the Federal Highway Administration

(FHWA). The project DTFH61-02-X-00029 was a 2-year pool funded-research project [TPF-5(023) on <http://www.pooledfund.org>], which started in March 2002 in the Civil and Environmental Engineering Department at the University of Illinois at Urbana-Champaign (UIUC). The study partners were the National Center for Asphalt Technology (NCAT), the state highway agencies of Alabama, Georgia, Indiana, Minnesota, Mississippi, Missouri, Montana, and South Carolina, and the FHWA Central Federal Lands and Highways Division. A mid-year research progress meeting also took place on the campus of the University of Illinois in the first week of July 2003, which brought together the project technical team, administrative monitors, and the representatives from the participant states to evaluate the progress made in the pool-funded study and provide valuable inputs and research directions.

OBJECTIVES AND SCOPE OF THE POOLED FUND STUDY

The objectives of the pooled fund research project DTFH61-02-X-00029 include the measurement of imaging based volumetric and morphological indices of coarse aggregates and their correlations with laboratory and field performance results of asphalt concrete mixes as a wave of future in the development of asphalt pavement science and technology. The readily available image analysis device, University of Illinois Aggregate Image Analyzer (UIAIA), was used for validation and development of imaging based coarse aggregate shape indices. To fulfill the prospected application of UIAIA, aggregate materials with a broader range of shape irregularities were processed for generating imaging based morphological indices with the final goal to use these indices in the investigation of the effects of coarse aggregate shape and size properties on HMA performance. The project made strong efforts to develop parameters that could be used to supplant in speed, cost, objectivity, and precision/accuracy of the traditional test procedures used to characterize aggregate shape, volume, angularity, and texture properties. The scope of the project consisted of two phases:

Phase I: Evaluation of the Shape and Size Properties and Validation of UIAIA

In Phase I of the pooled fund research project DTFH61-02-X-00029, coarse aggregate samples were received from the National Center for Asphalt Technology (NCAT) Pavement Test Track Facility in Auburn, Alabama. These aggregate samples collected from 9 sponsoring States and the Federal Highway Administration were used to make various asphalt concrete mixtures (SMA, fine or coarse mixes, blended mixes, modified binder asphalt mixes, etc.) designed to withstand 10 million ESALs of accelerated full-scale testing at the NCAT Pavement Test Track Facility in two years. In addition to NCAT aggregates, participant state highway agencies of Georgia, Indiana, Minnesota, Mississippi, Missouri, Montana, and

South Carolina, and the Central Federal Lands and Highways Division shipped to UIUC their coarse aggregate samples (crushed, uncrushed, and partially crushed aggregates requested as available) together with the required amounts of asphalt binder, fine aggregate, and mineral filler for making in the laboratory their exact Superpave HMA mixes following the provided job mix formulas.

The automated procedure using the UIAIA was utilized to quantify three-dimensional shape, size, angularity, and surface texture properties of the pooled fund study aggregate samples and define proper imaging based morphological indices. Among the shape and size properties determined for each aggregate particle were: (i) maximum, intermediate, and minimum dimensions; (ii) flat and elongated (F&E) ratio; (iii) volume (and weight knowing its specific gravity); (iv) a computed Angularity Index (AI) to indicate how many crushed faces are there or how rounded or angular the particle is; and finally, (v) a computed Surface Texture (ST) Index to indicate how smooth or rough the aggregate particle surface is. Having the intermediate dimension for each particle, the particle size distribution, i.e., gradation, for each coarse aggregate sample was also accurately determined from imaging. With a coarse aggregate size and shape property database established this way, property variations reported by the various developed imaging based indices validated the UIAIA quantifications for shape, angularity, texture, and gradation properties.

Work items of Phase I therefore consisted of:

- (1) Acquisition of NCAT aggregate;
- (2) Acquisition of aggregate samples from the participating states;
- (3) Testing of participating states' aggregate samples with the UIAIA;
- (4) Testing of NCAT aggregate samples with the UIAIA; and
- (5) Image processing for shape indices.

Phase II: Evaluation of Shape and Size Effects on Hot Mix Performance

The UIAIA determined imaging based properties of the NCAT Test Track aggregates and the participant States' coarse aggregates were put to use in Phase II of the pooled fund research project DTFH61-02-X-00029 for evaluating shape and size effects on HMA performance. Being primarily a field rutting study, the NCAT Test Track findings were first used to evaluate the performances of the various Superpave mixes with traffic. The results from 46 different flexible pavement test sections installed at the NCAT Test Track, each at a length of 200 feet, were collected from the Test Track to provide a good statistical basis for AC structural layer rutting performance comparisons. The detailed UIAIA determined NCAT Test Track aggregate shape properties were then essentially correlated to the individual NCAT test

section asphalt surface rutting data for a better understanding of coarse aggregate shape effects on field Superpave mix rutting performances.

Phase II of the research project also included preparation and testing of asphalt concrete mixes made using the aggregate samples collected separately from the participating States and the FHWA Central Federal Lands and Highways Division. This activity extended field results from the NCAT study to other States' aggregates to assist in aggregate selection for performance. The laboratory evaluations of the Superpave mix performances of the participant States' mix designs, including the Central Federal Land and Highways Division's mixes, were performed at the Advanced Transportation Research and Engineering Laboratory at the UIUC. Three Superpave gyratory asphalt specimens were made for each asphalt mix design. Two of the specimens were tested for determining permanent deformation behavior in the laboratory. From the third gyratory specimen, three indirect tension type resilient modulus disc specimens were obtained and tested for determining in the laboratory the resilient modulus properties at 25°C. The UIAIA determined coarse aggregate shape properties were then correlated to the laboratory resilient modulus and permanent deformation test results of the Superpave asphalt mix specimens in an effort to quantify the influence of coarse aggregate particle shape on asphalt concrete mix performance and establish proper aggregate criteria.

Work items of Phase II therefore consisted of:

- (1) Preparation and laboratory testing of asphalt samples;
- (2) NCAT performance data collection;
- (3) Laboratory and field data analysis;
- (4) Final report preparation.

REPORT OUTLINE

Basic concepts and terminologies used in digital imaging to quantify the shape and size of coarse aggregate particles are introduced in Chapter 2. Previous research efforts on aggregate particle size and shape characterization are also reviewed with a highlight on the successful image analysis techniques. The physical configuration of the UIAIA imaging system is then described by detailing on the need for 3-dimensional aggregate imaging and volume computation. The image processing algorithms and virtual tools developed specifically for use with the UIAIA are also described to define the imaging based aggregate shape indices for Flat and Elongated (F&E) ratio, Angularity Index (AI), and Surface Texture (ST) Index.

In Chapter 3, detailed lists are given of all the aggregate materials received from the pooled fund study partners. The properties of the aggregates are listed to show the variations in sizes and shape irregularities these materials possessed, which was essentially intended to further validate the size and

shape quantification features of the UIAIA imaging system. The different State's asphalt mix designs are instead given in Appendix I. All the aggregate materials received are considered in Chapter 3 separately as coming from the NCAT Test Track pavement test sections and the other pooled fund participating States including the Central Federal Lands and Highways Division. As part of the Phase I activities, the imaging based size properties and shape indices of all the processed aggregates are documented in Tables. Only representative sample charts for the shape indices are presented in Chapter 3. All other detailed aggregate image analysis results are given in Appendix II.

Chapter 4 deals with the investigation of coarse aggregate shape effects on the rutting performances of the NCAT Test Track asphalt pavement test sections. The NCAT Pavement Test Track study that took place took place between September of 2000 and January of 2003 is first described to identify the location, test section designations, and the test parameters. The computed shape indices are first normalized to account for various coarse aggregate weight percentages used in different hot mix asphalt lifts and individual lift thicknesses. The normalized indices of the NCAT aggregate samples, i.e., F&E ratio, Angularity Index and Surface Texture Index, are then correlated to the asphalt pavement rut depth data of the individual NCAT pavement test sections to draw possible conclusions on how each of these morphological coarse aggregate properties could affect the field performances of asphalt mixes.

Chapter 5 investigates relationships between the imaging based coarse aggregate morphologies and the stability or permanent deformation behavior of asphalt mixtures prepared using the image processed coarse aggregate materials. A total of 18 asphalt mix designs mixes received from a total 10 state highway agencies, i.e., the 8 pooled fund participating states and the Central Federal Lands and Highways Division providing asphalt mixes and mix designs of New Mexico and Oklahoma, are followed to make specimens in the laboratory. The stability and deformation characteristics of the asphalt mixtures are studied by means of repeatedly applying traffic loads in a triaxial test setup. The differences in the laboratory test data, i.e., different trends in the permanent deformation accumulation with the number of load applications, are then analyzed for possible linkages to the UIAIA imaging based morphological indices of the coarse aggregate materials used in the asphalt mixes. A possible mechanism of coarse aggregate morphology affecting the stability of asphalt mixture is also proposed as defined by the concept of particle geometrical interference in hot mix asphalt.

In Chapter 6, coarse aggregate morphological properties quantified from the UIAIA analysis as angularity and surface texture indices are primarily used to investigate the effects of these shape properties on the resilient modulus of hot mix asphalt. The indirect tensile test using the specimen diametral loading as per ASTM D 4123 is the adopted procedure for resilient modulus, M_R , testing in the laboratory. Based on the 18 asphalt mixes prepared and tested in the University of Illinois ATREL, it will be shown that when coarse aggregates with more irregular morphologies are used in asphalt mixes, the

resilient modulus of the asphalt mixture is often improved. The resilient modulus test data will also be grouped according to gradation, asphalt binder grade, and asphalt stiffnesses to better indicate possible linkages and mechanisms of the aggregate morphologies with the resilient moduli.

In Chapter 7, conclusions are drawn and recommendations are given for future image analysis research in the area of aggregate size and shape effects on asphalt mix behavior and performance.

CHAPTER 2

UNIVERSITY OF ILLINOIS AGGREGATE IMAGE ANALYZER

The performance-based Superpave volumetric design procedure specifies coarse aggregate consensus properties for quality asphalt mixture designs. After evaluating most of the existing image analysis systems developed for aggregate consensus property determinations and identifying the need for accurate volume (and weight) computation for a proper 3-dimensional (3-D) shape reconstruction of an aggregate particle, Tutumluer et al. (2000) developed a new image analysis system, the University of Illinois Aggregate Image Analyzer (UIAIA), to provide accurate and automated measurement of the shape and size properties of coarse aggregate. In addition to the preliminary validation of the UIAIA image analysis results by Tutumluer et al. (2000), the pooled fund research project DTFH61-02-X-00029 further evaluated and validated the UIAIA system for its practical application in coarse aggregate image collection and data acquisition and the accuracy of its imaging based shape indices describing a broader range of aggregates in terms of both size and shape. The UIAIA will therefore be described in this chapter as a device that can sufficiently capture images and characterize size and shape of coarse aggregate particles in compliance with the currently used test procedures and by emphasizing the need for 3-D volume computation, basic image analysis concepts, detailed physical configuration of the UIAIA system, and the imaging based indices developed to quantify the size and shape properties.

NEED FOR 3-DIMENSIONAL IMAGE ANALYSIS

In video imaging based aggregate gradation and shape analyses, estimating the volume of an individual particle has a significant effect on the computed grain size distribution and the estimation of percentage flat and elongated particles by weight in a given sample. Once the volume is estimated, the ratio of the volume of the flat and elongated particles to the total volume of all the particles in the sample will be equivalent to their ratios by weight. This equivalency arises due to the fact that the weight and the volume differ by a constant factor, the specific gravity, with the condition that all aggregates processed are from a homogeneous parent material.

Any technique that utilizes a single 2-D image of a particle to estimate the volume assumes the particle size in the third dimension. Although this assumption reduces the image capturing setup and simplifies the analysis, it introduces serious errors in calculating the volume and consequently, the weight. Two orthogonal views provide sufficiently more information about the depth of the particle than

the projected image from one camera. However, getting an additional view of the particle from the third orthogonal direction clearly shows any non-uniformity in its depth and hence aids in a more realistic estimation of the volume. Figure 2-1 illustrates this point clearly. The 3-D views of two regular shaped solids, a rectangular and a triangular prism, are shown. Clearly, both the top and side views of the two solids are identical rectangles. Imagine a 2-D video image analysis setup consisting of only top and side cameras. Capturing images of these two views of each solid would not be effective in discriminating the 3-D shapes of the solids. In reality, the rectangular prism has twice as much volume as that of the triangular prism. Incorporating the front view obtained from an additional third camera would certainly be beneficial in getting a more realistic 3-D view of the solids, which is needed for the proper shape analysis and the 3-D volume determination. Although this example deals with theoretical shapes, the concepts presented are valid even for irregularly shaped aggregates.

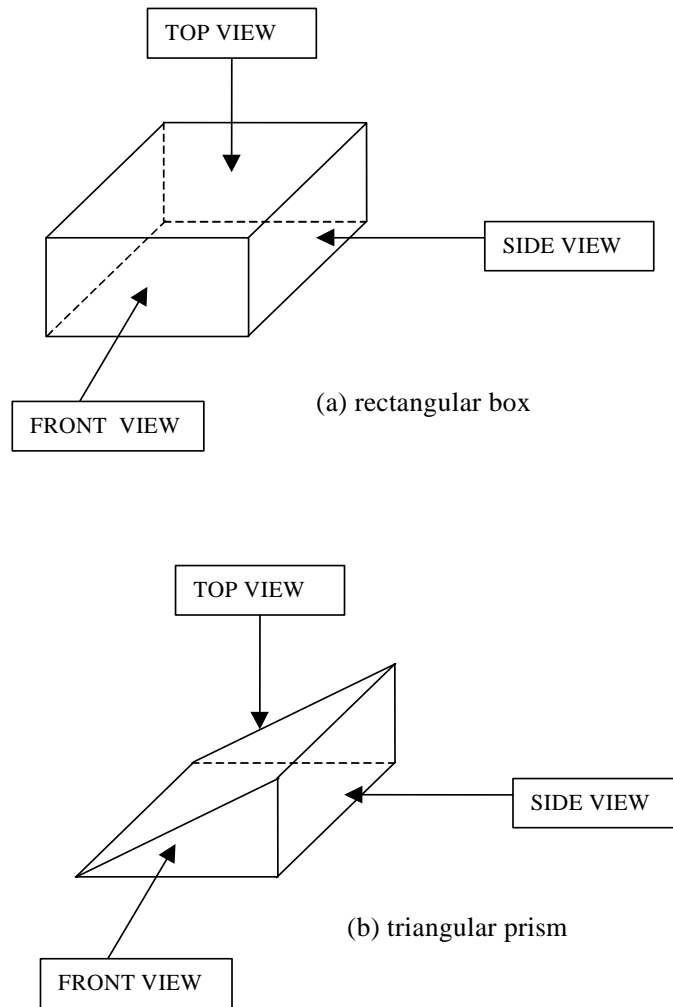


Figure 2-1 Three-dimensional Views of Two Regular Shaped Solids

For the triangular prism shown in Figure 2-1, the correct positioning of only two cameras to capture the front and side views would be sufficient to determine the 3-D shape of this regular shaped solid. However, aggregates are not regular shaped particles and hence the outline of an aggregate image in any view does not ever continue into the third dimension that is not visible. Therefore, the use of at least three cameras to obtain three orthogonal (front, top and side) views is essential in establishing an accurate 3-D shape of each particle.

IMAGE ANALYSIS CONCEPTS

Image analysis is conducted on digital images. A digital image is a numerical representation of an object and allows image processing by performing numerical calculations by discrete units. Bitmap graphic formats treat each graphic as a collection of picture elements called pixels, assigning a specific color to each pixel. When viewed as a whole, the collection of pixels forms an image as shown in Figure 2-2.

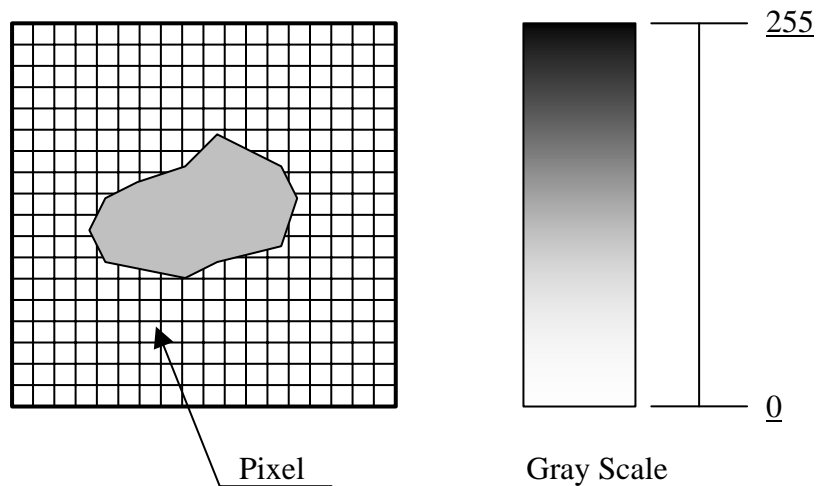


Figure 2-2 Image Digitization

The process of converting an image to an array of pixels is called digitization. Assuming a continuous tone capture, the image must go through a spatial digitization and a gray tone quantization. It must be placed into computation in a functional form $f(x, y)$, where (x, y) is a discrete pixel (picture element) in the grid and $f(x, y)$ is a discrete gray value. A digital image may be binary (1-bit), have multiple levels of gray (8-bits) or be color (24-bits). It is often assumed that capturing and sampling form a block of activity prior to digital processing and that digital processing commences with a sampled (digitized and quantized) image stored in a computer. Gray levels are quantified on a scale of 0 to 255, 0 to indicate black and 255 to indicate white. All intermediate gray shades are assigned values between 0

and 255. So, each pixel in an image has a gray level in the range of 0 to 255. On the other hand, a color image has 24 bits per pixel and is essentially a combination of three 8-bit integer arrays. The array consists of three brightness values corresponding to each of the three primary colors.

Often, to recognize an object in an image, a thresholding operation is performed on the image, which allows the recognition of regions in the image that belong to the object of interest. Image thresholding is essentially a computational operation and helps define disjoint regions and helps identify the object from the contrasting background. On assigning a threshold value to the image, all pixels with gray levels below this threshold value are reduced to '0' (black) while all pixels with gray levels greater than the threshold value are made equal to '255' (white). Clearly, the choice of the threshold value will depend upon the color of the background, and the brightness of the object to be identified in the image.

Image analysis is the process of measuring features (properties) of the object(s) in the image. The features extracted, depending on the application involved, can belong either to the image or to an object in the image. Linear measurements such as measuring the length of a line are typically performed by counting the number of pixels representing the line. Knowing the calibration for a particular resolution, the pixels are converted to length units. Also, the area or any 2-D measurement involves measuring the number of pixels occupying the area followed by conversion to engineering units.

UNIVERSITY OF ILLINOIS AGGREGATE IMAGE ANALYZER

The University of Illinois Aggregate Image Analyzer (UIAIA) uses 3 cameras to collect aggregate images from three orthogonal directions and in essence captures an "actual" 3-D view of each aggregate particle. The choice of using 3 cameras to collect the front, top and side views was to provide the unique capability of determining accurately the volume of each particle, which is essential for the automation of the Superpave consensus property test procedures.

Figure 2-3 shows a schematic of the UIAIA illustrating the operating principle and the various components of the UIAIA. Particles to be analyzed are continuously fed on to a conveyor belt system, which carries them towards the orthogonally positioned cameras. As the individual particles travel along the conveyor, each particle comes into the field of view of a sensor that detects the particle and immediately triggers the cameras. Once triggered, the three synchronized cameras capture the images of the front, top, and side views of the particle. There is a small time delay between the detection of the particle by the sensor and the actual image acquisition. This allows enough time for the particle to move into the field of the three camera views. The captured images are then processed using software developed specifically for this application and the needed size and shape properties are determined.

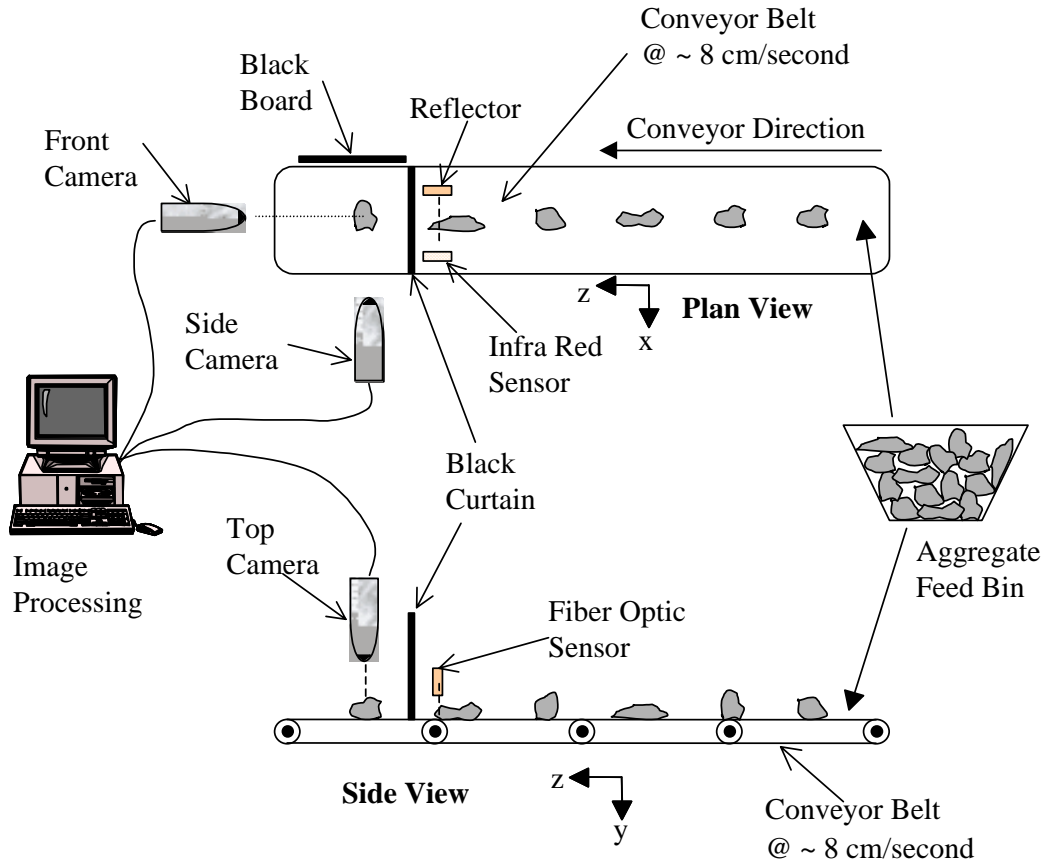


Figure 2-3 Schematic of the University of Illinois Aggregate Image Analyzer

The design and construction efforts of both the physical components such as fixtures for mounting and positioning the cameras, as well as the software components to acquire and process images in the UIAIA were undertaken at the University of Illinois. The mechanical details of the UIAIA include a working conveyor belt operated using a variable speed AC motor, which provides smooth and steady operation at speeds as low as 3 inches/sec. Three fluorescent lights were positioned behind the cameras to provide adequate brightness. A black background was provided for all three views in order to provide a contrast and collect sharp images. A cloth curtain was placed in front of the sensors (see Figure 2-3) not only to obtain a black background for the front view but also to hide the sensors and other fixtures from the camera.

Extensive research was conducted for finding the optimum configuration of hardware components for the system, i.e., frame grabber boards, cameras, image processing software, etc. A typical device for an image digitizing application of this nature would be a Charged Couple Device, commonly known as a CCD camera, which is essentially a solid-state camera with a light-sensitive crystalline silicon chip. A rectangular array of photo-detector on the silicon substrate holds the

photoelectrons produced in the local area, which gets shifted as a charge packet to an external terminal. CCD cameras are compact and also have the advantage of having no geometric distortion and offer high linearity in their response to light. They hence lend themselves to several image-sensing applications.

Due to the moving nature of aggregates on the conveyor in the UIAIA, the choice was to use progressive scan CCD cameras, which are commonly used in motion control applications. The Sony XC-55 analog progressive scan camera was selected for its ability to capture sharp, unblurred images of moving objects using high shutter speeds and for its impressive resistance to shock and vibration. The cameras were synchronized to take images of the aggregate particle at every 1/30th of a second in succession. Several issues such as the optimum distance of cameras, adjustment of lighting fixtures and selection of camera lenses were studied during the experimentation phase of the system integration.

An analog frame grabber board, the National Instruments (NI) PCI 1408, which is a high accuracy monochrome image acquisition device, was used to capture digital images. The board is essentially an analog-to-digital converter that converts video signals to digital images and can be controlled with the image acquisition driver software NI-IMAQ, which serves as an interface between the board and any programming environment. The board supports four video sources with four input/output lines, three of which were used for the three cameras and one for the trigger mechanism. Although the more recently available boards can synchronize all functions to a single trigger or time event using a Real-Time System Integration (RTSI) bus, the board used in the UIAIA does not have this capability. Hence the image processing tasks have to accommodate images captured in succession with a 1/30th of a second time delay between successive cameras. Nevertheless, this does not affect any good operational features of the UIAIA as will be discussed in this thesis.

The National Instruments LabVIEW™ software and its image analysis advanced package IMAQ Vision library was used to create the necessary user-programmed functions for capturing and analyzing aggregate images. The IMAQ vision package provides built-in functions exclusively for scientific imaging applications and includes an extensive set of MMX-optimized functions that allows high quality gray scale, color, and binary image display, image processing, shape matching, blob analysis, gauging and measurement. In addition, the LabVIEW™/IMAQ Vision combined platform currently offers researchers the unique opportunity to program in user-defined image processing/analysis functions by using the LabVIEW's Graphical (G) Programming Language.

The UIAIA integrated system includes two external sensors needed for recognizing the approach of an aggregate particle and for triggering the cameras to capture images as the particle comes into the field of view of the cameras. The sensor fixtures are shown in Figure 2-4. Two sensors were used in the prototype because of the sensor range limitations. The first sensor shown in Figure 2-4 is an infrared sensor that triggers when an infrared beam is cut by the passage of an aggregate particle. A second fiber

optic sensor was installed on top of the belt to sense moving aggregates of all sizes, particularly the thin and, flat particles (having thicknesses less than 5 mm, 0.2-in.). The use of sensors, in general, eliminated the timing requirements for aggregate placement or image capturing, and provided adequate control over conveyor belt operations.

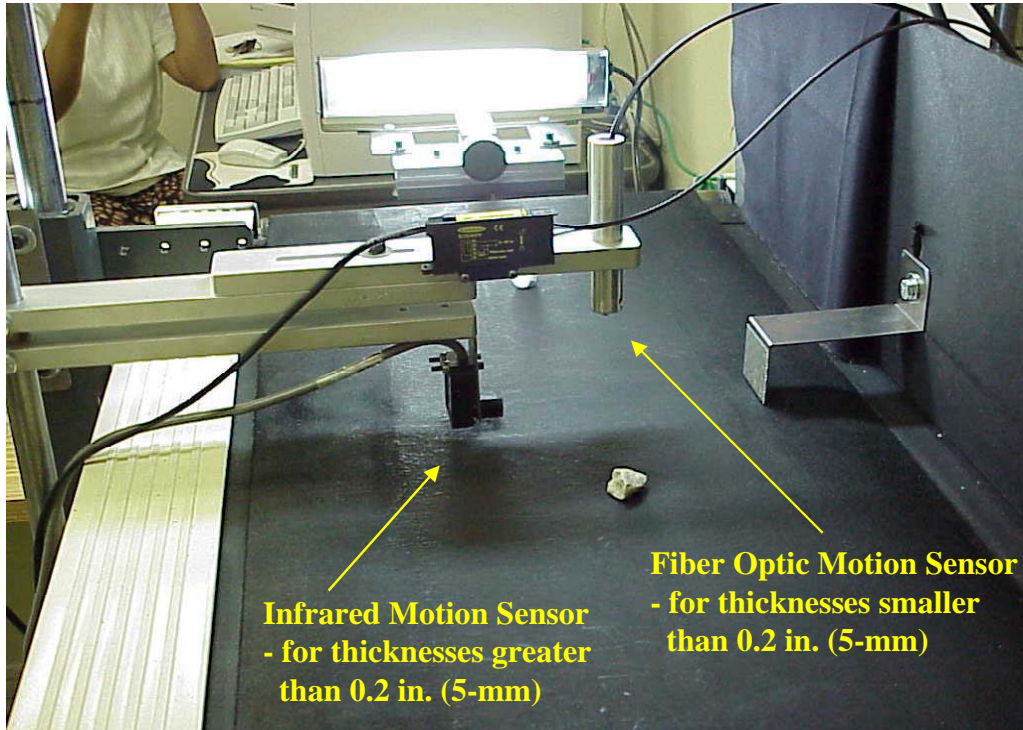


Figure 2-4 Installations of Sensors for the UIAIA

Finally, the complete assembly of UIAIA is shown in Figure 2-5. A black box is used to help eliminate any variable lighting conditions due to the swinging of the cloth curtain when a particle passes underneath it. Furthermore, a small opening in the back of the box was also provided to guide the system operator to drop aggregate particles in the right location, i.e., at the centerline of the belt. Close attention was also paid to maintain a constant belt speed with no lateral wander so as to preserve the set focus and calibration.

The UIAIA operating software includes the following modules: image acquisition, aggregate volume computation, particle size determination (flat and elongated ratio and controlling sieve size), aggregate angularity index computation, and aggregate surface texture index computation. The image acquisition module primarily aids in capturing images of aggregate particles during the operation of the conveyor belt. The volume computation, particle size determination, angularity index and surface texture index determination modules perform the “image processing” tasks needed for this application.



Figure 2-5 Photograph Showing the University of Illinois Aggregate Image Analyzer

COARSE AGGREGATE SIZE AND SHAPE INDICES IN UIAIA

The imaging based indices developed in UIAIA for coarse aggregate fall into two categories: (i) particle size indices, which include maximum, intermediate and minimum dimensions of the particle, grain size distribution, and volume computation (Tutumluer et al., 2000; Rao, 2001); (ii) particle morphological or shape indices, which include the flat and elongated ratio (Rao et al., 2001), angularity index AI (Rao et al., 2002) and surface texture ST index (Rao et al., 2003). Preliminary validations of these two categories of imaging based indices were performed by successfully measuring aggregate properties and linking results to corresponding laboratory strength data (Tutumluer et al., 2000; Rao et al., 2003).

Particle Size Determination

The basic application of image analysis techniques to aggregate particle was to determine particle size and hence gradation. Wilson et al. (1996 and 1997) determined aggregate gradation by comparing the width of each particle to standard sieve sizes and estimating the sieve size it would be retained on. To

extend this gradation on the basis of weight, assumed that the square of the weight, $(W_i)^2$, was proportional to the cube of the surface area, A^3 , determined from the image analysis, i.e., $W_i \propto A^{3/2}$.

A two-dimensional image captured by a camera is simply the projection of a 3-D structure on the plane parallel to the camera lens. For quantitative volume computation, powerful tools such as stereology (Underwood, 1970; Wiebel, 1979) have been employed to convert measurements from 2-D images to 3-D values. As the measurement of volume fractions, surface areas of interfaces, mean thicknesses, and size distribution is statistically “estimated” from a random section, it fails to capture the real sense of the 3-D structure.

On the other hand, tomographic images have been widely used to reconstruct a 3-D structure from a series of 2-D images (projections) captured at predetermined depths (sections at regular intervals) of the object(s) of interest. Tomographic images can be produced using magnetic resonance, sound waves, isotope emission or X-ray scattering techniques. The resolution and the thickness adopted for each section can vary depending on the application. Typical section thicknesses are in kilometers for seismic tomography, in centimeters for medical scans, in millimeters for industrial applications, and in nanometers for reconstruction of viruses and atomic lattices. Image processing from tomographic reconstruction is perhaps the most accurate technique for measuring densities or elemental compositions of solid specimens (Russ, 1992).

A common method for 3-D reconstruction is to combine the serial sections and compute the number of cubic pixels in the objects, commonly referred to as voxels (Russ, 1992) in these applications. However, these image processing methods are very time consuming and require the use of an elaborate test setup that is not very suitable to an application involving coarse aggregate testing in sample sizes typical of pavement engineering. An aggregate image analysis system has to be equipped with the ability to perform volume computation so that a relative estimate of its weight can be obtained. The relative proportionality is used here because of the assumed uniform specific gravity of each particle in a sample. By first computing the volume of a particle, its weight can be determined knowing its specific gravity. To express results in compliance with the Superpave specifications, it would be necessary to establish the weight of each aggregate particle in the sample.

A volume computation module was developed in the UIAIA to form a vital component of the image analysis system. The benefit of having images of an individual particle from three orthogonal views in the UIAIA was best realized in computing the particle volume. The procedure essentially involved the reconstruction of a particle volume by combining the three 2-D images, the front, top, and side views. Figure 2-6 shows three orthogonal views of a particle obtained from the three cameras of the UIAIA.

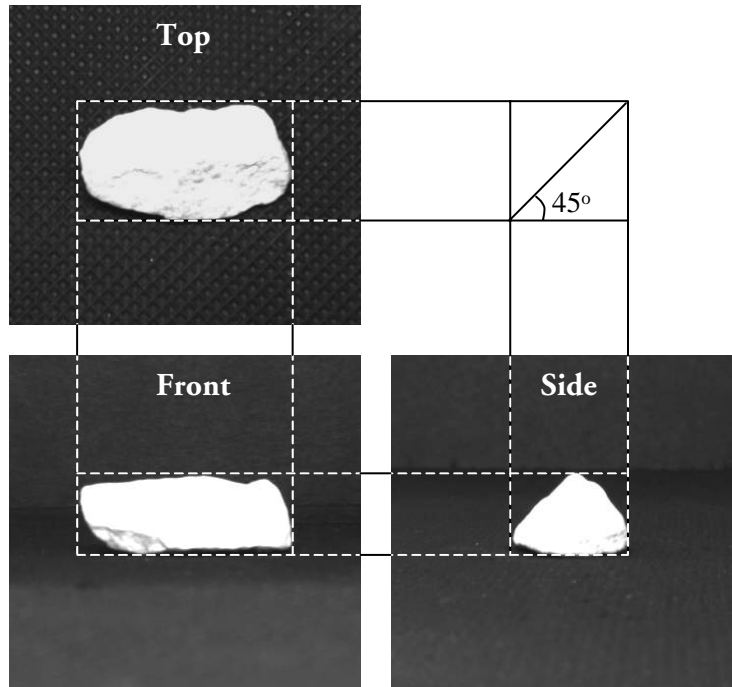


Figure 2-6 Three Orthogonal Views of a Particle Captured by the UIAIA

The image analysis approach for volume computation is based on identifying these gray scale values that belong to the particle and eliminating those that belong to the background. The procedure uses all three captured views of the particle simultaneously. The steps used in the volume computation program consist of image thresholding, converting image to an array, choosing the particle in the array subset, and determining number of solid pixel cubes.

Thresholding is one of the most widely used segmentation procedures that help extract useful information from an image. In order to recognize an object in a gray scale image, the regions that belong to the object need to be distinguished from those that belong to the background. The simplest way to identify these regions corresponding to the object is to perform a threshold operation, which essentially separates the two main regions in an image, namely the object and the background. By thresholding, a gray scale image is converted to a binary image. This binary image has only black or white (gray level 0 or 255) pixels to clearly identify the particle against its background. By thresholding, all pixels having a gray scale value larger than the threshold value are made white, i.e. assigned a value of 255. Similarly, all pixels having a value less than the threshold value are assigned a value of 0 and hence converted to black.

In applications involving routine image analysis of standard or fabricated items, the value of the threshold gray level can be held constant as the contrast of both the background and the object in the image is constant. However, as aggregates have varying colors and shades, the threshold value used should be chosen appropriate to the color of each individual particle. This is to make sure that the

threshold operation leaves the entire aggregate particle white and distinguishable from the black background. Since aggregate particles in a sample are not always of the same color, using a constant threshold value may result in incorrect thresholding. Therefore, to eliminate the subjectivity involved in choosing the right threshold value, an automatic thresholding scheme was adopted to objectively choose a threshold value befitting the color of each individual particle. In situations when the lighting conditions are not optimal, or when the particle has drastically varying shades on its surface, or when the particle is almost the same color as the background, errors in thresholding may however be inevitable.

Each image captured by the UIAIA is in a frame of 640x480 pixel resolution, i.e., it has 640 pixels in the horizontal direction and 480 in the vertical. Note that this is not the case for images shown in Figure 2-6 since these images had to be cropped for presentation purposes. The thresholded image is typically converted to a 2-D array having 480 rows and 640 columns, identical to the dimensions of the image. Each element in the array has the value of the gray level of the corresponding pixel. In essence, all elements of the array associated with the particle take the value of '255' while all the others of the background take the value of '0'. The mathematical algorithm developed for volume computation is operated upon this array from this stage forward.

Each thresholded image consists of two distinct regions, one belonging to the particle and the other belonging to the background. The particle occupies an area that is only a part of the image, as shown in Figure 2-6. This region containing the particle is of interest for image processing and hence is extracted from the array formed in the previous section. An array subset of the particle is obtained which essentially represents the smallest rectangle enclosing the particle. This is achieved by the elimination of all rows and columns in the matrix that do not contain any portion of the particle. The process is applied to all the three views and the created subset arrays are combined to determine the smallest 3-D rectangular box in which the particle can exactly fit. Figure 2-7 illustrates this mathematical operation pictorially. The use of this subset array significantly reduces the computation involved in the volume determination process.

In rare cases, due to different shades existing in the same particle or due to variation in light intensities, thresholding can result in noise in the images, i.e., visually small dots can be seen around the particle. As this can be detected early on, the array extraction is performed only for the blob having the largest area in the image. Here, the blob with the largest area is reasonably assumed to represent the particle. This process has been validated to work quite effectively.

The UIAIA operating software includes the following modules: image acquisition, aggregate volume computation, particle size determination (flat and elongated ratio and controlling sieve size), aggregate angularity index computation, and aggregate surface texture index computation. The image acquisition module primarily aids in capturing images of aggregate particles during the operation of the

conveyer belt. The volume computation, particle size determination, angularity index and surface texture index determination modules perform the “image processing” tasks needed for this application.

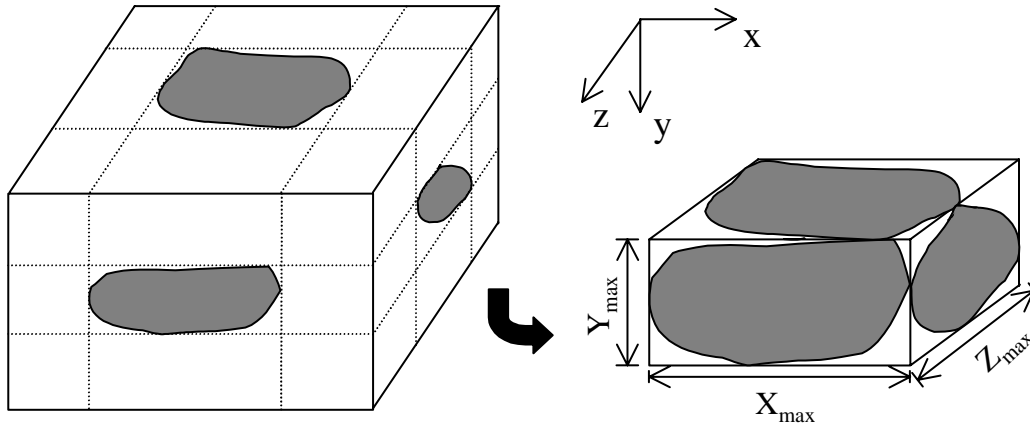


Figure 2-7 Acquiring Array Subsets for Images

In image analysis procedures, the length measurement is commonly done by counting the number of pixels that corresponds to the object. The actual length is then obtained by multiplying the pixel count by a calibration factor. The volume computation method adopted in the UIAIA employs a 3-D analogy of this measurement technique based on pixel units. The 3-D equivalent of a pixel, a cubic pixel, is termed as a voxel (Russ, 1992). A 3-D space consists of a cubic array of voxels. The main objective in volume computation is to estimate the number of voxels corresponding to the particle circumscribed in the rectangular box shown in Figure 2-7. Eliminating the portions of the rectangular box that do not contain the solid particle gives a numerical volume measurement of the aggregate particle.

The volume computation program used in the UIAIA iteratively scans over the entire 3-D space and examines if each voxel belongs to the particle from all views. For each voxel belonging to the particle, the corresponding three pixels in the x-y, y-z, and z-x planes have gray scale values of 255 (white). For this condition to be true, the corresponding element in the array extracted in the previous step must have a value of 255. The number of voxels that satisfies this condition of occupying the mass of the particle from all three directions, finally, gives the volume of the particle in units of pixel length cube. Knowing the uniform calibration factor used in three cameras, the volume can be easily converted to cubic centimeters or cubic inches. For most part of this research study, the UIAIA was adjusted for a calibration factor of $1'' = 158.6$ pixels or $1 \text{ pixel} = 0.006305''$.

Comparison of particle weights serves as a convenient method to verify and validate the volume computation technique for aggregate particles. However, in the case of Superpave coarse aggregate tests

for flat and elongated particles, gradation, and aggregate angularity, the computation of particle weights is a redundant. The ratio of volume is equivalent to the ratio of weights for a constant calibration factor and specific gravity, as is typically the case while testing an aggregate sample. This is to say, the percentage particles by weight satisfying a given test criteria is equivalent to the percentage of particles by volume satisfying the same criteria if the volume computation is accurate. The UIAIA hence uses the percent of particles by volume to obtain the gradation and flat and elongated ratio of results.

With all the necessary knowledge introduced in the determination of the volume, it is comparatively simple to define the “maximum”, “minimum”, and “intermediate” dimensions of an aggregate particle. Figure 2-7 shows the smallest rectangular box that can contain the front, top, and side projections of an aggregate particle obtained from the three cameras of the UIAIA system. The maximum dimension is defined as the longest size of the particle from all three views, which corresponds to the longest side of the rectangular box shown in Figure 2-7. The definition of the minimum and intermediate dimensions are somewhat linked to the position of the maximum dimension. When the position of the maximum dimension is determined, the minimum dimension is found as the smaller of the two perpendicular intercepts of the particle that is located in the direction perpendicular to the maximum dimension. The minimum dimension corresponds to the shortest side or height of the rectangular box shown in Figure 2-7. The intermediate dimension is also found as the bigger of the two perpendicular intercepts located in the direction perpendicular to the maximum dimension. The intermediate dimension corresponds to the width of the rectangular box shown in Figure 2-7.

Particle Morphology Determination

The coarse aggregate particle morphological indices used in the UIAIA imaging system include the Flat and Elongated Ratio (F&E Ratio), Angularity Index (AI) and Surface Texture (ST) Index. These three indices were developed to represent the three key morphological descriptors of coarse aggregate materials as the shape or form, angularity and surface texture as shown in Figure 2-8. Each one of them characterizes a different aggregate morphological property at a different magnification linked to overall aggregate performances in unbound and hot mix asphalt applications. The UIAIA image analysis modules, each developed individually as a Labview Virtual Instrument (VI) with a set of unique algorithms, are executed through the Labview IMAQ Vision analysis software to determine these three key shape indices. A description of each imaging based shape index is given in the following paragraphs.

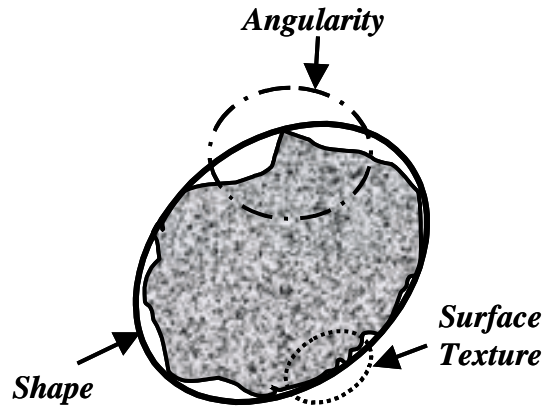


Figure 2-8 Three Key Morphological Descriptors of Coarse Aggregate Particles

Flat and Elongated Ratio

The SHRP Superpave program allows no more than 10% by weight particles having an aspect ratio greater than 5:1 for the aggregate blend used in asphalt pavements having greater than 3 million equivalent single axle loads in the design life. Because flat and elongated particles have a tendency to break during construction and under traffic loads cubical and angular particles are preferred. The flat and elongated (F&E) ratio is defined as the ratio of the longest dimension of the particle to its minimum dimension. In the standard manual test procedure, a proportional caliper is used to determine the maximum to minimum dimensional aspect ratios as 2:1, 3:1, and 5:1 (ASTM D 4791-99). The minimum dimension is often measured in a direction that is considered perpendicular to the longest dimension based on the operator's visual judgment.

In analyzing the UIAIA captured images, a similar approach was adopted for determining the longest and the shortest dimensions from the image (see Equation 2-1). The particle is analyzed for the longest dimension and the shortest dimension, which is perpendicular to the longest dimension, from each view of the 3-camera front, top, and side images. Also discussed by Rao et al. (2001), the ratio of the longest dimension to the shortest finally gives the desired F&E ratio as illustrated in Figure 2-9.

$$F \ \& \ E \ Ratio = \frac{Longest \ Dimension}{Shortest \ Perpendicular \ Dimension} \quad (2-1)$$

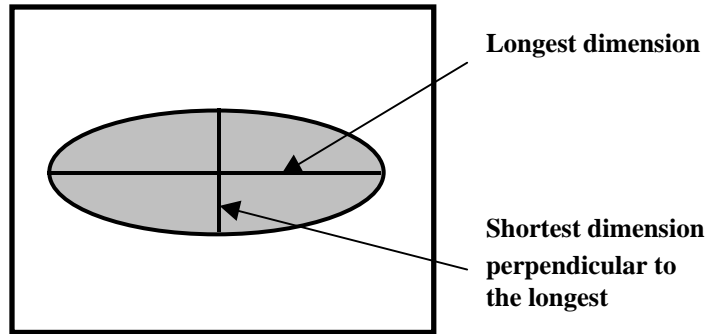


Figure 2-9 Illustration of the Longest and Shortest Perpendicular Dimensions

Angularity Index (AI)

Presently, coarse aggregate angularity is determined manually by counting the number of fractured faces on an aggregate particle (ASTM D 5821-95). Coarse aggregate angularity, in turn, controls the level of internal shear resistance that can be developed in a particulate medium. A required percentage by weight of crushed particles is determined based on projected traffic level and the depth of the pavement layer.

A quantitative “Angularity Index” (AI) is developed based on image analysis from the images captured by the UIAIA (Rao et al., 2002). The new AI methodology is based on tracing the change in slope of the particle image outline obtained from each of the top, side and front images. Accordingly, the AI procedure first determines an angularity index value for each 2-D image. Then, a final AI is established for the particle by taking a weighted average of its angularity determined for all three views.

To determine angularity for each 2-D projection, an image outline, based on aggregate camera view projection, and its coordinates are extracted first. Next, the outline is approximated by an n -sided polygon as shown in Figure 2-10. The angle subtended at each vertex of the polygon is then computed. Relative change in slope of the n sides of the polygon is subsequently estimated by computing the change in angle (β) at each vertex with respect to the angle in the preceding vertex. The frequency distribution of the changes in the vertex angles is established in 10-degree class intervals. The number of occurrences in a certain interval and the magnitude are then related to the angularity of the particle profile.

Equation 2-2 is used for calculating angularity of each projected image. In this equation, e is the starting angle value for each 10-degree class interval and $P(e)$ is the probability that change in angle β and has a value in the range e to $(e+10)$.

$$\text{Angularity, } A = \sum_{e=0}^{170} e * P(e) \quad (2-2)$$

The “Angularity Index” (AI) of a particle is then determined by averaging the Angularity values (see Equation 2-2) calculated from all three views when weighted by their areas as given in the following equation:

$$AI = \frac{\sum_{i=1}^3 \text{Angularity}(i) * \text{Area}(i)}{\sum_{i=1}^3 \text{Area}(i)} \quad (2-3)$$

where, i takes values from 1 to 3 for top, front, and side orthogonal views. The final AI value for the entire sample is simply an average of the Angularity values of all the particles weighted by the particle weight, which measures overall degree changes on the boundary of a particle.

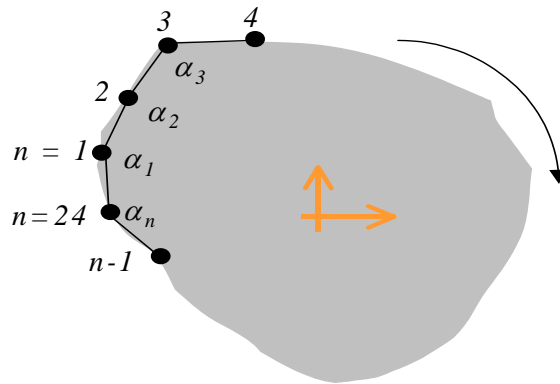


Figure 2-10 Illustration of An n-sided Polygon Approximating the Outline of a Particle

Surface of Texture (ST) Index

Coarse aggregate surface texture has been known to affect mix properties of both asphalt concrete and Portland cement concrete pavement surface courses. The current standard manual test procedures ASTM C1252-03 and ASTM D3398-00 do not make any objective measurements of surface texture but instead provide an indirect estimation of surface profile roughness or irregularity at both a macro and micro level combined. Whereas, digital imaging techniques offer a direct and objective measurement of surface irregularities or surface texture from images of aggregate particles to quantitatively determine various

roughness (or smoothness) levels. A methodology to determine surface texture can best be accomplished by defining a quantifiable index using representative aggregate samples with varying levels of texture characteristics, rough to smooth.

In the UIAIA system, the image analysis technique known as “erosion and dilation” is used to determine Surface Texture (ST) of an aggregate particle (Rao et al., 2003). Erosion of certain structuring-elements is a morphological process by which boundary image pixels are removed from an object surface leaving the object less dense along the perimeter or outer boundary. Dilation of the same structuring-elements is the reverse process of erosion and a single dilation cycle increases the particle shape or image dimension by the same pixels around its boundary. Erosion cycles followed by the same number of dilation cycles tend to smooth the surface of a particle by losing shape peaks and patching sharp dents on the boundary. In essence, the image area difference before and after erosion and dilation cycles of the same number of cycles is directly related to the surface micro-irregularities, which leads to the definition of the ST for one of the three particle projection images (see Equation 2-4).

$$ST = \frac{A_1 - A_2}{A_1} * 100 \quad (2-4)$$

where:

ST = Surface texture parameter for each image;

A_1 = Area (in pixels) of the 2-D projection of the particle in the image;

A_2 = Area (in pixels) of the particle after performing a sequence of “ n ” cycles of erosion followed by “ n ” cycles of dilation.

Similar to the definition of the AI, the image analysis procedure first provides an ST value for each of the three images obtained from three orthogonal views. Next, an ST index, denoted as $ST_{particle}$, is established for the particle by taking a weighted average of each ST determined from all three views.

To set up a ST index independent of particle size, the optimum number of cycles of erosion and dilation, n , to be applied can be obtained as follows:

$$n = L/\beta \quad (2-5)$$

where:

L = Longest or maximum intercept of a particle in image;
 β = Scaling factor for erosion and dilation operations.

The optimal n value is determined at which $ST_{particle}$ of a set of smooth-surfaced coarse aggregate is recognized as significantly separated from the $ST_{particle}$ of a set of rough-surfaced aggregate. The change of the surface texture of a crushed aggregate particle before and after the optimum of erosion and dilation cycles is shown in Figure 2-11.

The final aggregate surface texture, $ST_{particle}$, which measures overall degree surface irregularities of a particle, is computed as the weighted average of each ST determined from all three views as follows:

$$ST_{particle} = \frac{\sum_{i=1}^3 ST(i) * Area(i)}{\sum_{i=1}^3 Area(i)} \quad (2-6)$$

where i takes values from 1 to 3 for top, front, and side views.

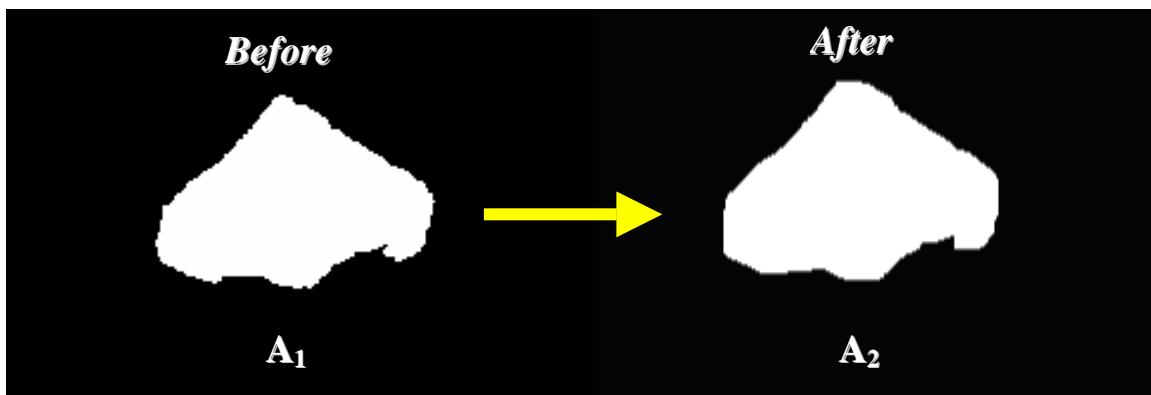


Figure 2-11 Change of an Aggregate Particle Surface Texture Before and After the Application of Optimum Cycles of Erosion and Dilation

The UIAIA imaging based shape or morphological indices, F&E Ratio, Angularity Index (AI), and Surface Texture (ST) Index, have all been validated in several research projects at the University of Illinois by the use of a variety of coarse aggregate sources and types ranging from cubical, angular, rough to flat and elongated, rounded, smooth aggregates that provided satisfactory results from all UIAIA tests.

SUMMARY

This chapter summarizes the research efforts made in developing the 3-dimensional (3-D) image analysis system, the University of Illinois Aggregate Image Analyzer (UIAIA). The need for 3-D particle shape reconstruction and the basic image analysis concepts were first discussed briefly. The physical components, image acquisition software, and operation procedure of the UIAIA system were described in detail next. The imaging based indices for coarse aggregate size and shape evaluation in UIAIA were classified into two groups and discussed accordingly. The first group was on particle size determination, which dealt with particle volume computation, and determination of maximum, intermediate and minimum dimensions of the particle. The second group briefly summarized particle morphological or, shape indices covering the three key morphological properties, i.e., shape or form defined with the imaging based flat and elongated ratio, angularity defined with the imaging based angularity index AI , and finally, the UIAIA imaging based surface texture ST index for quantifying coarse aggregate surface roughness.

CHAPTER 3

MATERIALS AND IMAGING BASED INDICES

The UIAIA developed as an imaging system with the capabilities and merits presented in Chapter 2 can possibly replace four of the standard coarse aggregate shape test procedures, i.e., ASTM D4791, ASTM D5821, ASTM D3398, AASHTO TP56. A future production device developed based on the UIAIA and its routine use in the State DOT material testing laboratories is anticipated to provide a significant cost savings to be realized in materials testing. To further validate the UIAIA system and demonstrate its practical applicability in aggregate size and shape determination, the FHWA DTFH61-02-X-00029 pooled fund study partners, i.e., the National Center for Asphalt Technology (NCAT), the state highway agencies of Alabama, Georgia, Indiana, Minnesota, Mississippi, Missouri, Montana, and South Carolina, and the FHWA Central Federal Lands and Highways Division, shipped aggregate materials with a broader range of shape irregularities to the Civil and Environmental Engineering Department at the University of Illinois. The coarse aggregate materials were then processed using the UIAIA system to establish a database of aggregate size and shape indices from image analysis. This chapter summarizes these indicial properties obtained from the UIAIA analysis to set up a property database of aggregate materials with a broader range of shape irregularities and additionally documents all the required amounts of asphalt binder, fine aggregate, and mineral filler also received for making the laboratory HMA mixes. In the subsequent chapters, the imaging based indices will be related to resilient modulus and permanent deformation characteristics of the HMA mixes in an effort to investigate the effects of shape and size properties on the Superpave asphalt mix performances and to help future design and maintenance of asphalt pavements.

MATERIAL ACQUISITION

The pooled fund study aggregate materials were shipped to the Advanced Transportation Research and Engineering Laboratory (ATREL) at the University of Illinois in two different sets during the project. The first set of 36 different aggregate materials arrived first from the National Center for Asphalt Technology (NCAT) Pavement Test Track Facility in Auburn, Alabama as summarized in Table 3-1. These and other aggregate samples originally collected from the NCAT study sponsoring states were used to make HMA surfaces constructed and tested in 46 different flexible pavement test sections installed at the NCAT Facility, each at a length of 200 feet (61 meters). The NCAT aggregates potentially provided

an ideal range of materials possessing broad shape varieties in terms of different levels of surface irregularities. Accordingly, they were quite suitable in this study to: (i) further validate the size and shape indices defined in UIAIA for quantifying three-dimensional shape, size, angularity, and surface texture properties of aggregate materials and (ii) investigate how these coarse aggregate materials would affect the field rutting performances of the NCAT asphalt pavement test sections.

Table 3-1 Aggregate Materials Received from the NCAT Pavement Test Track Field Evaluation Study

SOURCE	AGGREGATE MATERIAL	TYPE
Alabama	<i>Calera 67</i>	Limestone
	<i>Calera 7</i>	Limestone
	Calera 821	Limestone
	Calera 822	Limestone
	<i>Calera 89</i>	Limestone
	Calera 892	Limestone
	<i>Jemison 1/2 Crushed gravel</i>	Gravel
	<i>Jemison 3/8 crushed gravel</i>	Gravel
	Jemison Concrete sand	Sand
	<i>Summit sandstone 8</i>	Sandstone
	Summit sandstone sand	Sand
	<i>Gadsden slag 78</i>	Slag
	Gadsden slag 8910	Slag
Indiana	Indiana 1	Limestone
Georgia	<i>Columbus 6</i>	Granite
	<i>Columbus 7</i>	Granite
	Columbus 89	Granite
	Columbus M10	Granite
	Columbus W10	Granite
	<i>Lithia springs 7</i>	Granite
	Lithia springs 89	Granite
Mississippi	<i>Blain 1/2 crushed gravel</i>	Gravel
	<i>Blain 3/4 crushed gravel</i>	Gravel
	Blain coarse sand	Sand
	Blain 3/8 crushed gravel	Gravel
	Falco agricultural lime	Limestone
South Carolina	Blacksburg regular screens	Granite
	<i>Blacksburg 67</i>	Granite
	<i>Blacksburg 78M</i>	Granite
	Blacksburg manufactured sand	Sand
	Gray court #10 manufactured sand	Sand
	<i>Gray court 6M</i>	Granite
	Gray court 789	Granite
	Gray court regular screenings	Granite
Tennessee	<i>Gilbertville 57</i>	Limestone
	<i>Gordonville 78</i>	Limestone

The NCAT aggregate materials included both coarse and fine aggregate samples. The coarse aggregate materials highlighted in bold in Table 3-1 were those selected for image analysis, which constituted the most commonly used crushed aggregate types in the paving industry, i.e., limestone, gravel, sandstone, and granite. These NCAT aggregates were light colored and also came with a broad range of shape irregularities in terms of angularity and surface texture to establish an ideal means to test the validity of the UIAIA imaging system. Moreover, the diversity of the NCAT coarse aggregate samples in terms of shape irregularities and their effects on HMA behavior could possibly be more easily singled out among many other factors in comparing rutting performances of the NCAT test sections.

The second set of project materials were requested from each study partner other than NCAT and consisted of three types of coarse aggregate materials, greater than 4.75 mm (No. 4 sieve) in size and preferably with a top size of 25 to 37 mm (1 to 1.5 inches): (1) 100% crushed, (2) uncrushed gravel, and (3) partially crushed (possibly a blend of the 100% crushed and uncrushed) aggregates. They had to be light colored since dark aggregate could not be easily processed via imaging using the UIAIA system. For all three aggregate materials, crushed, partially crushed, and uncrushed if at all used as coarse aggregate in HMA making in that State, the following were also requested from the study partner: (1) the required amounts of asphalt binder, fine aggregate, and mineral filler to be used for making in the laboratory the HMA mix designs that are representative of those typically constructed in that State and (2) the job mix formulas used in the asphalt mix designs.

The second set of aggregate materials arrived at ATREL during and after the UIAIA data acquisition and image processing of the NCAT aggregate materials in the project. As summarized in Table 3-2, these aggregate and additional asphalt binders came from the study partners that participated in the FHWA pooled fund project DTFH61-02-X-00029. These were the state highway agencies of Alabama, Georgia, Indiana, Minnesota, Mississippi, Missouri, Montana, and South Carolina. The FHWA Central Federal Lands and Highways Division also provided materials from the states of New Mexico and Oklahoma as listed in Table 3-2. Table 3-2 also summarizes the number of asphalt mixes and mix designs received from each state. The participating state coarse aggregate materials were actually used in field constructed asphalt pavements by the individual state highway agencies. Having received the job mix formulas and the component materials that were used in designing the asphalt mixes of these pavements, the approach in the project was to produce laboratory Superpave asphalt mix specimens using the same designs and subsequently to test them for modulus, strength, and resistance to permanent deformation for investigating the effects of coarse aggregate shape properties on the mechanical responses of hot mix asphalt in a controlled way. Since this set of coarse aggregates came from the different states and sources and therefore possessed a broad range of irregularities at different morphology levels they could be used to verify the capability of the UIAIA system in characterizing the shape properties.

Table 3-2 Aggregates and Binders Received from the Participating Pooled Fund Partners

STATE No.	MATERIALS RECEIVED & SOURCES	No. of MIXES
1	Central Federal Lands and Highways (New Mexico)	1 mix
	7/8" Rock	
	Coarse Aggregate	
	Intermediate Aggregate	
	Hydrated Lime	
	Crushed Fines	
2	Central Federal Lands and Highways (Oklahoma)	1 mix
	1" Rock	
	1/2" Rock	
	Screenings	
	Stone Sand	
	Sand	
3	Minnesota	2 mixes
	<i>Maple Grove Mix</i>	
	Meridian St. Cloud 3/4" Unwashed Sand	
	Meridian St. Cloud CA-50	
	Meridian St. Cloud FA-3	
	Barton Elk River #1 Washed Sand	
	Kraemer Burnsville Washed Sand	
	Meridian Washed Sand, <u>Mn-DOT PG64-22</u>	
	<i>Red Rock Mix</i>	
	Barton Denmark BA-2	
	Kraemer Burnsville 9/16" Chip	
	Kraemer Burnsville Class 2	
	Camas "Shiely" West Lakeland Washed Sand	
Camas Nelson Man. Sand (Class D)		
<u>Mn-DOT PG58-28</u>		
4	Mississippi	2 mixes
	<i>Dickerson Bowen Madison Mix</i>	
	Crushed Gravel (4 bags), -1" and -0.5"	
	Crushed Limestone (2 bags) #11 , *#78 LST	
	Agricultural Limestone	
	Hydrated Lime	
	Coarse Sand	
	<u>Asphalt Binder PG67-22</u>	
	<i>Jackson County Mix</i>	
	#7 Granite, #89 Granite	
	1/4 in. Granite Screens	
	Coarse Sand, Hydrated Lime	
<u>Asphalt Binder PG67-22</u>		

Table 3-2 Aggregates and Binders Received from the Participating Pooled Fund Partners (continued)

STATE No.	MATERIALS RECEIVED & SOURCES	No. of MIXES
5	Missouri	3 mixes
	<i>Brickey's Mix</i> Brickeys 1", *Brickeys 1/2" Brickeys 3/4", * Brickeys 3/8" Tower Rock Stone Man Sand PG 70-22 Asphalt Binder <i>Burlington Mix</i> 1/2" Joorn. J.H. Q. B. 3/4" Joornagan J.H. Q. 1/2" Joorn. J.H. Q. R. 1/2" Base, PG 64-22 Asphalt Binder <i>Clean Mix</i> 1 1/2" Clean Stone 1/2" Clean Stone 3/4" Clean Stone LOF Man. Sand MOR Life TRSG Man. Sand Screenings PG 64-22 Asphalt Binder	
6	South Carolina	3 mixes
	Blacksburg 67 (NCAT) Blacksburg 78M (NCAT) Gray Court 6M (NCAT) Gray Court 789 Marlboro 67 Marlboro 789 Blacksburg Man. Sand Blacksburg Regular Screening Gray Court Regular Screenings Binders for the 3 designs, PG76-2 (2), PG67-22	
7	Georgia	3 mixes
	Georgia M10 Lithia Springs Georgia 89 M10 W10 Lime (binder) Fine aggregate liquid AC lime (binder) Binders for the 3 designs, PG67-2 (2), PG76-22	

Table 3-2 Aggregates and Binders Received from the Participating Pooled Fund Partners (continued)

8	Indiana	2 mixes
	#23 Natural Sand, Interstate Sand & Gravel, Williamsport (2164)	
	QAFM-01 stone sand Newton County Stone, Kentland (2445)	
	#11 Gravel Cowles Sand & Gravel, Williamsport (2164)	
	<u>Asphalt Binders for both designs, PG64-22</u>	
	#23 Natural Sand Cowles Sand & Gravel, Kewanna (2432)	
	QA # 12 stone Vulcan Materials, Francisville (2461)	
	#11 Gravel Cowles Sand & Gravel, Kewanna (2432)	
9	Alabama	NCAT mixes
	Calera 7 (NCAT)	
	Calera 89 (NCAT)	
	Columbus 7 Granite 7 (NCAT)	
	Jemison 1/2 crushed gravel (NCAT)	
	Jemison 3/8 crushed gravel	
	Summit sandstone 8 (NCAT)	
	Calera 821	
	Calera 892	
	Columbus 89 Granite 89	
	Columbus M10 granite M10	
	Columbus W10 Granite W10	
	Jemison concrete sand natural sand	
	Summit sandstone sand	
10	Montana	2 mixes
	Crushed Fines	
	Washed Crushed Fines	
	3/8 Inch Chips	
	Coarse Aggregate 1	
	Fines	
	Intermediate Aggregate	
	Coarse Aggregate 2	
	<u>Binders of both designs, PG58-28, PG70-28</u>	

As listed in Table 3-2, the designations of the aggregates and binders received from the participating state highway agencies established a complete set of materials for making the laboratory asphalt mixes following the job mix formulas. The detailed aggregate gradations, percent aggregate blends, asphalt binder and air voids information, and mixing and compaction temperatures are given in

Appendix I for each laboratory asphalt mix design summarized from the corresponding state highway agency job mix formula sheet. The aggregate samples highlighted in bold in Table 3-2 are the selected light colored coarse aggregate materials for the UIAIA data acquisition and image processing. Similar to the NCAT coarse aggregate materials selected for image analysis, the selected participating state coarse aggregate materials also included the most commonly used crushed aggregate types in the paving industry, i.e., limestone, gravel, sandstone, granite. No State used uncrushed aggregates only in their asphalt mixes. The selected coarse aggregate materials again possessed a broad range of shape irregularities in terms of angularity and surface texture, which made them eligible in validating the UIAIA system and investigating the effects of shape properties on the modulus, stability, and permanent deformation behavior of the laboratory asphalt mix specimens.

IMAGING RESULTS OF NCAT AGGREGATES

As highlighted in bold in Table 3-1, 17 coarse aggregate (retained on No.4 square opening sieve) samples from the NCAT were selected as representatives for testing and image processing with the UIAIA system. Depending on the average sizes and gradation results, anywhere from 300 to 2500 particles were selected for testing to establish a representative bag sample for each material having statistically sufficient particles. For materials having mainly smaller particles, a larger number of particles was typically needed to have anywhere from half a kilogram to 2 kilograms of aggregate by weight. Each aggregate sample was processed through the UIAIA system at least twice to verify the repeatability of the results. Only two of the samples had slightly darker particles, which could not be properly detected by the cameras and had to be removed for image processing purposes. In total, images of approximately 15,000 particles from 17 samples were acquired and properly documented for image processing to obtain their shape indices.

The imaging based morphology analyses were next conducted on the NCAT aggregate materials using the UIAIA image processing modules. The analyses of shape indices were first completed for the volume and weight (using specific gravities), gradation, flat and elongated ratio, and angularity index imaging based indices. The remaining surface texture analyses of the NCAT aggregates were performed after the modification and final development of the imaging based surface texture (ST) index outlined in Chapter 2. In summary, the automated UIAIA procedure produced imaging based shape indices for the following coarse aggregate properties: (i) maximum, intermediate, and minimum dimensions, (ii) flat and elongated ratio; (iii) volume and knowing its specific gravity, therefore, its weight; (iv) a computed Angularity Index (AI) to indicate how many crushed faces are there or how rounded or angular the particle is; and finally, (v) a computed Surface Texture Index to indicate how smooth or rough the aggregate surface is. Having the intermediate dimension for each particle, the particle size distribution,

i.e., gradation, for each aggregate sample bag was also accurately determined based on imaging. All the 17 aggregate samples were processed using the UIAIA for determining size and shape indices from image analysis. Accuracy, repeatability, and significance of the imaging results were evaluated by comparing with the measured and further by analyzing using statistical techniques.

Weight Computation

Most standard tests developed to determine the coarse aggregate properties require test results to be expressed as percent by weight of the materials satisfying a given test criterion. For example, no more than 10% by weight of the flat and elongated (F&E) particles with ratios greater than 5 to 1 (5:1) is allowed by Superpave for asphalt pavements having greater than three million equivalent single axle loads in their design lives. Also, for determining aggregate angularity, the ASTM D5821 procedure adopted by Superpave requires that the percent crushed particles by weight not exceed a specified limit. With the ability to compute the total particle volume in a sample, the UIAIA system can easily determine the total weight using a known bulk specific gravity, G_{sb} , in accordance with the Superpave criteria.

To verify the accuracy of the imaging based volume computation, the actual weights and bulk specific gravities G_{sb} of aggregate bag samples were measured manually in the laboratory. Table 3-3 compares for each bag sample the imaging based weights with the manual measurements. The typical percent errors of all the coarse aggregate samples were within 9% with an average absolute error of 4.77% for all the samples. When these weights were used in the F&E computation, the imaging based weights proved to be satisfactory for the analysis of NCAT aggregate materials. These error percentages are directly affected by the image pixel quality or the resolution and the uniformity in the type and mineralogical composition of the aggregate particles assigned with the laboratory measured average G_{sb} value. Therefore, the low overall average error of 4.77% in weight determination demonstrates that the volume computation approach adopted in the UIAIA system can reasonably estimate individual aggregate particle volume and weight from image analysis.

Gradation Analysis

Aggregate gradation is critical to achieve good packing and target air voids in asphalt mixtures. Imaging based gradation analysis is accomplished by the use of the intermediate dimension of the aggregate particles. In ASTM D136-96a, the diagonal length of the sieve opening is usually the dimension that controls the passing or retaining of a particle. The intermediate dimension obtained from image analysis controls the sieve size on which the particle is retained because perpendicular dimensions that are bigger than the diagonal length of the sieve opening cannot pass through a sieve opening. Therefore, if two

orthogonal (intermediate and maximum) dimensions of an aggregate particle are greater than the diagonal length of a given sieve size, then the particle is retained on that sieve.

Table 3-3 UIAIA Imaging Based Weight Predictions for the NCAT Aggregate Samples

Aggregate Sample	Specific Gravity	Actual Weight (g)	UIAIA Weight (g)	% Error
Blacksburg 67	2.747	1176.1	1177.585	+0.13%
Blacksburg 78M	2.690	535.03	508.54	-4.95%
Blain 1/2 crushed gravel	2.429	1278	1364.58	+6.77%
Blain 3/4 crushed gravel	2.442	1513.9	1514.53	+0.04%
Calera 67	2.690	1868.4	1840.17	-1.51%
Calera 7	2.752	1237.7	1343.56	+8.55%
Calera 89	2.709	295.5	318.9	+7.90%
Columbus 6	2.670	1937.9	1799.91	-7.12%
Columbus 7	2.611	1354.5	1308.77	-3.38%
Gadsden slag 78	2.270	982.1	1033.51	+5.23%
Gilbertsville 57	2.651	1602.1	1579.44	-1.41%
Gordonville 78	2.735	1711.2	1860.75	+8.74%
Gray Court 6M	2.622	1614.6	1590.26	-1.51%
Jemison 1/2 Crushed gravel	2.548	986.3	1037.2	+5.16%
Jemison 3/8 crushed gravel	2.546	986.4	1037.7	+5.20%
Lithia Springs 7	2.558	1774.3	1872.35	+5.53%
Summit sandstone 8	2.435	1078.4	1163.68	+7.91%
Average Absolute Error (%)				4.77%

To verify the accuracy and repeatability of the imaging based determination of the particle size distributions, gradation curves of aggregate bag samples were drawn in the laboratory following the sieve analysis procedure specified in ASTM D136-96a. Each aggregate sample was processed twice in sieve shaking to confirm the accuracy of the gradation data and to adequately check the validity and repeatability of the imaging based results. In general, the gradation curves matched exactly with the sieve shaking results. Due to the size limitation of this chapter, comparison of the imaging based gradation curves and the manually measured ones of all the NCAT aggregate samples are presented in Appendix II of this report. Here, only an example chart is shown in Figure 3-1, which presents the accuracy and repeatability of gradation analyses of the aggregate sample Blacksburg 67. For all the coarse aggregate samples, the imaging based gradation curves agreed very well with the distributions from the sieve analysis. This agreement actually not only validates the accuracy with which the UIAIA system measures the intermediate sizes or dimensions of the NCAT coarse aggregate materials, it also proves the feasibility of using the intermediate dimensions to determine the imaging based gradation as compared to the manual sieve analysis.

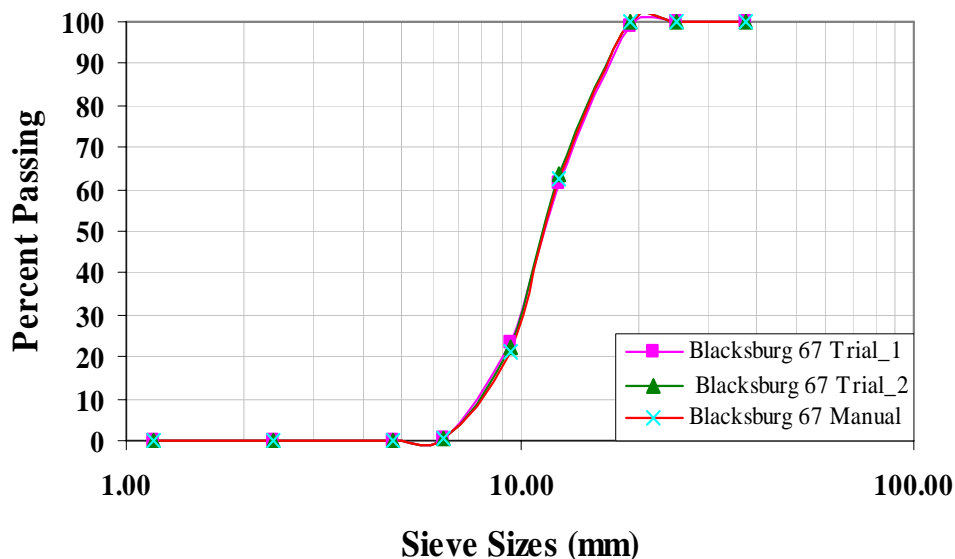


Figure 3-1 UIAIA Imaging Based Particle Size Distributions for the Blacksburg 67 Sample

Flat and Elongated Ratio

Table 3-4 presents repeatability results of the imaging based F&E ratios, two trials for each of the following three categories: less than 3 to 1 (<3:1), between 3 to 1 and 5 to 1 (3:1 to 5:1), and greater than 5 to 1 (>5:1). The predictions from two trials of each NCAT aggregate sample are listed in Table 3-4 as percent by (imaging based) weight. Flat and elongated particles by proportion of the NCAT coarse aggregate materials were found conforming to the Superpave criteria in that none of these coarse aggregate samples has flat and elongated particles exceeding 10% by weight of greater than 5 to 1 (>5:1). Since the F&E ratio is defined as the ratio of the maximum to minimum dimensions, generally repeatable F&E ratio predictions also verified the UIAIA imaging based approach and the analysis procedures for determining the maximum and minimum coarse aggregate dimensions.

Angularity and Surface Texture

To evaluate the accuracy and repeatability of using UIAIA to measure coarse aggregate angularity, the Angularity Index (AI) analyses described in Chapter 2 were conducted on all the NCAT coarse aggregate samples. Table 3-5 presents repeatability results of the imaging based Angularity analysis by the UIAIA imaging system. Due to the size limitation of this chapter, comparisons of the two trial imaging based AI results of each NCAT aggregate sample with the AI of a standard uncrushed gravel sample and a standard crushed limestone sample are presented in Appendix II of this report. Here, only an example chart is shown in Figure 3-2, which presents the repeatability of angularity analyses of the aggregate sample

Blacksburg 67. A similarity can be observed between the AI distributions of the two trials for Blacksburg 67 and all other NCAT aggregate samples, which further demonstrates the repeatability of using UIAIA in characterizing angularity property of coarse aggregate particles.

Table 3-4 UIAIA Flat and Elongated (F&E) Ratio Results for the NCAT Aggregate Samples

Aggregate Sample	No. of Particles	Trial 1			Trial 2		
		Flat and Elongated Ratio			Flat and Elongated Ratio		
		<3:1	3:1-5:1	>5:1	<3:1	3:1-5:1	>5:1
Blacksburg 67	497	66.1%	30.5%	3.3%	73.0%	25.3%	1.8%
Blacksburg 78M	1030	82.8%	16.7%	0.5%	80.6%	18.5%	0.9%
Blain 1/2 crushed gravel	1404	96.5%	3.5%	0.0%	95.5%	4.5%	0.0%
Blain 3/4 crushed gravel	814	95.9%	4.1%	0.0%	95.6%	4.4%	0.0%
Calera 67	539	90.5%	9.2%	0.2%	87.7%	12.0%	0.2%
Calera 7	1593	84.5%	15.2%	0.4%	86.3%	13.5%	0.2%
Calera 89	600	84.50%	15.00%	0.50%	85.80%	13.70%	0.50%
Columbus 6	306	87.4%	12.5%	0.1%	88.2%	11.8%	0.0%
Columbus 7	1098	88.4%	11.5%	0.1%	88.0%	11.9%	0.1%
Gadsden slag 78	1390	99.0%	1.0%	0.0%	99.4%	0.6%	0.0%
Gilbertsville 57	363	75.6%	22.9%	1.5%	77.2%	21.8%	1.0%
Gordonville 78	1670	91.0%	8.8%	0.3%	90.3%	9.3%	0.4%
Gray Court 6M	344	86.9%	12.7%	0.4%	85.3%	14.2%	0.5%
Jemison 1/2 crushed gravel	1809	92.80%	6.80%	0.40%	92.60%	7.00%	0.50%
Jemison 3/8 crushed gravel	1843	92.40%	7.40%	0.20%	92.60%	7.20%	0.20%
Lithia Springs 7	1199	93.9%	6.1%	0.0%	92.5%	7.5%	0.0%
Summit Sandstone 8	2480	96.4%	3.4%	0.1%	96.5%	3.4%	0.1%

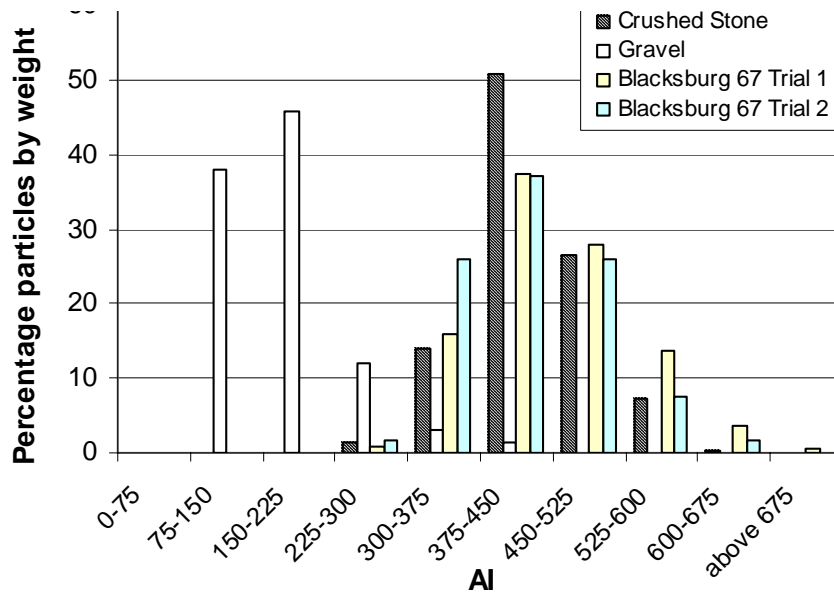


Figure 3-2 Imaging Based Angularity Index (AI) Repeatability Analysis of the Blacksburg 67 Sample

Table 3-5 UIAIA Imaging Based Angularity Indices (AI) of NCAT Aggregate Samples

Aggregate Sample	Trial 1		Trial 2	
	AI - mean	Std Dev	AI - mean	Std Dev
Blacksburg 67	441	82	418	70
Blacksburg 78M	439	73	436	76
Blain 1/2 crushed gravel	400	78	396	76
Blain 3/4 crushed gravel	405	85	407	87
Calera 67	392	70	395	69
Calera 7	393	65	395	66
Calera 89	446	66	440	74
Columbus 6	453	86	459	97
Columbus 7	515	97	523	89
Gadsden slag 78	477	86	473	88
Gilbertsville 57	415	71	405	76
Gordonville 78	477	86	473	88
Gray Court 6M	476	81	472	83
Jemison 1/2 crushed gravel	380	78	362	82
Jemison 3/8 crushed gravel	375	84	371	88
Lithia Springs 7	432	72	428	73
Summit Sandstone 8	419	69	413	73

To evaluate the accuracy and repeatability of using UIAIA to measure coarse aggregate angularity, the Surface Texture (ST) index analyses described in Chapter 2 were conducted on all the NCAT coarse aggregate samples. Table 3-6 presents repeatability results of the imaging based Surface Texture analysis by the UIAIA imaging system. Here, only the ST index distribution of Blacksburg 67 is shown as an example in Figure 3-3. Due to the size limitation of this chapter, comparisons of the two trial imaging based ST index results of the NCAT aggregate samples are presented in Appendix II of this report. The similarity between the ST index distributions of the two trials for each NCAT aggregate sample once again demonstrates the repeatable results obtained for characterizing surface texture property of coarse aggregate particles. Therefore, the mean values of the imaging based AI and surface texture (ST) indices given in Tables 3-5 and 3-6 show reasonably good repeatability for all the NCAT coarse aggregate samples evaluated by the UIAIA imaging system.

Table 3-6 UIAIA Imaging Based Surface Texture (ST) Indices of NCAT Aggregate Samples

Aggregate Sample	Trial 1		Trial 2	
	ST - mean	Std Dev	ST- mean	Std Dev
Blacksburg 67	2.45	1.75	1.94	1.37
Blacksburg 78M	1.74	1.41	1.66	1.28
Blain 1/2 crushed gravel	1.15	0.59	1.11	0.53
Blain 3/4 crushed gravel	1.33	0.79	1.28	0.75
Calera 67	1.29	0.67	1.29	0.67
Calera 7	1.19	0.61	1.23	0.73
Calera 89	1.14	0.90	1.15	0.87
Columbus 6	2.14	1.55	2.19	1.88
Columbus 7	1.94	1.34	1.87	1.24
Gadsden slag 78	1.41	0.65	1.44	1.34
Gilbertsville 57	1.59	0.89	1.60	1.19
Gordonville 78	1.46	1.06	1.36	0.95
Gray Court 6M	2.27	1.77	2.13	1.54
Jemison 1/2 crushed gravel	1.09	0.70	1.10	0.88
Jemison 3/8 crushed gravel	1.14	0.94	1.15	0.87
Lithia Springs 7	1.70	1.07	1.41	0.85
Summit Sandstone 8	0.93	0.48	0.95	0.96

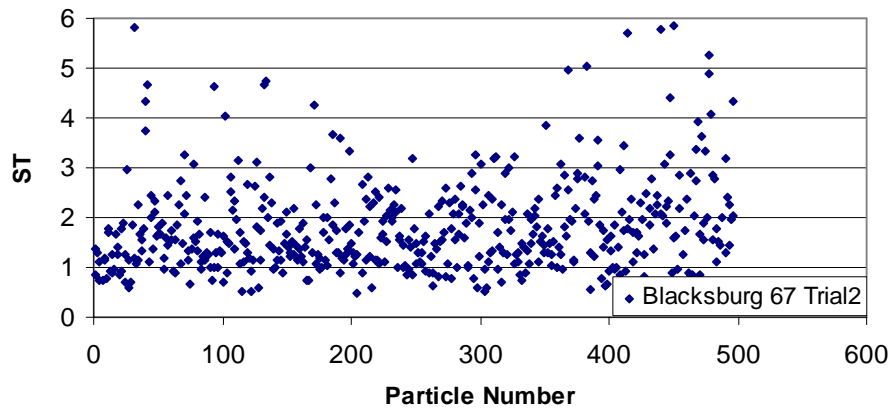
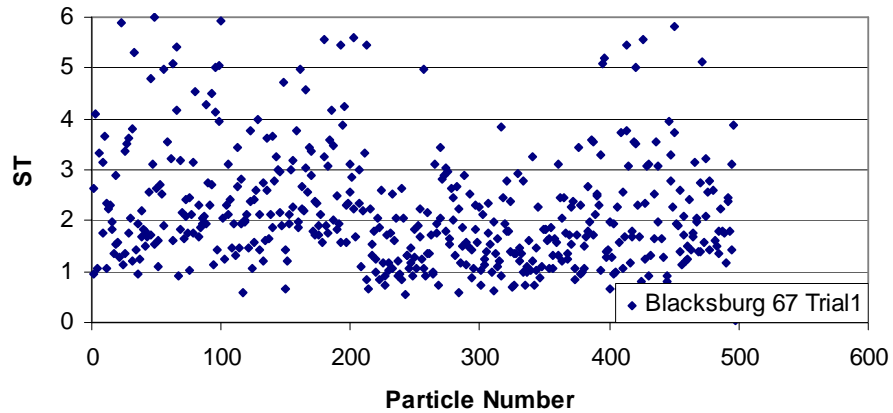


Figure 3-3 Imaging Based Surface Texture (ST) Repeatability Analysis of the Blacksburg 67 Sample

As indicated in Tables 3-4 through 3-6 and also from the individual NCAT aggregate results given in Appendix II, charts detailing gradation, AI, and ST index distributions of the NCAT aggregates, the UIAIA imaging based morphological indices, i.e., the F&E ratio, angularity index (AI) and the surface texture (ST) index, demonstrated adequate capability in distinguishing the various shape, angularity and surface texture characteristics of the different types of NCAT aggregate samples. For all the NCAT coarse aggregate studied, the percent by weight with F&E ratios greater than 5:1 ranged from 0 to 2%; the range for AI was between 150 and 700, and the maximum and minimum ST indices varied between 0.5 and 2.5. The good repeatability typically observed in determining similar individual shape indices from the two trials of the NCAT coarse aggregate image acquisition and processing further validated the UIAIA system as a robust and repeatable image analysis device. Note that the F&E ratios, AI, and ST indices of the NCAT aggregate samples reflect overall the different levels of shape irregularities of the aggregate samples, which will be linked to the rutting performances of the NCAT Test Track asphalt pavement test sections in the next chapter.

IMAGING RESULTS OF AGGREGATE FROM PARTICIPATING STATES

As the second set of aggregate samples shipped to UIUC, a total of 48 different coarse aggregate materials, as listed in Table 3-2, were received from seven state highway agencies and the Central Federal Lands and Highways Division participated in the pooled fund study. Representative samples of these coarse aggregate materials with statistically sufficient particles were then processed using the UIAIA for determining size and shape indices from image analysis. Accuracy, repeatability, and significance of the imaging results were evaluated similar to what is presented for the NCAT aggregate samples, by comparing the imaging results with the measured and by further analyzing using statistical techniques.

Weight Computation

The actual weights and bulk specific gravities, G_{sb} , of the pooled fund participating agency aggregate bag samples were first measured manually in the laboratory to verify the accuracy of the imaging based volume/weight computations. Table 3-7 compares the imaging based weights with the manual measurements of the analyzed coarse aggregate samples. The percent errors of all the coarse aggregate samples were found again to be within 9% with an absolute average error of 3.67% for all the samples. Note that these error percentages are directly affected by the image pixel quality or the resolution and the uniformity in the type and mineralogical composition of the aggregate particles assigned with the laboratory measured average G_{sb} value.

Table 3-7 UIAIA Imaging Based Weight Predictions for the Participating Agency Aggregate Samples

Aggregate Source	Aggregate Sample	No. of Particles	Actual Weight (g)	UIAIA Weight (g)	Percent Error	Specific Gravity G_{sb}
Federal Lands & Highways Division (NM)	7/8" Rock	400	1971.8	1899.5	-3.67%	2.617
	Coarse Aggregate	350	917.7	860.3	-6.26%	2.596
	Intermediate Aggregate	600	282.3	283.7	+0.50%	2.503
Federal Lands & Highways Division (OK)	1" Rock	350	1423.1	1378.7	-3.12%	2.699
	1/2" Rock	400	362.5	362.6	+0.01%	2.685
Minnesota	Meridian St. C.CA-50	600	456.2	442.1	-3.19%	2.712
	Meridian St. C. FA-3	600	369.5	367.9	-0.43%	2.698
	Barton Denmark BA-2	150	157.4	166.8	+5.97%	2.495
	Kraemer B. 9/16" Chip	729	1088	1136.5	+4.46%	2.655
	Kraemer B. Class 2	1339	966.4	1005.3	+4.02%	2.57
Mississippi	#7 Granite	600	486.8	482.2	-0.95%	2.658
	#89 Granite	600	412.5	401.6	-2.71%	2.702
	Crushed Gravel-1"	1000	735.3	766.8	+4.28%	2.444
	Crushed Gravel-0.5"	600	433.2	425.6	-1.79%	2.584
	Crushed Limestone #78	1000	645.7	652.1	+0.99%	2.706
	Crushed Limestone # 11	600	415.9	413.8	-0.51%	2.716
Missouri	Brickeys 1"	199	993.8	1012.9	+1.92%	2.515
	Brickeys 1/2"	2059	984.5	1043.4	+5.98%	2.546
	Brickeys 3/4"	1905	988.9	1024.5	+3.60%	2.586
	Brickeys 3/8"	1000	428.5	437.2	+2.02%	2.546
	1/2" Joorn. J.H. Q. B.	1006	993.4	1077.4	+8.46%	2.618
	3/4" Joornagan J.H. Q.	509	1988.9	1997.4	+0.42%	2.591
	1/2" Joorn. J.H. Q. R.	265	995.5	1054.3	+5.91%	2.615
	1 1/2" Clean Stone	150	2685.3	2684.3	-0.04%	2.447
	1/2" Clean Stone	1820	991.9	915.3	-7.73%	2.572
3/4" Clean Stone	527	993.4	1007.1	+1.37%	2.636	
South Carolina	Blacksburg 67	230	880.8	847.3	-3.80%	2.74
	Blacksburg 78M	600	627.8	585.1	-6.80%	2.805
	Gray Court 6M	500	1964.3	1891.5	-3.71%	2.609
	Gray Court 789	600	398.9	425.8	+6.73%	2.541
	Marlboro 67	743	1793.1	1819.7	+1.48%	2.626
	Marlboro 789	1000	637.3	621.9	-2.42%	2.609
Georgia	Lithia Springs-007	1100	889.4	931	+4.68%	2.558
	Georgia 89	443	1218.2	1111.4	-8.77%	2.916
	Georgia M10	600	498.9	485.8	-2.70%	2.721

Table 3-7 UIAIA Imaging Based Weight Predictions for the Participating Agency Aggregate Samples
(Continued)

Aggregate Source	Aggregate Sample	No. of Particles	Actual Weight (g)	UIAIA Weight (g)	Percent Error	Specific Gravity G_{sb}
Indiana	#11 gravel W. (2164)	675	505	518.5	+2.67%	2.549
	QA # 12 stone (2461)	600	424.3	415.4	-2.14%	2.659
	#11 gravel K. (2432)	600	418.9	409.8	-2.22%	2.713
Alabama	Calera 7	1000	1094.2	1137.5	+3.95%	2.708
	Calera 89	600	295.5	318.9	+7.90%	2.709
	Columbus 7 Granite 7	600	1134	1046.2	-7.74%	2.64
	Jemison 1/2 cr. gravel	1809	986.3	1037.2	+5.16%	2.548
	Jemison 3/8 cr. gravel	1843	986.4	1037.7	+5.20%	2.546
	Summit sandstone 8	600	1110.2	1076.5	-3.04%	2.435
Montana	3/8 Inch Chips	600	421.4	429.9	+2.01%	2.545
	Coarse Agg. - MD2	833	1633.2	1657.6	+1.49%	2.572
	Intermediate Agg.	600	354.9	336.3	-5.24%	2.561
	Coarse Agg. - MD1	600	1989.3	2103.9	+5.76%	2.628
Average Absolute Error (%)					3.67%	

Gradation Analysis

As for the accuracy of the UIAIA in measuring the imaging based particle size distributions of the participating agency aggregate materials, gradation curves of these aggregate bag samples were measured manually in the laboratory following the sieve analysis procedure specified in ASTM D136-96a, and compared to the results of the imaging based gradation curves. It was found that all the gradation curves matched the sieve shaking results. Due to the size limitation of this chapter, the gradation curves of three aggregate samples from the Federal Lands and Highways Division-New Mexico (FLHD-NM) are only shown here in Figure 3-4. For all the three coarse aggregate samples, the imaging based gradation curves matched very well with the distributions obtained from sieve analyses. This actually concludes that the UIAIA system also measured accurately the intermediate sizes or dimensions of all the pooled fund study coarse aggregate materials. For all the other participating agency aggregate samples, comparison charts of the imaging based gradation curves to the manually measured ones are presented in Appendix II.

Flat and Elongated Ratio

Table 3-8 presents the imaging based F&E ratios of the aggregate samples from the participating agencies, i.e., less than 3 to 1 (<3:1), between 3 to 1 and 5 to 1 (3:1 to 5:1), and greater than 5 to 1 (>5:1). The predictions from the two trials of each aggregate sample are also given in Table 3-8 as percent by

weight based on imaging. The flat and elongated particles by proportion of the pooled fund study coarse aggregate materials also conformed to those provided by the state highway agencies and none of them exceeded 10% by weight of greater than 5 to 1 (>5:1) in accordance with the Superpave criteria. The repeatability in F&E ratio predictions further validated the UIAIA imaging based approach as well as the analysis procedures for determining the maximum and minimum coarse aggregate dimensions since the F&E ratio is defined as the ratio of the maximum to minimum dimensions.

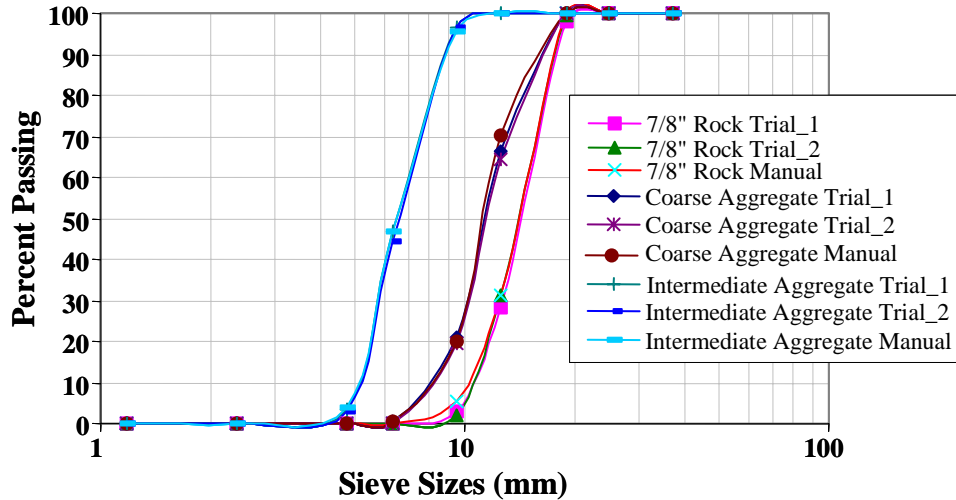


Figure 3-4 Imaging Based Particle Size Distributions for the FLHD-NM Aggregate Samples

Table 3-8 UIAIA Flat and Elongated (F&E) Ratio Results for the Participating Agency Aggregate

Aggregate Source	Aggregate Sample	No. of Particles	Trial 1			Trial 2		
			F&E Ratio			F&E Ratio		
			<3:1	3:1 to 5:1	>5:1	<3:1	3:1 to 5:1	>5:1
Federal Lands & Highways Division (NM)	7/8" Rock	400	87.10%	12.00%	0.80%	85.90%	13.30%	0.70%
	Coarse Aggregate	350	89.70%	9.90%	0.40%	89.40%	10.40%	0.20%
	Intermediate Aggregate	600	78.30%	19.80%	1.90%	78.40%	19.70%	2.00%
Federal Lands & Highways Division (OK)	1" Rock	350	71.90%	24.30%	3.80%	73.30%	22.90%	3.80%
	1/2" Rock	400	95.70%	4.20%	0.70%	95.70%	4.20%	0.70%
Minnesota	Meridian St. C.CA-50	600	85.23%	13.57%	1.20%	84.46%	14.64%	0.90%
	Meridian St. C. FA-3	600	97.30%	2.40%	0.30%	95.85%	3.34%	0.81%
	Barton Denmark BA-2	150	89.60%	10.40%	0.00%	92.30%	7.50%	0.10%
	Kraemer B. 9/16" Chip	729	96.20%	3.80%	0.00%	95.10%	4.90%	0.00%
	Kraemer B. Class 2	1339	93.30%	6.40%	0.30%	92.70%	7.00%	0.30%

Table 3-8 UIAIA Flat and Elongated (F&E) Ratio Results for the Participating Agency Aggregate
(Continued)

Aggregate Source	Aggregate Sample	No. of Particles	Trial 1			Trial 2		
			F&E Ratio			F&E Ratio		
			<3:1	3:1 to 5:1	>5:1	<3:1	3:1 to 5:1	>5:1
Mississippi	#7 Granite	600	91.25%	8.25%	0.50%	90.19%	9.19%	0.62%
	#89 Granite	600	87.59%	10.26%	2.15%	88.67%	9.48%	1.85%
	Crushed Gravel-1''	1000	97.90%	2.10%	0.00%	94.70%	5.30%	0.00%
	Crushed Gravel-0.5''	600	86.12%	13.26%	0.62%	89.15%	9.23%	1.62%
	Crushed Limestone #78	1000	82.30%	17.30%	0.40%	83.20%	16.60%	0.20%
	Crushed Limestone #11	600	94.29%	5.10%	0.61%	91.58%	8.21%	0.21%
Missouri	Brickeys 1''	199	85.10%	14.50%	0.40%	85.90%	13.70%	0.40%
	Brickeys 1/2''	2059	80.00%	18.90%	1.10%	78.70%	20.00%	1.30%
	Brickeys 3/4''	1905	79.30%	19.70%	1.00%	79.50%	19.20%	1.30%
	Brickeys 3/8''	1000	94.80%	4.90%	0.30%	94.40%	5.10%	0.60%
	1/2'' Joorn. J.H. Q. B.	1006	94.50%	5.40%	0.10%	94.40%	5.40%	0.10%
	3/4'' Joornagan J.H. Q.	509	94.00%	5.90%	0.10%	91.20%	8.50%	0.30%
	1/2'' Joorn. J.H. Q. R.	265	96.50%	3.50%	0.00%	95.90%	4.10%	0.00%
	1 1/2'' Clean Stone	150	95.60%	4.40%	0.00%	93.70%	6.30%	0.00%
	1/2'' Clean Stone	1820	95.70%	4.30%	0.00%	94.80%	5.10%	0.20%
3/4'' Clean Stone	527	97.40%	2.60%	0.00%	97.10%	2.90%	0.00%	
South Carolina	Blacksburg 67	230	68.60%	26.00%	5.50%	70.90%	25.60%	3.40%
	Blacksburg 78M	600	86.70%	12.70%	0.60%	85.10%	14.30%	0.60%
	Gray Court 6M	500	93.60%	6.20%	0.20%	88.50%	11.00%	0.50%
	Gray Court 789	600	80.40%	19.20%	0.40%	79.60%	20.10%	0.30%
	Marlboro 67	743	92.80%	6.80%	0.40%	91.50%	8.50%	0.00%
	Marlboro 789	1000	90.50%	9.20%	0.30%	95.20%	4.80%	0.00%
Georgia	Lithia Springs-007	1100	84.50%	15.40%	0.00%	84.90%	15.10%	0.00%
	Georgia 89	443	77.80%	21.90%	0.20%	79.20%	20.50%	0.20%
	Georgia M10	600	79.58%	20.11%	0.31%	81.64%	17.79%	0.57%
Indiana	#11 gravel W. (2164)	675	95.40%	4.60%	0.00%	96.90%	3.10%	0.00%
	QA # 12 stone (2461)	600	90.26%	7.98%	1.76%	87.61%	11.37%	1.02%
	#11 gravel K. (2432)	600	83.21%	14.11%	2.68%	85.67%	12.68%	1.65%
Alabama	Calera 7	1000	79.00%	20.40%	0.60%	78.30%	21.00%	0.70%
	Calera 89	600	84.50%	15.00%	0.50%	85.80%	13.70%	0.50%
	Columbus 7 Granite 7	600	88.10%	11.90%	0.00%	90.40%	9.50%	0.10%
	Jemison 1/2 cr. gravel	1809	92.80%	6.80%	0.40%	92.60%	7.00%	0.50%
	Jemison 3/8 cr. gravel	1843	92.40%	7.40%	0.20%	92.60%	7.20%	0.20%
	Summit sandstone 8	600	96.30%	3.70%	0.00%	95.90%	4.00%	0.10%
Montana	3/8 Inch Chips	600	78.70%	19.80%	1.60%	79.70%	19.00%	1.30%
	Coarse Agg. - MD2	833	94.20%	5.70%	0.00%	93.00%	6.90%	0.10%
	Intermediate Agg.	600	83.50%	15.00%	1.50%	85.40%	13.30%	1.30%
	Coarse Agg. - MD1	600	86.60%	12.70%	0.70%	81.50%	16.90%	1.60%

Angularity and Surface Texture

The Angularity Index (AI) analysis as defined in UIAIA was conducted on all the coarse aggregate samples from the participating agencies to evaluate the accuracy and repeatability of using UIAIA to measure particle angularity. The mean AI results with the standard deviations are given in Table 3-9 as obtained from the two trial analyses of the participating agency coarse aggregate. The detailed AI distribution figures for the individual aggregate samples can be found in Appendix II of this report. As an example, Figure 3-5 shows the AI distributions for the FLHD-NM 7/8-inch Rock aggregate sample. The good agreement between the AI distributions of the two trials for this and all the other aggregate samples demonstrates the good repeatability of UIAIA in characterizing angularity property of coarse aggregate particles. The UIAIA imaging based Surface Texture (ST) index results given in Table 3-10 also indicate very good repeatability for all the participating agency coarse aggregate samples. The ST index distributions for the FLHD-NM 7/8-inch Rock aggregate sample is also shown in Figure 3-6 with the details and comparisons of the two trial imaging based ST index results of other individual aggregate samples presented in Appendix II of this report.

Table 3-9 UIAIA Imaging Based Angularity Index (AI) Results for Participating Agency Aggregate

Aggregate Source	Aggregate Sample	Trial 1		Trial 2	
		AI - mean	Std Dev	AI - mean	Std Dev
Federal Lands & Highways Division (NM)	7/8" Rock	459	94	449	96
	Coarse Aggregate	426	102	440	112
	Intermediate Aggregate	439	93	451	95
Federal Lands & Highways Division (OK)	1" Rock	541	98	547	102
	1/2" Rock	494	80	482	76
Minnesota	Meridian St. C.CA-50	552	106	540	98
	Meridian St. C. FA-3	525	134	539	116
	Barton Denmark BA-2	451	124	453	130
	Kraemer B. 9/16" Chip	405	71	401	67
	Kraemer B. Class 2	425	71	419	65
Mississippi	#7 Granite	563	69	551	75
	#89 Granite	549	85	542	93
	Crushed Gravel-1"	404	78	402	76
	Crushed Gravel-0.5"	411	67	413	63
	Crushed Limestone #78	411	64	405	66
	Crushed Limestone #11	426	78	420	72

Table 3-9 UIAIA Imaging Based Angularity Index (AI) Results for Participating Agency Aggregate
(Continued)

Aggregate Source	Aggregate Sample	Trial 1		Trial 2	
		AI - mean	Std Dev	AI - mean	Std Dev
Missouri	Brickeys 1"	391	73	401	67
	Brickeys 1/2"	418	68	408	72
	Brickeys 3/4"	404	74	416	62
	Brickeys 3/8"	455	69	449	81
	1/2" Burlington	400	63	410	71
	3/4" Joornagan J.H. Q.	513	90	531	98
	1/4" Chips T. Rock	413	68	423	76
	1 1/2" Clean Stone	538	100	526	106
	1/2" Clean Stone	445	79	425	71
	3/4" Clean Stone	417	65	413	71
South Carolina	Blacksburg 67	488	88	472	82
	Blacksburg 78M	445	79	431	69
	Gray Court 6M	520	92	512	86
	Gray Court 789	553	89	529	85
	Marlboro 67	331	97	351	91
	Marlboro 789	326	74	336	78
Georgia	Lithia Springs-007	448	74	444	76
	Georgia 89	381	59	373	63
	Georgia M10	508	118	499	106
Indiana	#11 gravel W. (2164)	432	78	428	74
	QA # 12 stone (2461)	428	87	425	85
	#11 gravel K. (2432)	423	74	439	82
Alabama	Calera 7	432	69	448	75
	Calera 89	446	66	440	74
	Columbus 7 Granite 7	515	97	523	89
	Jemison 1/2 cr. gravel	380	78	362	82
	Jemison 3/8 cr. gravel	375	84	371	88
	Summit sandstone 8	419	69	413	73
Montana	3/8 Inch Chips	477	90	475	82
	Coarse Agg. - MD2	467	107	459	89
	Intermediate Agg.	545	121	519	119
	Coarse Agg. - MD1	454	136	446	128

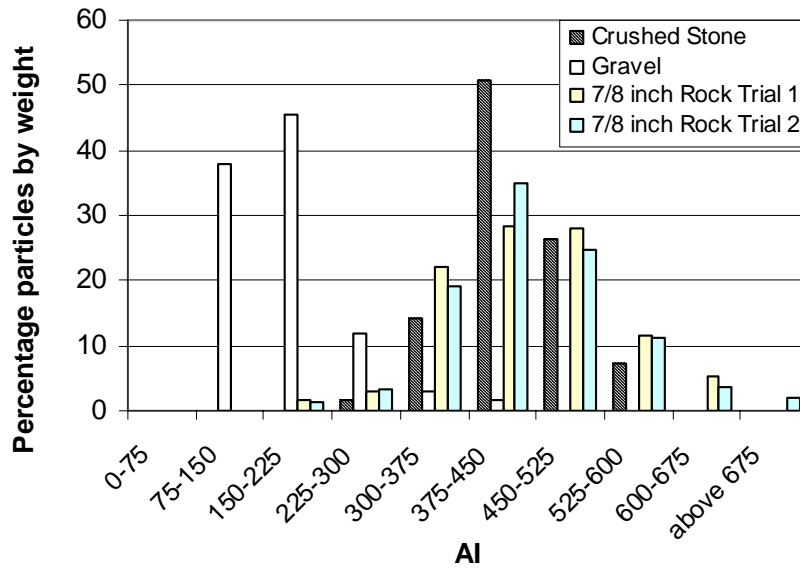


Figure 3-5 Imaging Based Angularity Index (AI) Repeatability Analysis of the FLHD-NM 7/8-inch Rock

Table 3-10 UIAIA Imaging Based Surface Texture (ST) Indices of the Participating Agency Aggregate

Aggregate Source	Aggregate Sample	Trial 1		Trial 2	
		ST - mean	Std Dev	ST - mean	Std Dev
Federal Lands & Highways Division (NM)	7/8" Rock	2.21	1.09	2.22	1.07
	Coarse Aggregate	2.01	1.1	2.02	1.13
	Intermediate Aggregate	1.81	1.09	1.78	1.07
Federal Lands & Highways Division (OK)	1" Rock	2.7	1.24	2.67	1.25
	1/2" Rock	1.81	0.89	1.78	0.81
Minnesota	Meridian St. C.CA-50	1.61	1.01	1.53	0.95
	Meridian St. C. FA-3	1.95	1.31	2.07	1.25
	Barton Denmark BA-2	1.58	0.87	1.63	0.75
	Kraemer B. 9/16" Chip	1.33	0.68	1.21	0.62
	Kraemer B. Class 2	1.34	0.87	1.36	0.85
Mississippi	#7 Granite	2.19	0.96	2.27	0.98
	#89 Granite	2.22	1.23	2.08	1.27
	Crushed Gravel-1"	1.32	0.77	1.34	0.8
	Crushed Gravel-0.5"	1.38	0.35	1.46	0.41
	Crushed Limestone #78	1.4	0.88	1.49	0.76
	Crushed Limestone #11	1.45	0.96	1.41	1.00

Table 3-10 UIAIA Imaging Based Surface Texture (ST) Indices of the Participating Agency Aggregate
(Continued)

Aggregate Source	Aggregate Sample	Trial 1		Trial 2	
		ST - mean	Std Dev	ST - mean	Std Dev
Missouri	Brickeys 1"	1.36	0.53	1.36	0.5
	Brickeys 1/2"	1.55	0.9	1.51	0.85
	Brickeys 3/4"	1.44	0.78	1.45	0.92
	Brickeys 3/8"	1.38	0.7	1.39	0.71
	1/2" Joorn. J.H. Q. B.	1.38	0.75	1.41	0.7
	3/4" Joornagan J.H. Q.	2.25	1.09	2.27	1.05
	1/2" Joorn. J.H. Q. R.	1.32	0.54	1.38	0.53
	1 1/2" Clean Stone	2.09	0.94	2.07	0.94
	1/2" Clean Stone	1.39	1.00	1.55	0.94
	3/4" Clean Stone	1.3	0.6	1.21	0.53
South Carolina	Blacksburg 67	2.68	1.15	2.58	1.11
	Blacksburg 78M	1.88	1.18	2.03	1.28
	Gray Court 6M	2.28	0.96	2.75	1.8
	Gray Court 789	2.3	1.3	2.28	1.33
	Marlboro 67	1.05	0.62	1	0.55
	Marlboro 789	1.03	0.67	0.79	0.46
Georgia	Lithia Springs-007	1.71	0.97	1.7	0.91
	Georgia 89	1.43	0.72	1.4	0.66
	Georgia M10	2	1.1	2.06	0.94
Indiana	#11 gravel W. (2164)	1.4	0.76	1.34	0.66
	QA # 12 stone (2461)	1.62	0.62	1.5	0.74
	#11 gravel K. (2432)	1.35	0.81	1.37	0.75
Alabama	Calera 7	1.09	0.7	1.1	0.88
	Calera 89	1.14	0.90	1.15	0.87
	Columbus 7 Granite 7	2.74	1.87	3.06	2.04
	Jemison 1/2 cr. gravel	1.09	0.70	1.10	0.88
	Jemison 3/8 cr. gravel	1.14	0.94	1.15	0.87
	Summit sandstone 8	1.55	0.87	1.42	0.71
Montana	3/8 Inch Chips	2.06	1.18	2.09	1.19
	Coarse Agg. - MD2	1.88	0.96	2.13	1.31
	Intermediate Agg.	2.04	0.93	2.17	1.04
	Coarse Agg. - MD1	2.01	1.04	2.21	1.29

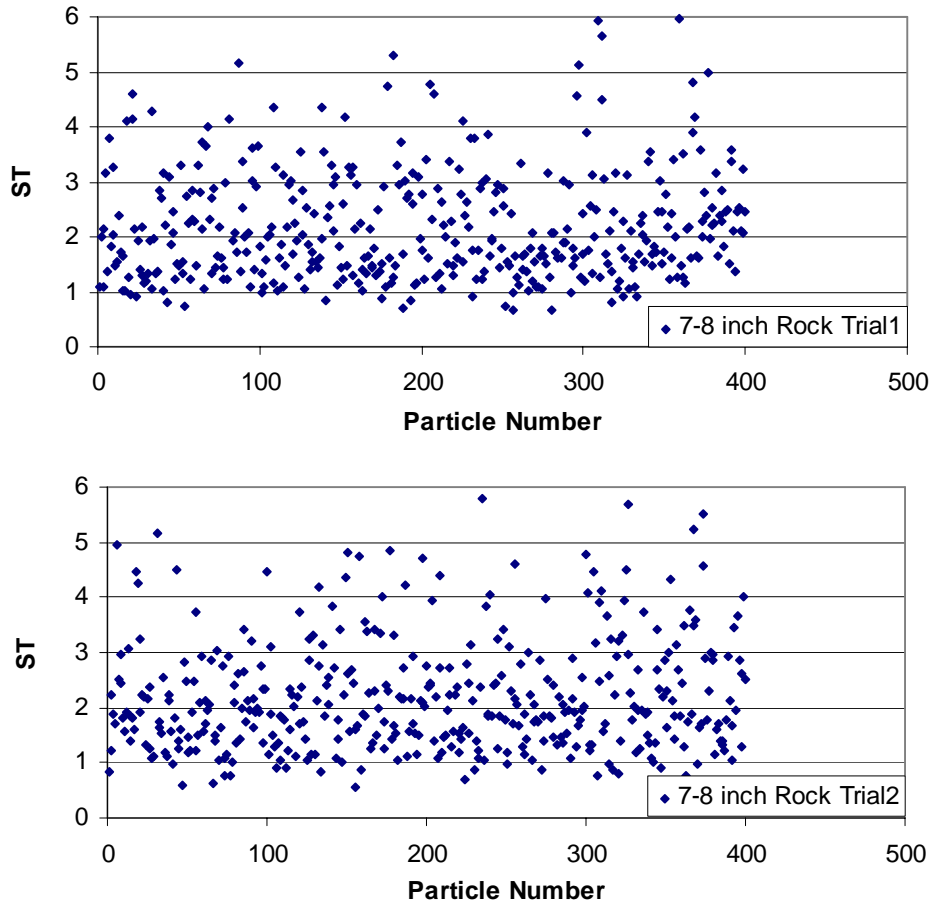


Figure 3-6 Imaging Based Surface Texture (ST) Repeatability Analysis of the FLHD-NM 7/8-inch Rock

Table 3-11 presents the means and standard deviations of the imaging based AI and ST index results from the two trials for the participating agency coarse aggregate, from which an overall knowledge of the surface irregularities of the 48 aggregate samples can be gathered. As a result, four categories can be established in terms of angularity and surface texture ranges using statistical clustering techniques. Table 3-12 lists these categories, which coincided with the typical AI and ST index values identified for the uncrushed gravel, crushed gravel, crushed limestone, and crushed granite evaluated in this pooled fund study. As the surface irregularity levels of the aggregate materials increase from uncrushed to crushed, both the AI and ST indices increase for the 48 different aggregates evaluated. This finding is consistent with the common experience and perception. Further analysis indicated a definite relationship, with a coefficient of determination R^2 of 0.79, existed between the aggregate surface texture and angularity index values as shown in Figure 3-7. Note that there are some special aggregate materials such as obsidian and precious stones that may not follow this trend and instead possess rather high angularity and very smooth surface texture properties.

Table 3-11 Imaging Based Angularity and Surface Texture Indices of the Participating Agency Aggregate

Aggregate Source	Aggregate Sample	Angularity Index (AI)		Surface Texture (ST) Index	
		Mean	Std Dev	Mean	Std Dev
Federal Lands & Highways Division (NM)	7/8" Rock	454	95	2.22	1.08
	Coarse Aggregate	433	107	2.01	1.12
	Intermediate Aggregate	445	94	1.79	1.08
Federal Lands & Highways Division (OK)	1" Rock	544	100	2.68	1.24
	1/2" Rock	488	78	1.80	0.85
Minnesota	Meridian St. C.CA-50	546	102	1.57	0.98
	Meridian St. C. FA-3	532	125	2.01	1.28
	Barton Denmark BA-2	452	127	1.61	0.81
	Kraemer B. 9/16" Chip	403	69	1.27	0.65
	Kraemer B. Class 2	422	68	1.35	0.86
Mississippi	#7 Granite	557	72	2.23	0.97
	#89 Granite	546	89	2.15	1.25
	Crushed Gravel-1"	403	77	1.33	0.78
	Crushed Gravel-0.5"	412	65	1.42	0.38
	Crushed Limestone #78	408	65	1.44	0.82
	Crushed Limestone #11	423	75	1.43	0.98
Missouri	Brickeys 1"	396	70	1.36	0.52
	Brickeys 1/2"	413	70	1.53	0.88
	Brickeys 3/4"	410	68	1.44	0.85
	Brickeys 3/8"	452	75	1.39	0.70
	1/2" Joorn. J.H. Q. B.	405	67	1.40	0.72
	3/4" Joornagan J.H. Q.	522	94	2.26	1.07
	1/2" Joorn. J.H. Q. R.	418	72	1.35	0.53
	1 1/2" Clean Stone	532	103	2.08	0.94
	1/2" Clean Stone	435	75	1.47	0.97
3/4" Clean Stone	415	68	1.26	0.56	
South Carolina	Blacksburg 67	480	85	2.63	1.13
	Blacksburg 78M	438	74	1.95	1.23
	Gray Court 6M	516	89	2.51	1.38
	Gray Court 789	541	87	2.29	1.32
	Marlboro 67	341	94	1.03	0.59
	Marlboro 789	331	76	0.91	0.57
Georgia	Lithia Springs-007	446	75	1.71	0.94
	Georgia 89	377	61	1.42	0.69
	Georgia M10	503	112	2.03	1.02

Table 3-11 Imaging Based Angularity and Surface Texture Indices of the Participating Agency Aggregate
(Continued)

Aggregate Source	Aggregate Sample	Angularity Index (AI)		Surface Texture (ST) Index	
		Mean	Std Dev	Mean	Std Dev
Indiana	#11 gravel W. (2164)	430	76	1.37	0.71
	QA # 12 stone (2461)	427	86	1.56	0.68
	#11 gravel K. (2432)	431	78	1.36	0.78
Alabama	Calera 7	440	72	1.83	1.25
	Calera 89	443	70	1.60	0.90
	Columbus 7 Granite 7	519	93	2.90	1.96
	Jemison 1/2 cr. gravel	371	80	1.09	0.79
	Jemison 3/8 cr. gravel	373	86	1.15	0.90
	Summit sandstone 8	416	71	1.49	0.79
Montana	3/8 Inch Chips	476	86	2.08	1.19
	Coarse Agg. - MD2	463	98	2.00	1.13
	Intermediate Agg.	532	120	2.11	0.98
	Coarse Agg. - MD1	450	132	2.11	1.17

Table 3-12 Typical Ranges of Angularity and Surface Texture Indices

Aggregate Type	Angularity Index (AI)		Surface Texture (ST) Index	
	Range	Mean	Range	Mean
Uncrushed Gravel	250-350	300	0.5-1.20	0.900
Crushed Gravel	300-450	400	1.00-1.50	1.200
Crushed Limestone	400-550	500	1.20-1.80	1.600
Crushed Granite	500-650	550	1.80-2.90	2.200

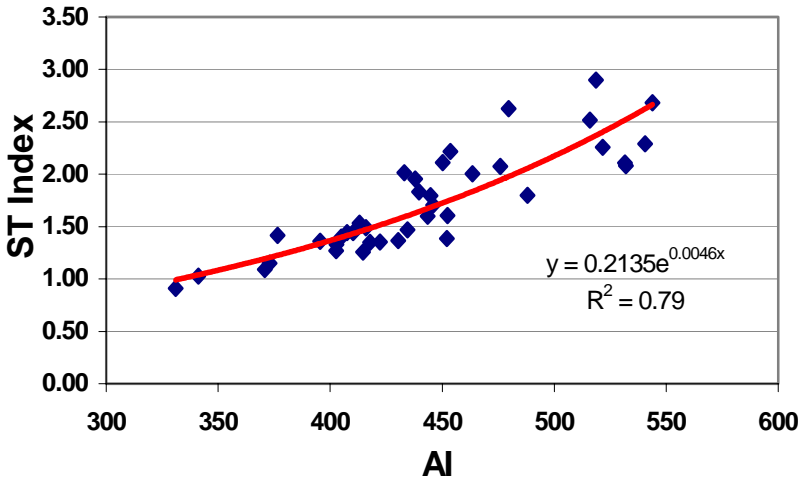


Figure 3-7 Relationship between Coarse Aggregate Angularity (AI) and Surface Texture (ST) Indices

In the following chapters, the AI and ST indices of the pooled fund study aggregate materials will be related to the field and laboratory stability or permanent deformation (rutting) properties and the laboratory modulus characteristics of the asphalt mixes designed with these coarse aggregate materials. Field rutting data collected from the NCAT pavement test track will be analyzed. Laboratory permanent deformation and resilient modulus tests will be performed on asphalt specimens fabricated following the mix designs used by the pooled fund study participant state highway agencies. Results of these field and laboratory test data will be used to establish relationships between HMA performances and the imaging based aggregate morphological indices to better understand effects of the aggregate shape properties on asphalt mixture performance.

SUMMARY

To validate the effectiveness of the University of Illinois Aggregate Image Analyzer (UIAIA) in imaging based quantification of coarse aggregate size and shape properties, different types and sources of coarse aggregate materials with varying shape irregularities were collected from the study partners in the FHWA Project DTFH61-02-X-00029. These are the National Center for Asphalt Technology (NCAT), the participating state highway agencies of Alabama, Georgia, Indiana, Minnesota, Mississippi, Missouri, Montana, and South Carolina, and the Central Federal Lands and Highways Division. Imaging based size and shape properties of the coarse aggregate samples were then determined using the UIAIA for maximum, intermediate and minimum dimensions, individual particle volume and weight, percent flat and elongated ratio by weight, angularity index (AI), and the surface texture (ST) index, in order to study effects of coarse aggregate shape on the permanent deformation and modulus characteristics of asphalt mixtures. Accuracy and repeatability of the imaging based volume computations were validated by successfully comparing the imaging based weights of the aggregate samples to their actual weights measured in the laboratory. Imaging based particle size distributions were also accurately computed and compared to gradation curves obtained from manual sieve analyses. Individual aggregate types with unique particle morphologies were documented and classified according to the imaging based shape indices. Using statistical clustering techniques, four categories were established for commonly used coarse aggregate types based on the image analysis shape property database. A definite relationship was shown to exist between coarse aggregate angularity and surface texture.

CHAPTER 4

EFFECT OF COARSE AGGREGATE MORPHOLOGY ON RUTTING PERFORMANCES OF ASPHALT MIXES IN THE NCAT TEST TRACK

Aggregate shape factors such as angularity and flat and elongated ratio as well as surface texture influence hot mix asphalt behavior and performance. The imaging based analysis of the coarse aggregate materials also used in the National Center for Asphalt Technology (NCAT) Test Track asphalt mixes were performed using the three-dimensional imaging system, University of Illinois Aggregate Image Analyzer (UIAIA). The imaging based shape indicial results of the NCAT aggregate samples, i.e., flat and elongation ratio, angularity index (AI) and surface texture (ST) index were well documented in Chapter 3. Being primarily a field rutting study, the NCAT Test Track findings will be used in this chapter to evaluate the performances of the various Superpave mixes with traffic. The results from 46 different flexible pavement test sections installed at the NCAT full scale study were collected from the Test Track to provide a good statistical basis for AC structural layer rutting performance comparisons. An attempt is made in this chapter to link the detailed UIAIA determined NCAT Test Track coarse aggregate shape properties to the individual NCAT test section asphalt surface rutting data for a better understanding of the coarse aggregate shape effects on Superpave mix rutting field performances.

SIGNIFICANCE OF THE NCAT COARSE AGGREGATE STUDY

Coarse aggregate constitutes the largest proportion by weight of the majority of asphalt concrete (AC) pavement surface courses. The significant role played by coarse aggregate in the volumetric design of hot mix asphalt naturally links physical properties of coarse aggregate to the strength, stability, and performance of AC pavements. Coarse aggregate shape factors such as angularity, flat and elongated ratio and surface texture have been recognized to be critical factors affecting the performance of asphalt concrete pavements (Monismith, 1970; Barksdale et al., 1992; Buchanan, 2000).

To design a long service life asphalt mixture, the aggregates must have the proper gradation and shape. In general, it is preferable to have somewhat cubical and angular particles rather than flat, thin, or elongated ones (Barksdale et al., 1992; Kennedy, 1994). The Strategic Highway Research Program (SHRP) Superpave mix design system currently specifies a maximum limit of 10 percent of flat and elongated particles at the 5:1 ratio for the design aggregate blend. Recent research has shown that even flat and elongated particles at the 3:1 ratio can influence rutting to different extents depending on aggregate types and the percentage of flat and elongated particles used in asphalt mixtures (Buchanan,

2000). A better correlation to reduced pavement rutting has also been obtained for aggregate blends having rough surface texture than those with smooth surface properties (Fletcher, 2002).

Flat and elongated ratio, angularity, and surface texture are therefore the three key aggregate properties determined based on imaging for the morphological description of coarse aggregate processed in the UIAIA system. In the previous chapters of this report, the image analysis modules of UIAIA including programs were described as the means to determine these three shape indices. A database of the UIAIA imaging based shape indices was established for the two sets of coarse aggregate materials, i.e., the NCAT aggregates and those from the other participating agencies, obtained from throughout the country from various sources and having aggregate types ranging from cubical to flat and elongated, rounded to angular, and smooth to rough coarse aggregates.

A conventionally proven way to investigate factors such as the coarse aggregate shape effects on AC pavement performance is to collect field performance data under controlled traffic repetitions and environmental conditions. Brown and Cross (2002) tentatively regarded pavement test track as the most realistic way to test pavement under accelerated conditions with actual truckloads applied. The research approach taken was therefore to relate the coarse aggregate shape indices determined from imaging for flatness and elongation, angularity and surface texture to NCAT Test Track asphalt mix rutting performance data (Brown and Cross, 2002; Powell, 2001). This was accomplished by means of individually accounting for the weight percentage of each coarse aggregate material used in the hot mix asphalt designs of different pavement sections and also the contributions of each constructed hot mix lift on the overall pavement rut depth performances in the NCAT test sections.

NCAT PAVEMENT TEST TRACK STUDY AND FIELD RESULTS

As shown in Figure 4-1, the NCAT Pavement Test Track is a full-scale AC pavement test track constructed in the year 2000 to evaluate various mixture types placed in 46 different flexible pavement sections. In the NCAT Test Track study, the materials and asphalt mix methods, especially the Superpave design, were the study variables to determine which mixes would perform better under actual traffic. The goal was also to identify laboratory tests that would best indicate field performances, primarily the rutting performances of various Superpave asphalt mixes with traffic.

Each of the 46 different flexible pavement test sections installed at the NCAT Test Track Facility was constructed at a length of approximately 61 m (200 ft.) designed overall to provide a good statistical basis for field rutting comparisons and performance evaluations of various Superpave mixes with traffic. The NCAT Pavement Test Track study asphalt mix constituents including coarse aggregate were collected from 9 sponsoring States and the Federal Highway Administration to make various asphalt

concrete mixtures (SMA, fine or coarse mixes, blended mixes, modified binder asphalt mixes, etc.) designed to withstand 10 million ESALs in 2 years. The trafficking of these year 2000 Test Track pavement sections took place between September of 2000 and January of 2003 (Brown and Cross, 2002; Powell, 2001; and <http://www.pavetrack.com/>). Figure 4-2 shows the designations of the NCAT pavements consisting of the North, South, East, and West test sections.

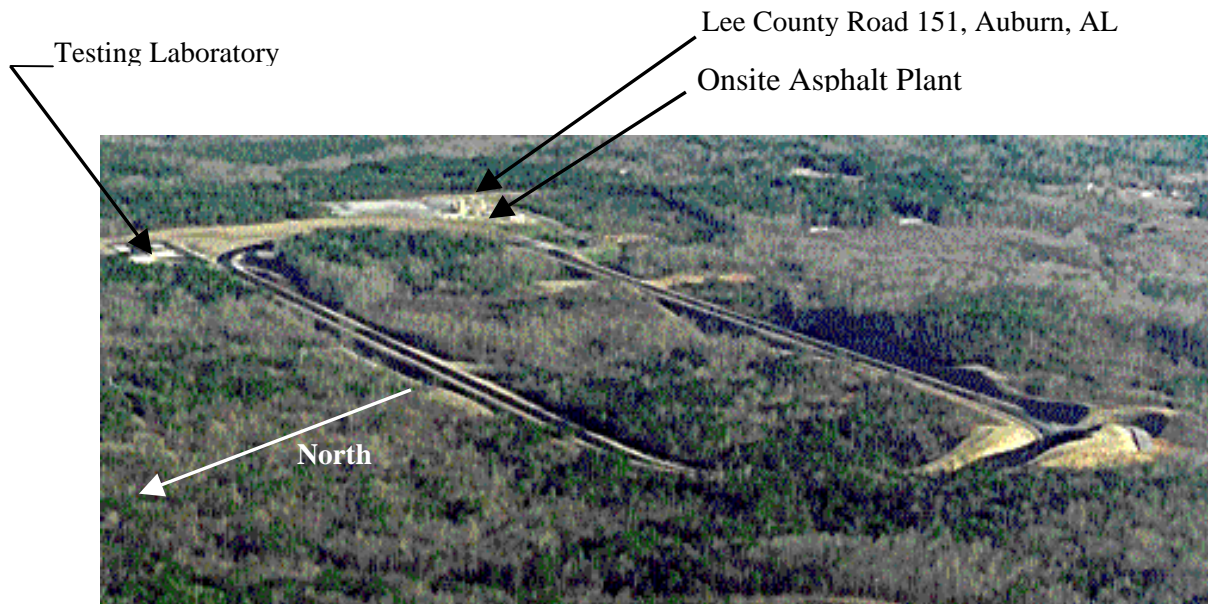


Figure 4-1 NCAT Pavement Test Track in Auburn, Alabama (courtesy of NCAT)

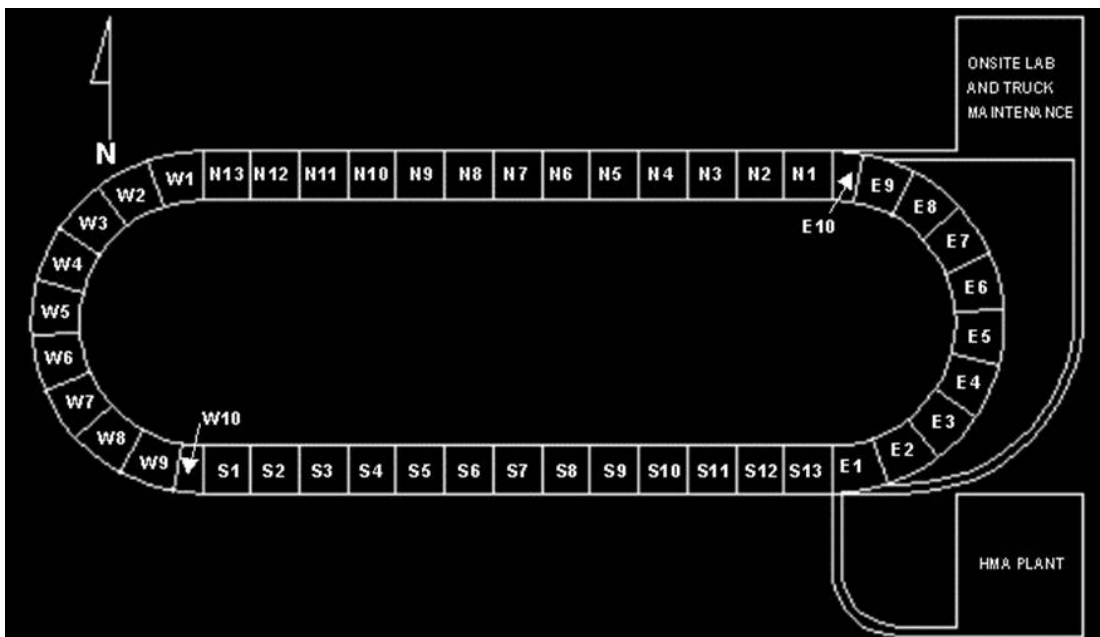


Figure 4-2 Section Assignment of the NCAT Pavement Test Track (courtesy of NCAT)

Each of the selected aggregate samples from the NCAT asphalt pavement sections corresponds to a type of coarse aggregate from a certain source and is of the same specific gradation and properties as that adopted in on site construction of NCAT Pavement Test Track (Powell, 2001). Tables 4-1 and 4-2 list the pertinent information of all the coarse aggregate samples processed by the UIAIA and the corresponding NCAT Test Track pavement sections in which the aggregate materials were used in construction and testing and their rutting performances (Brown and Cross, 2002 and <http://www.pavetrack.com>). In both tables, the letters “B” and “T” following the designations of sections refer to the bottom lift and top lift, respectively. The letter “O” is adopted here to designate an open-graded friction course (OGFC) used in the top lift.

The pavement section transverse profiles were measured using an ARAN type laser profiling device and continuous 3-point approximations served the basis for reporting each section’s historical rutting performance over time (see <http://www.pavetrack.com>). The individual section wheel-path rut depths presented in Tables 4-1 and 4-2 were therefore obtained from the NCAT web site as reported after a total traffic application of 8,972,237 ESALs at the end of warmer summer months in 2002.

NCAT COARSE AGGREGATE SHAPE INDICES AND NORMALIZATION

Table 4-3 lists the three key aggregate shape properties, flat and elongated ratio, angularity, and surface texture, determined based on imaging for the morphological description of NCAT coarse aggregate processed in the UIAIA system. Details of these imaging based shape indices of these aggregate samples can be found from Chapter 3.

Statistically sufficient aggregate particles were processed for each coarse aggregate. Accordingly, Table 4-3 also presents for each aggregate material the mean and standard deviation values for angularity and surface texture indices, AI and ST, respectively. The F&E ratios also listed in Table 3 were determined for each coarse aggregate as percent by weight of particles having flat and elongated ratios larger than 5 to 1 (5:1). For all the NCAT coarse aggregate studied, the percent by weight with F&E ratios greater than 5:1 ranged from 0 to 2%; the range for AI was between 150 and 700, and the maximum and minimum ST indices determined varied between 0.5 and 2.5.

Coarse aggregates used in hot mix asphalt (HMA) designs often represent a blend of different aggregate materials used to satisfy a certain gradation requirement, which also defines a certain mix type such as fine, coarse, stone matrix, etc. As in the case of NCAT Test Track pavement sections, each aggregate type in a blended gradation also exhibits unique morphological shape properties (see Table 4-3). Moreover, an asphalt concrete (AC) structural layer is often composed of different HMA lifts with

different coarse aggregate blends used in each lift, which further complicates the investigation of coarse aggregate shape effects on the rutting performance of the AC layer. A “composite” aggregate shape index needs to be computed for each lift using the imaging based shape indices of the individual coarse aggregate materials blended and used in that lift.

Table 4-1 NCAT Test Track South and West Sections, Rutting Performances, and Coarse Aggregate Used In Mix Designs

NCAT Pavement Test Track – South Side			
Section & Lift Designation	Lift Thickness (mm)	Rut Depth (mm)	Percent by Weight of Coarse Aggregate in Mix Design
S11B	53	2.29	37% Blacksburg 67, 41% Blacksburg 78M
S11T	38		49% Blacksburg 78M
S8B	53	2.54	32% Blacksburg 67, 41% Blacksburg 78M
S8T	38		49% Blacksburg 78M
S5B	64	2.03	33% Gilbertsville 57
S4B	64	2.54	25% Gordonville 78
S3B	64	2.54	26% Calera 67, 40% Calera 89
S3T	38		14% Calera 89
S2B	64	2.29	38% Blain 3/4 crushed gravel
S2T	38		15% Blain 1/2 crushed gravel
S1B	64	2.29	52% Gray Court 6M
S1T	38		10% Gray Court 6M
NCAT Pavement Test Track – West Side			
W1	102	2.03	73% Columbus 7
W2	102	1.52	74% Gadsden slag 78, 10% Calera 89
W3B	84	0.51	48% Columbus 7
W3O	18		20% Calera 7, 75% Gadsden slag 78
W4B	84	3.05	82% Calera 7
W5O	18	2.03	75% Columbus 7
W5B	84		82% Calera 7
W6	102	2.03	39% Gadsden slag 78
W7	102	1.02	82% Calera 7
W8	102	3.56	30% Calera 7, 34% Gadsden slag 78, 19% Summit Sandstone 8
W9	102	3.05	74% Jemison 1/2, 10% Jemison 3/8
W10	102	2.79	74% Jemison 1/2, 10% Jemison 3/8

Table 4-2 NCAT Test Track North and East Sections, Rutting Performances, and Coarse Aggregate Used In Mix Designs

NCAT Pavement Test Track – North Side			
Section & Lift Designation	Lift Thickness (mm)	Rut Depth (mm)	Percent by Weight of Coarse Aggregate in Mix Design
N1	102	3.05	32% Gadsden slag 78
N2	102	3.05	32% Gadsden slag 78
N3	102	7.62	32% Gadsden slag 78
N4	102	5.84	32% Gadsden slag 78
N5	102	6.10	53% Gadsden slag 78
N6	102	3.56	53% Gadsden slag 78
N7	102	2.29	53% Gadsden slag 78
N8	102	2.29	53% Gadsden slag 78
N9	102	2.03	53% Gadsden slag 78
N10	102	2.54	53% Gadsden slag 78
N11B	64	2.03	27% Columbus 6, 17% Columbus 7
N11T	38		38% Columbus 7
N12T	38	3.05	60% Lithia Springs 7
N13T	38	5.84	72.5% Blain 1/2 crushed gravel
NCAT Pavement Test Track – East Side			
E1	102	6.10	36% Jemison 1/2, 18% Jemison 3/8
E2	102	2.54	48% Columbus 7
E3	102	0.51	48% Columbus 7
E4	102	1.27	48% Columbus 7
E5	102	1.78	33% Columbus 7
E6	102	2.03	33% Columbus 7
E7	102	1.27	33% Columbus 7
E8	102	2.03	30% Columbus 7
E9	102	2.03	30% Columbus 7
E10	102	2.79	30% Columbus 7

The field rut depth data collected from the NCAT Test Track pavement sections, also reported in Tables 4-1 and 4-2, correspond to an overall AC surface deflection, which is actually a simple summation of permanent deformation accumulations in the different HMA lifts. However, due to the lack of individual rutting data for each lift, it is almost impossible to compare the coarse aggregate shape effects on the overall rutting performances of different pavement sections by directly comparing the composite aggregate shape indices for each lift. In essence, the philosophy behind developing a composite aggregate shape index for each HMA lift necessitates a “normalized” aggregate shape index also to be defined for each NCAT pavement test section in order to adequately evaluate coarse aggregate shape effects by

taking individual lift thicknesses into account and linking them to pavement section rutting performances. Based on these constraints inherent in the pavement geometries and field data collection approaches, each of the following shape indices, F&E ratio, angularity, and surface texture, therefore, had to be evaluated separately to show how individual shape factors would affect the field rutting performances.

Table 4-3 Imaging Based Indices Determined for Selected NCAT Coarse Aggregate Used In Mix Designs

Sample Designation	Percent by Weight With F&E Ratio > 5:1	Angularity Index, AI		Surface Texture Index, ST	
		Mean	Std. Dev.	Mean	Std. Dev.
Blacksburg 67	1.1	429.78	75.9	2.2	1.56
Blacksburg 78M	0.85	437.93	74.43	1.7	1.35
Blain 1/2 crushed gravel	0.565	398.19	77.08	1.13	0.56
Blain 3/4 crushed gravel	0.655	406.09	85.92	1.31	0.77
Calera 67	0.645	393.58	69.49	1.29	0.67
Calera 7	0.605	394.14	65.53	1.21	0.67
Columbus 6	1.085	456.06	91.36	2.17	1.72
Columbus 7	0.95	466.95	93.48	1.9	1.29
Gadsden slag 78	0.71	474.92	86.62	1.42	1
Calera 89	0.8	443.47	69.94	1.6	0.9
Jemison 1/2 crushed gravel	0	370.77	79.8	1.09	0.79
Gilbertsville 57	0.8	409.86	73.45	1.6	1.04
Gordonville 78	0.705	405.9	67.01	1.41	1.01
Gray Court 6M	1.1	473.92	81.83	2.2	1.65
Lithia Springs 7	0.78	429.76	72.43	1.56	0.96
Jemison 3/8 crushed gravel	0.8	373	85.59	1.15	0.9

Accordingly, a composite aggregate shape index for one HMA lift design was defined first to account for all the coarse aggregate materials used in that lift. This composite index was for any of the three key imaging shape indices, F&E ratio, angularity AI, or surface texture ST indices. The following formula shown in Equation 4-1 was used in the definition of the composite aggregate shape index:

$$Composite\ Index = \frac{\sum_{i=1}^n [(a_i)(index_i)]}{\sum_{i=1}^n (a_i)} \quad (4-1)$$

where *Composite Index* is the composite aggregate shape index for each design HMA lift, which is a weighted sum of the individual shape indices of the UIAIA-processed coarse aggregate materials used in the lift; the variable a_i is the percentage by weight of the i^{th} coarse aggregate material used in the lift; the variable $index_i$ is the imaging shape index of the i^{th} coarse aggregate material used in the lift; and finally the summation counter n is the number of the coarse aggregate materials used in that lift, which may be 1, 2, or 3 in this study depending on the number of coarse aggregate types used in that lift and processed by the UIAIA.

As for the constraint associated with the field rutting data collection approach, a normalization process was essentially conducted on the *Composite Index* based on individual lift thickness data as follows:

$$\text{Normalized Composite Index} = \frac{\sum_{j=1}^m \{(b_j)[(\text{Composite Index})_j]\}}{\sum_{j=1}^m (b_j)} \quad (4-2)$$

where *Normalized Composite Index* is the composite aggregate shape index of each design HMA layer normalized based on individual lift thickness used in the NCAT pavement test section; $(\text{Composite Index})_j$ is the composite shape index previously defined in Equation 1; the variable b_j is the thickness of the j^{th} HMA lift in the AC structural layer; and finally the summation counter m is the number of lifts comprising the AC structural layer, which may be 1 or 2 in this study since all the NCAT pavement sections had either 1 (dual) HMA lift or 2 lifts in construction.

RELATING COARSE AGGREGATE SHAPE INDICES TO NCAT TEST TRACK FIELD PERFORMANCE DATA

A complete review of the construction and testing performance data of the NCAT Pavement Test Track revealed that all pavement sections performed reasonably well with average wheel-path rutting reported as 3.05 mm (0.12 in.) considered as “minimal” at the Test Track (Brown et al., 2002 and <http://www.pavetrack.com>). All the rut depths were within 12.7 mm (0.5 in.), a value up to which rutting is typically not considered to be a problem on road and airfield pavements. The maximum rut depths reported, up to 7.62 mm (0.3 in.) for Section N3 (see Table 4-2), occurred in sections that did not use a modified asphalt binder and in which an additional 0.5% asphalt binder was added.

Rutting of an AC structural layer relates to many factors besides just the coarse aggregate shape that makes it extremely difficult to single out any individual shape effect. For the NCAT Test Track

sections, these factors could have been any or in combination of all of the following items: temperature; moisture contents of the HMA and subgrade; mixture types influenced by aggregate gradations, such as fine, coarse, SMA, and open-graded friction courses; mix design properties and volumetrics, such as asphalt binder grade, asphalt content and modifier type, design gyrations, and aggregate gradations affecting Superpave mix properties above, through, and below restricted zone ARZ, TRZ, and BRZ; construction related factors such as field compactive effort, in-place air voids, quality control; traffic load magnitudes and repetitions, etc. To isolate the coarse aggregate shape factors from this group of complex data so that statistical analysis could be conducted has surely been challenging and required all properties or factors kept similar for relating just the coarse aggregate shape factors to rutting performances. Since this goal was not easily attainable even with the most carefully constructed NCAT Test Track facility ever conceived for evaluating asphalt pavement rutting, the analysis approach adopted in this section has been to simply consider coarse aggregate imaging shape indices as independent variables and field rut depth data as dependent variables to study any relationships and linkages between the two sets of results.

Based on the field performance results, the NCAT Pavement Test Track rutting performance data overall had a limited range. This was especially the case for the rutting data measured on the south side sections of the NCAT Pavement Test Track, which are the series of sections beginning with capital letter “S” in Table 4-1. The rut depths of the S-series sections ranged from 2.03 to 2.54 (0.8 to 1 in.) as listed in Table 4-1. From a statistical point of view, it was not viable to correlate the normalized composite aggregate shape indices of these sections to a set of rutting data varying within such a small range.

As for the North and East NCAT pavement sections, 10 of the 13 North side sections and 9 of the 10 East side sections used the same sets of aggregate blends, of which only one coarse aggregate could be processed by the UIAIA due to the light color and aggregate size requirements. These were Gadsden slag 78 for the North side sections and Columbus 7 for the East side sections. For each of the three normalized composite shape indices, i.e., F&E ratio, AI and ST indices, of the North and East side sections, the limited number of coarse aggregate types produced a set of zero to very low index values since there was only one coarse aggregate processed by the UIAIA. It was therefore not possible to develop a relationship of some statistical significance between the rutting data and each of the three aggregate shape indices.

The West side NCAT pavement sections, on the other hand, generally provided adequate data with fair to good representations of most coarse aggregate materials in the blended gradations for proper statistical analysis. To study how the defined coarse aggregate shape factors affected permanent deformation accumulation of the West side pavement test sections, statistical analyses were carried out using the West side pavement rutting data and the imaging based shape indices of the coarse aggregate materials. For establishing the independent variables, normalized composite aggregate shape indices were

computed using Equations 4-1 and 4-2 to combine the shape factors of all the coarse aggregate materials used in a pavement section into a unique index value to account for various coarse aggregate weight percentages used in different HMA lifts and individual lift thicknesses. For establishing the rut depth data listed in Table 4-1 as the dependent variables, the following assumptions were made: (i) traffic load magnitudes and repetitions were the same for all the sections (8.97 million ESALs, see <http://www.pavetrack.com>); (ii) the environmental factors, such as on-site temperature, moisture contents of the HMA and subgrade were similar throughout testing as indicated by Powell (Powell, 2001); (iii) construction issues such as compactive effort and in-place density or air voids were close and somewhat similar (Powell, 2001).

The asphalt mixture types influenced by aggregate gradations (fine, coarse, SMA, and open-graded friction courses) are actually functions of coarse aggregate shape factors, and, therefore, were included indirectly in the statistical analyses. Note that some other factors such as mix design properties and volumetrics, asphalt binder grade, asphalt content and modifier type, fine aggregate content and gradation, design gyrations, etc. most definitely influenced rutting behavior of the AC structural layer with different HMA designs and yet could not be studied using the results of the current statistical analyses on how they contribute to the different NCAT pavement section rut depth performances.

Table 4-4 presents the weight percentages of the UIAIA processed coarse aggregate materials used in the NCAT Test Track West side pavement sections selected for statistical analysis. These pavements were all sponsored by the state of Alabama and built consistently in accordance with their Superpave asphalt mix design specifications. Again, the letters “B” and “T” following the designations of sections refer to the bottom lift and top lift, respectively, and the letter “O” designates an open-graded friction course (OGFC) also used in the top lift of W3 and W5 sections.

Table 4-4 Weight Percentages of the UIAIA Processed Coarse Aggregate Used
In the NCAT West Side Pavement Mix Designs

Aggregate Designation	W2	W3O	W3B	W4B	W5O	W5B	W9	W10
Columbus 7	—	—	48	—	75	—	—	—
Gadsden Slag 78	74	75	—	—	—	—	—	—
Calera 89	10	—	—	—	—	—	—	—
Calera 7	—	20	—	82	—	82	—	—
Jemison 1/2	—	—	—	—	—	—	74	74
Jemison 1/2	—	—	—	—	—	—	10	10

Table 4-5 lists the normalized composite aggregate shape indices computed using Equations 4-1 and 4-2 to combine the shape factors of all the coarse aggregate materials used in the “W” pavement

sections into a unique index value to account for various coarse aggregate weight percentages used in different HMA lifts and the individual lift thicknesses. The normalization of the composite aggregate shape indices was done for only those West side sections listed in Table 4-5 with their rut depths presented. The normalized composite F&E ratio refers to the percent by weight of coarse aggregate with flat and elongated ratios greater than 5 to 1 (5:1).

Table 4-5 Rut Depth Data Presented with Normalized Composite Shape Indices for Selected NCAT West Side Pavement Sections

Section Designation	Rut Depth (mm)	Normalized Composite Percent by Weight with F&E Ratio > 5:1	Normalized Composite AI	Normalized Composite ST
W2	1.52	0.06	471	1.44
W3	0.51	0.09	465	1.81
W4	3.05	0.30	394	1.21
W5	2.03	0.27	407	1.33
W9	3.05	0.42	371	1.10
W10	2.79	0.42	371	1.10

Simple linear regression models were first developed to correlate the rut depth data of these selected West side sections to each of the normalized composite shape indices for the F&E ratio, AI and ST. Figure 4-3 shows the relationship obtained when the amount (percentage) of flat and elongated particles larger than 5:1 ratio was used only to predict rut depths of the West side sections. As percent of flat and elongated particles increased, rut depth predictions typically increased. Buchanan (2000) indicated recently that flat and elongated particles used in AC mixtures with F&E ratios greater than 3:1 did not significantly influence rutting behavior. For a limestone aggregate, when a low amount of flat and elongated particles at the 3:1 ratio was used, no observable influence was noted. While for a granite aggregate, this kind of influence was more apparent but still depended on the amount of flat and elongated particles used in the AC mixture. Although the amounts (percentages) of flat and elongated particles larger than 5:1 ratio given in Table 4-5 are considerably low (less than 1%), with a fairly high correlation coefficient R^2 of 0.75, Figure 4-3 shows a good linkage and significance between F&E ratios and rutting performances of NCAT West side pavement sections.

Figures 4-4 and 4-5 show the relationships obtained when the normalized composite angularity (AI) and surface texture (ST) indices, respectively, were used individually to predict rut depths of the West side sections. As expected, when both shape indices increased, rut depth predictions typically decreased. With high correlation coefficients, R^2 values of 0.80 and 0.94, these relationships establish excellent relationships between coarse aggregate angularity and surface texture and rutting performances of NCAT West side pavement sections.

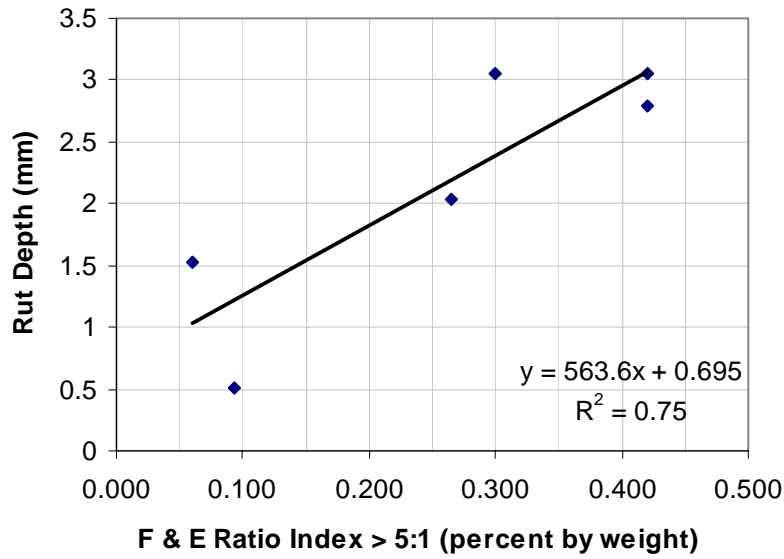


Figure 4-3 NCAT Test Track Pavement Rut Depth Data Correlated to Percent Coarse Aggregate with % F&E Ratios > 5:1

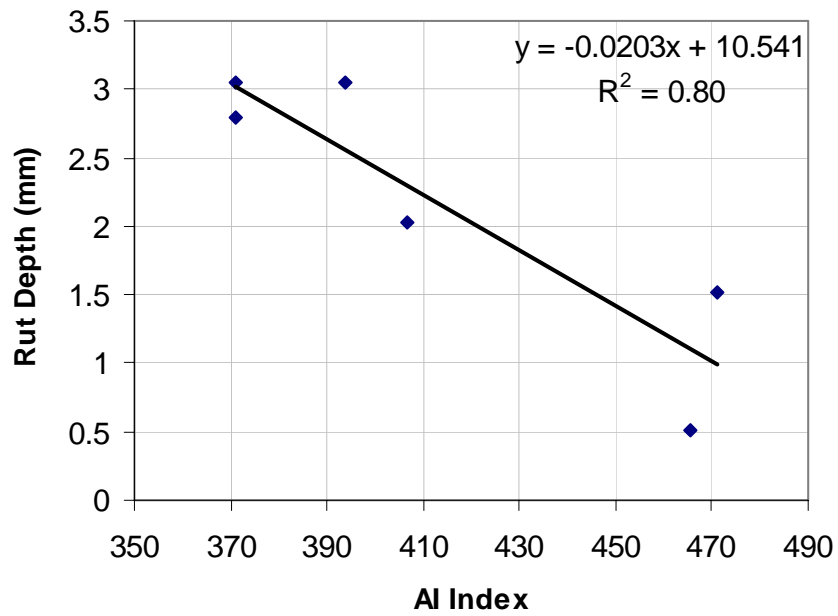


Figure 4-4 NCAT Test Track Pavement Rut Depth Data Correlated to Angularity Indices (AI) of Coarse Aggregate

Several research studies have indicated asphalt mixes having angular and rough aggregate materials to provide the highest resistance to permanent deformation accumulation (Brown and Cross,

1992; Epps et al., 2001). An earlier NCAT study by Brown et al. (Brown and Cross, 1992) showed that angular, crushed rough textured aggregates would control rutting when in-place air voids content was above 2.59 percent. Aggregate particles were considered crushed when they had two or more fractured faces. Epps et al. (2001) also successfully correlated some of the consensus aggregate properties, such as coarse aggregate angularity (CAA), fine aggregate angularity (FAA) and F&E ratios, to rut depths obtained in the WesTrack full-scale asphalt pavement test sections. Masad and Button (2000) recently recognized the effects of fine aggregate morphological properties on asphalt mixture behavior by quantifying based on imaging the angularity and surface texture properties of fine aggregates. His findings are vastly parallel to the imaging based results presented in this paper for relating coarse aggregate shape effects to rutting performances of NCAT Test Track pavements.

A multiple linear regression analysis was conducted next to evaluate the combined effects of all three imaging based coarse aggregate shape indices on the rut depth data from the NCAT West side pavement sections. The intent was to identify which of the three indices, each characterizing a certain domain in the morphological descriptive hierarch of coarse aggregate physical properties, might have influenced the most the NCAT field rutting performances. The results of the statistical analysis are given in Table 4-6, and the linear equation developed as a function of the three shape indices is presented as follows by Equation 4-3:

$$Rut\ Depth = -0.033AI - 798.840FE - 2.754ST + 21.619 + \varepsilon \quad (4-3)$$

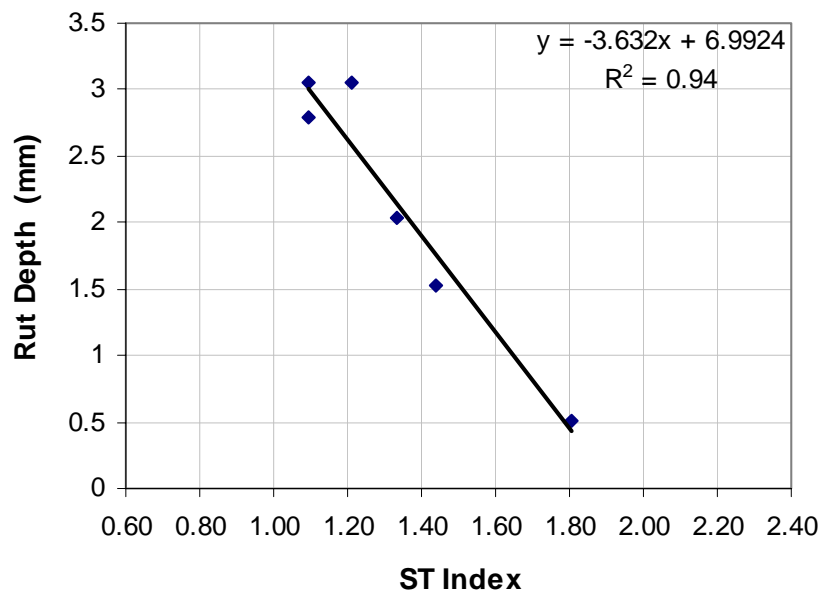


Figure 4-5 NCAT Test Track Pavement Rut Depth Data Correlated to Surface Texture (ST) Indices of Coarse Aggregate

Table 4-6. Results of the Statistical Analysis between Aggregate Shape Indices and NCAT Test Track Pavement Rut Depth Data

	Coefficients	Standard Error	t-Stat	P-value
Intercept	21.619	13.160	1.643	0.242
Normalized Composite AI	-0.033	0.028	-1.173	0.361
Normalized Composite % by Weight With F&E Ratio > 5:1	-798.840	763.669	-1.046	0.405
Normalized Composite ST	-2.754	1.091	-2.523	0.128

Table 4-6 presents in detail the results of an associated t-test, which is meaningful when used together with the obtained multiple linear regression equation (see Equation 4-3). Among the three independent variables listed in Table 4-6, the normalized composite ST index has the lowest P-value, which means that there is the least probability of denying the coefficient of ST in the multiple-linear equation compared with the coefficient of the other two shape indices. The imaging based ST index related better to the rutting data than the F&E ratio percentages and the angularity (AI) indices as shown previously in Figure 4-5 with the highest correlation coefficient R^2 of 0.94.

SUMMARY

Aggregates make up more than 95 percent of asphalt pavements of which coarse aggregate occupies by far the highest weight or volume. Morphological shape properties of coarse aggregate have been successfully linked to the strength, stability, and performance of asphalt pavements. This chapter investigated how physical shape properties of coarse aggregate used in asphalt mixtures would affect field-rutting performances of the full-scale asphalt pavement sections constructed and tested at the National Center for Asphalt Technology (NCAT) Test Track facility.

NCAT coarse aggregate materials were shipped to University of Illinois and processed by the validated image analysis system, the University of Illinois Aggregate Image Analyzer (UIAIA). Imaging based shape indices, percent flat and elongated ratio by weight, angularity index, and surface texture index, were calculated for the NCAT coarse aggregate. The computed shape indices were normalized to account for various coarse aggregate weight percentages used in different hot mix asphalt lifts and individual lift thicknesses, and correlated to the field rutting data collected from the NCAT Pavement Test Track.

Statistical analyses were performed to relate the three normalized imaging based shape indices to the rut depth data from the West side pavement sections of the NCAT Test Track. All shape indices, percent flat and elongated ratio by weight, angularity index, and surface texture index, indicated good correlations individually with the field rutting data from the NCAT Pavement Test Track with surface texture giving the highest correlation coefficient R^2 of 0.94. Among the three imaging based shape indices, surface texture related the best with the field rutting data from the NCAT Pavement Test Track, as indicated by the lowest p-value in the t-test performed for the multiple linear regression analysis.

CHAPTER 5

EFFECT OF COARSE AGGREGATE MORPHOLOGY ON PERMANENT DEFORMATION BEHAVIOR OF LABORATORY ASPHALT MIXES

Rutting resistance of asphalt concrete under traffic and environmental loads depends on the aggregate structure in the asphalt mix. Aggregate gradation and aggregate shape properties or morphology of aggregate materials have been recognized by the Strategic Highway Research Program (SHRP) among the top factors that influence the stability of hot mix asphalt (HMA). In certain asphalt mixes such as the stone mastic or stone skeleton asphalt, coarse aggregate particles are more likely to establish physical contact due to their large sizes to form the skeleton of the aggregate structure. This type of particle contact is commonly referred to as interlock and has been shown to be very effective for designing rut resistant surface courses in high volume roads. Even in dense graded asphalt mixes, coarse aggregate size and shape properties are believed to some extent contribute to the rutting resistance of asphalt concrete.

Previous research studies that realized the important role the coarse aggregate plays in the rutting behavior of HMA related aggregate structure stability to coarse aggregate morphologies. Effects of coarse aggregate morphologies on the rutting resistance of HMA have been highlighted according to different shape irregularities, such as shape, angularity, and texture, by both field observations and laboratory standard tests (Barksdale et al., 1992; Ahlrich, 1996). In these studies, asphalt mixes that included particles with angular shape and/or rough texture were found to have higher aggregate structure stability.

Review of the currently adopted standard specifications regarding the coarse aggregate shape properties and the previously performed research studies show that while there is a general understanding of the influence of aggregate shape properties on the rutting performance of HMA mixtures, the specifics have been somewhat elusive because the current methods used to characterize particle shape and surface texture are imprecise and cannot be applied across the broad range of aggregate materials without ambiguity. For example, current particle index test method for evaluating coarse aggregate morphology usually ends up indirectly measuring the different levels aggregate shape irregularities as combined effects of shape, texture, and angularity (ASTM D3398). There are currently no standard test methods for directly and objectively measuring aggregate angularity, surface texture, and surface area.

The UIAIA imaging based coarse aggregate morphological indices were successfully linked to asphalt concrete rut depths of the NCAT pavement test sections in Chapter 4. Permanent deformation or rut development in an HMA pavement surface can in fact be due to many other factors also contributing

in combinations, for example, temperature changes, moisture contents of the HMA and subgrade, mixture types influenced by aggregate gradations, mix design properties and volumetrics, and construction related factors such as field compactive effort, in-place air voids, quality control, traffic load magnitudes and repetitions, etc. Further, the behavior of asphalt mixture under traffic loading also possesses a creep nature, which cannot be studied alone based on the cumulative permanent deformations, which was essentially the case with the rut depth measurements used from the NCAT pavement test sections.

Laboratory testing with controlled applied stress conditions may provide a better insight into the aggregate structure and the coarse aggregate shape properties affecting the stability of asphalt mixes. This chapter describes permanent deformation tests performed on asphalt mix specimens prepared in the laboratory following the mix designs received from a total 10 state highway agencies, i.e., the 8 pooled fund participating states and the Central Federal Lands and Highways Division (CFLHD) providing asphalt mixes and mix designs of New Mexico and Oklahoma. The stability and deformation characteristics of the asphalt mixtures were studied by means of repeatedly applying traffic loads in a triaxial test setup. The differences in the laboratory test data, i.e., different trends in the permanent deformation accumulation with the number of load applications, were then analyzed for possible linkages to the UIAIA imaging based morphological indices of the coarse aggregate materials used in the asphalt mixes.

EXPERIMENTAL DESIGN OF THE STUDY

To set up a laboratory study and investigate effect of coarse aggregate morphology on the HMA aggregate structure and the stability of asphalt concrete (AC) pavements, aggregate morphologies that capture all the different levels of shape irregularities have to be properly taken into account together with the aggregate sizes or gradations, test temperature, asphalt binder grades, and other asphalt mix properties. In this study, regarding the coarse aggregate morphologies, the complete set of imaging based morphological indices defined in UIAIA, i.e., flat and elongated ratio (F&E Ratio), angularity index (AI), and surface texture (ST) index, was included as the aggregate shape factors. The F&E Ratio, AI, and ST are the three key shape indices that can capture the morphologies of an aggregate particle in three magnification levels, each of which is believed to control a different aspect of the rutting behavior of asphalt mixes. For example, asphalt mix designs having significant number of flat and elongated particles were found more likely to develop severe rutting due to directional orientation and/or breaking of the flat and elongated particles (Buchanan, 2000). Similarly, angularity defined by AI can be critical for the aggregate contact and interlock in the way that angular aggregate particles have higher chances of particle contact and less room for relative particle movement once the interlock is established. Furthermore, the

aggregate texture defined by ST here is known to directly influence friction between aggregate particles and hence contribute to the shear strength of the aggregate interlock.

To properly establish different coarse aggregate morphologies and investigate their effects on the aggregate structure stability of asphalt mixtures, a total of 18 Superpave volumetric HMA mix designs were included in this study. As listed in Table 3-2, the designations of the aggregates and binders received from the participating state highway agencies were used to make the laboratory asphalt mixes following the job mix formulas. The detailed aggregate gradations, percent aggregate blends, asphalt binder and air voids information, and mixing and compaction temperatures are given in Appendix I for each laboratory asphalt mix design summarized from the corresponding state highway agency job mix formula sheet. The HMA mix designs and the asphalt concrete ingredients, materials were received from a total 10 state highway agencies, i.e., the 8 pooled fund participating states and the Central Federal Lands and Highways Division (CFLHD) providing asphalt mixes and mix designs of New Mexico and Oklahoma.

Table 5-1 shows the 18 mix designs designated according to the State abbreviation indicating each mix is used by the corresponding highway agency. These asphalt mixes show diversity in terms of the percent coarse aggregate blends, the asphalt binder PG grade, and the final aggregate gradations. The type of aggregate gradation chosen for a specific asphalt mix design no doubt has a major influence on the mix properties and performance.

Fine- or coarse-graded asphalt mixtures, having either more fine aggregate or more coarse aggregate in the mix, respectively, often result in different rutting performances under traffic loads. This effect was highlighted many times in the literature; for example, by the NCAT stone mastic asphalt (SMA) and the work of Seward et al. (Kandhal and Cooley, 2002; Seward et al., 1996). To design a stable aggregate structure in an asphalt mix, Superpave mix design requires that the gradation of the aggregate structure go above or below the restricted zone as indicated on the Superpave aggregate gradation chart with the sieve sizes expressed as raised to 0.45 power on the x-axis. Nevertheless, there are still contradicting research findings about the influence of gradation on the HMA behavior, such as the study conducted at the NCAT facility, which showed no significant differences between the rutting performances of coarse- and fine-graded Superpave mixtures (Kandhal and Cooley, 2002).

To investigate the effect of gradation on the stability of asphalt mix specimens and the aggregate structure, a total of 18 asphalt mixes, obtained from the 10 state highway agencies, were grouped into 2 main categories according to the aggregate gradation curves used in the mixes. The first category considered those mixes with the gradation curves passing below the restricted zone (BRZ), while the second category grouped the other mixes whose aggregate gradation curves were either going through or above the restricted zone (TRZ or ARZ). Table 5-1 shows the final gradation types in the asphalt mix

designs indicated by TRZ, ARZ, and BRZ. The gradation curves of all the 18 mixes satisfied the maximum density line requirements by passing between the control points as required by the Superpave volumetric HMA mix design.

Table 5-1 Mix Designs and Permanent Deformation Results of the Laboratory Superpave HMA Specimens

Mix Design Designation	Binder Grade	% Coarse Aggregate	Gradation	FN_{log}	SS	PS
CFLHD-NM	PG 58-34	48.0%	TRZ	3.015	1.10E+01	10.30
CFLHD-OK	PG 70-28	33.0%	ARZ	2.913	1.30E+01	1.06
GA1	PG 67-22	56.0%	BRZ	3.712	9.87E+00	4.19
GA2	PG 76-22	46.0%	BRZ	3.789	3.35E+00	3.74
GA3	PG 76-22	58.0%	TRZ	3.564	1.19E+01	3.24
IN1	PG 64-22	53.0%	BRZ	2.740	1.73E+01	26.99
IN2	PG 64-22	63.0%	BRZ	2.493	2.01E+01	32.17
MN1	PG 64-22	51.0%	BRZ	4.143	5.00E+00	30.97
MN2	PG 58-28	60.0%	TRZ	2.225	1.94E+01	30.96
MO1	PG 70-22	76.0%	BRZ	3.269	1.30E+01	2.09
MO2	PG 64-22	90.0%	BRZ	3.974	3.03E+00	17.13
MO3	PG 64-22	77.1%	BRZ	3.269	1.19E+01	4.75
MS1	PG 67-22	90.0%	TRZ	2.125	2.08E+01	7.60
MS2	PG 67-22	59.0%	TRZ	3.081	1.49E+01	21.67
MT1	PG 58-28	64.0%	BRZ	4.008	7.09E+00	10.48
MT2	PG 70-28	52.0%	BRZ	4.618	1.04E+00	1.46
SC1	PG 76-22	65.0%	BRZ	5.227	7.00E-03	12.15
SC2	PG 67-22	73.0%	BRZ	4.115	5.17E-01	1.56

To isolate the effects of coarse aggregate shape and size properties on the permanent deformation characteristics of AC pavements, Kandhal and Parker (1998) indicated that the fine aggregate content and gradation would need to be similar in all AC mixes studied. To minimize the influence of different asphalt PG-grade binders used in the 18 asphalt mixes, the permanent deformation tests were performed at a temperature of approximately 50° C. Such a high temperature was selected to better bring out the influence of aggregate shape properties and also to address how permanent deformation buildup would vary in the different mixes according to gradation, aggregate morphological properties and the aggregate structure. Further, this temperature also represents a possible average 7-day highest temperature of the year at which pavement ruts can develop the fastest in North America.

PERMANENT DEFORMATION TESTING OF ASPHALT MIXES

Phase II of the research project involved preparation and testing of asphalt concrete mixes made using the aggregate samples collected from the participating States and the FHWA Central Federal Lands and

Highways Division. The laboratory evaluations of the Superpave asphalt mix performances were performed at the University of Illinois Advanced Transportation Research and Engineering Laboratory (ATREL). Three Superpave gyratory asphalt specimens were made for each asphalt mix design. Two of the specimens were tested for permanent deformation accumulation in the specimens with increasing number of load applications. The following sections give details of the specimen fabrication and laboratory triaxial testing for characterizing permanent deformation behavior of the 18 asphalt mixes.

Specimen Preparation and Testing

The asphalt mix designs, given in Appendix I, were used to fabricate specimens for permanent deformation testing at ATREL. The asphalt mixtures were prepared strictly following the SuperPave volumetric mix design specifications. To minimize test sample disturbance, which usually occurs due to sawing or cutting of an asphalt specimen from Superpave gyratory compactor (SGC), the 150 mm (6-in.) high by 150-mm (6-in.) in diameter specimens were produced directly in the SGC. All the specimens were compacted to a 7% laboratory final air void content, which is a rather high value, but commonly measured in the newly paved field AC layers. The intention was to make the findings from this research study practically relevant to the field condition of the newly paved asphalt surface courses. Therefore, to produce in the laboratory an asphalt specimen at 7% air voids, the following equation was used to compute the amount of asphalt concrete to go in the 150-mm (6-in.) high by 150-mm (6-in.) in diameter gyratory mold:

$$M_{HMA} = G_{mm} \gamma_w \left(1 - \frac{(\text{AirVoid}(\%) + CA_{\text{initial}}(\%))}{100} \right) * \text{Area} * h \quad (5-1)$$

where

M_{HMA} = weight of the asphalt specimen at 7% air void content;

G_{mm} = maximum specific gravity of asphalt mixture (no air voids);

γ_w = density of water = 1000 kgf/m³ = 10⁻³ grf/mm³;

Area = area of the mold base, mm² = $\frac{\pi(150)^2}{4} = 17,671.5$ mm²;

h = 150 mm, height of the gyratory sample.

With the advantage to simulate realistic dynamic loading of highway traffic in the laboratory, repeated load permanent deformation tests have become popular in measuring the rutting potential of asphalt mixes. Two types of repeated load permanent deformation tests commonly used in laboratories

are the unconfined and the confined tests. The confined test additionally applies a confining pressure to the HMA specimen during testing. From both types of tests, the permanent deformation behavior of an asphalt mixture specimen can be characterized by a series of test parameters, i.e., flow number (FN) and slopes of the three permanent deformation accumulation phases as the primary slope (PS), the secondary slope (SS) and the tertiary slope (TS) as shown in Figure 5-1. Of the four test parameters, the flow number (FN) that measures the stability of the mixes has been evaluated and recommended as one of the most important parameters to characterize the rutting susceptibility of HMA (Witczak et al., 2002).

The laboratory permanent deformation testing was performed using an Industrial Process Controls (IPC) universal testing machine, UTM V2.23B39, with an environmental chamber temperature controlled setting at 50° C. Figure 5-2 shows a photo of the repeated load triaxial setup used in permanent deformation testing of the asphalt specimens at ATREL. The load was applied by lowering the ram on to the specimen and by repeatedly applying an axial stress level measured by the load cell and maintained by the feedback controller and the data acquisition system. The axial deformations were measured on top of the specimen through two LVDTs, which were mounted vertically on diametrically opposite specimen sides. To simplify the test procedure, the unconfined test was adopted with a low axial stress level of 138 kPa (20 psi) to simulate a low-end highway traffic loading. Such a low stress corresponded to only a fraction of the asphalt mix strength thus preventing any premature shear failure. The load cycle consisting of a 0.1-second haversine pulse load and a 0.9-second rest period was applied to each specimen. All the specimens were tested until collapse. Results from the repeated load tests were presented in terms of the Cumulative Permanent Strain (CPS) versus the number of loading cycles as shown in Figure 5-1.

Permanent Deformation Test Results of the Asphalt Mixes

Each of the 18 cumulative permanent strain curves in the unconfined repeated load permanent deformation tests was found comprising of three phases as shown in Figure 5-1, i.e., the primary phase, the secondary phase, and the tertiary one. The primary phase is usually referred to as densification, in which aggregate particles get closer and air is expelled at a high rate. The primary phase occurs with a quick volume drop in the specimen due to the relatively loose state of the mixture materials. Therefore, this phase does not stand many load repetitions. During the secondary phase, the specimen volume continues dropping, however at a much lower rate than that occurs in the primary phase. During the tertiary phase, the specimens were observed experiencing quick vertical deformation due to the shear failure that involved very little volume change. The load cycle number at which tertiary flow started was judged as the so-called flow number (FN). Since in the tertiary phase, the vertical permanent deformation

developed at a much higher rate than those occurred during the primary and secondary phases, FN was also referred to as the critical point in evaluating the stability of the asphalt specimen and it measures the number of load repetitions the specimen can sustain before shear failure. At the set environmental chamber temperature of 50°C, the asphalt specimens that sustained high load repetitions before the flow number were therefore believed to possess stronger aggregate structures than those sustained low load repetitions before the flow number.

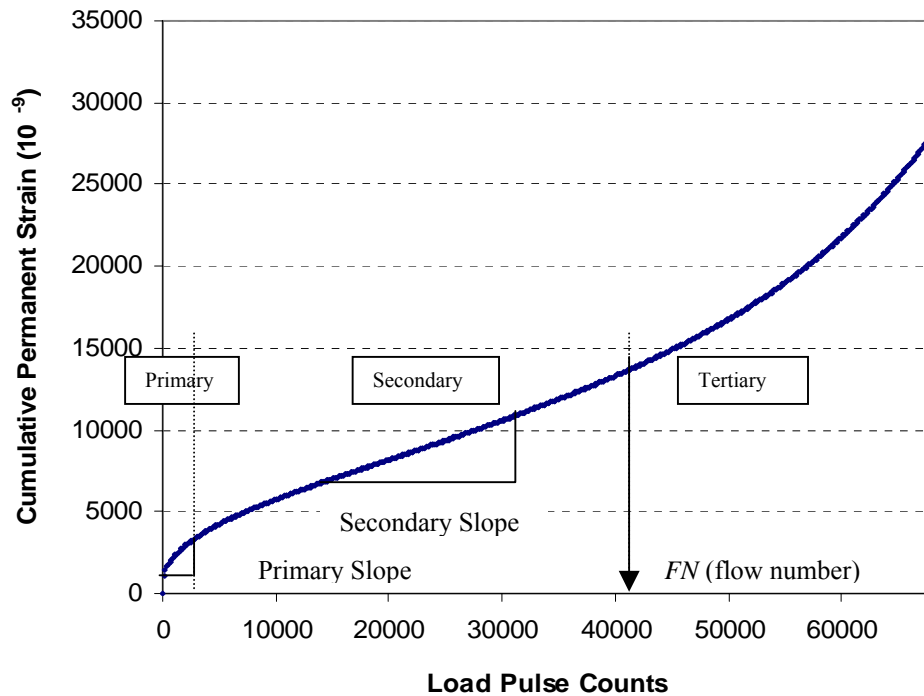


Figure 5-1 Schematic of Permanent Strain Accumulation in a Repeated Load Triaxial Test

Figure 5-3 shows three typical ranges of the Cumulative Permanent Strains (CPS) varying with the number of loading cycles from testing of the 18 asphalt mixes. Range I corresponds to a high measurement of CPS before FN with high measurements of primary and secondary slopes and a low measurement of FN as shown in Figure 5-3. Asphalt mix designs falling into this category usually have weak aggregate structure and fail fast. Among the 18 mix designs, CFLHD-NM and MN2, for example, belonged to this range. Range II typically indicates a low measurement of CPS before FN with low measurements of primary and secondary slopes and a high FN. Such a mixture is also deemed to be good. Among the 18 mix designs, CFLHD-OK and GA2, for example, belonged to this range. Finally, Range III gives a moderate CPS before FN with a moderate measurement of FN and either a high primary slope or a secondary slope as shown in Figure 5-3. All the other 14-mix designs of the 18 fell into this category.



Figure 5-2 Repeated Load Triaxial Setup Used in Permanent Deformation Testing of Asphalt Specimens at ATREL

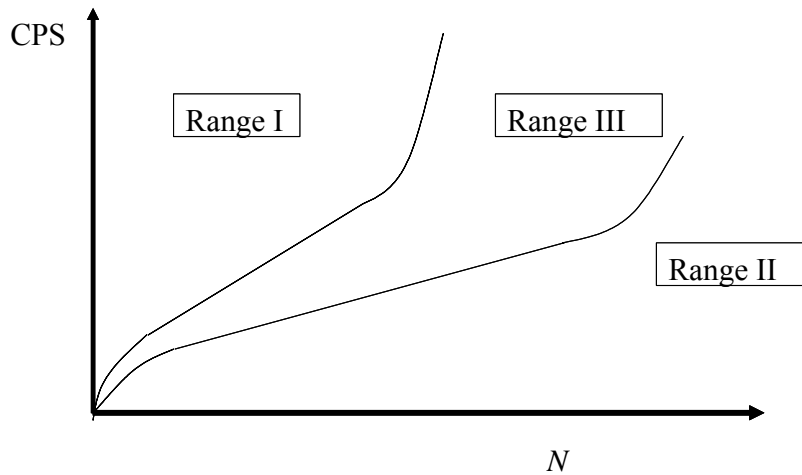


Figure 5-3 Typical Ranges of Cumulative Permanent Strains with Number of Load Applications

To quantify the permanent deformation features of the mixes and relate them to the imaging based aggregate morphologies, the flow number FN was included as a major parameter since it measures the load repetitions of the specimen before failure. The primary slope PS and the secondary slope SS characterize the rate of vertical permanent deformation under the repeated loads, which were believed to be related to the morphologies of the coarse aggregate and were therefore adopted to characterize the

primary phase and the secondary phase, respectively. Since the tertiary phase characterized the behavior of the specimen after shear failure, it was of no significance and was not considered in this study. Table 5-1 gives the flow number FN logarithm, the primary slope PS, and the secondary slope SS with the mix design information. Note that these are the average results obtained from testing two samples of each asphalt mix design.

IMAGING INDICES OF COARSE AGGREGATE BLENDS IN ASPHALT MIXES

Following the test procedures previously established for the UIAIA system, imaging based results of the F&E Ratio, angularity AI and surface texture ST indices were obtained for the coarse aggregate materials also used in making the asphalt specimens for permanent deformation testing. Due to the varying combinations or blends of coarse aggregate materials used for each of the 18 mix designs, a composite aggregate shape index was defined for one HMA mix design to account for all the different coarse aggregate materials used in that mix. This composite index was for any of the three key imaging shape indices, F&E ratio, angularity AI, or surface texture ST indices. The following formula shown in Equation 5-2 was used in the definition of the composite aggregate shape index:

$$Composite\ Index = \frac{\sum_{i=1}^n [(a_i)(index_i)]}{\sum_{i=1}^n (a_i)} \quad (5-2)$$

where *Composite Index* is the composite aggregate shape index for a certain HMA mix design, which is a weighted sum of the individual mean indices of the UIAIA-processed coarse aggregate materials used in the design; the variable a_i is the percentage by weight of the i^{th} coarse aggregate material used in the design; the variable $index_i$ is the mean imaging based index of the i^{th} coarse aggregate material used in the design; and finally the summation counter n is the number of the coarse aggregate materials used in that design, which may be 1, 2, 3 or 4 for each of the 18 mix designs, depending on the number of coarse aggregate materials used in that design (see Appendix I) and processed by the UIAIA. The composite indices for the eighteen mix designs are listed in Table 5-2.

With the parameters measured from the permanent deformation tests, i.e., the flow number FN, the primary slope PS, and the secondary slope SS, possible influences of the coarse aggregate morphologies on the HMA stability and the aggregate structure of the 18 asphalt mixes was studied through a series of regression analyses. The three imaging based indices of each

mixture, i.e., the F&E ratio, angularity index AI, and surface texture ST indices, were correlated to the individual test parameters of the corresponding asphalt mixture specimen. Results of the statistical correlations are presented in the following sections.

Table 5-2 Imaging Based Composite Indices of the Coarse Aggregate Blends of the Asphalt Mix Designs

Mix Design Designation	Composite F&E Ratio>5:1	Composite AI	Composite ST
CFLHD-NM	0.9% by weight	442	2.00
CFLHD-OK	2.7%	524	2.46
GA1	0.1%	446	1.71
GA2	0.3%	503	2.03
GA3	0.1%	446	1.71
IN1	0.0%	430	1.37
IN2	0.0%	429	1.44
MN1	1.5%	540	1.75
MN2	0.2%	429	1.42
MO1	0.9%	417	1.44
MO2	0.2%	522	2.26
MO3	0.0%	442	1.45
MS1	0.0%	403	1.33
MS2	0.5%	479	1.82
MT1	1.3%	469	2.09
MT2	1.4%	519	2.10
SC1	0.6%	550	2.56
SC2	2.3%	519	2.25

DATA ANALYSIS

To better interpret the test results for the measured permanent deformation parameters, the flow numbers, FN, of the 18 specimens were taken logarithms and the data analyses were performed using the logarithms of the flow numbers denoted as FN_{\log} (see Table 5-1). For each mix design, in order to link the coarse aggregate morphologies to the permanent deformation test parameters, a total of nine regression analyses had to be performed between the three morphological indices and the three test parameters. Before performing the regression analyses, screening t-tests were performed for each of the permanent deformation test parameters as dependent variables and the independent variables, coarse aggregate morphological indices, to screen out the pairs that have a *P-value* higher than the specified significance level of 5% ($\alpha = 0.05$). These pairs were judged as having poor correlations between the dependent and the independent variables. Results of the t-tests are given in Table 5-3, in which only the

four pairs underlined were selected for further regression analysis since they had the lowest P-value and indicated the least probability of denying meaningful correlations.

Table 5-3 Screening t-test for Regression Analysis

Regression Pairs	<i>t-Stat</i>	<i>P-value</i>
FE-PS	-1.39	1.85E-01
FE-SS	-1.94	7.03E-02
FE-FN	1.12	2.79E-01
AI-PS	-0.42	6.82E-01
<u>AI-SS</u>	-5.81	<u>2.65E-05</u>
<u>AI-FN</u>	4.38	<u>4.65E-04</u>
ST-PS	-1.57	1.36E-01
<u>ST-SS</u>	-4.76	<u>2.11E-04</u>
<u>ST-FN</u>	3.44	<u>3.33E-03</u>

Correlations of Coarse Aggregate Morphologies with the Primary Slope

In the screening t-tests, the composite coarse aggregate morphologies were very poorly correlated to the primary slope PS for the eighteen asphalt mixes. A possible explanation could be that the mixture materials at the initial air voids content of 7% were in a comparatively loose state in the primary phase. The coarse-to-coarse and fine-to-coarse particle contacts were probably at very low levels when compared to those established in the secondary phase. Therefore, little or no particle contacts were probably observed in these dense-graded asphalt mixes for the aggregate structure to show any resistance against the applied load. Accordingly, the coarse aggregate morphologies indicated poor correlations with the primary slope.

Correlations of Coarse Aggregate F&E Ratio with HMA Stability and Aggregate Structure

It is well accepted that AC surface course rut depths tend to increase as the percentage of flat and elongated particles in the asphalt mixture increases. Recent research has indicated that flat and elongated particles used in asphalt mixes with F&E ratios greater than 3:1 did not significantly influence rutting behavior (Buchanan, 2000). The SHRP Superpave program, however, allows no more than 10% by weight of those particles having an aspect ratio greater than 5:1 for aggregate blends used in asphalt concrete pavements that have greater than 3 million equivalent single axle loads (ESALs) in the design life.

In the screening t-tests, the composite percentages of flat and elongated particles in the 18 asphalt mixes were very poorly correlated to the primary slope, secondary slope and the flow number. This

phenomenon could be attributed to the fact that flat and elongated particles in general occupied a very low proportion in all the mix designs. As shown in Table 5-2, aggregate particles with F&E ratios greater than 5:1 actually constituted much lower than 10% by weight in all the 18 mix designs with the largest being 2.7% for the CFLHD-OK mix. Therefore, there was apparently a very little chance that any particle breakage and/or directional orientation under applied repeated loading would happen in these mixes.

Correlations of Coarse Aggregate Angularity with HMA Stability and Aggregate Structure

In the screening t-test, the angularity AI index was found to correlate well with the logarithm of the flow number FN_{log} and the secondary slope SS from the permanent deformation tests. To further investigate the mechanism of coarse aggregate angularity affecting these two permanent deformation test parameters of asphalt mixes under repeated loads, two regression analyses were performed, one between the FN_{log} and the AI and the other one between the SS and the AI.

Figures 5-4(a) and 5-4(b) show the composite AI correlations for FN_{log} and SS, respectively. Figure 5-4(a) presents a somewhat decent linear relationship with a correlation coefficient R^2 of 0.54 between the flow number FN_{log} and the AI index for all the 18 asphalt mixes. As the composite AI index increases for all the mixes, the flow number FN_{log} also steadily increases. Therefore, using in asphalt mixes more of the angular or better-crushed coarse aggregate particles (having 2 or more crushed faces) can improve the stability of the HMA and its aggregate structure. To further investigate the influence of aggregate gradation on the possible improvement of the relationship between the FN_{log} and AI, separate regression analyses were also performed for the different category mix design aggregate gradations given in Table 5-1. Accordingly, the results of the regression analyses are given in Figure 5-4(b) for: (i) mixes that had aggregate gradation curves designated as below the restricted zone (BRZ) and (ii) mixes that had aggregate gradation curves designated as through and above the restricted zone (T-ARZ). For the BRZ mixes, the relationship between the FN_{log} and AI was greatly improved as indicated by the higher coefficient of determination R^2 of 0.73. Yet, for the T-ARZ mixes, the regression performed between the FN_{log} and AI was found to be extremely poor giving only low coefficient of determination R^2 of 0.094, which indicated that there was no measurable relationship between FN_{log} and AI for the TRZ and ARZ mixes. This finding is indeed very reasonable considering that the mixes with BRZ aggregate gradations have higher percentages of larger sized aggregate particles and therefore higher chances of providing aggregate particle interlock and stone-on-stone contacts to carry the load similar to the aggregate skeleton formed in the SMA type mixes.

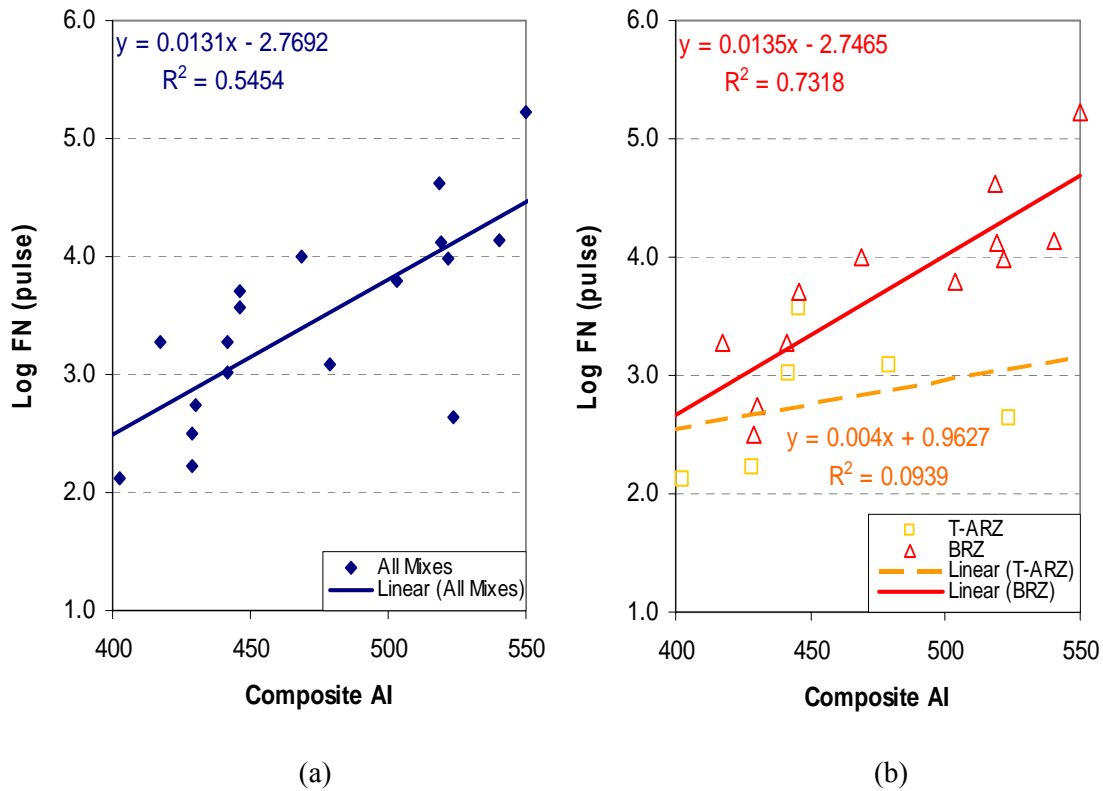


Figure 5-4 Correlations between Log (FN) and Composite AI for the 18 Asphalt Mixes

To determine how coarse aggregate angularity would affect the rate of vertical permanent deformation, another set of separate regression analyses was performed between the secondary slope SS and the composite AI. The results are shown in Figures 5-5(a) and 5-5(b) together with the corresponding regression equations and the correlation coefficients. The findings, in general, indicate that the asphalt mixes containing more angular coarse aggregate particles possessed stronger aggregate structures and higher stability. Moreover, the SS-composite AI correlation with an R^2 of 0.6785 was even better than that observed between the FN_{log} and AI for all the mixes. Similarly, a high correlation coefficient R^2 of 0.81 was obtained for the mixes that had BRZ type aggregate gradation curves. The slight improvements in the correlations might indicate that the angularity property of coarse aggregate was more pronounced and controlling in the secondary stage of permanent deformation accumulation.

Correlations of Coarse Aggregate Texture with HMA Stability and Aggregate Structure

In the screening t-tests, the surface texture ST indices of the UIAIA processed coarse aggregate were also correlated well to the flow number FN_{log} and the secondary slope SS from the permanent deformation test data. Accordingly, separate correlations through linear regression

analyses were established between the FN_{log} and composite ST and the SS and composite ST. The results are presented in Figures 5-6 and 5-7 together with the corresponding regression equations and the correlation coefficients.

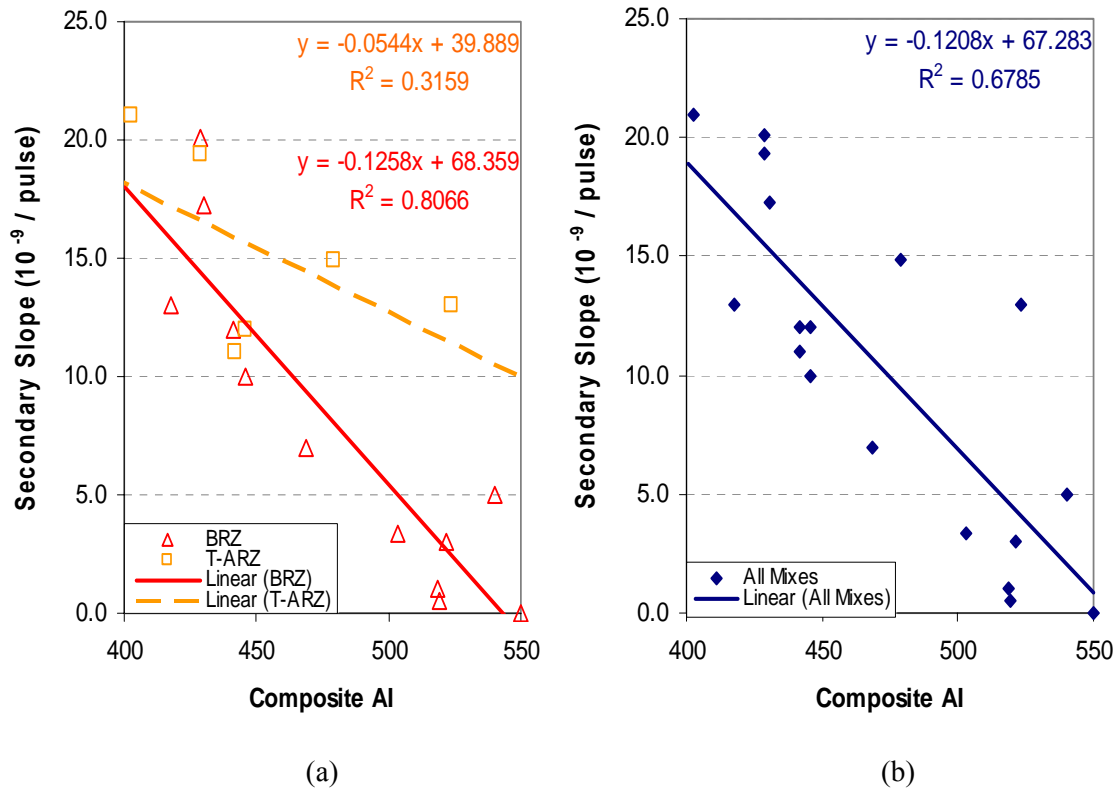


Figure 5-5 Correlations between Secondary Slope (SS) and Composite AI for the 18 Asphalt Mixes

In Figure 5-6(b), an overall positive trend in the way the composite ST was linked to the FN_{log} parameter can be easily identified. The asphalt mixes containing rougher textured aggregate particles possessed possibly stronger aggregate structures and higher stability or longer lives. Also, this relationship appeared to be significantly affected by the gradation of the aggregate structure as shown in Figure 5-6(a). The regression analysis performed between the FN_{log} and composite ST index for the BRZ mixes gave a higher coefficient of determination R^2 of 0.77. However, the FN_{log} and ST index for those mixes that went through or above the restricted zone (TRZ and ARZ) still yielded a low regression coefficient of R^2 of 0.12 indicating that there was no measurable relationship between the coarse aggregate surface texture and permanent deformation behavior for these mixes.

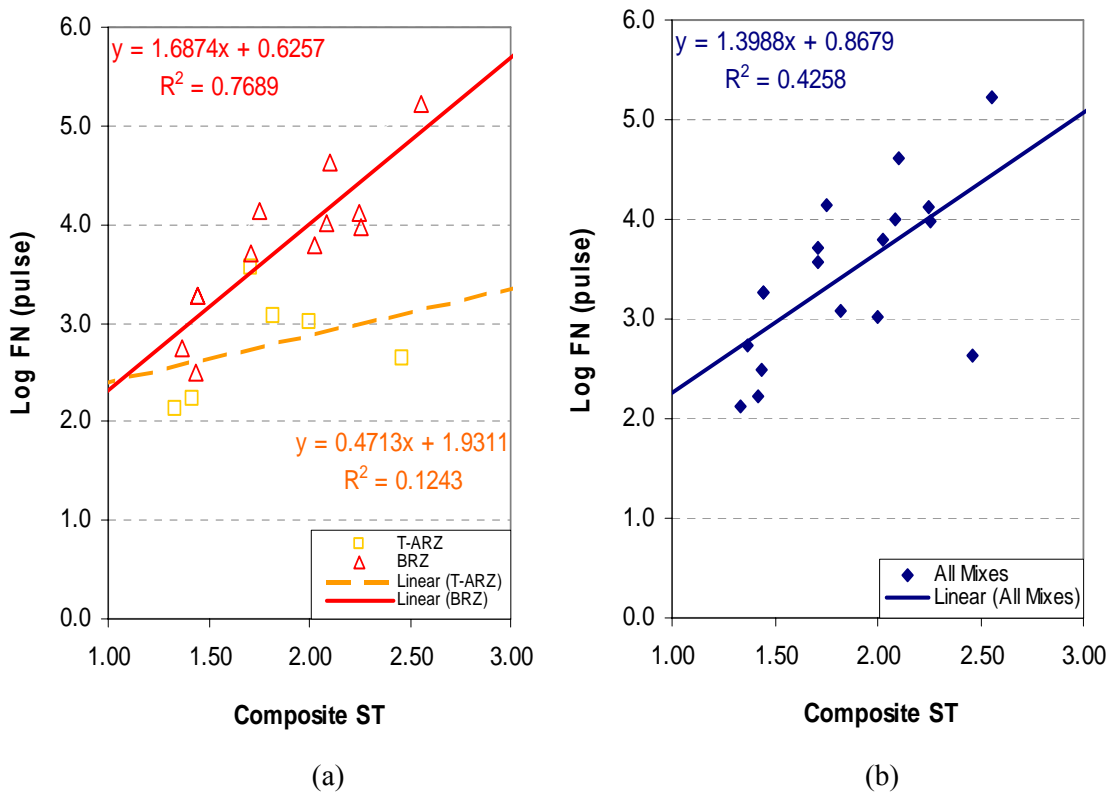


Figure 5-6 Correlations between Log (FN) and Composite ST index for the 18 Asphalt Mixes

The secondary slope SS was next related to the composite ST indices. As shown in Figure 5-7(b), the ST index gave inverse correlations with the secondary slope SS for all the mixes, which further demonstrated that asphalt mixes containing aggregate particles with rougher texture possessed better rutting resistance. The relationship between the SS and composite ST index also appeared to be significantly affected by the gradation of the aggregate structure as shown in Figure 5-7(a). The contribution of a higher ST index to a better HMA stability and longer performance life was obvious for the BRZ mixes. However, contrary to what was observed in the SS-composite AI relationship, a more decent correlation was also found between the SS and composite ST index for the TRZ and ARZ mixes, which can be attributed to a possible bigger influence of surface texture than angularity on the rutting performances of the TRZ and ARZ mixes.

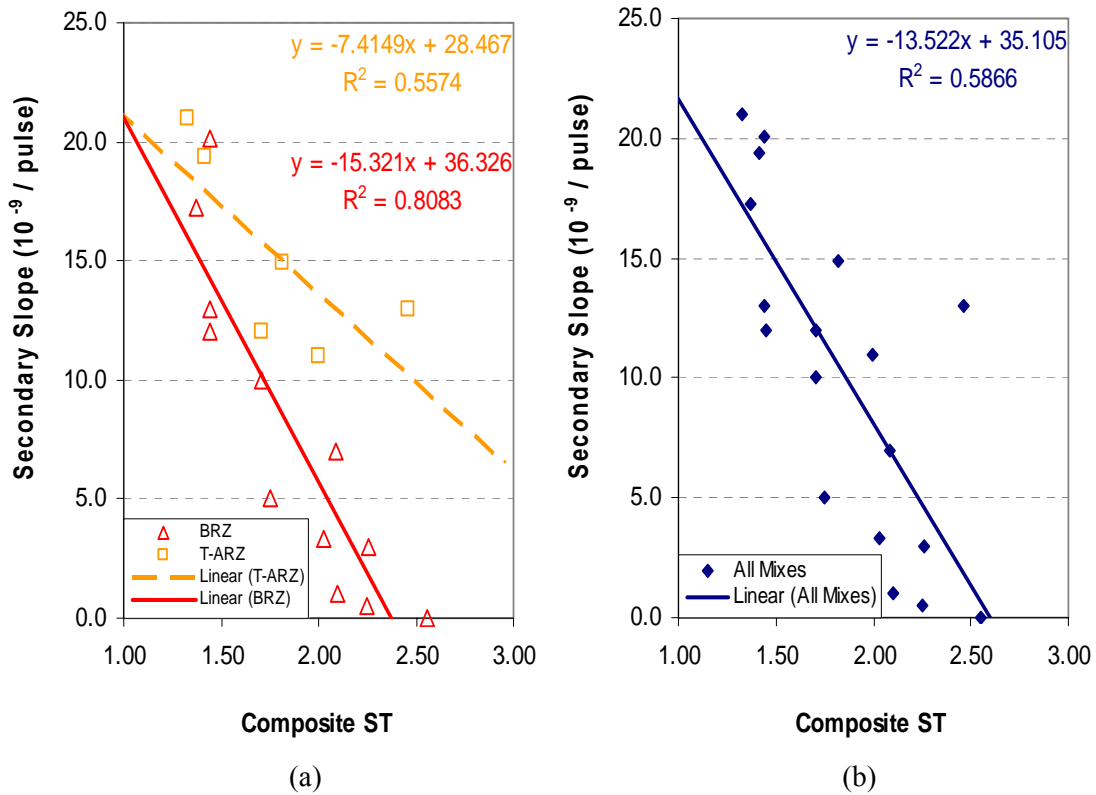


Figure 5-7 Correlations between the Composite ST and the Secondary Slope (SS)

Possible Mechanism of Coarse Aggregate Morphologies Affecting HMA Stability and Aggregate Structure

In studying an asphalt mixture’s rutting resistance, three phases of this composite material can be identified as the coarse aggregate particles, fine aggregate particles, and the mastic. The mastic phase consists of the asphalt binder, air voids, and a small amount of solid fines or fillers (passing 0.075 mm or No. 200 sieve in mechanical sieve analysis). Both the coarse aggregate phase and the fine aggregate phase have a high uniformity in composition and high physical stiffness and resistance to permanent deformation. Having a composite nature and a much lower stiffness, the mastic material has a higher potential to generate permanent deformation under traffic loads and therefore has a minor contribution to the rutting resistance of asphalt mixture compared to that of the two aggregate phases.

The coarse aggregate particles in asphalt mixes refer to the portion of aggregate retained above the No. 4 sieve in the mechanical analysis. As discussed in the introductory paragraphs, due to the dominant usage and big particle sizes, coarse aggregate particles contribute more to the rutting resistance of HMA through particle interlock. However the effect of the fine aggregate phase on the rutting

resistance of HMA is also important. Fine aggregate particles refer to the portion between No. 4 sieve and No. 200 sieve in a mechanical sieve analysis, which are usually used as the intermediate sized materials filling the voids between the coarse aggregate particles. Research studies based on conventional laboratory tests have reported contradictory findings about fine aggregate contributions to rutting performances of asphalt mixes (Ahlrich, 1996; Kandhal and Cooley, 2002).

Based on the data analysis, which involved the complete set of coarse aggregate morphologies and the measured features of the permanent deformation tests, a mechanism of coarse aggregate morphologies affecting the aggregate structure stability of asphalt mixture can be proposed in terms of the geometrical interference of aggregate particles in the asphalt mixture. This concept of Particle Geometrical Interference in HMA (PGI-HMA), as such termed here in this study, can be possibly used to characterize the behavior of different asphalt mixes under traffic loads considering compositions and interactions of the coarse aggregate with the fine aggregate and the asphalt binder or mastic. Note that PGI-HMA is different from the concept of interlock in asphalt mixes.

Interlock characterizes behavior of a group of physically connected particles, which possess a somewhat stable structure and allows little relative movement between the particles. In asphalt mixtures having such an aggregate skeleton, such as the SMA mixes, the interlock occurs mainly among coarse aggregate particles, or among coarse aggregate particles with a small portion of fine aggregate particles. The PGI-HMA concept, on the other hand, characterizes all kinds of physical interactions between aggregate particles of any size contained in the assembly of granular materials under applied traffic loads and its level of intensity determines the stability of HMA and the aggregate structure.

The PGI-HMA concept is based on the three types of aggregate particle interactions, i.e., coarse-to-coarse aggregate interaction, the fine-to-coarse aggregate interaction, and the fine-to-fine aggregate interaction. Accordingly, coarse aggregate interlock only accounts for part of the aggregate structure stability. Any level of the PGI-HMA depends on the magnitude of traffic or shear loading as well as the volumetric and morphological properties of the component aggregates, such as the particle size, percent in the aggregate blend, gradation, angularity, and texture properties. What happens in the aggregate matrix of an asphalt mixture is also related to aggregate interactions that exist with respect to the fine aggregate particles, i.e., the fine-to-coarse interaction and the fine-to-fine particle interaction. These two types of aggregate interactions in asphalt mixes are more complicated than the coarse-to-coarse particle interlock and have not been clearly understood so far. Further, the fine-to-coarse particle interaction can prevent the interlocking among the coarse particles but at the same time can provide the load transfer through HMA by the physical connections established between any separated coarse aggregate particles. This bridging helps set up interlock among separately located coarse particles. This type of interlock through fine-to-coarse particle touch is of a minor level in the aggregate matrix due to the ease of fine particle to displace

and rotate. Moreover, the fine-to-fine particle interaction contributes even less to the stability of aggregate structure due to the greater ease for movement in the aggregate assembly.

The BRZ mixes studied in the previous section had higher percentage of coarse aggregate particles than the TRZ and ARZ mixes. Therefore, relatively lower FN values observed from the TRZ and ARZ mixes when compared to the BRZ mixes suggested that the interlock among the coarse aggregate particles is an important factor for the rutting resistance of asphalt mixes. The significance of interlock among the coarse aggregate particles was further highlighted by the greater sensitivity the AI-FN, AI-SS, ST-FN, and ST-SS relationships showed with changes in the gradation characteristics of the 18 asphalt mixes.

Although both the angularity and surface texture indices of the coarse aggregate were better correlated to the permanent deformation trends in the BRZ mixes than in the TRZ and ARZ mixes, these two morphological properties possibly played different roles in the overall PGI-HMA concept. Angularity represents the irregularity of particle surface in a magnitude much higher than the texture. High stress concentrations often exist at sharper corners in the contacting angular aggregates, which make interlock the primary mechanism for stability. On the other hand, surface texture measures roughness of the particle surface, which rests on a much smaller, micro scale compared to angularity. Surface texture contributes to the stability of aggregate structure by increasing the chance of its “short-range” interactions at the contacting interface of particles, such as the van der Waals attraction, primary valence attraction, and bonding, etc. These short-range interactions, if between two touching aggregate particles, are often quantified by the coefficient of friction due to a given level of normal stress at the contacting interface of the particle surface. Hence, both angularity and surface texture work through particle contact, and gradation tends to equally affect the contributions of coarse aggregate angularity and surface texture to interlock.

The mechanism is probably different when the asphalt mixes are moving towards finer gradations with less coarse aggregate usage as in the TRZ and ARZ mixes. This time, fine aggregate interaction particle becomes more important in the PGI-HMA concept. There are more short-range interactions established at the fine-to-coarse and fine-to-fine interfaces. However, with the lower levels of stress concentration that can be tolerated at these fine-to-coarse and fine-to-fine interfaces, the rutting resistance and the stability of HMA as a function of the aggregate structure is reduced when compared to the coarse asphalt mixes. This was indeed shown clearly when surface texture ST index better characterized the platform where fine-to-coarse interactions occurred, i.e., the ST showed higher correlation to the SS than the AI for the TRZ and ARZ mixes. It is still possible that in some asphalt mixes that use fine particles of extreme morphologies, the interactions at the fine-to-coarse and/or the fine-to-fine interfaces influencing the behavior can be significant enough to mask the effect of coarse aggregate interlock. This may explain

why some previous studies showed similar rutting behavior for the different BRZ, TRZ, and ARZ mixes regardless of the different aggregate gradation characteristics.

SUMMARY

This chapter investigated relationships between the imaging based coarse aggregate morphologies and the stability or permanent deformation behavior of asphalt mixtures prepared using the same coarse aggregate materials. There were a total of eighteen HMA specimens prepared in the laboratory following the mix designs received from a total 10 state highway agencies, i.e., the 8 pooled fund participating states and the Central Federal Lands and Highways Division (CFLHD) providing asphalt mixes and mix designs of New Mexico and Oklahoma. The stability and deformation characteristics of the asphalt mixtures were studied by means of repeatedly applying traffic loads in a triaxial test setup. The differences in the laboratory test data, i.e., different trends in the permanent deformation accumulation with the number of load applications, were then analyzed for possible linkages to the UIAIA imaging based morphological indices of the coarse aggregate materials used in the asphalt mixes. The effects of the AI and ST indices on the permanent deformation were especially significant when the test results were evaluated according to the aggregate gradations. The F&E ratio index, however, showed no measurable effect on the permanent deformation due to low percentages of flat and elongated particles used in all the specimens. Based on these findings, a possible mechanism of coarse aggregate morphology affecting the stability of asphalt mixture was proposed as defined by the concept of Particle Geometrical Interference in HMA (PGI-HMA). The PGI-HMA considers all HMA coarse and fine aggregate particle interactions including the asphalt mastic and attempts to explain possible different effects of the aggregate angularity and surface texture properties on HMA stability and aggregate structure in the study of asphalt pavement field rutting behavior.

CHAPTER 6

EFFECT OF COARSE AGGREGATE MORPHOLOGY ON RESILIENT MODULUS OF ASPHALT MIXES

The coarse aggregate morphology quantified by the flat and elongated (F&E) ratio, angularity index (AI) and surface texture (ST) index should also link to the resilient modulus of asphalt mixes, but the relationship is not yet well understood due to the lack of quantitative measurement of coarse aggregate morphology. Resilient modulus (M_R) measured in the indirect tensile mode as per ASTM D4123 reflects effectively the elastic properties of asphalt mixtures under repeated load. It is believed that using coarse aggregates with more irregular morphologies could improve the resilient modulus of asphalt mixtures. This chapter presents findings of the pooled fund laboratory study directed at revealing the effects of the coarse aggregate morphology on the resilient moduli of asphalt mixes tested at an intermediate temperature of 25°C. The stiffness of the asphalt binder is known to have a strong influence on modulus. To be complete, other asphalt properties that would influence the relationship between the coarse aggregate morphology and the resilient modulus, such as the stiffness of the asphalt binder, the aggregate gradation, and the nominal maximum aggregate size are also included in the study as major factors.

RESILIENT MODULUS AND STUDY GOALS

Resilient modulus and dynamic complex modulus are the two most commonly used methods to test for the elastic modulus of asphalt mixes under repeated loading. Although the dynamic complex modulus of asphalt mixes has been recently proposed as the primary input property used in the flexible pavement design procedure of the 2002 Design Guide, it has limited use with most laboratories due to the excessive time involved, complex equipment needed to conduct the test, and the size required for the testing specimen (Robert et al., 1996).

The concept of resilient modulus was first introduced by Seed et al. (1962) in characterizing the elastic response of subgrade soils and their relation to fatigue failures in asphalt pavements. Since then, owing to its simplicity and applicability to test both field cores and laboratory fabricated mix specimens, resilient modulus measured in the diametral test as per ASTM D4123 has been selected by most engineers as the preferred method to measure the resilient modulus of asphalt mixes. The resilient modulus was once regarded as the most commonly used method of measuring the stiffness modulus of the hot mix

asphalt (Robert et al., 1996). Moreover, previous research showed that the resilient modulus was more appropriate for use in multilayer elastic theories compared to the other common methods of measurement of elastic properties of asphalt mixes, such as the Young's modulus and dynamic complex modulus (Mamlouk and Sarofim, 1988). The resilient modulus measurement by the indirect tensile tests was also indicated as the most promising in terms of repeatability by Baladi and Harichandran (1989). With the merits of using diametral test in determining elastic properties of asphalt mixtures under repeated load, resilient modulus provides a platform on which the factors that affect the elastic property of asphalt mixtures can be evaluated.

Previous research studies also recognized that coarse aggregate morphological properties could be related to the stiffness of asphalt mixes (Monismith, 1970). However, the relationship is not well understood due to the lack of quantitative measurements of coarse aggregate morphology. Moreover, some other properties of the aggregate structure, such as aggregate gradation and nominal maximum size, also affect the resilient modulus of asphalt mixes. The unavailability of an effective and quantitative means to measure the coarse aggregate morphology was a limitation for studying the combined influences of these factors on the resilient modulus of asphalt mixes. With the accurate and objective measurements of the somewhat elusive coarse aggregate morphologies using the image analysis system UIAIA, it now becomes promising that the dilemma that hinders the aforementioned study of the relationship between the resilient modulus and the HMA component material properties be solved.

In this study, the main objective is to reveal the effect of coarse aggregate morphology on the elastic property of the HMA specimens under repeated loading. Research efforts were made to link the morphological indices, the F&E ratio, AI and ST index of the coarse aggregate materials to the resilient moduli of the asphalt mixes fabricated and subjected to diametral testing at the University of Illinois Advanced Transportation Research and Engineering Laboratory (ATREL). Other asphalt properties that would influence the relationship between the coarse aggregate morphology and the modulus, such as the stiffness of the asphalt binder, the aggregate gradation, and the nominal maximum aggregate size were also considered as major factors. This study included the following steps, with the results of the first step presented in Chapter 3:

- Processing the coarse aggregate materials using UIAIA to obtain the morphological indices;
- Fabricating and testing the asphalt mixture specimens to collect the resilient modulus data;
- Investigating the effect of coarse aggregate morphology on the resilient modulus of HMA.

EXPERIMENTAL DESIGN OF THE STUDY

Asphalt mixtures contain two types of basic materials, the asphalt binder and aggregate materials. The asphalt binder is used to hold together the aggregate particles, which constitute the aggregate structure/skeleton of the asphalt mixture. Coarse aggregate particles occupy the biggest volumetric portion in the aggregate structure due to the dominant usage and the big particle size they have. Having enough particle contacts among the coarse aggregates provides one of the prerequisites of a strong aggregate structure, which also depends on the shape properties of the aggregate particles. Particles with higher levels of angularities and surface irregularities usually demonstrate a higher level of interlock among the particles. Therefore, it is conceivable that the resilient property of the asphalt mixture is related to the properties of the asphalt binder and the coarse aggregate. Properties of these two basic materials were selected as the major factors that affect the resilient property of the asphalt mixture, and finally included in experimental design of this study.

Stiffness term is often loosely defined as the relationship between the applied stresses and the measured strain response as a function of loading time and temperature. For the asphalt binder or asphalt mixture, stiffness is often referred to characterizing the rheological behavior. At an intermediate temperature and very short load duration, the stiffness of an asphalt binder has been found to significantly affect the stiffness of the asphalt mixture that contains the binder by Van der Poel (Van der Poel, 1954). Since the resilient modulus characterizes the elastic part of the stiffness of asphalt mixture under repeated loading, it will inherently relate to the stiffness of the asphalt binder. Accordingly, the stiffness of the asphalt binder is selected as a main factor in studying the effect of the coarse aggregate morphology on the resilient property of the asphalt mixes.

Effects of the gradation of aggregate structure on the mechanical properties of asphalt mixture seem to be always at the center of controversy. Gradations of aggregate structures are often roughly categorized into coarse graded and fine graded, depending on the gradation curves going under the restricted zone or not. Another commonly used categorization includes more detailed grades, i.e. below the restricted zone (BRZ), through the restricted zone (TRZ) and above the restricted zone (ARZ). To see how gradation properties would affect the resilient modulus of the asphalt mixture and interact with other major factors, the aggregate structure gradation, as classified into the BRZ, TRZ and ARZ categories, was selected as a major factor in this study.

Asphalt mixture designs with larger nominal maximum sizes of coarse aggregate have been believed to possess higher stiffness properties than those with smaller ones. Accordingly, the nominal maximum size of the aggregate structure is also considered as a factor that would affect the elastic property of the asphalt mixes.

With the other component material properties selected that might potentially influence the resilient modulus of the asphalt mixture, i.e. the asphalt binder stiffness, aggregate gradation, nominal maximum aggregate size, the effect of the coarse aggregate morphology on the resilient modulus of the asphalt mixture can be performed without bias. Considering the focus of this study, the coarse aggregate morphology of aggregate structure is set as the principal factor, which means that this research altogether focuses on the effects of the coarse aggregate morphology and the influences of the other three factors on the resilient modulus of the asphalt mixture.

To properly establish different coarse aggregate morphologies and investigate their effects on the resilient modulus of asphalt mixtures, a total of eighteen HMA mix designs that use the Superpave volumetric mix design method were included in this study. These HMA mix designs and the materials used to make the mixes were obtained from eight different state highway agencies and the Central Federal Lands and Highways Division that participated in the subject FHWA pooled fund study; project DTFH61-02-X-00029. As shown in Table 6-1, the mix designs were selected considering the variations of the four major material properties as discussed previously. All the specimens were compacted to a 7% air void content level consistently. The 7% air void content matches the air void content commonly reached in the newly paved asphalt layers, which should make the findings from this research practically relevant for the study of the field elastic behavior of asphalt mixes.

IMAGING INDICIAL RESULTS OF COARSE AGGREGATE

The imaging based AI index in UIAIA measures the angularity property of a coarse aggregate particle by counting the relative differences of the adjacent vertex angles of the n-sided polygon that approximates the outline of the particle (see Figure 2-10). Therefore, the AI index in UIAIA directly measures the variation of a particle outline and is quite different from the manual method specified in ASTM D5821-01. On the other hand, the imaging based ST index is defined to directly quantify the average depth of surface irregularities of a particle, of which the scale is too small for the AI to measure as was shown in Figure 2-11. The two approaches taken in AI and ST index determinations are hence completely different. Accordingly, the philosophy involved in the algorithm of ST index is also different from what is specified in ASTM D1252-03, which measures a combined effect of particle shape, surface texture, and grading, and therefore only partially reflects the effect of surface texture property of coarse aggregate particles.

Following the test procedures previously established for the UIAIA system, imaging based results of the angularity and surface texture indices were obtained for the coarse aggregate materials also used in making the asphalt specimens for resilient modulus testing. Due to the varying combinations of coarse aggregate materials used for each of the 18 mix designs, the normalization procedure used first in Chapter

4 was also conducted on the mean of the two morphological indices for each mix design, transforming mean indices of the involved coarse aggregate materials contained in a certain mix into a composite index for that mix. The equation used for the normalization procedure is presented again as follows and the composite index results obtained for each mix design are shown in Table 6-2.

Table 6-1 Asphalt Mixes, Mix Properties, and Resilient Modulus Results

Mixes	Resilient Modulus (MPa)	Nominal Max Size	Binder* Stiffness	Gradation**
FLHD-NM	1056	19.0	58	T
FLHD-OK	4154	19.0	70	A
GA1	2471	12.5	67	B
GA2	3857	12.5	76	B
GA3	3659	9.5	76	T
IN1	2140	9.5	64	B
IN2	2016	9.5	64	B
MN1	2942	12.5	64	B
MN2	1011	12.5	58	T
MO1	1807	19.0	64	B
MO2	3213	19.0	67	B
MO3	2150	25.0	67	B
MS1	3082	19.0	70	T
MS2	2878	12.5	64	T
MT1	1992	19.0	58	B
MT2	3307	19.0	70	B
SC1	4617	12.5	76	B
SC2	2720	12.5	67	B

* High temperature performance grade of the asphalt binder in °C;

** “A” means the gradation curve goes above the restricted zone;

“B” means the gradation curve goes below the restricted zone;

“T” means the gradation curve goes through the restricted zone.

$$Composite\ Index = \frac{\sum_{i=1}^n [(a_i)(index_i)]}{\sum_{i=1}^n (a_i)} \quad (6-1)$$

where, *Composite Index* is the composite aggregate shape index for a certain HMA design, which is a weighted sum of the individual mean indices of the UIAIA-processed coarse aggregate materials used in the design; the variable a_i is the percentage by weight of the i^{th} coarse aggregate material used in the

design; the variable $index_i$ is the mean imaging based index of the i^{th} coarse aggregate material used in the design; and finally the summation counter n is the number of the coarse aggregate materials used in that design, which may be 1, 2, 3 or 4 for each of the 18 mix designs, depending on the number of coarse aggregate materials used in that design and processed by the UIAIA.

LABORATORY RESILIENT MODULUS TESTING

The resilient modulus tests were conducted at the University of Illinois ATREL according to ASTM D4123. A total of three specimens were fabricated for each mix design. Each specimen was tested twice at 25°C with a different orientation, the second test specimen positioned at a 90° rotation with respect to the first test. For the two measurements of the same specimen at the two orientations, the coefficient of variance (CV) for all the specimens were under 1.5%, with a minimum CV of 0.1% and a maximum CV of 1.4%. The generally low CV values indicated that the resilient moduli of the specimens were somewhat isotropic in radial direction. As for the resilient moduli of the three specimens, much higher CV values were computed for each mix design. The average CV for the resilient moduli was 3.7%, with a maximum CV of 6.1% observed for the MO3 specimens, which had the greatest nominal maximum size (see Table 6-2). The mix designs with bigger nominal maximum sizes gave higher CV values than those with smaller nominal maximum sizes, which demonstrated that higher homogeneity existed in specimens with smaller nominal maximum sizes. The average of the six resilient modulus values was reported as the resilient modulus of that asphalt mix.

Since the amount of stress applied to the sample during testing would have a significant effect on the measured resilient modulus values, it was necessary to estimate the tensile strength of asphalt mixes in order to estimate the applied stress as a percent of tensile strength. For each of the mixes, a specimen was tested to obtain the indirect tensile strength before the resilient modulus test, and a standard applied stress of 15% of the tensile strength was finally adopted and used in all the resilient modulus tests. The Poisson's ratio was assumed to be 0.35 for all the specimens tested at 25°C.

The resilient modulus testing device used in this study is shown in Figure 6-1. The resilient modulus test setup consisted of a pneumatic loading system to generate load pulses. The device was set to apply 1 Hz repeated haversine load waveform with load duration of 0.1 seconds and a rest period of 0.9 seconds on the test specimens as shown in Figure 6-2. The computer connected to the testing device recorded the load and deformation automatically, and resilient modulus was thereafter output with the assumed Poisson's ratio. Figure 6-3 gives a typical recorder output of a resilient modulus test performed in this study. The average resilient moduli of all the asphalt mixture specimens are listed in the second column of Table 6-1 as the resilient modulus of that asphalt mix.

Table 6-2 Imaging Results of Composite AI and ST Indices for the 18 Asphalt Mixes Studied

Designations	Composite AI	Composite ST
FLHD-NM	442	2.00
FLHD-OK	524	2.46
GA1	446	1.71
GA2	503	2.03
GA3	446	1.71
IN1	430	1.37
IN2	429	1.44
MN1	540	1.75
MN2	429	1.42
MO1	417	1.44
MO2	522	2.26
MO3	442	1.45
MS1	403	1.33
MS2	479	1.82
MT1	469	2.09
MT2	519	2.10
SC1	550	2.56
SC2	519	2.25



Figure 6-1 Resilient Modulus (M_R) Test Device Utilized at the University of Illinois ATREL

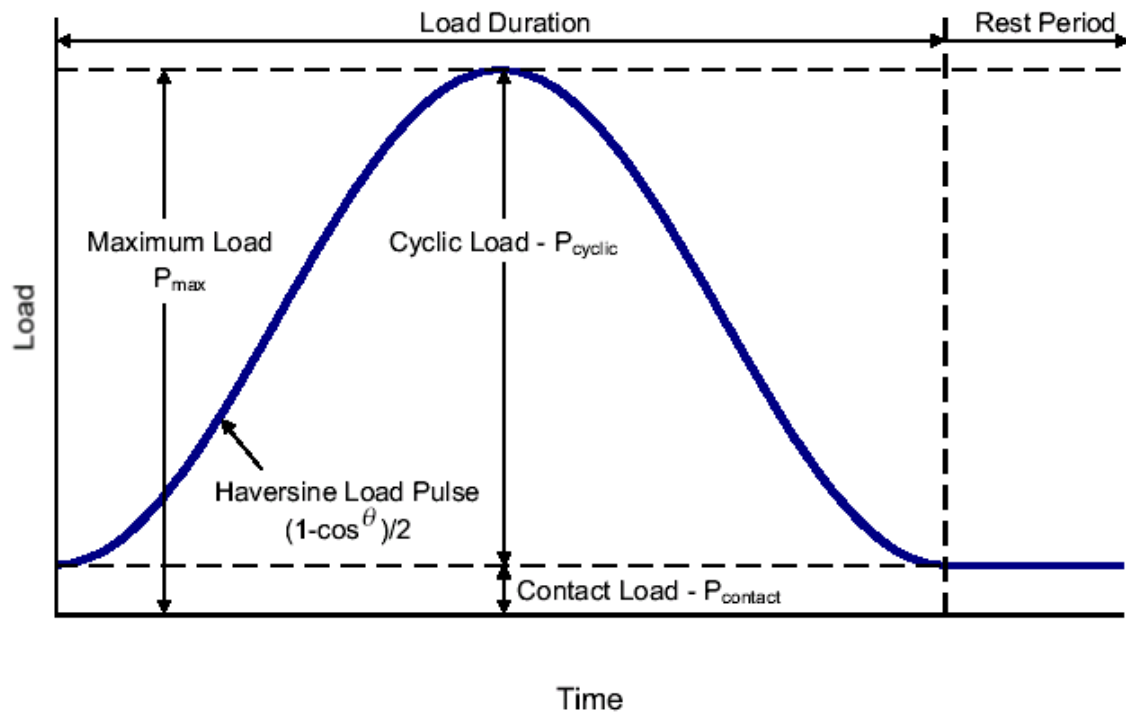


Figure 6-2 The 1-Hz Haversine Load Waveform with 0.1-sec. Load Duration and 0.9-sec. Rest

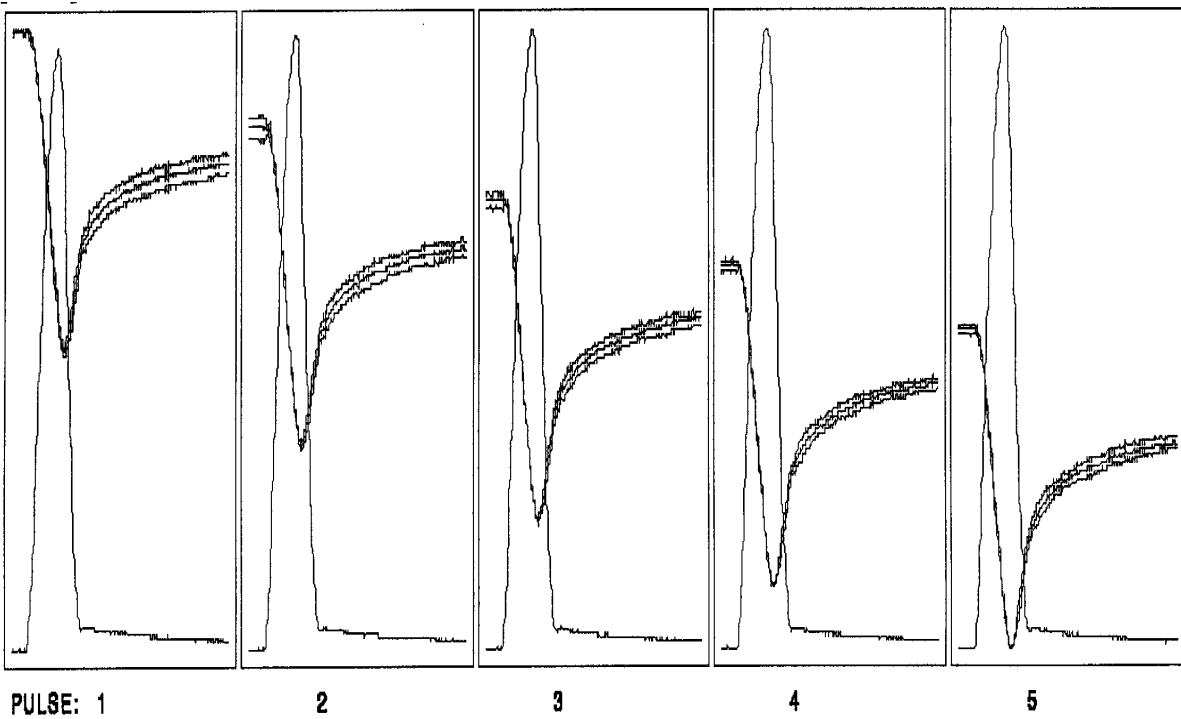


Figure 6-3 Typical Recorder Output of the Resilient Modulus Test

ANALYSIS OF THE RESULTS

With the coarse aggregate morphology chosen as the principal factor in this study, a simple linear regression was first performed between the resilient moduli and the imaging based AI and the ST indices respectively, as shown in Figures 6-4(a) and 6-4(b). Although the two correlation coefficients were not very high, there was still a trend; the asphalt mixes with high resilient moduli were likely to show high values of coarse aggregate morphology as denoted by the AI and ST indices. A comparison of the two coefficients further indicated that the coarse aggregate angularity related better to the resilient modulus than did the surface texture.

To further investigate how the interaction between the coarse aggregate morphology, as denoted by the AI and ST indices, and the other three selected major factors would influence the resilient modulus of hot mix asphalt, the resilient modulus data were grouped based on the classes of each of the other three selected factors. The grouped resilient modulus data were then correlated to the AI and ST indices within the individual groups. For any of the other three selected major factors, if the individual coefficients of determination significantly differed from overall coefficients of determination as shown in Figures 6-4(a) and 6-4(b), the interaction between the coarse aggregate morphology and that selected major factor could be regarded as significantly influencing the resilient modulus of hot mix asphalt.

To group the resilient modulus data based on the binder stiffness, a classification of the binder stiffness had to be established beforehand. The performance based Superpave asphalt binder specification as per AASHTO MPI-93 requires that the physical properties remain constant for all performance grades (PG), but the temperature at which these properties must be achieved varies from grade to grade depending on the climate in which the asphalt grade is expected to perform. Therefore, at a certain temperature, although the actual asphalt binder stiffness of different grades is unknown, the stiffness can still be roughly classified based on the PG grade. With the fact that binders used in this study had almost the same low temperature grade, the classification of the binder stiffness was finally performed based on the high temperature grades. Then the resilient modulus data were grouped based on these classes of binder stiffnesses. Feasibility of this tentative grouping method was thereafter verified by checking the relative ranges of resilient moduli in each group as shown in Figure 6-5. The mean resilient moduli of the groups shown in Figure 6-5 tend to increase with the increments of the high temperature grade, which demonstrates the effectiveness of using PG grade for the classification of binder stiffness.

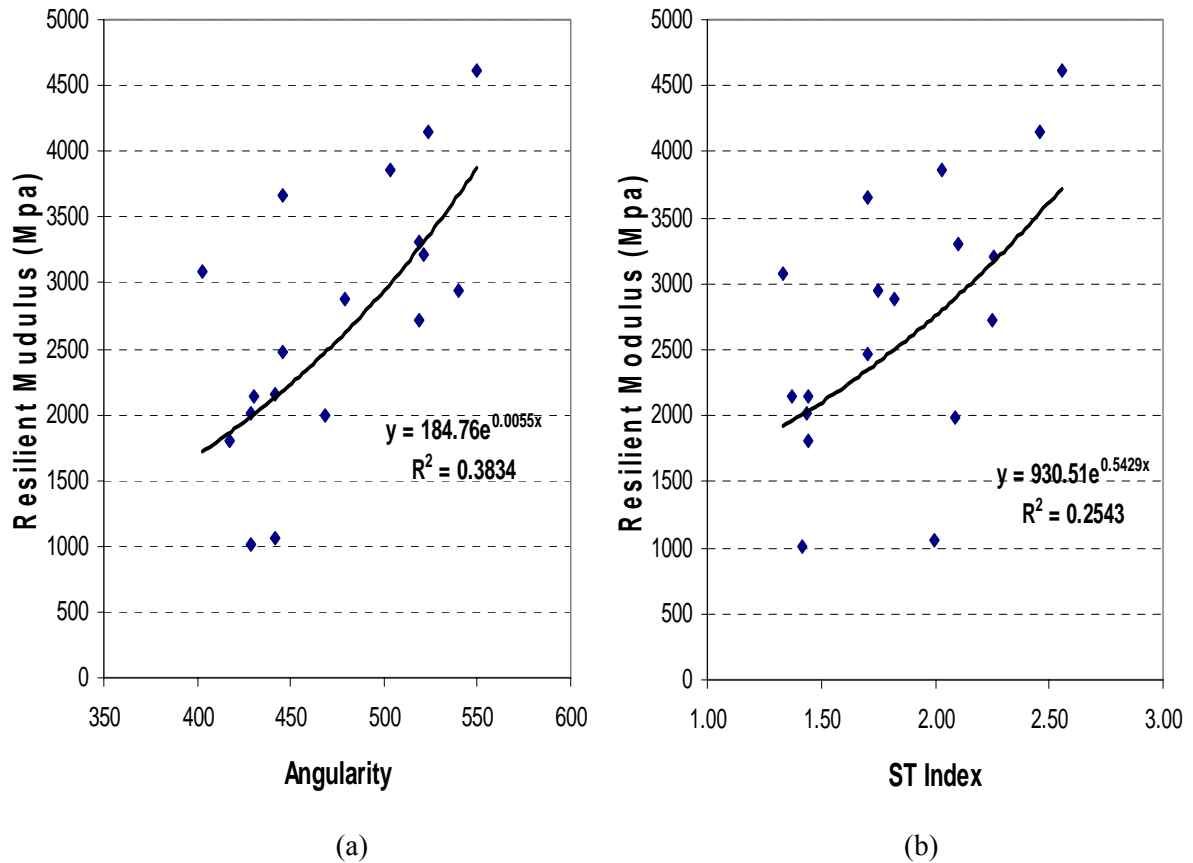


Figure 6-4 Relationships between the Resilient Modulus and the AI and ST Indices

The grouped resilient modulus data were then correlated to the AI and ST indices within each group, as shown in Figures 6-6 and 6-7, respectively. It can be observed from Figures 6-6 and 6-7 that, within all of the five groups of binder stiffness, resilient modulus increases exponentially with the increasing AI and ST indices. This phenomenon strengthens the preliminary conclusion based on Figures 6-4 findings that coarse aggregate materials with more irregular morphologies can improve the resilient modulus of the asphalt mixture. The positive correlations between the AI and ST indices and the resilient moduli showed much higher individual coefficients of determination than those of the ungrouped data correlations shown in Figure 6-4. Based on this observation, another conclusion can be made that the interaction between the coarse aggregate morphology and the binder stiffness significantly influences the resilient modulus of hot mix asphalt.

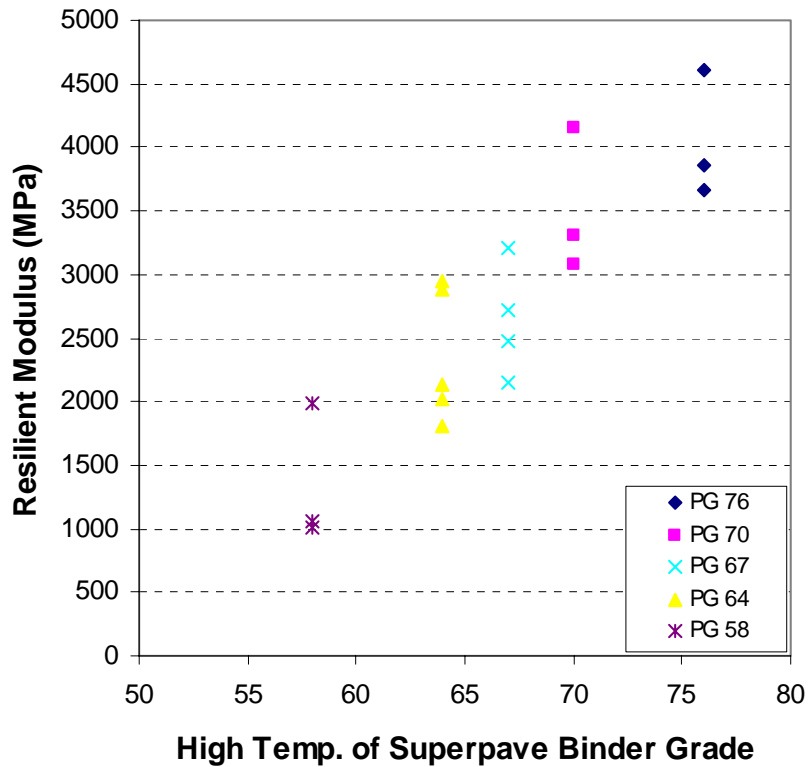


Figure 6-5 Resilient Moduli Grouped on the High Temperature of Superpave PG Grades

The resilient modulus data were next grouped on the classes of the aggregate gradation. Then, the grouped resilient moduli were correlated to the AI and ST indices within the BRZ and TRZ groups as shown in Figures 6-8(a) and 6-8(b) respectively. The ARZ group had only one mix and therefore was eliminated from the correlation. From Figure 6-8, it can be observed that although the AI and ST indices correlated quite well to the resilient moduli in the BRZ group, the correlations in the TRZ group were very low. In Figure 6-8(b), the increasing ST index even negatively affected the resilient modulus. As a result, the variations of the gradation did not consistently influence the relationship between the coarse aggregate morphology and the resilient modulus. The inconsistent effects of gradation on the resilient modulus can be attributed to the different levels of aggregate contacts in the BRZ and TRZ gradations. In order to achieve coarse aggregate interlock, the gradation must pass below the restricted zone (Seward et al., 1996); therefore, in the TRZ case, there might not be enough coarse aggregate contacts formed and the shape properties of coarse aggregate particle had little impact on the resilient modulus of the asphalt mixes.

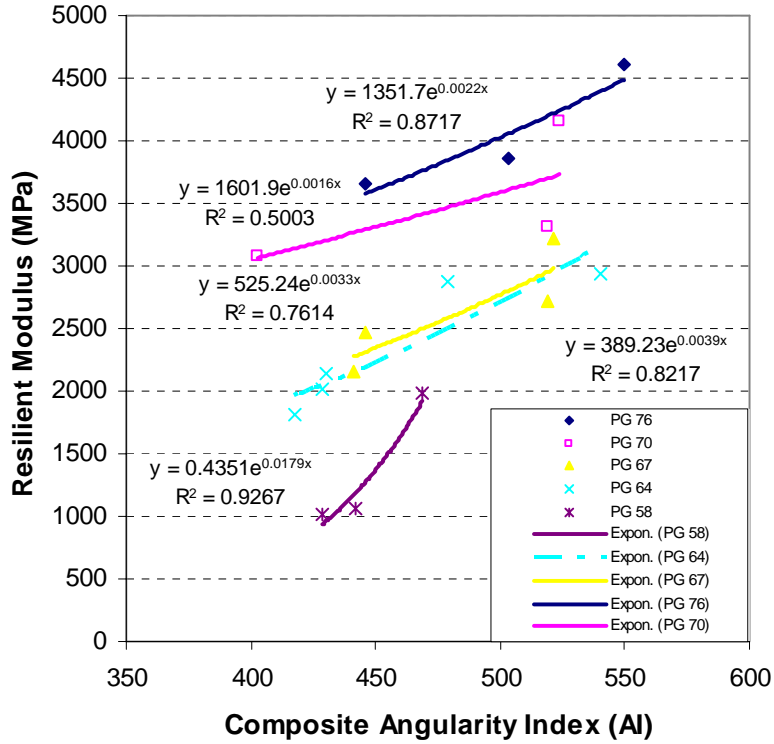


Figure 6-6 Effects of AI on Binder Stiffness-grouped Resilient Modulus

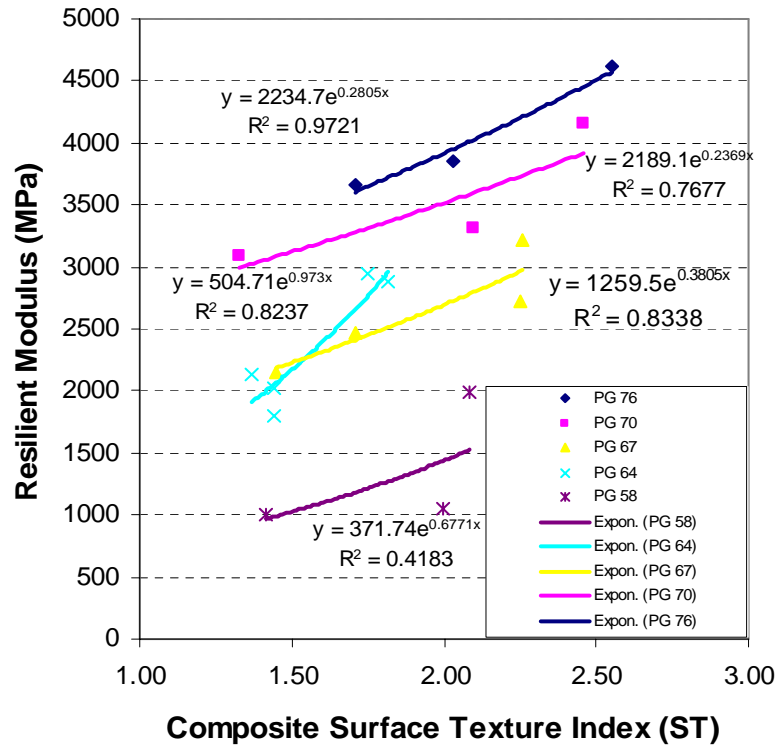


Figure 6-7 Effects of ST Index on Binder Stiffness-grouped Resilient Modulus

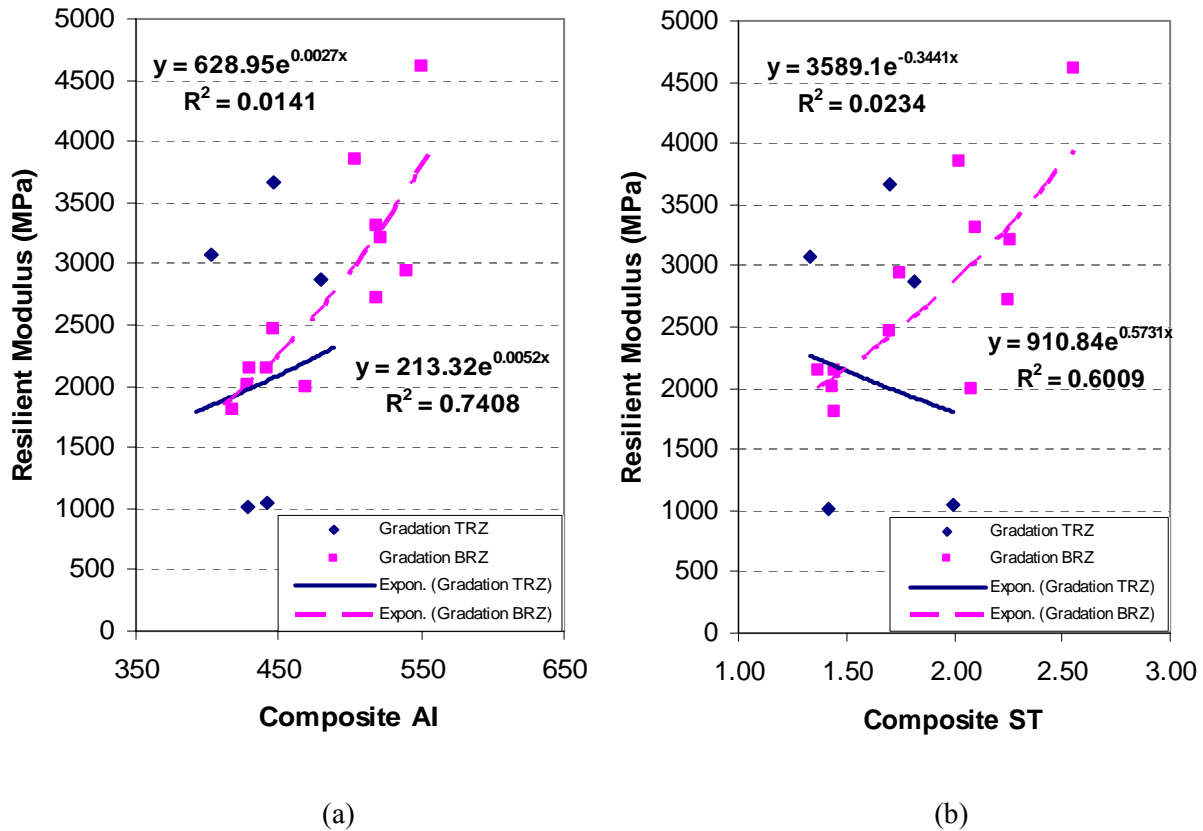


Figure 6-8 Effects of AI and ST Indices on Gradation-grouped Resilient Modulus

Similarly, the resilient modulus data were also grouped on the classes of the nominal maximum aggregate size. Since one asphalt mix only had the nominal maximum aggregate size of 25 mm, it was eliminated from the correlation study. The grouped resilient moduli based on the three other major classes of nominal maximum aggregate sizes, i.e. 19 mm, 12.5 mm and 9.5 mm, were next correlated to the AI and ST indices within each group as shown in Figures 6-9(a) and 6-9(b), respectively. For both AI and ST indices, the correlations among these groups showed large variations in terms of the coefficient of determination. So the variations of the nominal maximum aggregate size did not consistently influence the relationship between the coarse aggregate morphology and the resilient modulus. Very strong correlations were identified for the 9.5 mm nominal maximum aggregate size and the correlations got worse steadily as the nominal maximum aggregate size increased to 12.5 mm and 19 mm. Therefore, for fine mixes with nominal maximum aggregate sizes less than equal to 9.5 mm, the aggregate morphology, as identified by the AI and ST indices, had a major impact on the resilient modulus. This effect decreased significantly in coarser mixes having nominal maximum aggregate sizes greater than equal to 19 mm.

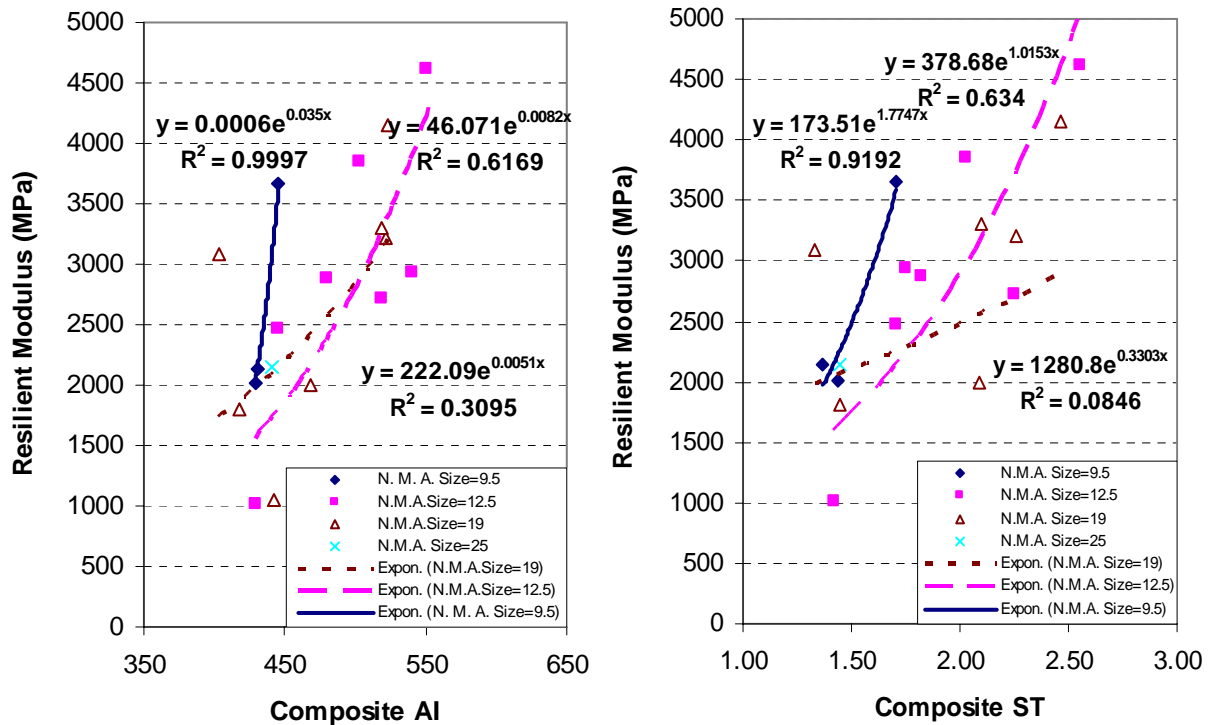


Figure 6-9 Effects of AI and ST Indices on Nominal Maximum Aggregate Size-grouped Modulus

SUMMARY

Coarse aggregate morphological properties were quantified from the UIAIA analysis as angularity and surface texture (AI and ST) imaging based indices to investigate the effects of these coarse aggregate shape properties on the resilient modulus of hot mix asphalt. Based on eighteen asphalt mixes prepared and tested in the University of Illinois Advanced Transportation Research and Engineering Laboratory (ATREL), it was observed that when coarse aggregates with more irregular morphologies were used in asphalt mixes, the resilient modulus of the asphalt mixture was improved. The stiffness of the asphalt binder also had a strong influence on modulus. The resilient modulus test data when grouped according to asphalt binder grade and stiffness typically demonstrated a much higher agreement to the coarse aggregate morphology than the ungrouped data. According to the observations made from the below and through the restricted zone (BRZ and TRZ) gradation groups, the gradation of aggregate structure showed contradicting effects on the relationship between the coarse aggregate morphology and the resilient modulus of asphalt mixes. The nominal maximum aggregate size did not consistently influence the contribution of the coarse aggregate morphology to the resilient modulus; a decrease in the nominal

maximum aggregate size from 19 mm to 9.5 mm typically indicated an increasing positive influence of aggregate morphology on the resilient modulus of asphalt mixes.

CHAPTER 7

SUMMARY AND CONCLUSIONS

To evaluate the prospected application of an aggregate image analysis system, the University of Illinois Aggregate Image Analyzer (UIAIA), research project DTFH61-02-X-00029: “Investigation of Aggregate Shape Effects on Hot Mix Performance” was initiated as a pool funded-research project, the TPF-5(023), in March of 2002 in the Civil and Environmental Engineering Department at the University of Illinois at Urbana-Champaign (UIUC). The study partners were the National Center for Asphalt Technology (NCAT), the state highway agencies of Alabama, Georgia, Indiana, Minnesota, Mississippi, Missouri, Montana, and South Carolina, and the FHWA Central Federal Lands and Highways Division. The objective of the study, as stated on the <http://www.pooledfund.org> web site, was as follows: “The measurement of imaging-based volumetric and morphological indices and their correlation with laboratory and field performance results as a wave of the future in the development of asphalt pavement science and technology.”

The project consisted of 2 main phases. In Phase I, coarse aggregate shape, size, angularity and texture properties were evaluated to define proper imaging based morphological indices. The UIAIA was used for the evaluation. The aggregates that were evaluated included: (1) Samples received from the National Center for Asphalt Technology (NCAT) Pavement Test Track study and (2) representative aggregate samples from the participating states and the Central Federal Lands and Highways Division. Among the shape and size properties determined for each aggregate particle were: (i) maximum, intermediate, and minimum dimensions; (ii) flat and elongated (F&E) ratio; (iii) volume (and weight knowing its specific gravity); (iv) a computed Angularity Index (AI) to indicate how many crushed faces are there or how rounded or angular the particle is; and finally, (v) a computed Surface Texture (ST) Index to indicate the smoothness or roughness of the aggregate particle surface.

In Phase II of the study, NCAT Pavement Test Track data were collected from the 46 field test section mixes studied by NCAT to correlate their detailed aggregate shape property indices to the asphalt mix field rutting performances. In addition, representative samples received from the participating states were also used to prepare asphalt concrete samples using the Superpave gyratory compactor. The samples were then tested for resilient modulus and permanent deformation characteristics. Stability and permanent deformation characteristics of the mixes were determined at the Advanced Research and Engineering Laboratory (ATREL) of the University of Illinois. The intent was to form a laboratory

database for studying the influence of particle shape on asphalt concrete mix performance and also to establish proper aggregate criteria.

In Chapter 1 of this final report, an overview was first given of the performance related aggregate properties. Currently available standard tests and specifications were reviewed next for determining coarse aggregate shape and size properties. The need and significance of investigating effects of coarse aggregate shape and size on the performance of asphalt mixes was established by presenting highlights of significant, noteworthy findings from previous research studies. As an introduction to the image analysis concepts and its advantages, a historical background was also given on the need and evolution of aggregate shape and size quantification from image analysis. Finally, the objectives and the scope of the pool-funded study were stated.

Chapter 2 mainly focused on presenting research efforts made in developing the three-dimensional (3-D) aggregate image analysis system, the University of Illinois Aggregate Image Analyzer (UIAIA). The need for 3-D image analysis and the basic image analysis concepts were also discussed briefly. The UIAIA system's physical configuration, main features, and the operational principles were described in detail to better understand the definitions of the indices and algorithms that quantify the coarse aggregate morphologies. The algorithm behind the development of the automated thresholding scheme used in UIAIA was indicated as a logical, efficient, and proven technique in determining the gray scale threshold value that can separate the particle from its background under varying conditions. The two categories of UIAIA imaging based indices for coarse aggregate were described for determining: (i) particle sizes, which include the maximum, intermediate and the minimum dimensions of the particle and the 3-D reconstruction of the particle volume; (ii) particle morphological or shape indices, which include the flat and elongated (F&E) ratio, angularity index AI, and the surface texture ST index.

Chapter 3 focused on Phase I project efforts for evaluating and validating the prospected features and the practical application of the UIAIA as an effective aggregate imaging system to quantify coarse aggregate size and shape properties. Aggregate materials with varying shape irregularities were shipped to the Civil and Environmental Engineering Department at the UIUC from the study partners in the FHWA Project DTFH61-02-X-00029, i.e., the NCAT Pavement Test Tracks, and the state highway agencies of Alabama, Georgia, Indiana, Minnesota, Mississippi, Missouri, Montana, and South Carolina, and the Central Federal Lands and Highways Division. Imaging based size and shape properties of these different coarse aggregate samples, which included maximum, intermediate and minimum dimensions, particle volume, percent F&E ratio by weight, angularity AI index, and surface texture ST index, were all obtained using the UIAIA and documented for further investigating effects of these coarse aggregate shape properties on the modulus and permanent deformation, or field rutting, performances of asphalt mixtures.

The accuracy and repeatability of the UIAIA imaging based volume computation was validated by successfully comparing the imaging based weights of the aggregate samples to their actual weights measured in the laboratory. The UIAIA imaging based particle size distributions were also accurately computed and compared to the gradation curves determined from the manual sieve analysis. Individual aggregate types having unique particle morphologies were documented and classified according to the developed flatness and elongations (F&E ratio) and angularity (AI) and surface texture (ST) shape indices. Using statistical clustering techniques, four categories were established for commonly used coarse aggregate types (uncrushed gravel, crushed gravel, limestone, and granite) based on the image analysis shape property data of the participating highway agencies aggregate samples. In addition, a definite relationship was shown to exist between coarse aggregate angularity and surface texture.

The pooled fund study aggregate materials processed using the UIAIA system established a coarse aggregate morphology database with a broad range of shape irregularities to investigate the effect of shape and size properties of coarse aggregate on the hot mix asphalt and to eventually help future design and maintenance of asphalt pavements. In that regard, the imaging based shape evaluation of coarse aggregate using the UIAIA system was noted to provide a fast, precise, and cost effective means to describe particle shape and size distribution characteristics of coarse aggregate. The UIAIA system together with its image processing algorithms for size and shape indices, therefore, has the potential to replace some of the currently used standard tests for aggregate gradation using sieve analysis as per ASTM C136, flat and elongated particles as per ASTM D4791, aggregate angularity as per ASTM D5821, uncompacted voids in coarse aggregate as per AASHTO TP56, and indirect aggregate shape property measurement for surface texture as per ASTM D3398.

Aggregates make up more than 95 percent of asphalt pavements of which coarse aggregate occupies by far the highest weight or volume and the coarse aggregate particles typically constitute the skeleton of the aggregate structure in Hot Mix Asphalt (HMA) believed to significantly affect the asphalt mix rutting performances. Chapter 4, therefore, investigated how the physical shape properties of coarse aggregate used in asphalt mixtures would affect field-rutting performances of the full-scale asphalt pavement sections constructed and tested at the National Center for Asphalt Technology (NCAT) Test Track facility. The NCAT coarse aggregate materials were shipped to UIUC ATREL and processed using the image analysis system. The UIAIA imaging based shape indices, percent F&E ratio by weight, angularity index AI, and the surface texture ST index, were calculated for the NCAT coarse aggregate. Composite shape indices were first established for the aggregate blends and weight percentages used in different hot mix asphalt lifts in the NCAT Pavement Test Track asphalt concrete surface courses. The composite indices were then normalized to account for the various numbers of hot mix asphalt lifts used and the individual lift thicknesses. This was in an effort to successfully correlate the shape indices of the

coarse aggregate used in the asphalt mixes to the field rutting performances of these mixes, test data collected at the NCAT Pavement Test Track.

Statistical analyses were performed to relate the three normalized imaging based shape indices to the rut depth data from the pavement sections of the NCAT Test Track. All shape indices, percent F&E ratio by weight, angularity index (AI), and surface texture (ST) index, indicated good correlations individually with the field rutting data from the NCAT Pavement Test Track with ST index giving the highest correlation coefficient R^2 of 0.94 and AI giving the next best correlation with an R^2 of 0.80. Among the three imaging based shape indices, surface texture related the best with the field rutting data from the NCAT Pavement Test Track, as indicated by the lowest p-value in the t-test performed for the multiple linear regression analysis. The success of the linkage between the physical shape properties of coarse aggregate and the affected field-rutting performances of the full-scale asphalt pavement sections constructed and tested at the NCAT Pavement Test Track facility also further verified the accuracy and repeatability of UIAIA in determining the shape and size of coarse aggregate particles.

Possible field disturbances, such as daily and seasonal temperature changes, can be easily controlled in a laboratory setting to better facilitate the study of the coarse aggregate shape effects on the HMA performances. In Phase II of the research study, asphalt mixture specimens were fabricated at UIUC ATREL using the pooled fund study coarse aggregate materials by following the mix designs received from a total 10 state highway agencies, i.e., the 8 pooled fund participating states and the Central Federal Lands and Highways Division (CFLHD) providing asphalt mixes and mix designs of New Mexico and Oklahoma. The Superpave asphalt specimens were produced in the laboratory at a target air void content of 7% to simulate the conditions of HMA layers commonly achieved in newly constructed highway pavements.

Chapter 5 described the permanent deformation tests conducted at a specified high temperature on two replicate specimens for a total of 18 Superpave asphalt mixes studied. The stability and permanent deformation characteristics of the asphalt mixtures were examined by means of repeatedly applying traffic loads in a triaxial test setup. The differences in the laboratory test data, i.e., different trends in the permanent deformation accumulation with the number of load applications, were then analyzed for possible linkages to the UIAIA imaging based morphological indices, i.e., the F&E ratio, angularity index (AI) and surface texture (ST) index, of the coarse aggregate materials used in the asphalt mixes.

During the repeated load permanent deformation tests, the Cumulative Permanent Strains (CPS) in a specimen were recorded as a function of load applications. Based on the laboratory test data and field measurements of highway pavement densities, inferences were made such that the primary phase of the CPS curve, in general, corresponds to the period during which the HMA air void content drops from 7-

8% to 4-5% in field pavements; secondary phase of CPS curve corresponds to the period during which the HMA air void content drops from 4-5% to 3%; and finally, the tertiary phase corresponds to the period during which the HMA air void content drops below 3%. From laboratory testing, it was found that the CPS did not conform to the flow number (FN) due to the variations of the primary slope (PS) and the secondary slope (SS). The primary slope of the CPS curve generally had no strong correlations with the FN and therefore did not significantly affect the stability of HMA specimens whereas the SS of the CPS curve related much better to the FN since most of the permanent strain accumulation occurred during the secondary phase of permanent strain accumulation.

When the shape effects were isolated with the help of composite shape indices established, the effects of the AI and ST indices on the HMA permanent deformations were especially significant from the test results evaluated according to the aggregate gradations. The contributions of higher AI and ST indices to a better HMA stability and longer performance life were very obvious for the BRZ (below-the-restricted-zone) type mixes, which had much higher coarse aggregate weights and percentages in the asphalt mix compositions. The F&E ratio index, however, showed no measurable effect on the permanent deformation due to low percentages of flat and elongated particles used in all the specimens.

The primary slope PS of the CPS curve was not significantly affected by the physical shape properties of coarse aggregate materials owing to the comparatively loose aggregate structure of the HMA concrete. Of the three key physical shape properties, the ST index was found to best correlate with the secondary slope (SS) and the flow number (FN) of the Cumulative Permanent Strain (CPS) curve that was recorded as a function of load applications during the repeated load permanent deformation tests. The AI also showed good relationship with the FN and the secondary slope SS.

Based on these findings, a possible mechanism of coarse aggregate morphology affecting the stability of asphalt mixture was proposed as defined by the concept of Particle Geometrical Interference in HMA (PGI-HMA). The PGI-HMA considers all HMA coarse and fine aggregate particle interactions including the asphalt mastic and attempts to explain possible different effects of the aggregate angularity and surface texture properties on HMA stability and aggregate structure in the study of asphalt pavement field rutting behavior. Accordingly, interlock among coarse aggregate particles provides the HMA stability and its aggregate structure. Surface texture and angularity properties are two prerequisites for the existence of interlock with surface texture determining the magnitude of friction between particles and high angularity enhancing the probability of establishing inter-particle contacts.

Chapter 6 presented the findings of another laboratory study undertaken as part of the pooled fund research project Phase II activities. In this study, the main objective was to reveal the effect of coarse aggregate morphology on the elastic, i.e., resilient modulus, property of the HMA specimens under repeated loading. Research efforts were made to link the morphological indices, the F&E ratio, AI and

ST index, of the coarse aggregate materials to the resilient moduli, M_R , of the asphalt mixes fabricated and subjected to diametral testing, in the indirect tensile mode as per ASTM D 4123, at an intermediate temperature of 25°C. Other asphalt properties that would influence the relationship between the coarse aggregate morphology and the modulus, such as the stiffness of the asphalt binder, the aggregate gradation, and the nominal maximum aggregate size were also considered as major factors.

Based on the 18 asphalt mixes prepared and tested in the laboratory, it was observed that when coarse aggregates with more irregular morphologies were used in asphalt mixes, the resilient modulus of the asphalt mixture was improved. The stiffness of the asphalt binder also had a strong influence on modulus. The resilient modulus test data, when grouped according to asphalt binder grade and stiffness, generally demonstrated a much better relationship with the coarse aggregate morphology than the ungrouped data. According to the observations made from the below and through the restricted zone (BRZ and TRZ) gradation groups, the gradation of aggregate structure showed contradicting effects on the relationship between the coarse aggregate morphology and the resilient modulus of asphalt mixes. The nominal maximum aggregate size did not consistently influence the contribution of the coarse aggregate morphology to the resilient modulus; a decrease in the nominal maximum aggregate size from 19 mm to 9.5 mm typically indicated an increasing positive influence of aggregate morphology on the resilient modulus of asphalt mixes.

This study indicated that coarse aggregate shape and size properties could significantly affect both resilient modulus and permanent deformation or stability of asphalt mixes. In the development of end-use asphalt mix performance specifications for aggregate selection criteria, in addition to the size, coarse aggregate shape properties have to be also taken into account properly. It was found that the elastic property of an asphalt mixture under repeated load, as characterized by the resilient modulus of the mixture, seemed to be very closely related to both the angularity and surface texture properties of the coarse aggregate particles. As the coarse aggregate used in HMA became rougher and more angular, higher resilient moduli were typically achieved from the laboratory diametral tests. On the other hand, the increased stability and reduced permanent deformation or rutting potential of the dense graded asphalt mixtures studied herein were more favorably influenced primarily by the increased surface texture or roughness property of coarse aggregate particles.

There were no obvious effects of the coarse aggregate percent by weight F&E ratios on the performances of asphalt mixes from both the laboratory diametral and permanent deformation tests, although the F&E ratios of the NCAT coarse aggregate showed fairly good correlations with the rut depth data obtained from the NCAT Test Track pavement sections. A possible explanation for this is the small amount of flat and elongated particles generally found in the laboratory specimens made following the state agency asphalt mix designs. These mixes did not show directional orientations during laboratory

testing when compared to field test track mixes since there were no signs particle breakage observed in the laboratory.

RECOMMENDATIONS FOR FUTURE RESEARCH

The major challenge in this project has been to try to isolate the effects of coarse aggregate shape and size properties on the different asphalt mix performances. The laboratory measured resilient modulus and permanent deformation characteristics of the different asphalt mixes were possibly influenced to a much greater extent by the mixture types according to the mix design properties and volumetrics, such as the asphalt binder grade, asphalt content and modifier type, design gyrations, and the aggregate gradations affecting Superpave mix properties above, through, and below the restricted zone; ARZ, TRZ, and BRZ. One approach to pursue in a follow-up study will no doubt be to consider preparing one type of Superpave gyratory asphalt mix having similar aggregate gradations, coarse and fine aggregate weights and percentages, the same asphalt binder, the same fine aggregate type (preferably crushed gravel), and the same filler. The only ingredient to vary will have to be the coarse aggregate type to possibly isolate the effect of coarse aggregate shape (F&E), angularity (AI), surface texture (ST), and possibly the surface area (SA) on aggregate structure shear strength (friction angle), HMA modulus, and HMA laboratory permanent deformation and/or field rutting performances.

Nevertheless, having only certain asphalt mix designs to study these aggregate shape effects can also lead to partial answers to our questions in the investigation and general knowledge of the coarse aggregate morphologies affecting the HMA performances. The improvement in objectively measuring aggregate shape properties using the UIAIA system or any other imaging based systems offers the additional opportunity to develop adaptable design methods and specifications that accommodate aggregates with a wide range of physical characteristics. For example, for economic reasons, one may decide to use a hard but low-angularity/low-texture aggregate in HMA on a low-volume road. In this case, the optimum mixture design may minimize binder content and maximize stone-to-stone contact of the coarse aggregate, etc. Or, use of a softer aggregate in HMA may require reducing stone-to-stone contact and thus protect the coarse aggregate with a layer of fine aggregate and binder.

The results of future research in this area should be able to provide tools to allow highway agencies and the industry to efficiently utilize the sources of aggregates available to them. Hence, major benefits of optimized aggregate resource utilization and construction cost reductions can this way be realized. The identification and quantification of the influence of aggregate properties on end-use performance will essentially help resolve issues such as the acceptable limits of aggregate shape, angularity and texture to optimize performance.

REFERENCES

1. AASHTO PROVISIONAL STANDARDS, TP 56-03 “Uncompacted Void Content of Coarse Aggregate (As Influenced by Particle Shape, Surface Texture, and Grading),” Washington, D.C., American Association of State Highway and Transportation Officials, 2003.
2. Ahlrich, R. C., “Influence of Aggregate Gradation and Particle Shape/texture on Permanent Deformation of Hot Mix Asphalt Pavements,” Tech. Rep. GL-96-1, Department of the Army, Waterways Experiment Station, Vicksburg, Mississippi, 1996.
3. Anderson, R. M., Turner, P. A., and Peterson, R. L., “Relationship of Superpave Gyrotory Compaction Properties to HMA Rutting Behavior,” NCHRP Report 478, Transportation Research Board (TRB), National Research Council, Washington, D.C., pp. 33-39, 2002.
4. ASTM C88-99A, “Test Method for Soundness of Aggregates by Use of Sodium Sulphate or Magnesium Sulphate,” Annual Book of ASTM Standards, Vol. 04.02, American Society for Testing and Materials, West Conshohocken, PA, 2004.
5. ASTM C131-03, “Test Method for Resistance to Degradation of Small-Size Coarse Aggregate by Abrasion and Impact in the Los Angeles Machine,” Annual Book of ASTM Standards, Vol. 04.02, American Society for Testing and Materials, West Conshohocken, PA, 2004.
6. ASTM C142-97, “Clay Lumps and Friable Particles in Aggregates,” Annual Book of ASTM Standards, Vol. 04.02, American Society for Testing and Materials, West Conshohocken, PA, 2004.
7. ASTM D 1252-03, “Standard Test Methods for Uncompacted Void Content of Fine Aggregate (as Influenced by Particle Shape, Surface Texture, and Grading),” Annual Book of ASTM Standards, Vol. 04.02, American Society for Testing and Materials, West Conshohocken, PA, 2003.
8. ASTM D 136-96a, “Standard Test Method for Sieve Analysis of Fine and Coarse Aggregates,” Annual Book of ASTM Standards, Vol. 04.02, American Society for Testing and Materials, West Conshohocken, PA, 2000.
9. ASTM D 3398-00, “Standard Test Method for Index of Aggregate Particle Shape and Texture,” Annual Book of ASTM Standards, Vol. 04.03, American Society for Testing and Materials, West Conshohocken, PA, 2000.
10. ASTM D 4123-82(1995), “Indirect Tension Test for Resilient Modulus of Bituminous Mixtures,” Annual Book of ASTM Standards, Vol. 04.03, American Society for Testing and Materials, West Conshohocken, PA, 2002.
11. ASTM D 4791-99, “Standard Test Method for Flat Particles, Elongated Particles, or Flat and Elongated Particles in Coarse Aggregate,” Annual Book of ASTM Standards, Vol. 04.03, American Society for Testing and Materials, Philadelphia, PA, 1999.

12. ASTM D 5821-95, "Standard Test Method for Determining the Percentage of Fractured Particles in Coarse Aggregate," Annual Book of ASTM Standards, Vol. 04.03, American Society for Testing and Materials, Philadelphia, PA, 1999.
13. Baladi, G. Y. and Harichandran, R. S., "Asphalt Mix Design and the Indirect Test: a New Horizon," Asphalt Concrete Mix Design: Development of More Rational Approaches, ASTM STP 1041, W. Gartner, Jr. (ed.), American Society for Testing and Materials, Philadelphia, pp. 86-105, 1989.
14. Barksdale, R.D., "Performances of Crushed Stone Base Courses", Transportation Research Record, (TRB), National Research Council, Washington, D.C., No. 954, pp. 78-87, 1984.
15. Barksdale, R. D. and Itani, S.Y., "Influence of Aggregate Shape on Base Behavior", Transportation Research Record (TRB), National Research Council, Washington, D.C., No. 1227, pp. 173-182, 1989.
16. Barksdale, R. D., Pollard, C. O. Siegel, T. and Moeller, S., "Evaluation of the Effects of Aggregate on Rutting and Fatigue of Asphalt," Research Report, Georgia DOT Project 8812, GA Tech Project E20-835, Georgia Institute of Technology, 1992.
17. Benson, F. J., "Effects of Aggregate Size, Shape, and Surface Texture on the Properties of Bituminous Mixtures – A Literature Review," Highway Research Board Special Report 109, pp. 12-21, 1970.
18. Bentz, D. P. and Garboczi, E. J., "Digital Image Based Computer Modeling and Visualization of Cement-Based Materials, Transportation Research Record No. 1526, pp. 129-134, 1996.
19. Boutlier, O. D., "A study of the Relation between the Particle Index of the Aggregate and the Properties of Bituminous Aggregate Mixtures," Proceedings, Association of Asphalt Paving Technologists, Vol. 36, 1967.
20. Brown, E. R. and Cross, S. A., "A National Study of Rutting in Hot Mix Asphalt (HMA) Pavements - Part 1 & Part 2," NCAT Report No. 1992-05, May 1992, pp.1-15, 1992.
21. Brown, E. R., Cooley, A., Hanson, D., Lynn, C., Powell, B., and Watson, D., "NCAT Test Track Design, Construction, and Performance," NCAT Report No. 2002-12, 2002.
22. Brzezicki, J. M. and Kasperkiewicz, J., "Automatic Image Analysis in Evaluation of Aggregate Shape," Journal of Computing in Civil Engineering, Vol. 13, No. 2, pp. 123-128, 1999.
23. Buchanan, M. S., "Evaluation of the Effect of Flat and Elongated Particles on the Performance of Hot Mix Asphalt Mixtures," National Center for Asphalt Technology Report No. 2000-03, May 2000.
24. Cable, J. K. and Marks, V.J., "Proceedings for the Automated Pavement Distress Data Collection Equipment Seminar," Ames, Iowa, June 12-15, 1990.
25. Chang, L., Abdelrazig, Y., and Chen, P., "Optical Imaging Method for Bridge Painting Maintenance and Inspection," Final Report, FHWA/IN/JTRP-99/11, Joint Transportation Research Program, Purdue University, April 2000.
26. Choubane B., Wu, C. L., and Tia, M., "Coarse Aggregate Effects on Elastic Moduli of concrete," Transportation Research Record (TRB), No. 1547, National Research Council, Washington, D.C., pp. 29-34, 1996.

27. Epps, A. L., Hand, A. J., Epps, J. A., and Sebaaly, P. E., "Aggregate Contributions to the Performance of Hot Mix Asphalt at WesTrack," *Aggregate Contribution to Hot Mix Asphalt (HMA) Performance*, ASTM Stock Number: STP 1412, 2001.
28. Fan, L. T. and Yashima, M., "Analysis of Aggregate Shape by Means of Video Imaging Technology and Fractal Analysis," Report No. KSU-93-3 for Kansas Department of Transportation, prepared by the Kansas State University, Manhattan, Kansas, 1993.
29. Fletcher, T., Chandan, C., Masad, E., and Sivakumar, K., "Measurement of Aggregate Texture and its Influence on HMA Permanent Deformation," *ASTM Journal of Testing and Evaluation*, Vol. 30, No. 6, pp. 524-531, 2002.
30. Glaser, S. D. and Haud, M. K., "Active Imaging of Sub-Millimeter-Scale Fractures in Rocks," In *Symposium Proceedings on Nondestructive and Automated Testing for Soil and Rock Properties*, ASTM Committee D18 on Soil and Rock, San Diego, CA, January 15-16, 1998.
31. Garboczi, E. J., Bullard, J. W., and Bentz, D.P., "Virtual Testing of Cement and Concrete – USA 2004," *Concrete International* 26 (12), pp. 33-37, 2004.
32. Huang, E. Y., "A test for evaluating the Geometric Characteristics of Coarse Aggregate Particles," *Proceedings of American Society for Testing and Materials*, Vol. 62, 1962.
33. Huang, E. Y., "An improved Particle Index Test for the Evaluation of Geometric Characteristics of Aggregate," *American Society for Testing and Materials Journal of Materials*, Vol.2, No.1, 1967.
34. Kandhal, P. S. and Parker, F., "Aggregate Tests Related to Asphalt Concrete Performance in Pavements", *National Cooperative Highway Research Program Report 405*, 1998.
35. Kandhal, P. S., and Cooley, L. A. Jr. "Investigation of the Restricted Zone in the SuperPave Aggregate Gradation Specification," *NCHRP Project 9-14, Draft Final Report*, April 2001.
36. Kandhal, P. S. and Cooley, L. A. Jr., "Coarse Versus Fine graded SuperPave Mixtures: Comparative Evaluation of Resistance to Rutting," *NCAT Report No. 2002-02*, pp. 2-6, 2002.
37. Kasturi, R. and Trivedi, M. M., "Image Analysis Applications", Marcel Dekker, Inc., New York, 1990.
38. Kennedy, T. W., Huber, G.A., Harrigan, E.T., Cominsky, R.J., Hughes, C.S., Quintus, H.V., and Moulthrop, J.S., "Superior Performing Asphalt Pavements (Superpave), The Product of the SHRP Asphalt Research Program," *SHRP-A-410*, 1994.
39. Kose, S., Guler, M., Bahia, H. U. and Masad, E., "Distribution of Strains within Hot-Mix Asphalt Binders: Applying Imaging and Finite-Element Techniques," *Transportation Research Record No. 1728*, National Research Council, Washington, D.C., pp. 21-27, 2000.
40. Laboratories Central Des Ponts et Chaussees (LCPC), "VDG 40 Measurement of Particle Size Distribution of Granular Mixtures," *Commercial Catalogue*, also in the *VDG 40 Technical Bulletin*, *Ministere de l'Equipement*, July 1995.

41. Li, L., Chan, P., Zollinger, D. G., and Lytton, R.L., "Quantitative Analysis of Aggregate Shape Based on Fractals," *ACI Materials Journal*, Vol. 90, No.4, pp. 357-365, July-August 1993.
42. Li, M.C. and Kett, I., "Influence of Coarse Aggregate Shape on the Strength of Asphalt Concrete Mixtures," *Highway Research Record No. 178*, pp. 93-106, 1967.
43. Livneh, M. and Greenstein, J., "Influence of Aggregate Shape on Engineering Properties of Asphaltic Paving Mixtures," *Highway Research Record No. 404*, pp. 42-56, 1972.
44. Maerz, N. H., Palangio, T. C., and Franklin, J. A., "WipFrag Image Based Granulometry System," WipWare Inc.; also in the *WipFrag Technical Bulletin*, WipWare Inc., 1996.
45. Maerz, N. H., "Aggregate Sizing and Shape Determination Using Digital Image Processing," In *Proceedings of the Sixth Annual Symposium of the International Center for Aggregate Research (ICAR)*, St. Louis, Missouri, April 19-21, pp. 195-203, 1998.
46. Mamlouk, S. M. and Ramsis, S. T., "The Modulus of Asphalt Mixtures – An Unresolved Dilemma," *Transportation Research Board (TRB), National Research Council, 67th Annual Meeting Proceedings*, Washington, D.C., 1988.
47. Masad, E., Muhunthan, B., Shashidhar, N., and Harman, T., "Internal Structure Characterization of Asphalt Concrete Using Image Analysis" *Journal of Computing in Civil Engineering* Vol. 13, pp. 88-95, 1998.
48. Masad, E., Muhunthan, B., Shashidhar, N. and Harman, T., "Quantifying Laboratory Compaction Effects on the Internal Structure of Asphalt Concrete" *Transportation Research Record (TRB), National Research Council, No. 1681*, Washington, D.C., pp. 179-185, 1999.
49. Masad, E. and Button, J. W., "Unified Imaging Approach for Measuring Aggregate Angularity and Texture," *The International Journal of Computer-Aided Civil and Infrastructure Engineering – Advanced Computer Technologies in Transportation Engineering*, Vol. 15, No. 4, 2000, pp. 273-280, 2000.
50. Masad, E., Olcott, D., White, T., and Tashman, L., "Correlation of Imaging Shape Indices of Fine Aggregate with Asphalt Mixture Performance," Presented at the 80th Annual Meeting of the *Transportation Research Board, National Research Council*, Washington D.C., 2001.
51. Masad, E., Jandhyala, V. K., Dasgupta, J., Somadevan, N. and Shashidhar, N. "Characterization of Air Void Distribution in Asphalt Mixes using X-Ray CT," *Journal of Materials in Civil Engineering*, ASCE, Vol. 14, No. 2, pp. 122-129, 2002.
52. Maupin, G. W., "Effect of Particle Shape and Surface Texture on the Fatigue Behavior of Asphaltic Concrete," *Highway Research Record No. 313*, pp. 55-62, 1970.
53. McGennis, R. B., Anderson, R. M., Kennedy, T. W., and Solaimanian, M., "Background of Superpave Asphalt Mixture Design and Analysis," *Final Report No. FHWA-SA-95-003*, Federal Highway Administration, U.S. Department of Transportation, February 1995.
54. McLeod, N. W. and Davidson, J. K., "Particle Index Evaluation of Aggregates for Asphalt Paving Mixtures," In *Proceedings of the Association of Asphalt Paving Technologists*, Vol. 50, 1981.

55. Mindess, S. and Young, F., "Concrete," Prentice Hall, Englewood Cliffs, NJ, 1981.
56. Monismith, C. L., "Influence of Shape, Size, and Surface Texture on the Stiffness and Fatigue Response of Asphalt Mixtures," Highway Research Board Special Report No. 109, pp. 4-11, 1970.
57. National Stone Association, "The Aggregate Handbook," Edited by R.D. Barksdale, 1991.
58. Powell, B., "As-Built Properties of Experimental Sections on the 2000 NCAT Pavement Test Track," NCAT Report No.2001-02, National Center for Asphalt Technology, Auburn, AL, pp. 13-94, 2001.
59. Prowell, B. D. and Weingart, R. L., "Precision of Flat and Elongated Particle Tests: ASTM 4791 and VDG 40 Video Grader," Presented at the 78th Annual Meeting of the Transportation Research Board, Washington D.C., January 10-14, 1999.
60. Puzinauskas, V. P., "Influence of Mineral Aggregate Structure on Properties of Asphalt Paving Mixtures," Highway Research Record No. 51, pp. 1-18. 1964.
61. Rao, C., "Determination of 3-D Image Analysis Techniques to Determine Shape and Size Properties of Coarse Aggregates," Ph.D. Thesis, University of Illinois at Urbana-Champaign, 2001.
62. Rao, C., Tutumluer, E., and Stefanski, J. A. "Flat and Elongated Ratios and Gradation of Coarse Aggregates Using a New Image Analyzer," ASTM Journal of Testing and Standard, Vol. 29, No. 5, 2001, pp. 79-89, 2001.
63. Rao, C., Tutumluer, E., and Kim, I-T. "Quantification of Coarse Aggregate Angularity based on Image Analysis," Transportation Research Record (TRB), National Research Council, No. 1787, Washington, D.C., pp. 117-124, 2002.
64. Rao, C., Pan, T., and Tutumluer, E., "Determination of Coarse Aggregate Surface Texture Using Imaging Analysis," In Proceedings of the 16th ASCE Engineering Mechanics Conference, University of Washington, Seattle, 2003.
65. Raschke, S. A., "Automated Imaging Approach for Soil GSD Analysis," In Proceedings of the Symposium on Nondestructive and Automated Testing for Soil and Rock Properties, ASTM Committee D18 on Soil and Rock, San Diego, CA, January 15-16, 1998.
66. Ribble, C., Szecsy, R., and Zollinger, D., "Aggregate Macro shape & Micro Texture in Concrete Mix Design," Texas Section ASCE Spring Meeting, Fort Worth, Texas, April 24, 1992.
67. Robert, F. L., Kandhal, P. S., Brown, E. R., Lee, D. Y. and Kennedy, T.W., "Hot Mix Asphalt Materials, Mixture Design, and Construction," NAPA Education Foundation, Lanham MD, pp. 502-507, 1996.
68. Russ, J.C., "The Image Processing Handbook," 3rd Edition, CRC Press, Boca Raton, FL, 1992.
69. Seed, H.C., Chan, C. K., and Lee, C. E., "Resilient Characteristics of Subgrade Soils and Their Relation to Fatigue Failures in Asphalt Pavements," In Proceedings of the 1st International Conference on the Structural Design of Asphalt Pavements, University of Michigan, Ann Arbor, MI, 1962.

70. Seward, D. L, Hinrichsen, J. A., and Ries, J. L., "Structure Analysis of Aggregate Blends Using Strategic Highway Research Program Gyratory Compactor," Transportation Research Record (TRB), National Research Council, No. 1545, Washington, D.C., 1996.
71. Tutumluer, E., Rao, C., and Stefanski, J. A., "Video Image Analysis of Aggregates," Final Project Report, FHWA-IL-UI-278, Civil Engineering Studies UILU-ENG-2000-2015, University of Illinois Urbana-Champaign, Urbana, IL, 2000.
72. Underwood, E. E., "Quantitative Stereology", Addison Wesley, Reading, MA, 1970.
73. Van der Poel, C. A., "General System Describing the Viscoelastic Properties of Bitumens and its Relationship to Routine Test Data," Journal of Applied Chemistry, May 1954.
74. Vavrik, W. R., Fries, R. J., Carpenter, S. H. and Aho, B. D., "Effect of Flat and Elongated Coarse Aggregate on Characteristics of Gyratory Compacted Samples," Final Report, Project IHR-R22, Illinois Cooperative Highway Research Program, Illinois Department of Transportation, March, 2000.
75. Wang, L. B., Frost, J. D., and Lai, J. S. "Microstructure Study of WesTrack Mixes from X-ray Tomography Images," Presented at the Transportation Research Board Annual Meeting, National Research Council, Washington, D.C. 2001.
76. Weingart, R. L. and Prowell, B. D., "Flat and Elongated Aggregate Tests: Can the VDG 40 Video Grader Deliver the Needed Precision and be Economically Viable?" In Proceedings of the 6th Annual Symposium of the International Center for Aggregate Research (ICAR), St. Louis, Missouri, pp. 219-229, April 19-21, 1998.
77. Weingart, R. L. and Prowell, B. D., "Specification Development Using the VDG 40 Videograder for Shape Classification of Aggregates," In Proceedings of the 7th Annual Symposium of the International Center for Aggregate Research (ICAR), University of Texas, Austin, pp. B1-2-1 to B1-2-12, April 19-21, 1999.
78. Wiebel, E. R., "Stereological Methods," Volumes I and II, Academic Press, London, 1979.
79. Wilson, J. D. and Klotz, L. D., "Quantitative Analysis of Aggregate Based on Hough-Transform," Transportation Research Record No. 1530, TRB, National Research Council, Washington D.C., pp. 111-115, 1996.
80. Wilson, J. D., Klotz, L. D., and Nagaraj, C., "Automated Measurement of Aggregate Indices of Shape," Particulate Science and Technology, Vol. 15, pp. 13-35, October 1997.
81. Witeczak, M. W., Kaloush, K. T. Pellinen, M. El-Basyouny and Von Quintus, H., "Simple Performance Test for Superpave Mix Design," NCHRP Report 465, Transportation Research Board, National Research Council, Washington, D.C., pp. 11-13, 53, 58, 2002.
82. Yeggoni, M., Button, J. W. and Zollinger, D. G., "Influence of Coarse Aggregate Shape and Surface Texture on Rutting of Hot Mix Asphalt," Research Report 1244-6, Texas Transportation Institute, Texas A&M University System, October 1994.
83. Yue, Z. Q., Bekking, W. and Morin, I., "Application of Digital Image Processing to Quantitative Study of Asphalt Concrete Microstructure," Transportation Research Record (TRB), National Research Council, No. 1492, pp. 53-60, 1995.

APPENDIX I

MIX DESIGNS USED IN THE LABORATORY TESTS

Central FLHD (New Mexico)

General Description of Mix and Materials

Design Method: Superpave Mix Design
Binder Performance Grade: PG 58-34
Modifier Type: NA
Aggregate Type: NA
Gradation Type: TRZ

Mix Design From State Agency

Avg. Lab Properties of Plant Produced Mix

<u>Sieve Size:</u>	<u>% Passing:</u>
1"	100
3/4"	99
1/2"	84
3/8"	73
No. 4	55
No. 8	38
No. 16	26
No. 30	18
No. 50	13
No. 100	9
No. 200	5.6

Asphalt Binder Content: 5.2%
Target Air Voids: 4.0%

Target Blend Proportions

<u>Component:</u>	<u>%</u>	<u>Target Weight (g)</u>
7/8" Rock	12%	732
Coarse Aggregate	21%	1281
Intermediate Aggregate	15%	915
Crushed Aggregate	51%	3111
Hydrated Lime	1%	61
Total Agg. Weight:		6100

Mixing and Compaction Temperatures

Viscosity (Pa-s) @ 135 ° C: 0.285
Viscosity (Pa-s) @ 165 ° C: 0.110
Mixing Temperature Range: 144°C - 151 °C
Compaction Temperature Range: 131°C - 136 °C

Note: **The highlighted** are the coarse aggregate samples evaluated in this project by UIAIA.

Central FLHD (OK)

General Description of Mix and Materials

Design Method: Superpave Mix Design
Binder Performance Grade: PG 70-28
Modifier Type: N/A
Aggregate Type: N/A
Gradation Type: ARZ

Mix Design From State Agency

Avg. Lab Properties of Plant Produced Mix

<u>Sieve Size:</u>	<u>% Passing:</u>	
1"		100
3/4"		96
1/2"		86
3/8"		80
No. 4		67
No. 8		48
No. 16	N/A	
No. 30		24
No. 40		19
No. 50		14
No. 100	N/A	
No. 200		4.0
Asphalt Binder Content:		5.1%
Target Air Voids:		4.0%

Target Blend Proportions

<u>Component:</u>	<u>%</u>	<u>Target Weight (g)</u>
1 inch Rock	21%	1281
0.5 inch Rock	12%	732
Screens	30%	1830
Stone Sand	25%	1525
Sand	12%	732
Total Agg. Weight:		6100

Mixing and Compaction Temperatures

Viscosity (Pa-s) @ 135 ° C:
Viscosity (Pa-s) @ 165 ° C:
Mixing Temperature Range: 177 °C - 185°C
Compaction Temperature Range: 164 °C - 169 °C

Georgia 1 (047-12.5SP-10--004L)

General Description of Mix and Materials

Design Method:	Superpave Mix Design
Binder Performance Grade:	PG 67-22
Modifier Type:	N/A
Aggregate Type:	N/A
Gradation Type:	BRZ

Mix Design From State Agency

Avg. Lab Properties of Plant Produced Mix

<u>Sieve Size:</u>		<u>% Passing:</u>
1"		100
3/4"		100
1/2"		99
3/8"		79
No. 4		46
No. 8		32
No. 16		25
No. 30		19
No. 50		13
No. 100		9
No. 200		4.5
Asphalt Binder Content:	276.33	4.53%
Target Air Voids:		4.0%

Target Blend Proportions

<u>Component:</u>	<u>%</u>	<u>Target Weight (g)</u>
007	42%	2562
810	25%	1525
W10	18%	1098
89	14%	854
Hydr. Lime	1.0%	61
Total Agg. Weight:		6100

Mixing and Compaction Temperatures

Viscosity (Pa-s) @ 135 ° C:	
Viscosity (Pa-s) @ 165 ° C:	
Mixing Temperature Range:	150° C
Compaction Temperature Range:	150° C

Georgia 2 (121-12.SSP-14--016L)

General Description of Mix and Materials

Design Method:	Superpave Mix Design
Binder Performance Grade:	PG 76-22
Modifier Type:	N/A
Aggregate Type:	N/A
Gradation Type:	BRZ

Mix Design From State Agency

Avg. Lab Properties of Plant Produced Mix

<u>Sieve Size:</u>	<u>% Passing:</u>
1"	100
3/4"	100
1/2"	98
3/8"	80
No. 4	50
No. 8	36
No. 16	24
No. 30	19
No. 50	12
No. 100	8
No. 200	5.6

Asphalt Binder Content:	4.70%
Target Air Voids:	4.0%

Target Blend Proportions

<u>Component:</u>	<u>%</u>	<u>Target Weight (g)</u>
078	53%	3233
M10	46%	2806
Hydr. Lime	1.0%	61
Total Agg. Weight:		6100

Mixing and Compaction Temperatures

Viscosity (Pa-s) @ 135 ° C:	
Viscosity (Pa-s) @ 165 ° C:	
Mixing Temperature Range:	150° C
Compaction Temperature Range:	150° C

Georgia 3 (024-12.5SP-31--015L)

General Description of Mix and Materials

Design Method:	Superpave Mix Design
Binder Performance Grade:	PG 76-22
Modifier Type:	N/A
Aggregate Type:	N/A
Gradation Type:	TRZ

Mix Design From State Agency

Avg. Lab Properties of Plant Produced Mix

<u>Sieve Size:</u>	<u>% Passing:</u>
1"	100
3/4"	100
1/2"	100
3/8"	92
No. 4	68
No. 8	47
No. 16	30
No. 30	20
No. 50	13
No. 100	7.8
No. 200	4.71

Asphalt Binder Content:	4.73%
Target Air Voids:	4.0%

Target Blend Proportions

<u>Component:</u>	<u>%</u>	<u>Target Weight (g)</u>
007	33%	2013
89	25%	1525
M10	33%	2013
W10	8%	488
Hydr. Lime	1.0%	61
Total Agg. Weight:		6100

Mixing and Compaction Temperatures

Viscosity (Pa-s) @ 135 ° C:	
Viscosity (Pa-s) @ 165 ° C:	
Mixing Temperature Range:	150° C
Compaction Temperature Range:	150° C

Indiana 1
9.5 mm surface mixture (R-21466)

General Description of Mix and Materials

Design Method:	Superpave Mix Design
Binder Performance Grade:	PG 64-22
Modifier Type:	N/A
Aggregate Type:	N/A
Gradation Type:	BRZ

Mix Design From State Agency

Avg. Lab Properties of Plant Produced Mix

<u>Sieve Size:</u>	<u>% Passing:</u>
1"	100
3/4"	100
1/2"	100
3/8"	92.1
No. 4	57.3
No. 8	40.4
No. 16	29.2
No. 30	17
No. 50	8.7
No. 100	5.8
No. 200	4.7

Asphalt Binder Content:	5.5%
Target Air Voids:	4.0%

Target Blend Proportions

<u>Component:</u>	<u>%</u>	<u>Target Weight (g)</u>
#11 Cr Gravel Interstate-2164	53%	3233
QA FM-01 Stone Sand-2445	15%	915
# 23 Natural Sand-2164	30%	1830
Composite Baghouse return	2%	122
Total Agg. Weight:		6100

Mixing and Compaction Temperatures

Viscosity (Pa-s) @ 135 ° C:	
Viscosity (Pa-s) @ 165 ° C:	
Mixing Temperature Range:	154 °C
Compaction Temperature Range:	143 °C

Indiana 2

9.5 mm surface mixture (M-26489)

General Description of Mix and Materials

Design Method:	Superpave Mix Design
Binder Performance Grade:	PG 64-22
Modifier Type:	N/A
Aggregate Type:	N/A
Gradation Type:	BRZ

Mix Design From State Agency

Avg. Lab Properties of Plant Produced Mix

<u>Sieve Size:</u>	<u>% Passing:</u>
1"	100
3/4"	100
1/2"	100
3/8"	94.5
No. 4	61.0
No. 8	39.0
No. 16	29.0
No. 30	20.5
No. 50	11.0
No. 100	5.5
No. 200	3.7

Asphalt Binder Content:	4.9%
Target Air Voids:	4.0%

Target Blend Proportions

<u>Component:</u>	<u>%</u>	<u>Target Weight (g)</u>
#11 Cr Gravel-2432	40%	2440
QA #12 Stone-2461	23%	1403
# 23 Natural Sand-2432	35%	2135
Composite Baghouse return	2%	122
Total Agg. Weight:		6100

Mixing and Compaction Temperatures

Viscosity (Pa-s) @ 135 ° C:	
Viscosity (Pa-s) @ 165 ° C:	
Mixing Temperature Range:	127-154 °C
Compaction Temperature Range:	132 °C

Minnesota 1

General Description of Mix and Materials

Design Method:	Superpave Mix Design
Binder Performance Grade:	PG 64-22
Modifier Type:	N/A
Aggregate Type:	N/A
Gradation Type:	BRZ

Mix Design From State Agency

Avg. Lab Properties of Plant Produced Mix

<u>Sieve Size:</u>	<u>% Passing:</u>
1"	100
3/4"	100
1/2"	93
3/8"	80
No. 4	52
No. 8	35
No. 16	23
No. 30	14
No. 50	7
No. 100	3
No. 200	2.5

Asphalt Binder Content:	5.4%
Target Air Voids:	4.0%

Target Blend Proportions

<u>Component:</u>	<u>%</u>	<u>Target Weight (g)</u>
Meridian St. Cloud 3/4 " Unwashed Sand	9%	549
Meridian St. Cloud CA-50	30%	1830
Meridian St. Cloud FA-3	21%	1281
Meridian Washed Sand	20%	1220
Kraemer Burnsville Washed Sand	15%	915
Barton Elk River #1 Washed Sand	5%	305
Total Agg. Weight:		6100

Mixing and Compaction Temperatures

Viscosity (Pa-s) @ 135 ° C:	
Viscosity (Pa-s) @ 165 ° C:	
Mixing Temperature Range:	145°C-150°C
Compaction Temperature Range:	131°C-136°C

Minnesota 2

General Description of Mix and Materials

Design Method:	Superpave Mix Design
Binder Performance Grade:	PG 58-28 Without A.S.
Modifier Type:	N/A
Aggregate Type:	N/A
Gradation Type:	TRZ

Mix Design From State Agency

Avg. Lab Properties of Plant Produced Mix

<u>Sieve Size:</u>	<u>% Passing:</u>
1"	100
3/4"	100
1/2"	96
3/8"	79
No. 4	60
No. 8	49
No. 16	36
No. 30	25
No. 50	13
No. 100	5
No. 200	3

Asphalt Binder Content:	5.2%
Target Air Voids:	4.0%

Target Blend Proportions

<u>Component:</u>	<u>%</u>	<u>Target Weight (g)</u>
Barton Denmark BA-2	18%	1098
Kraemer Burnsville Class 2	8%	488
Kraemer Burnsville 9/16" Chip	34%	2074
Camas Nelson Man. Sand (Class D)	20%	1220
Camas West Lakeland Washed Sand	20%	1220
Total Agg. Weight:		6100

Mixing and Compaction Temperatures

Viscosity (Pa-s) @ 135 ° C:	
Viscosity (Pa-s) @ 165 ° C:	
Mixing Temperature Range:	145°C-150°C
Compaction Temperature Range:	131°C-136°C

Missouri 1 (AC-SP190HB)

General Description of Mix and Materials

Design Method: Superpave Mix Design
Binder Performance Grade: PG 70-22
Modifier Type: Morlife 5000 (0.5% by WT. of AC)
Aggregate Type: N/A
Gradation Type: BRZ

Mix Design From State Agency

Avg. Lab Properties of Plant Produced Mix

<u>Sieve Size:</u>	<u>% Passing:</u>
1"	100
3/4"	98.1
1/2"	88.9
3/8"	79.2
No. 4	39.7
No. 8	27.9
No. 16	17
No. 30	10.2
No. 50	5.3
No. 100	2.9
No. 200	2.2

Asphalt Binder Content:	4.9%
Target Air Voids:	4.0%

Target Blend Proportions

<u>Component:</u>	<u>%</u>	<u>Target Weight (g)</u>
Brickey's Stone 1 inch	13%	793
Brickey's Stone 3/4 inch	23%	1403
Brickey's Stone 1/2 inch	24%	1464
Brickey's Stone 3/8 inch	16%	976
Tower Rock Stone Man Sand	24%	1464

Total Agg. Weight:	6100
--------------------	------

Mixing and Compaction Temperatures

Viscosity (Pa-s) @ 135 ° C:
Viscosity (Pa-s) @ 165 ° C:
Mixing Temperature Range: 320°F-330°F
Compaction Temperature Range: 290°F-300°F

Missouri 2 (AC-SP190MC)

General Description of Mix and Materials

Design Method:	Superpave Mix Design
Binder Performance Grade:	PG 64-22
Modifier Type:	Ultra Pave 5000 (1.0 lb. / ton Aggregate)
Aggregate Type:	N/A
Gradation Type:	BRZ

Mix Design From State Agency

Avg. Lab Properties of Plant Produced Mix

<u>Sieve Size:</u>	<u>% Passing:</u>
1"	100
3/4"	100
1/2"	89.5
3/8"	73.1
No. 4	41.9
No. 8	24.6
No. 16	15
No. 30	10.1
No. 50	7.6
No. 100	6.6
No. 200	5.8

Asphalt Binder Content:	5.5%
Target Air Voids:	4.0%

Target Blend Proportions

<u>Component:</u>	<u>%</u>	<u>Target Weight (g)</u>
Joornagan, Joe Howard	17%	1037
Joornagan, Joe Howard 1/2 inch (Burl)	13%	793
Joornagan, Joe Howard 1/2 inch (Reeds)	60%	3660
Man Sand	10%	610
Total Agg. Weight:		6100

Mixing and Compaction Temperatures

Viscosity (Pa-s) @ 135 ° C:	
Viscosity (Pa-s) @ 165 ° C:	
Mixing Temperature Range:	320°F-330°F
Compaction Temperature Range:	290°F-300°F

Missouri 3 (AC-SP250MC)

General Description of Mix and Materials

Design Method:	Superpave Mix Design
Binder Performance Grade:	PG 64-22
Modifier Type:	LOF 65-00LS1(0.5% by WT. of AC)
Aggregate Type:	N/A
Gradation Type:	BRZ

Mix Design From State Agency

Avg. Lab Properties of Plant Produced Mix

<u>Sieve Size:</u>	<u>% Passing:</u>
1.5 "	100
1"	93
3/4"	88.9
1/2"	79.1
3/8"	64.1
No. 4	34.4
No. 8	19.9
No. 16	13.7
No. 30	11.2
No. 50	8.3
No. 100	5.3
No. 200	3.3
Asphalt Binder Content:	5.10%
Target Air Voids:	4.00%

Target Blend Proportions

<u>Component:</u>	<u>%</u>	<u>Target Weight (g)</u>
APAC-Central #60113 1.5 inch	12.0%	732
APAC-Central #60113 3/4 inch	33.3%	2031.3
APAC-Central #60113 1/2 inch	31.8%	1939.8
APAC-Central #60113 SG	7.4%	451.4
APAC-Central #60113 Man Sand	15.5%	945.5
Total Agg. Weight:		6100

Mixing and Compaction Temperatures

Viscosity (Pa-s) @ 135 ° C:	
Viscosity (Pa-s) @ 165 ° C:	
Mixing Temperature Range:	303°F-313°F
Compaction Temperature Range:	283°F-293°F

Mississippi 1

General Description of Mix and Materials

Design Method:	Superpave Mix Design
Binder Performance Grade:	PG 67-22
Modifier Type:	N/A
Aggregate Type:	N/A
Gradation Type:	TRZ

Mix Design From State Agency

Avg. Lab Properties of Plant Produced Mix

<u>Sieve Size:</u>	<u>% Passing:</u>
1"	100
3/4"	99
1/2"	89
3/8"	76
No. 4	45
No. 8	31
No. 16	23
No. 30	17
No. 50	12
No. 100	7
No. 200	5.7

Asphalt Binder Content:	5.1%
Target Air Voids:	4.0%

Target Blend Proportions

<u>Component:</u>	<u>%</u>	<u>Target Weight (g)</u>
Minus 1 inch Crushed Gravel	17%	1037
Minus 0.5 inch Crushed Gravel	73%	4453
Course Sand	5%	305
Agricultural Limestone	4%	244
Hydrated Lime	1%	61
Total Agg. Weight:		6100

Mixing and Compaction Temperatures

Viscosity (Pa-s) @ 135 ° C:	
Viscosity (Pa-s) @ 165 ° C:	
Mixing Temperature Range:	315°F-325°F
Compaction Temperature Range:	297°F-306°F

Mississippi 2

General Description of Mix and Materials

Design Method: Superpave Mix Design
Binder Performance Grade: PG 67-22
Modifier Type: N/A
Aggregate Type: N/A
Gradation Type: TRZ

Mix Design From State Agency

Avg. Lab Properties of Plant Produced Mix

<u>Sieve Size:</u>	<u>% Passing:</u>
1"	100
3/4"	100
1/2"	99
3/8"	89
No. 4	62
No. 8	41
No. 16	28
No. 30	21
No. 50	12
No. 100	7
No. 200	5.9

Asphalt Binder Content: 5.3%
Target Air Voids: 4.0%

Target Blend Proportions

<u>Component:</u>	<u>%</u>	<u>Target Weight (g)</u>
#78 LST	10%	610
#7 Granite	15%	915
#89 Granite	14%	854
#11 LST	20%	1220
1/4 GRANITESCREEINGS	30%	1830
CS	10%	610
Hydrated Lime	1%	61

Total Agg. Weight: 6100

Mixing and Compaction Temperatures

Viscosity (Pa-s) @ 135 ° C:
Viscosity (Pa-s) @ 165 ° C:
Mixing Temperature Range: 300°F
Compaction Temperature Range: 290°F

Montana 1

General Description of Mix and Materials

Design Method:	Superpave Mix Design
Binder Performance Grade:	PG 58-28
Modifier Type:	N/A
Aggregate Type:	N/A
Gradation Type:	BRZ

Mix Design From State Agency

Avg. Lab Properties of Plant Produced Mix

<u>Sieve Size:</u>		<u>% Passing:</u>	
	1"		100
	3/4"		100
	1/2"		79
	3/8"		64
	No. 4		40
	No. 8		27
	No. 16		20
	No. 30		16
	No. 50		11
	No. 100		7
	No. 200		4.9

Asphalt Binder Content:	311.1	5.10%
Target Air Voids:		4.00%

Target Blend Proportions

<u>Component:</u>	<u>%</u>	<u>Target Weight (g)</u>
Crushed Fines	26%	1586
Washed Crushed Fines	10%	610
3/8 inch chips	18%	1098
Coarse Aggregate	46%	2806
Total Agg. Weight:		6100

Hydrated Lime (% Total weight)	1.40%	85.4
--------------------------------	-------	------

Mixing and Compaction Temperatures

Viscosity (Pa-s) @ 135 ° C:	
Viscosity (Pa-s) @ 165 ° C:	
Mixing Temperature Range:	157 ° C
Compaction Temperature Range:	132 ° C

Montana 2

General Description of Mix and Materials

Design Method:	Superpave Mix Design
Binder Performance Grade:	PG 70-28
Modifier Type:	Styrene
Aggregate Type:	N/A
Gradation Type:	BRZ

Mix Design From State Agency

Avg. Lab Properties of Plant Produced Mix

<u>Sieve Size:</u>	<u>% Passing:</u>
1"	100
3/4"	100
1/2"	84
3/8"	69
No. 4	48
No. 8	32
No. 16	22
No. 30	16
No. 50	12
No. 100	8
No. 200	6

Asphalt Binder Content:	5.2%
Target Air Voids:	4.0%

Target Blend Proportions

<u>Component:</u>	<u>%</u>	<u>Target Weight (g)</u>
Crushed Fines	48%	2928
3/8 in Crushed Chips	12%	732
3/4 in Crushed Rock	40%	2440
Total Agg. Weight:		6100
Hydrated Lime (% Total weight)	1.4%	85.4

Mixing and Compaction Temperatures

Viscosity (Pa-s) @ 135 ° C:	
Viscosity (Pa-s) @ 165 ° C:	
Mixing Temperature Range:	135 °C - 176 °C
Compaction Temperature Range:	121 °C - 154 °C

South Carolina 1 (A0191)

General Description of Mix and Materials

Design Method:	Superpave Mix Design
Binder Performance Grade:	PG 76-22
Modifier Type:	N/A
Aggregate Type:	N/A
Gradation Type:	BRZ

Mix Design From State Agency

Avg. Lab Properties of Plant Produced Mix

<u>Sieve Size:</u>	<u>% Passing:</u>
1"	100
3/4"	100
1/2"	100
3/8"	89
No. 4	57
No. 8	33
No. 16	22
No. 30	14
No. 50	10
No. 100	6.3
No. 200	4.3

Asphalt Binder Content:	4.6%
Target Air Voids:	4.0%

Target Blend Proportions

<u>Component:</u>	<u>%</u>	<u>Target Weight (g)</u>
Blacksburg #78 M Stone	65%	3965
Wash Scrn	29%	1769
Reg. Scrn	5%	305
Hydrated Lime (% Total weight)	1.0%	61
Total Agg. Weight:		6100

Mixing and Compaction Temperatures

Viscosity (Pa-s) @ 135 ° C:	
Viscosity (Pa-s) @ 165 ° C:	
Mixing Temperature Range:	
Compaction Temperature Range:	154 °C

South Carolina 2 (A0198)

General Description of Mix and Materials

Design Method:	Superpave Mix Design
Binder Performance Grade:	PG 67-22
Modifier Type:	N/A
Aggregate Type:	N/A
Gradation Type:	BRZ

Mix Design From State Agency

Avg. Lab Properties of Plant Produced Mix

<u>Sieve Size:</u>	<u>% Passing:</u>
1"	100
3/4"	100
1/2"	86
3/8"	70
No. 4	42
No. 8	26
No. 16	17
No. 30	12
No. 50	9
No. 100	5.6
No. 200	3.73

Asphalt Binder Content:	4.2%
Target Air Voids:	4.0%

Target Blend Proportions

<u>Component:</u>	<u>%</u>	<u>Target Weight (g)</u>
Blacksburg#67 Stone	32%	1952
Blacksburg#78 M Stone	41%	2501
Reg. Scrn	5%	305
Wash Scrn	21%	1281
Hydrated Lime (% Total weight)	1.0%	61
Total Agg. Weight:		6100

Mixing and Compaction Temperatures

Viscosity (Pa-s) @ 135 ° C:	
Viscosity (Pa-s) @ 165 ° C:	
Mixing Temperature Range:	
Compaction Temperature Range:	145 °C

APPENDIX II

IMAGING RESULTS OF THE POOLED FUND STUDY AGGREGATE SAMPLES

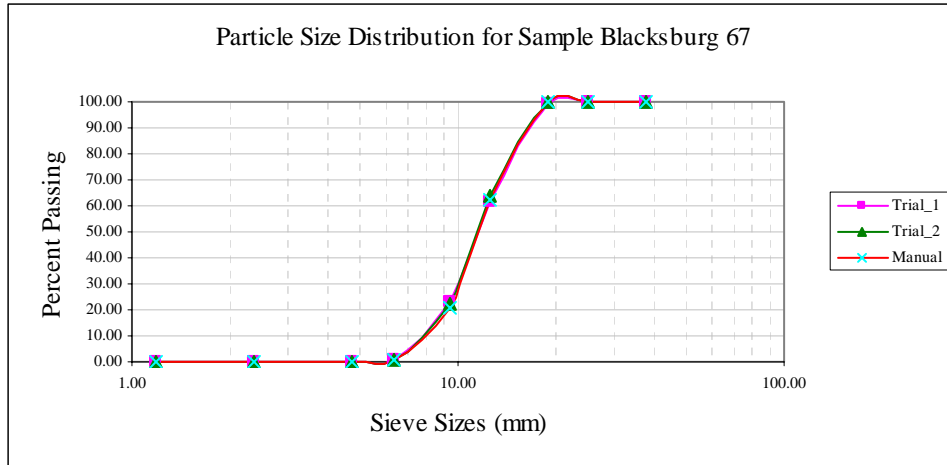


Figure AII-1 Imaging Based Particle Size Distributions of the Blacksburg 67 Sample

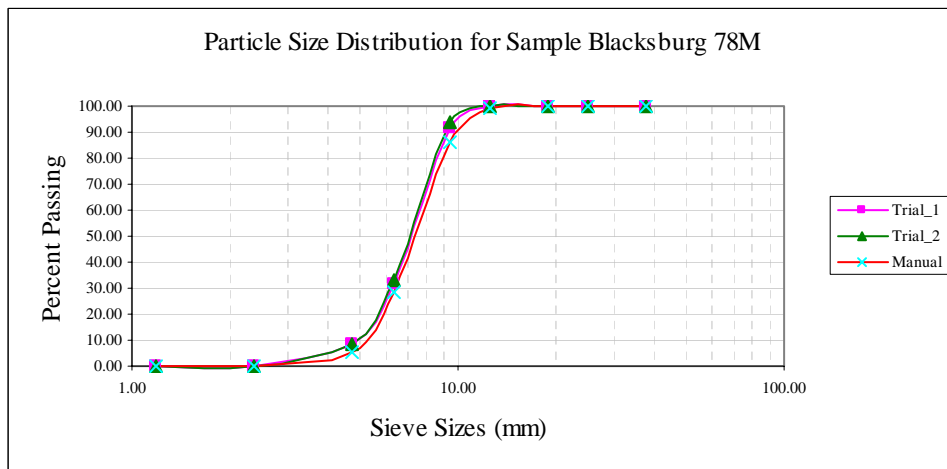


Figure AII-2 Imaging Based Particle Size Distributions of the Blacksburg 78M Sample

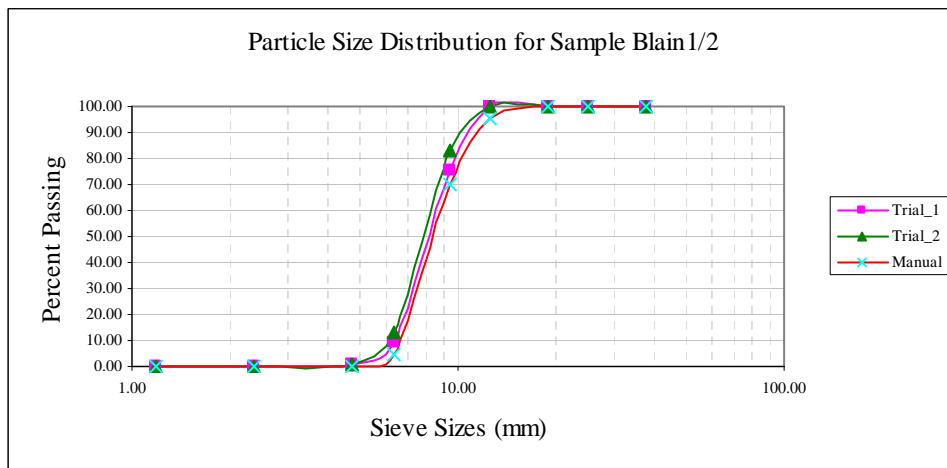


Figure AII-3 Imaging Based Particle Size Distributions of the Blain 1/2 in. Sample

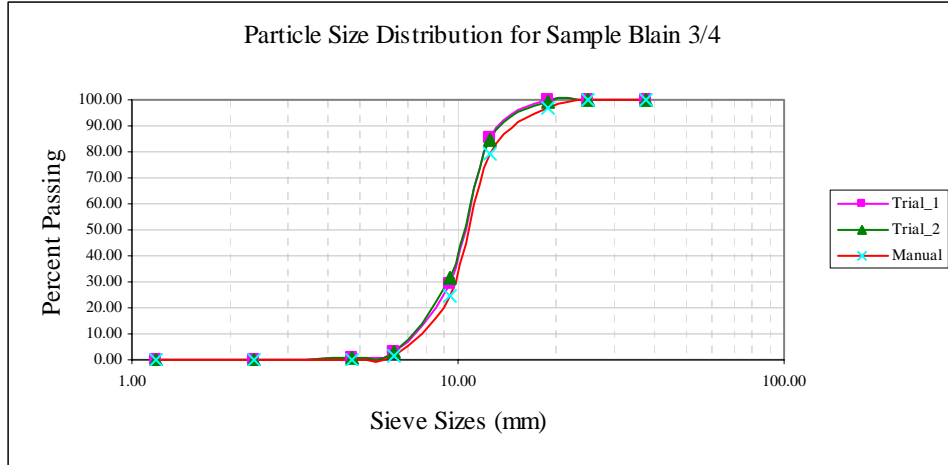


Figure AII-4 Imaging Based Particle Size Distributions of the Blain 3/4 in. Sample

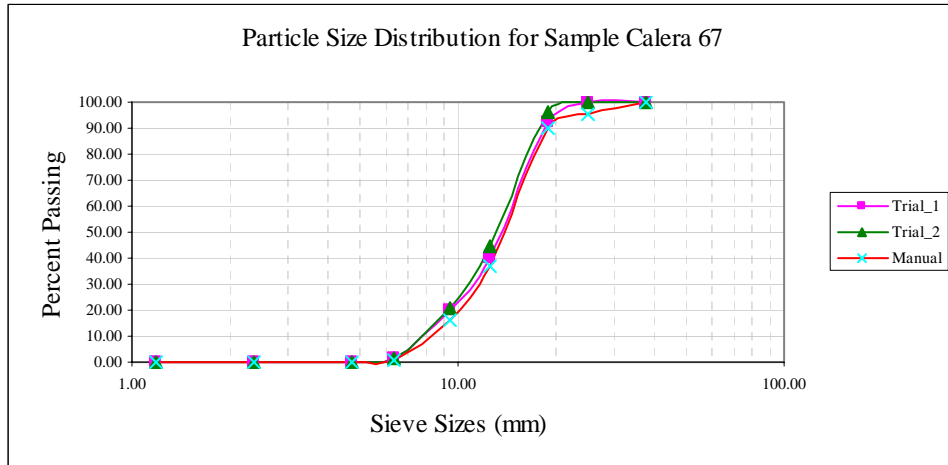


Figure AII-5 Imaging Based Particle Size Distributions of the Calera 67 Sample

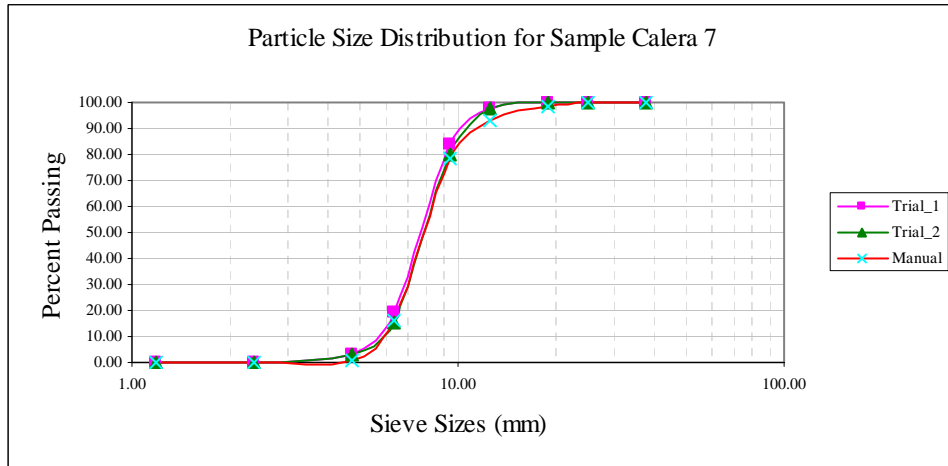


Figure AII-6 Imaging Based Particle Size Distributions of the Calera 7 Sample

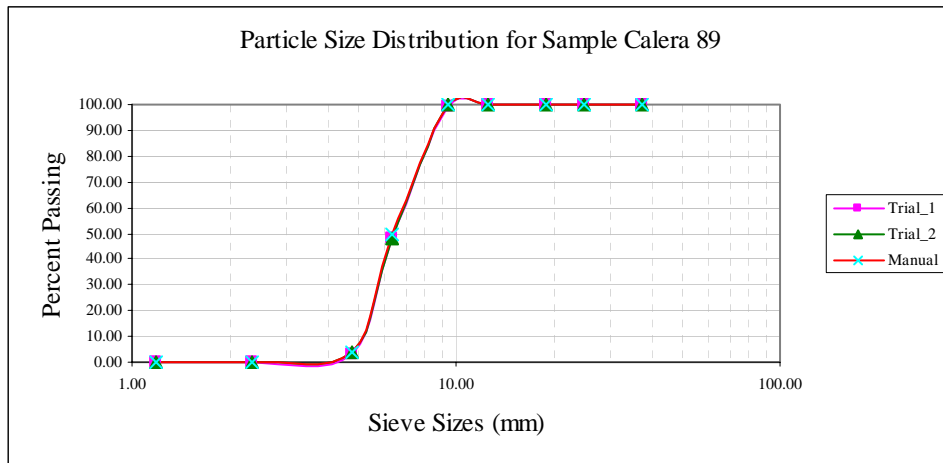


Figure AII-7 Imaging Based Particle Size Distributions of the Calera 89 Sample

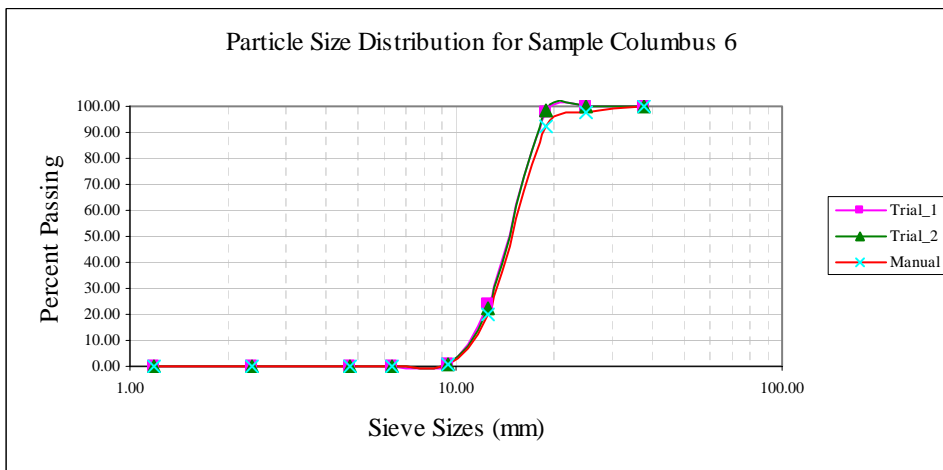


Figure AII-8 Imaging Based Particle Size Distributions of the Columbus 6 Sample

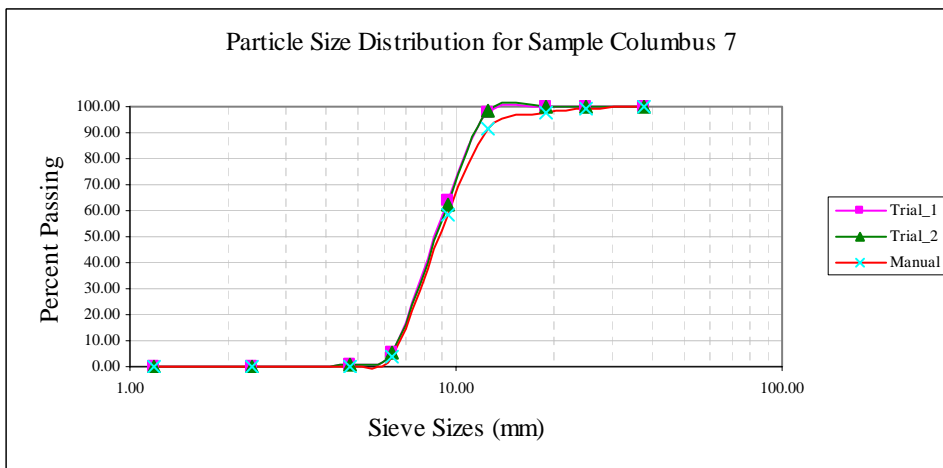


Figure AII-9 Imaging Based Particle Size Distributions of the Columbus 7 Sample

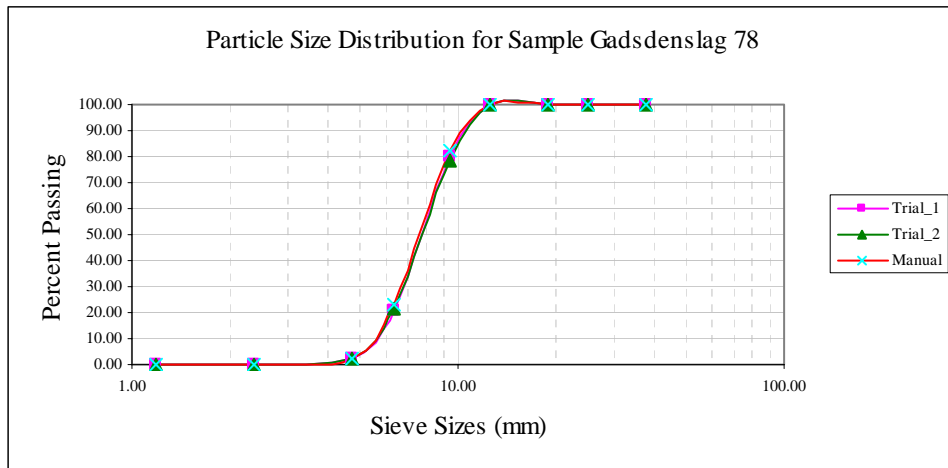


Figure AII-10 Imaging Based Particle Size Distributions of the Gadsdenslag 78 Sample

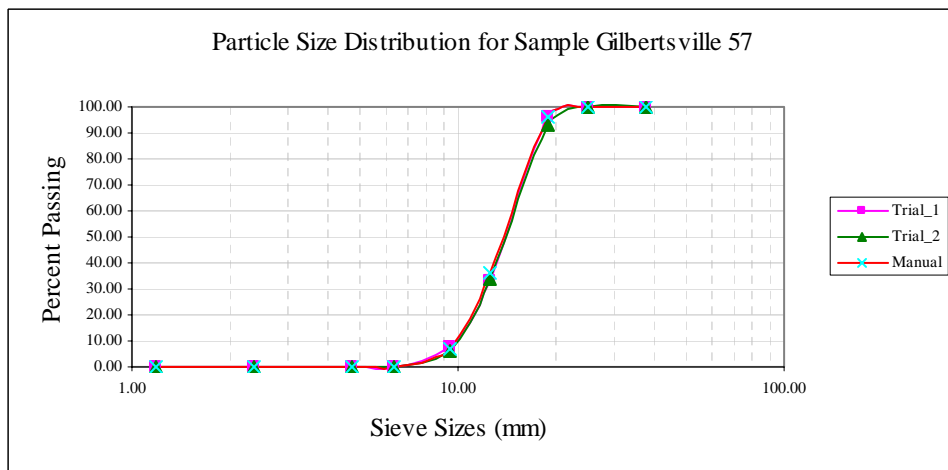


Figure AII-11 Imaging Based Particle Size Distributions of the Gilbertsville 57 Sample

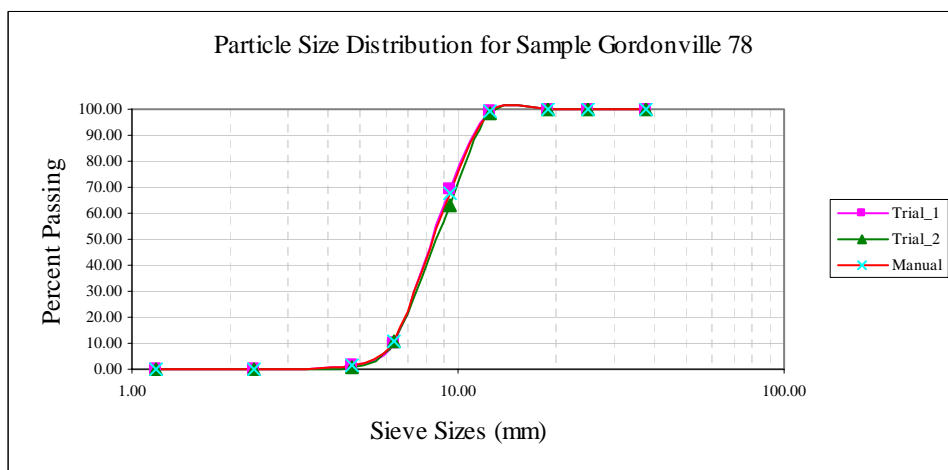


Figure AII-12 Imaging Based Particle Size Distributions of the Gordonville 78 Sample

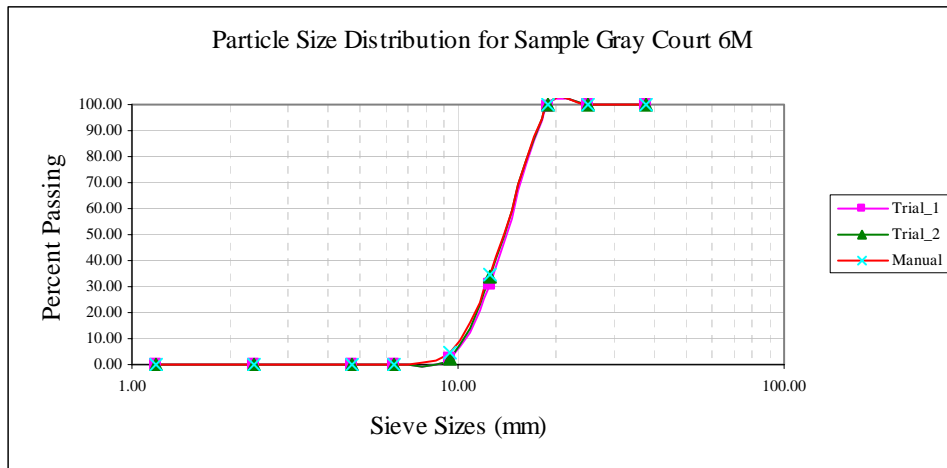


Figure AII-13 Imaging Based Particle Size Distributions of the Gray Court 6M Sample

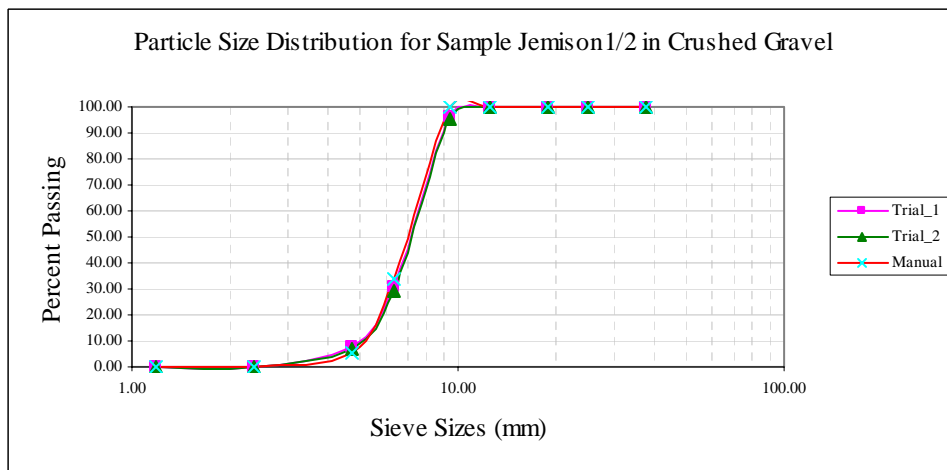


Figure AII-14 Imaging Based Particle Size Distributions of the Jemison 1/2 in. Sample

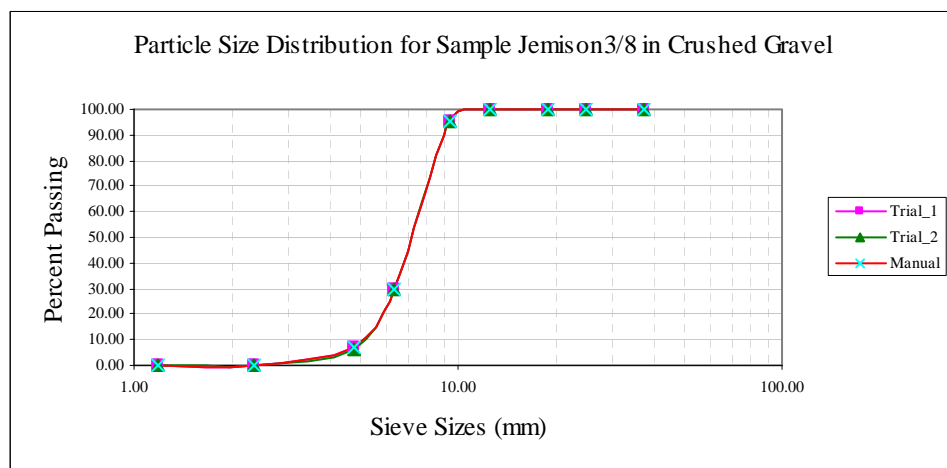


Figure AII-15 Imaging Based Particle Size Distributions of the Jemison 3/8 in. Sample

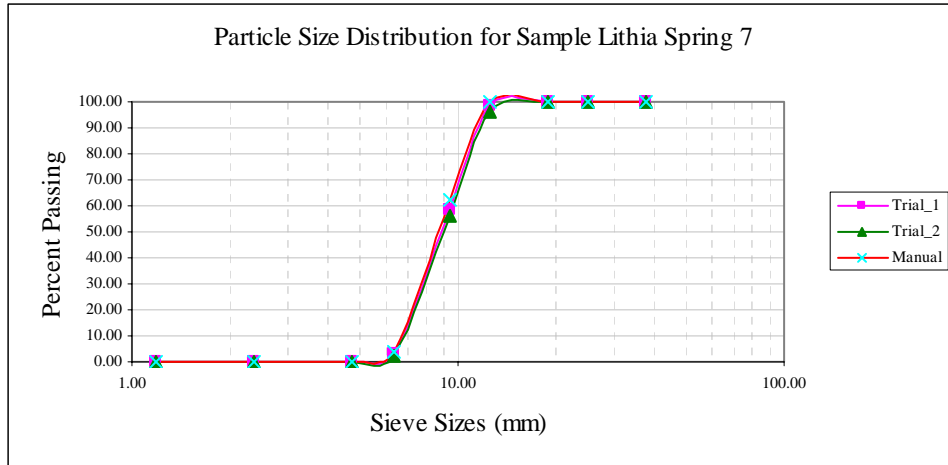


Figure AII-16 Imaging Based Particle Size Distributions of the Lithia Spring 7 Sample

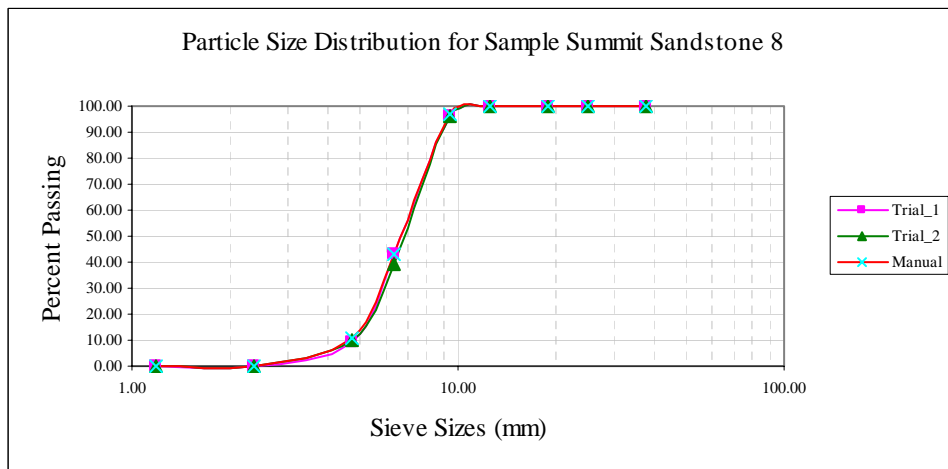


Figure AII-17 Imaging Based Particle Size Distributions of the Summit Sandstone 8 Sample

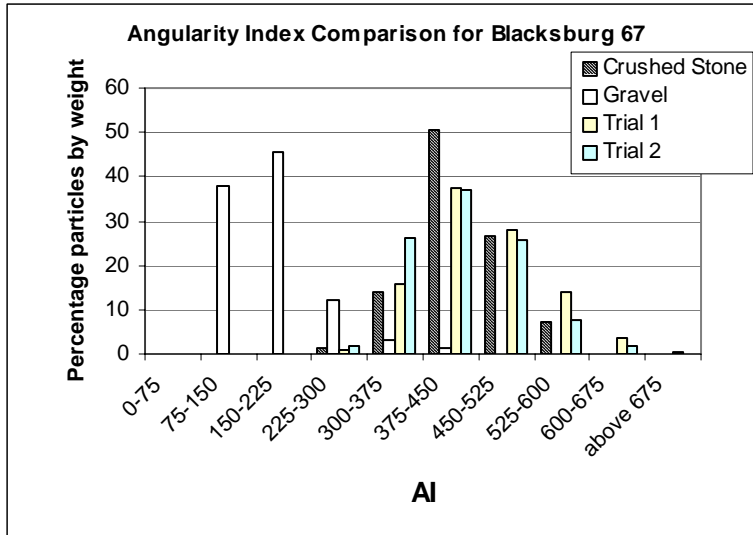


Figure AII-18 Imaging Based AI of the Blacksburg 67 Sample

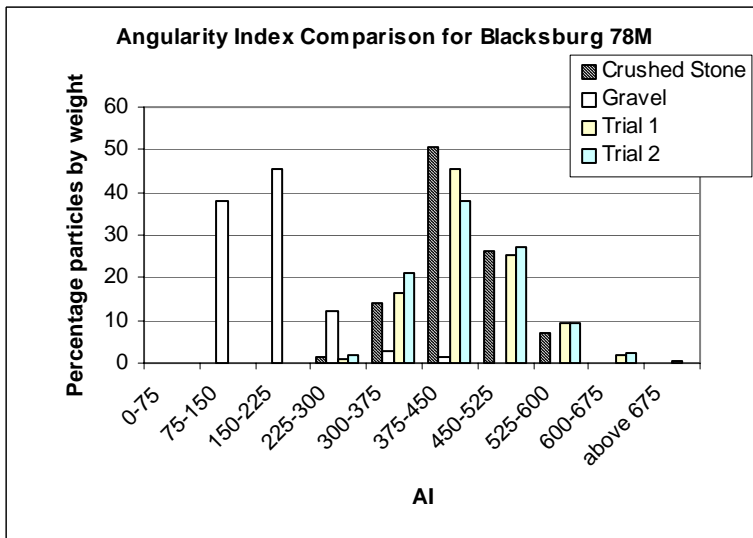


Figure AII-19 Imaging Based AI of the Blacksburg 78M Sample

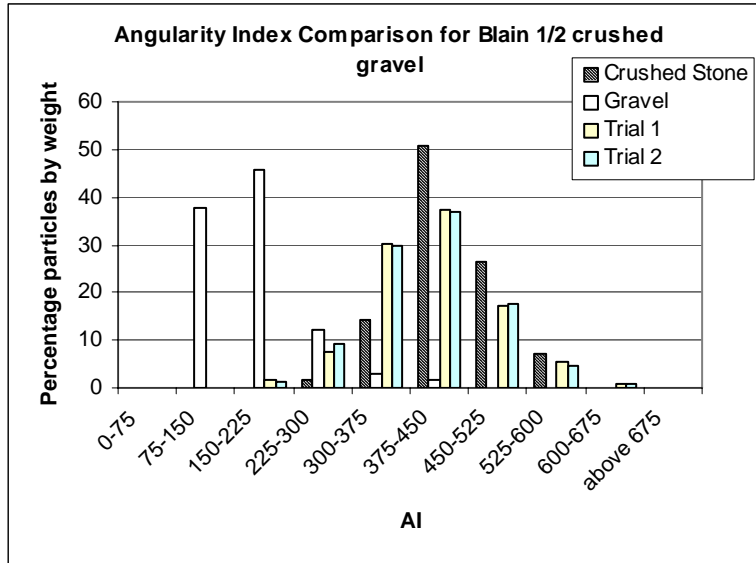


Figure AII-20 Imaging Based AI of the Blain 1/2 in. Sample

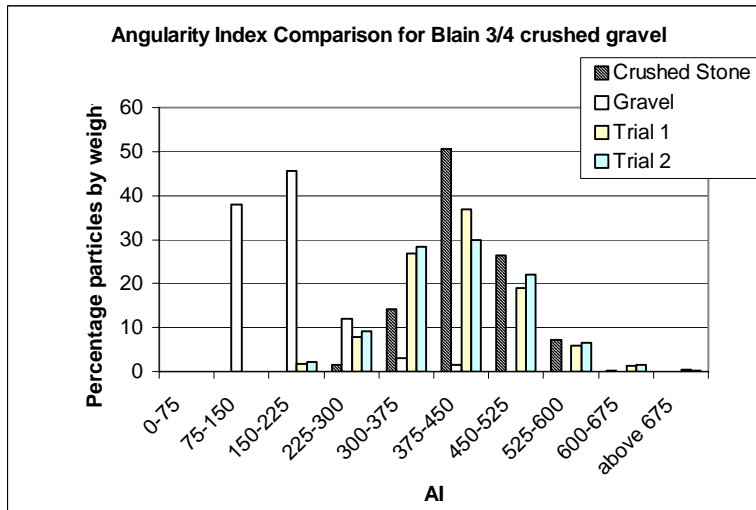


Figure AII-21 Imaging Based AI of the Blain 3/4 in. Sample

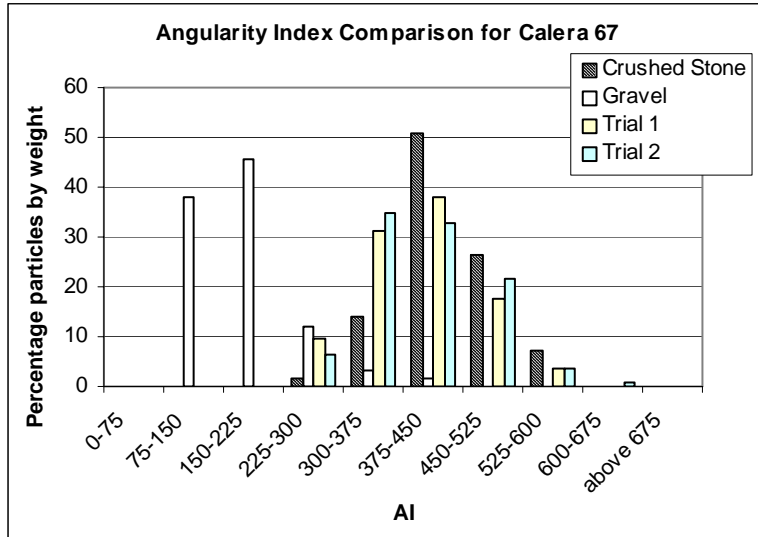


Figure AII-22 Imaging Based AI of the Calera 67 Sample

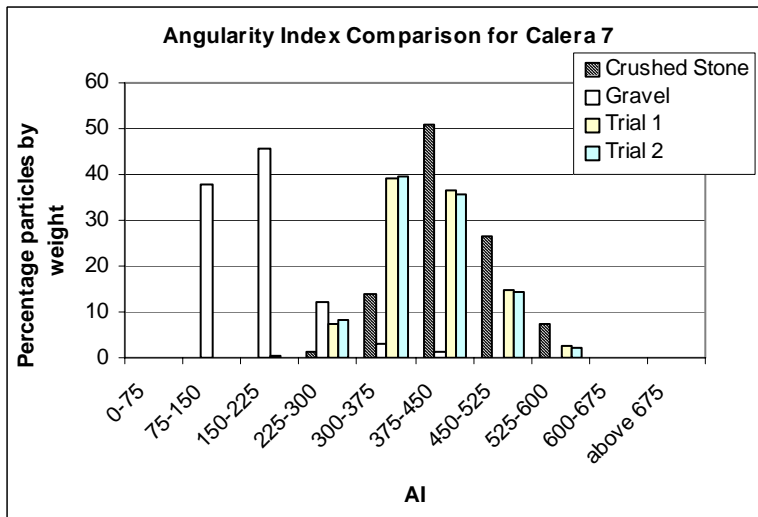


Figure AII-23 Imaging Based AI of the Calera 7 Sample

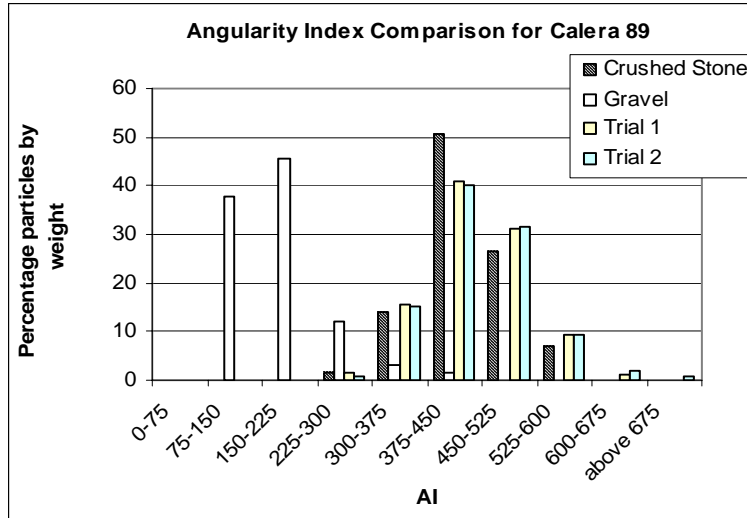


Figure AII-24 Imaging Based AI of the Calera 89 Sample

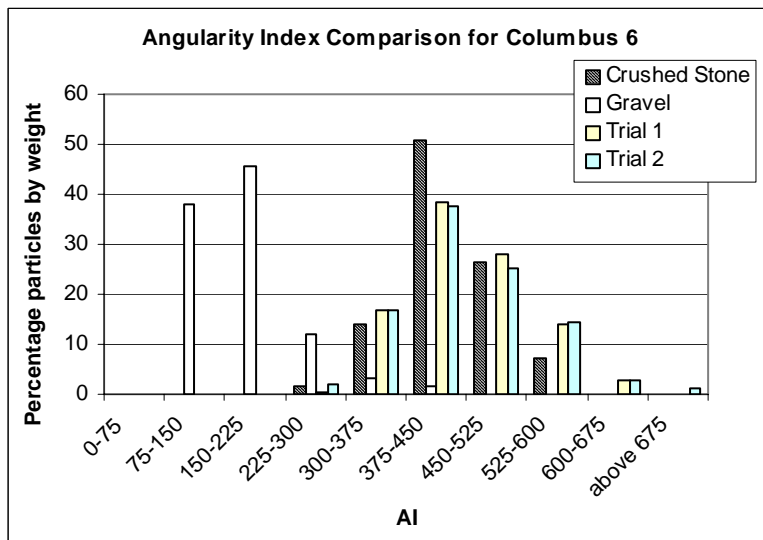


Figure AII-25 Imaging Based AI of the Columbus 6 Sample

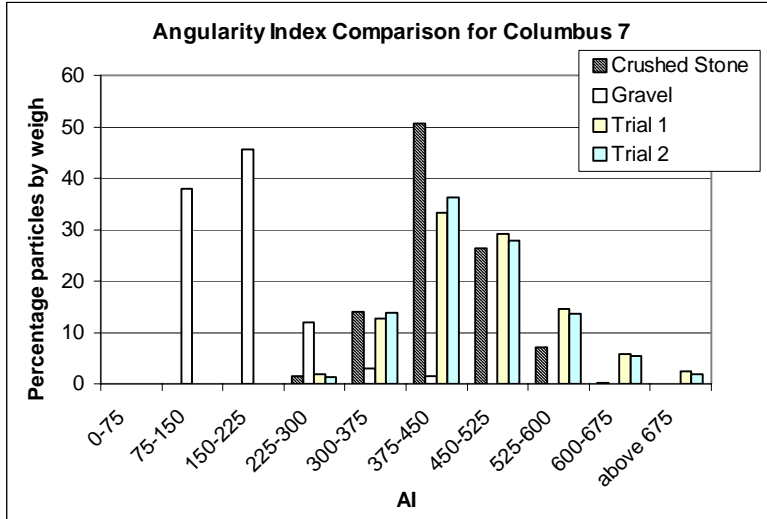


Figure AII-26 Imaging Based AI of the Columbus 7 Sample

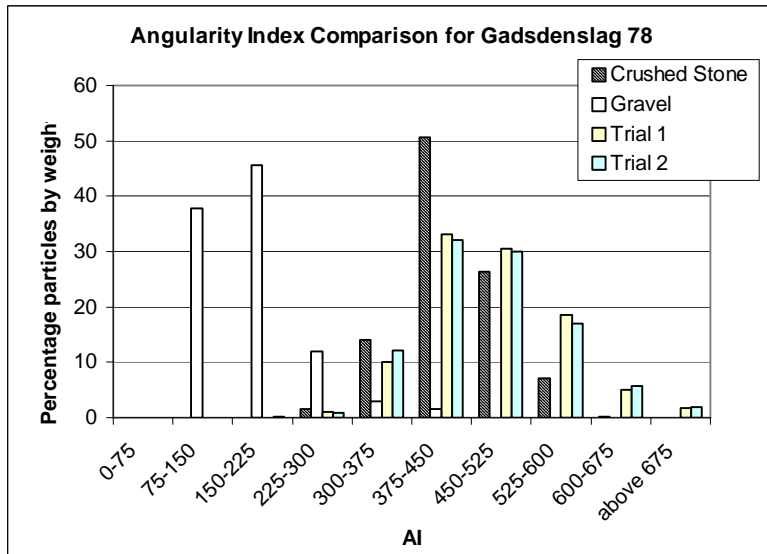


Figure AII-27 Imaging Based AI of the Gadsdenslag 78 Sample

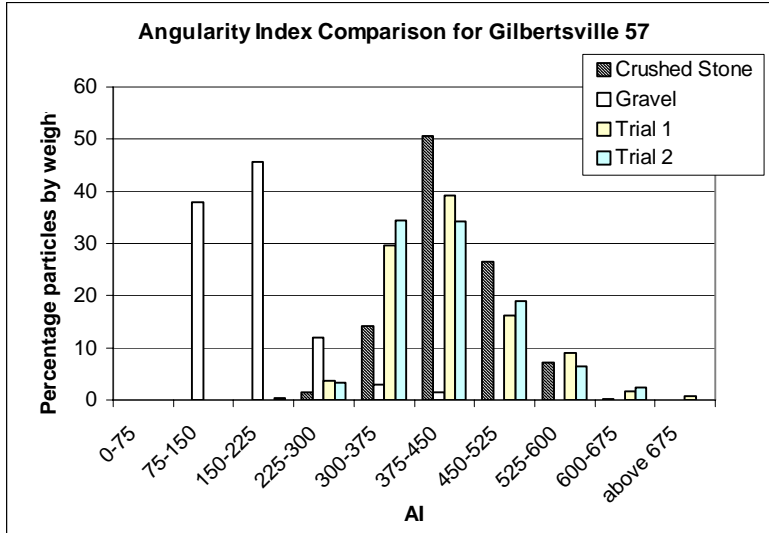


Figure AII-28 Imaging Based AI of the Gilbertsville 57 Sample

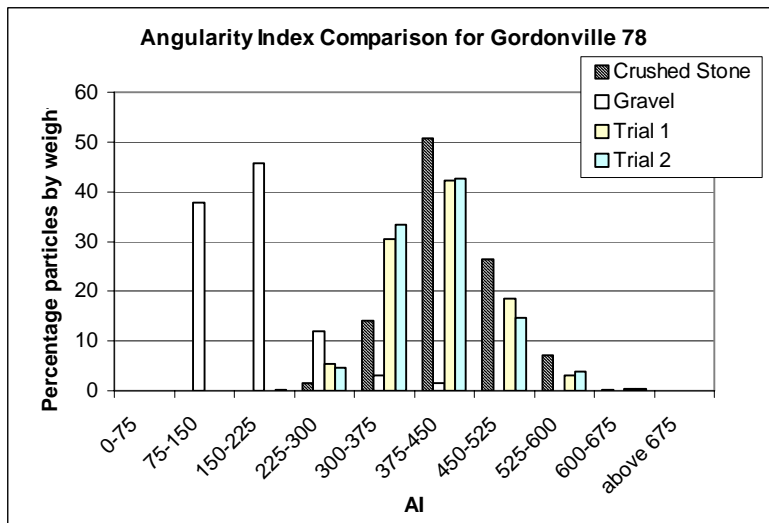


Figure AII-29 Imaging Based AI of the Gordonville 78 Sample

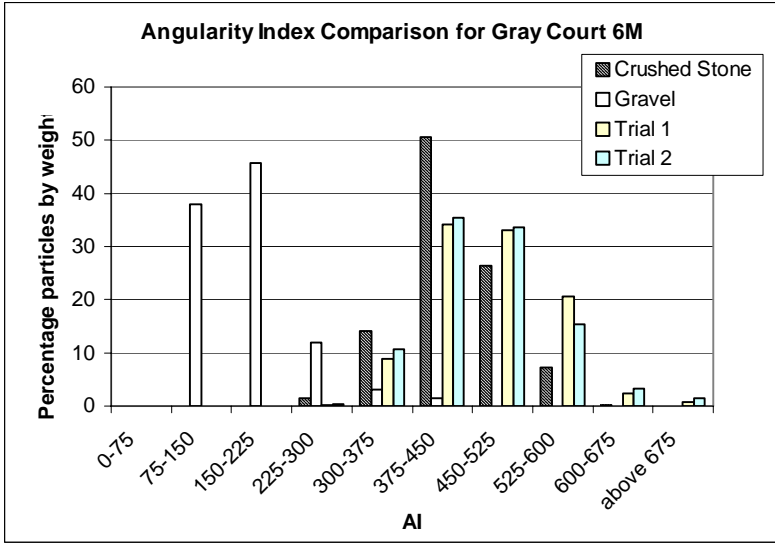


Figure AII-30 Imaging Based AI of the Gray Court 6M Sample

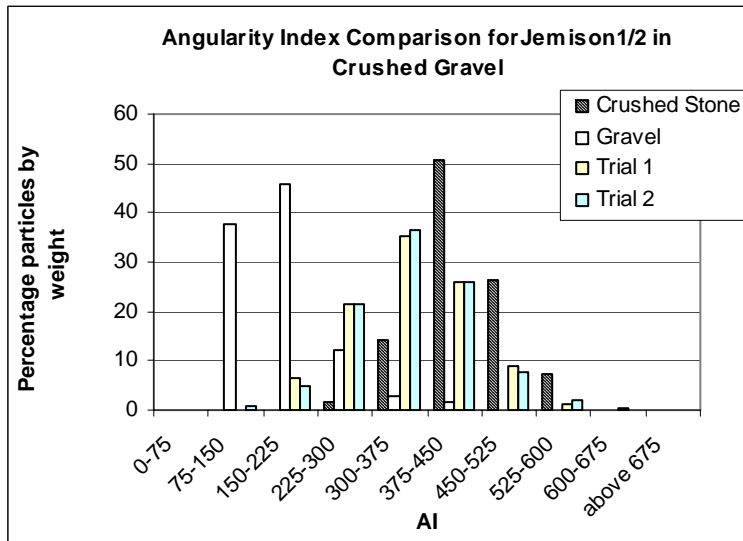


Figure AII-31 Imaging Based AI of the Jemison 1/2 Sample

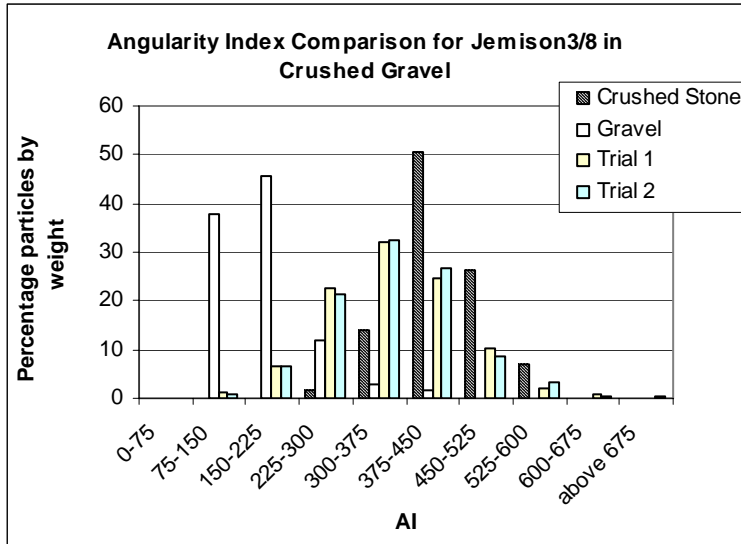


Figure AII-32 Imaging Based AI of the Jemison 3/8 Sample

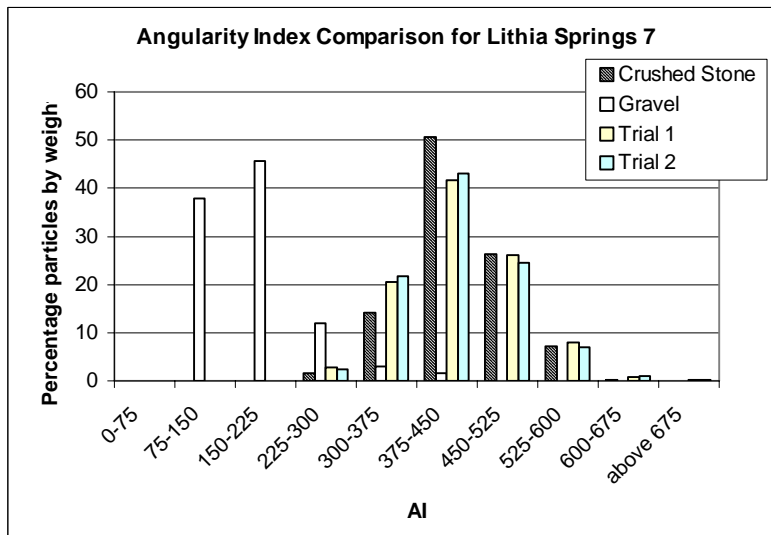


Figure AII-33 Imaging Based AI of the Lithia Spring 7 Sample

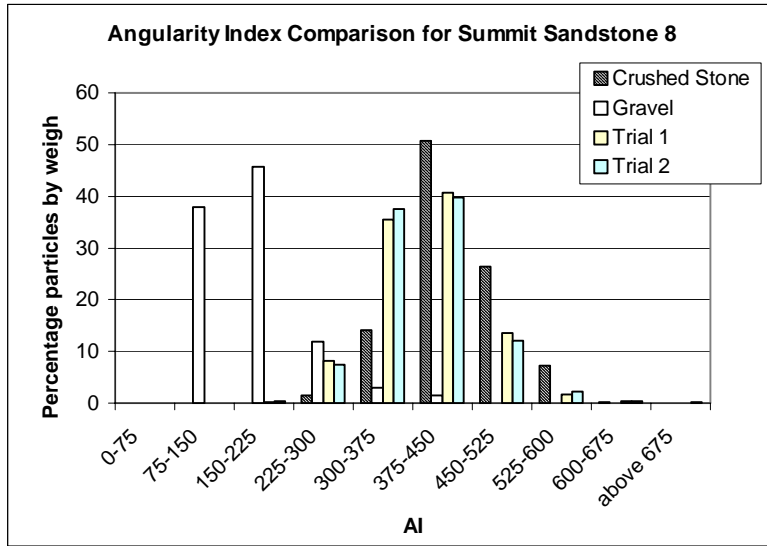


Figure AII-34 Imaging Based AI of the Summit Sandstone 8 Sample

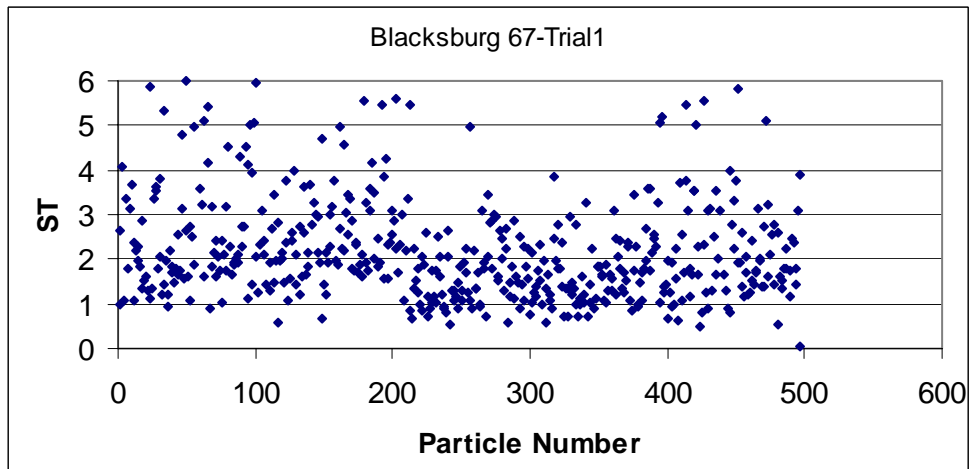


Figure AII-35 (a) Imaging Based ST of the Blacksburg 67 Sample-Trial 1

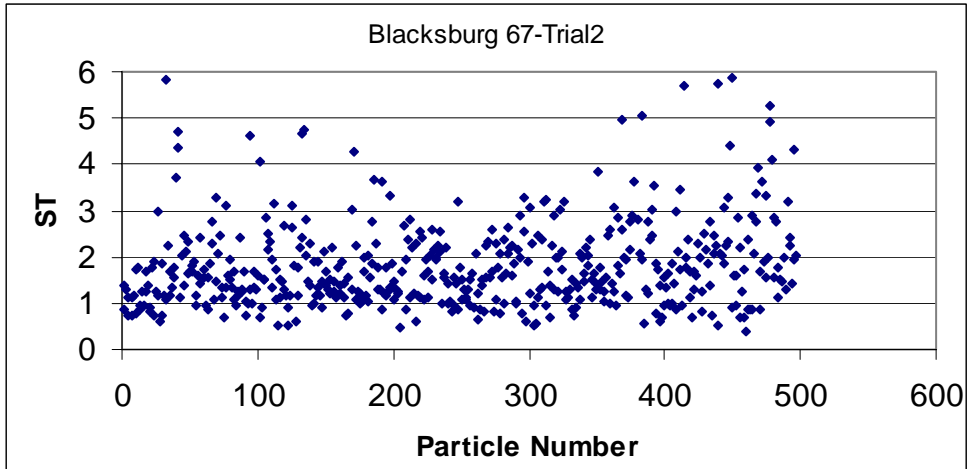


Figure AII-35 (b) Imaging Based ST of the Blacksburg 67 Sample-Trial 2

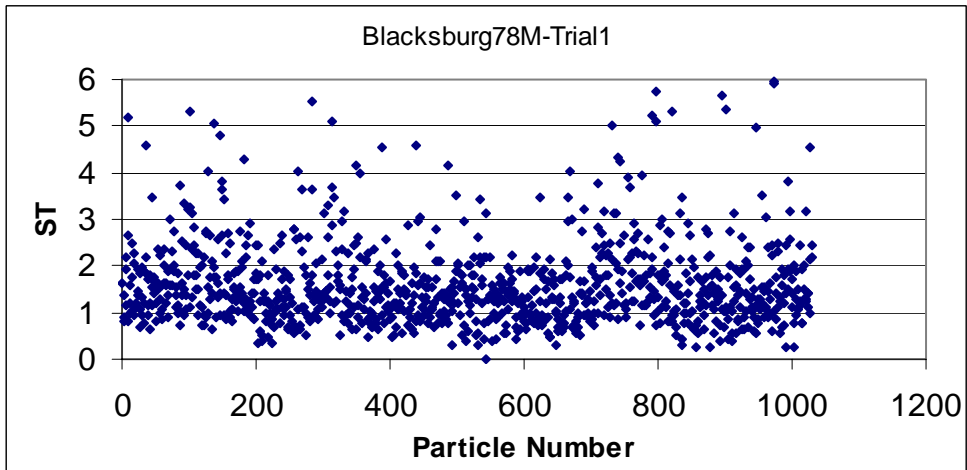


Figure AII-36 (a) Imaging Based ST of the Blacksburg 78M Sample-Trial 1

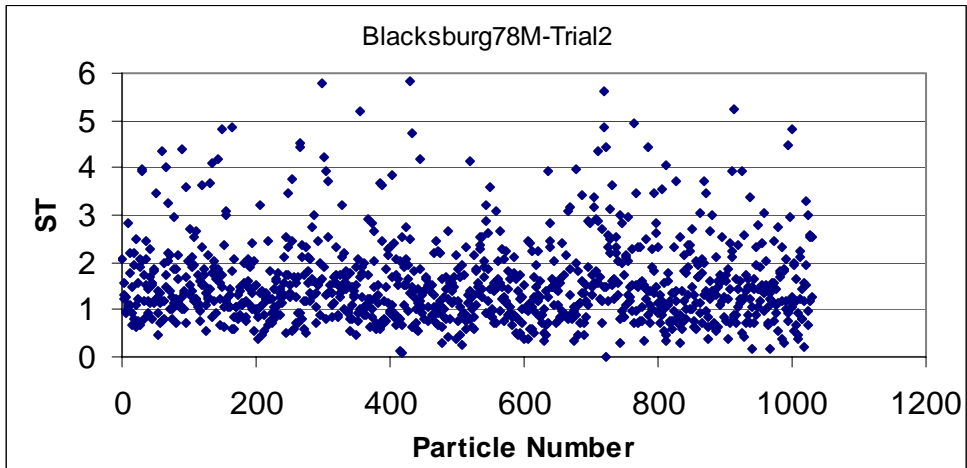


Figure AII-36 (b) Imaging Based ST of the Blacksburg 78M Sample-Trial 2

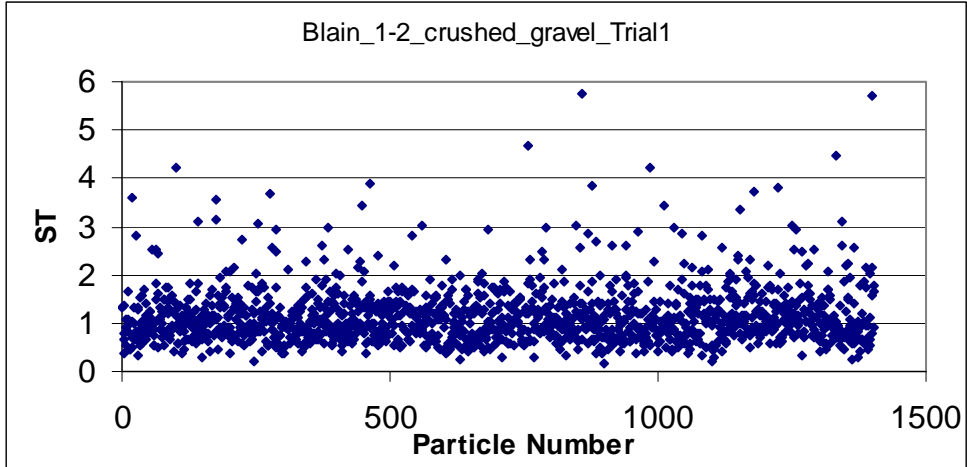


Figure AII-37 (a) Imaging Based ST of the Blain 1/2 in. Sample-Trial 1

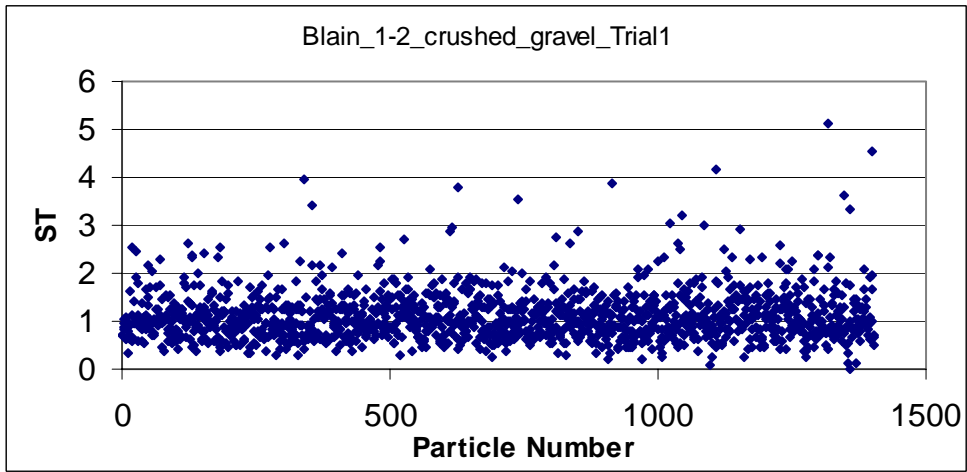


Figure AII-37 (b) Imaging Based ST of the Blain 1/2 in. Sample-Trial 2

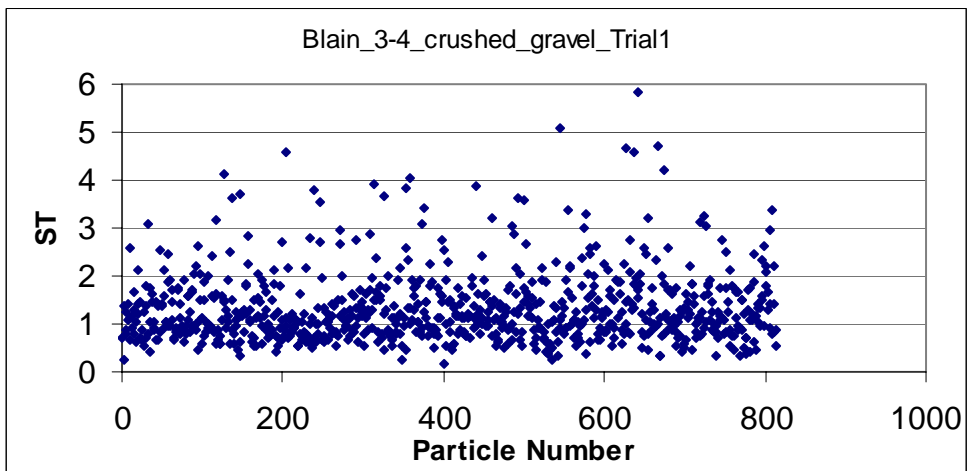


Figure AII-38 (a) Imaging Based ST of the Blain 3/4 in. Sample-Trial 1

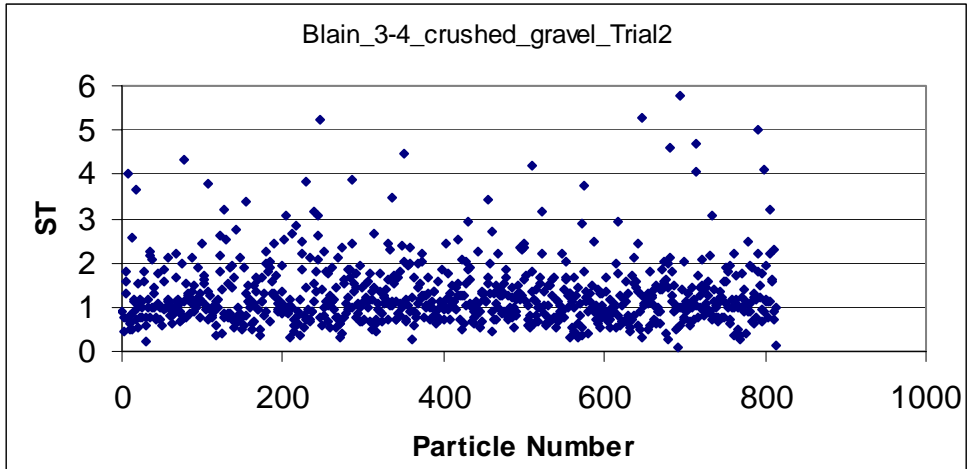


Figure AII-38 (b) Imaging Based ST of the Blain 3/4 in. Sample-Trial 2

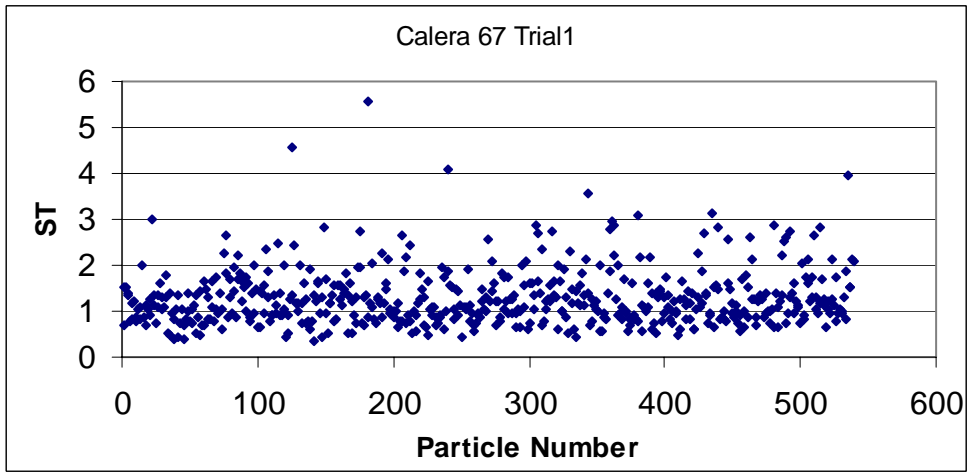


Figure AII-39 (a) Imaging Based ST of the Calera 67 Sample-Trial 1

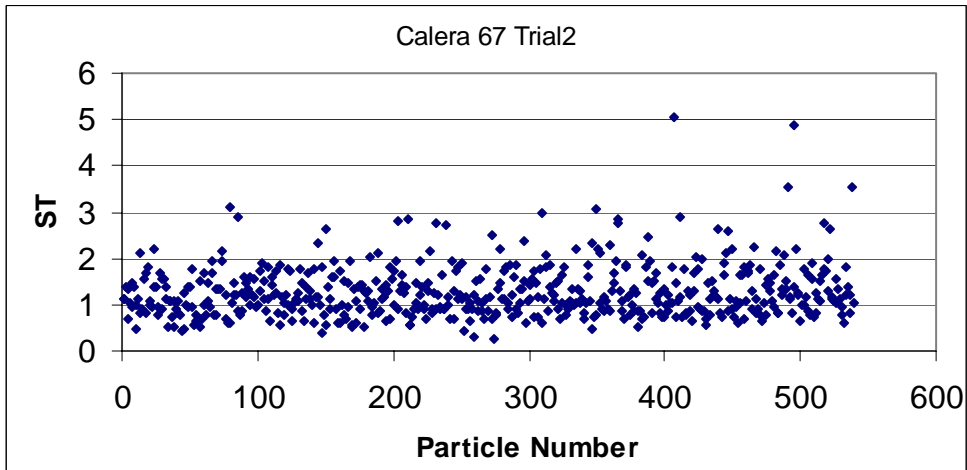


Figure AII-39 (b) Imaging Based ST of the Calera 67 Sample-Trial 2

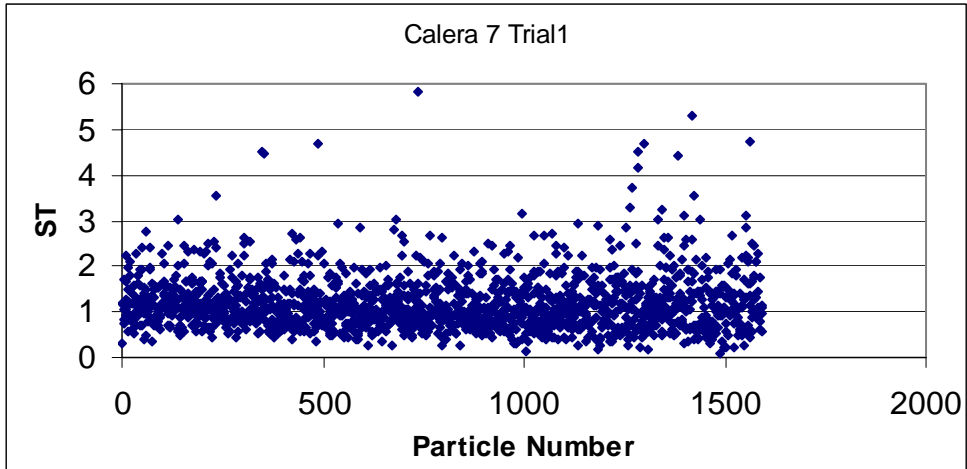


Figure AII-40 (a) Imaging Based ST of the Calera 7 Sample-Trial 1

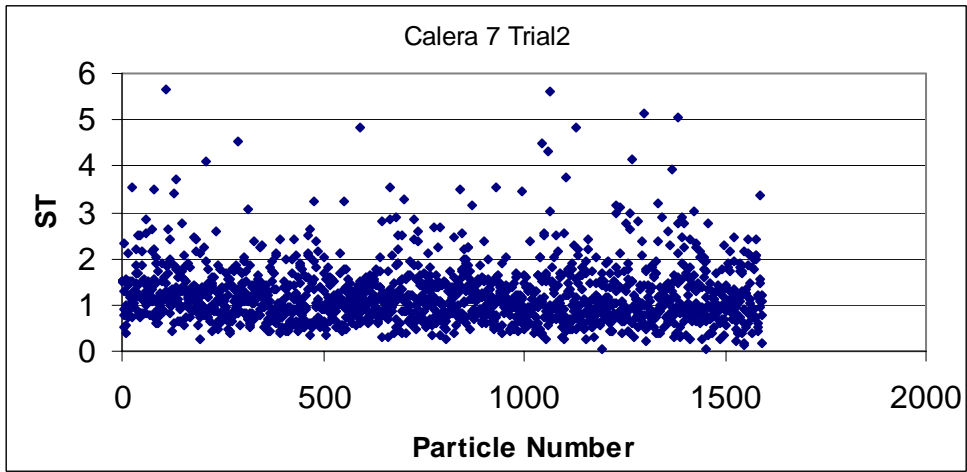


Figure AII-40 (b) Imaging Based ST of the Calera 7 Sample-Trial 2

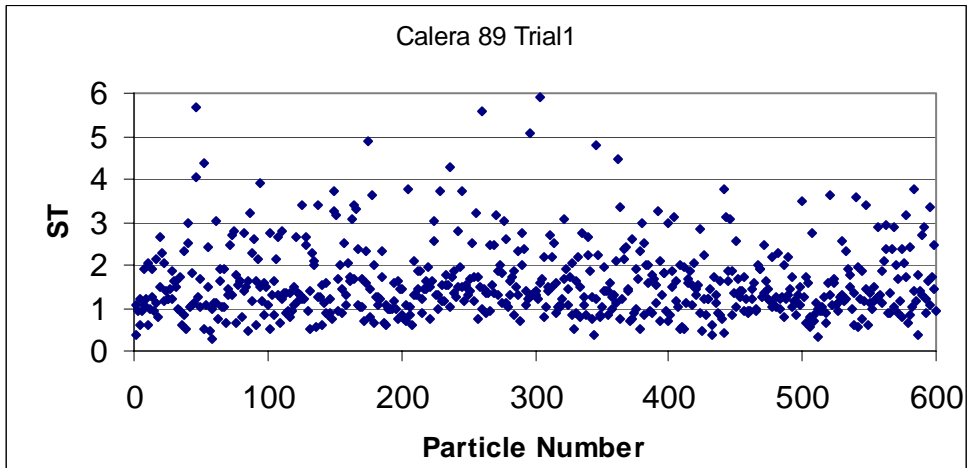


Figure AII-41 (a) Imaging Based ST of the Calera 89 Sample-Trial 1

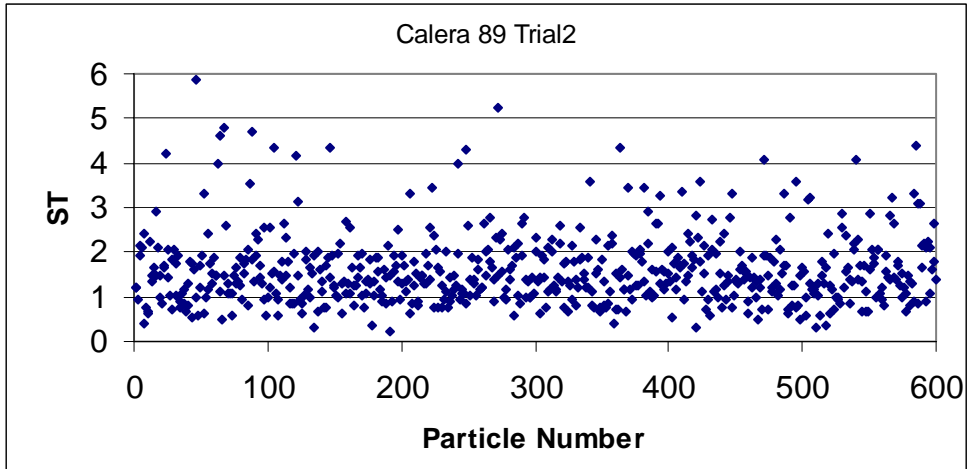


Figure AII-41 (b) Imaging Based ST of the Calera 89 Sample-Trial 2

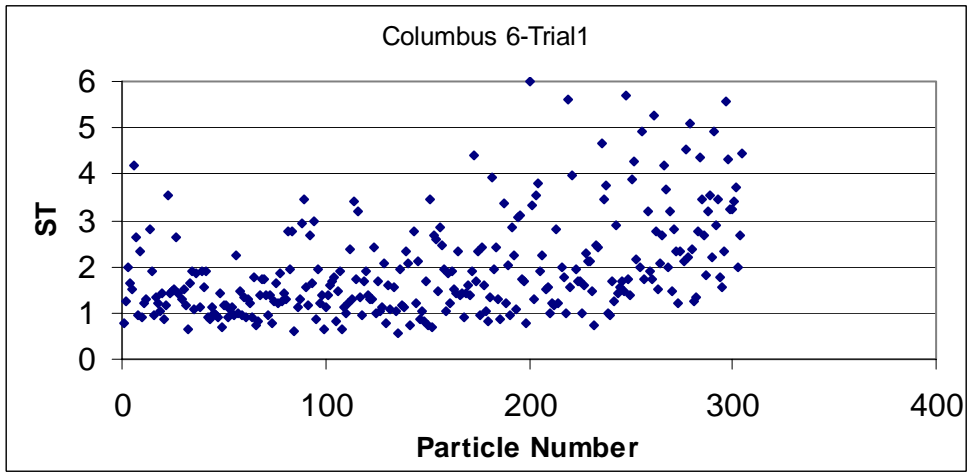


Figure AII-42 (a) Imaging Based ST of the Columbus 6 Sample-Trial 1

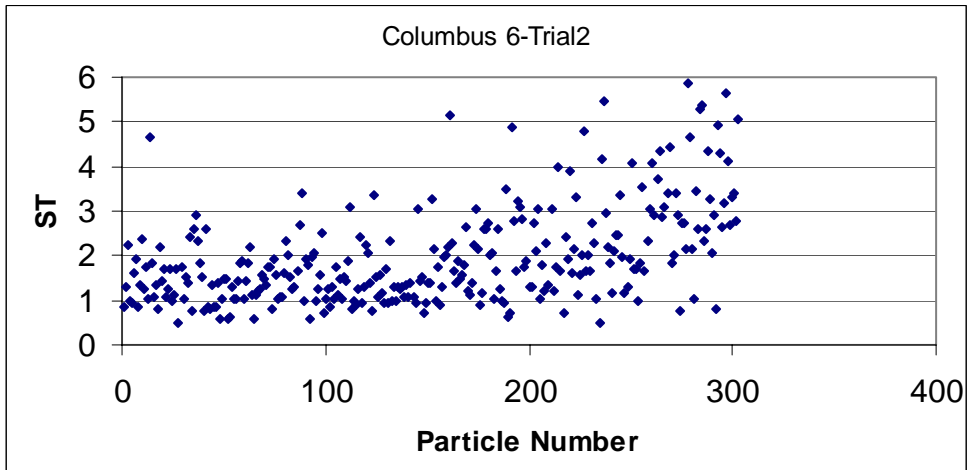


Figure AII-42 (b) Imaging Based ST of the Columbus 6 Sample-Trial 2

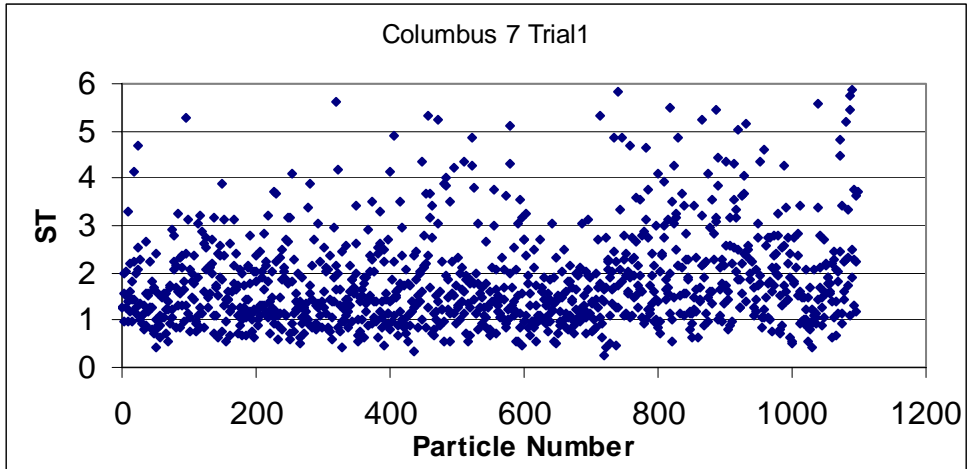


Figure AII-43 (a) Imaging Based ST of the Columbus 7 Sample-Trial 1

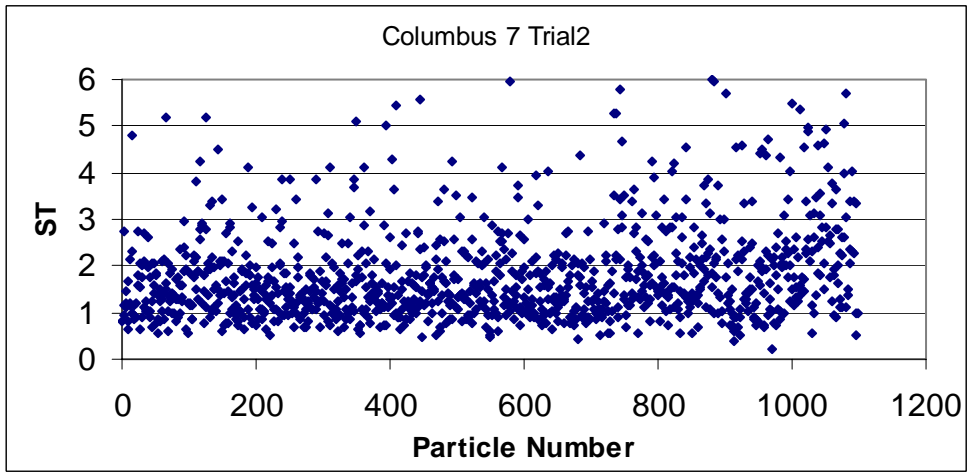


Figure AII-43 (b) Imaging Based ST of the Columbus 7 Sample-Trial 2

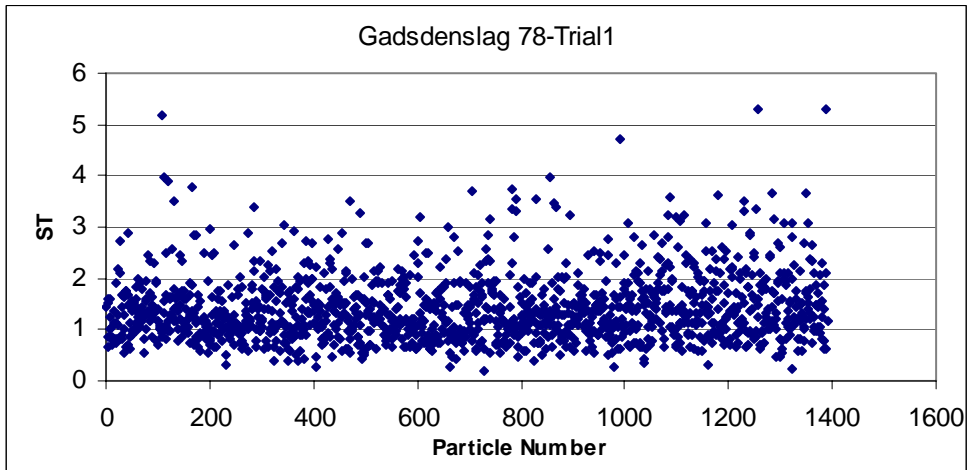


Figure AII-44 (a) Imaging Based ST of the Gadسدنslag 78 Sample-Trial 1

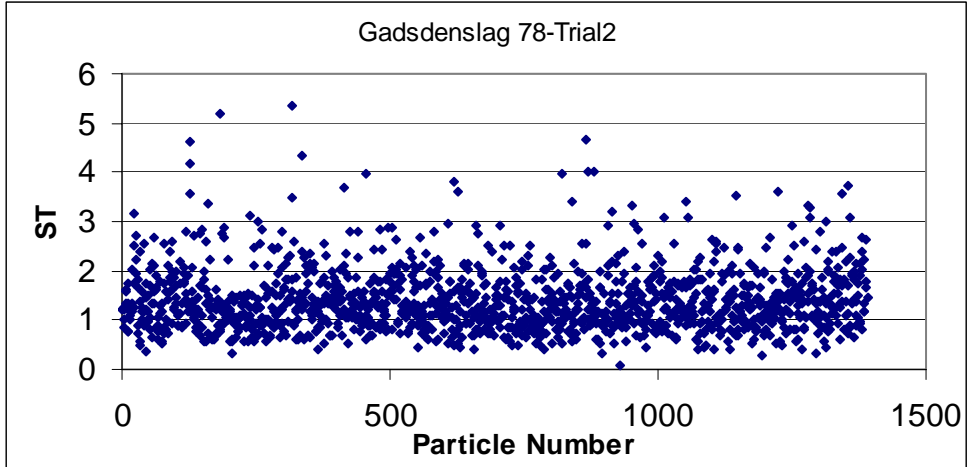


Figure AII-44 (b) Imaging Based ST of the Gadsdenslag 78 Sample-Trial 2

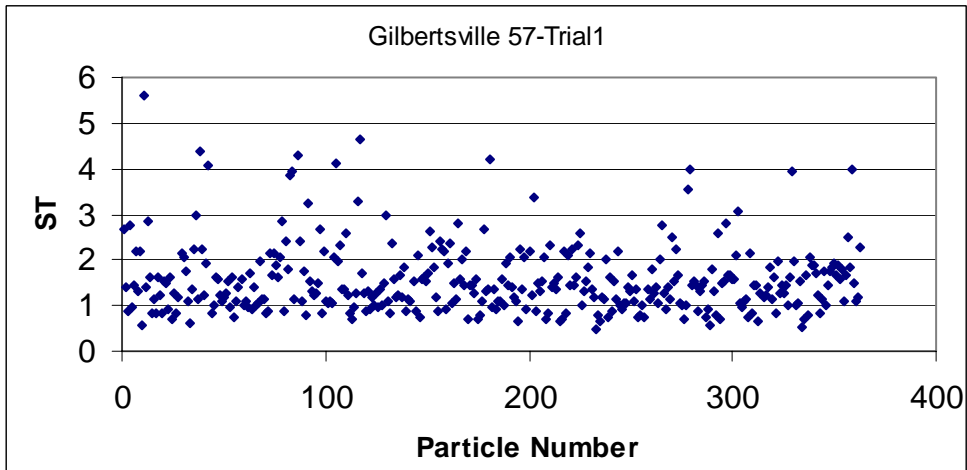


Figure AII-45 (a) Imaging Based ST of the Gilbertsville 57 Sample-Trial 1

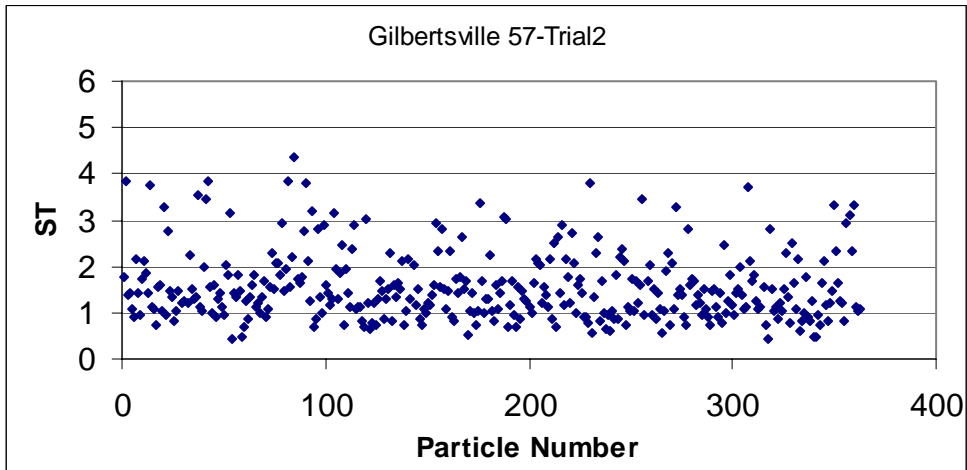


Figure AII-45 (b) Imaging Based ST of the Gilbertsville 57 Sample-Trial 2

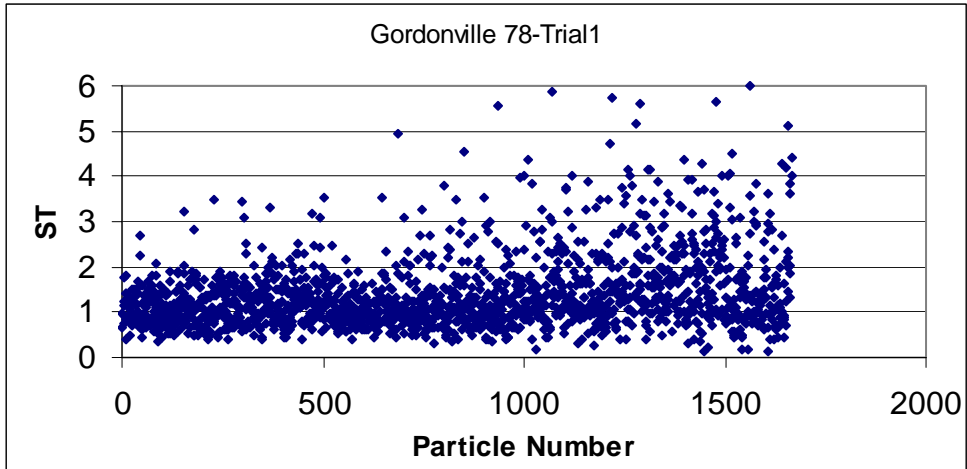


Figure AII-46 (a) Imaging Based ST of the Gordonville 78 Sample-Trial 1

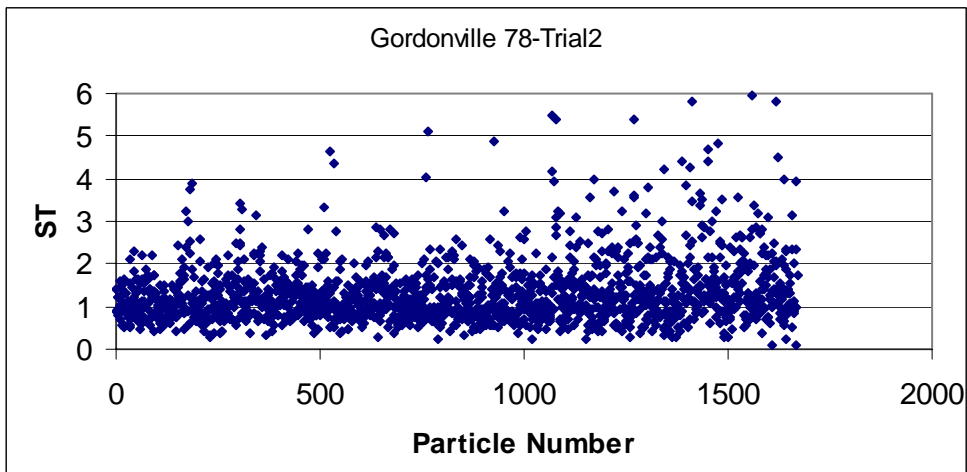


Figure AII-46 (b) Imaging Based ST of the Gordonville 78 Sample-Trial 2

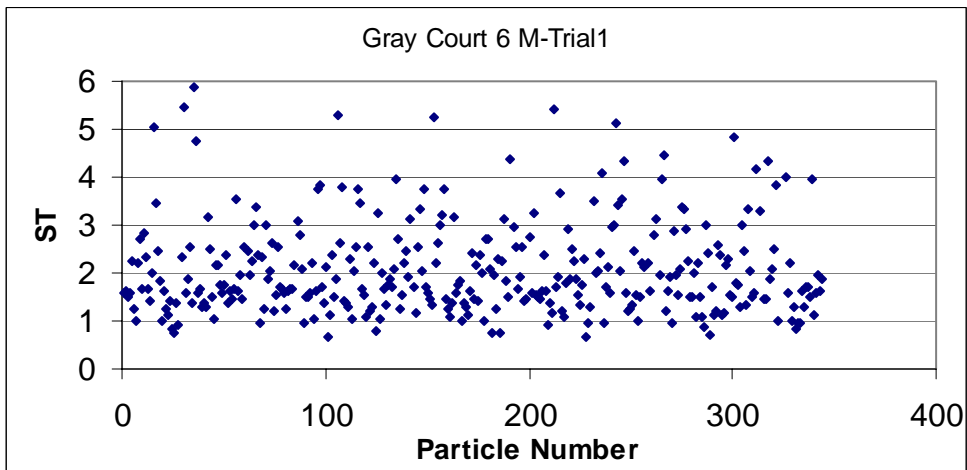


Figure AII-47 (a) Imaging Based ST of the Gray Court 6M Sample-Trial 1

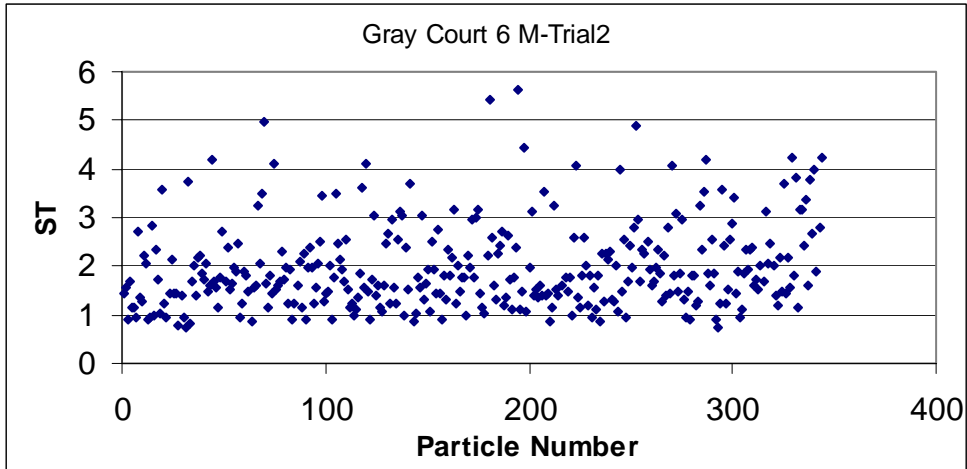


Figure AII-47 (b) Imaging Based ST of the Gray Court 6M Sample-Trial 2

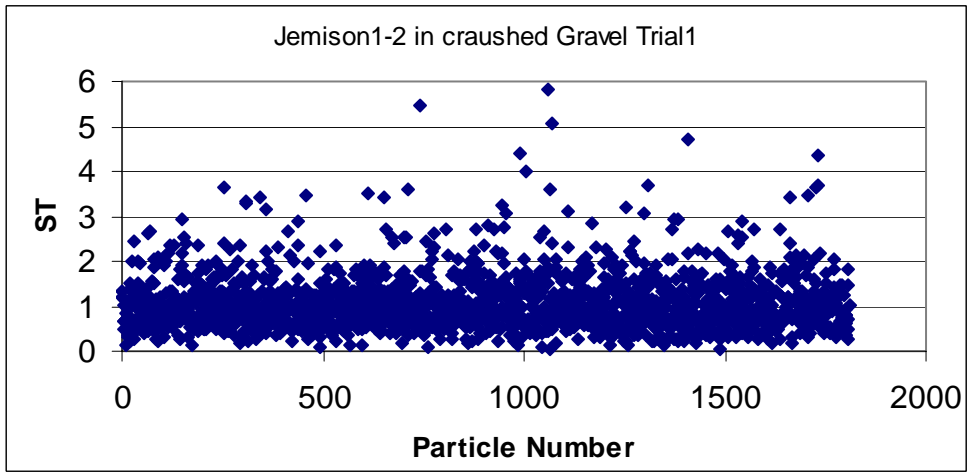


Figure AII-48 (a) Imaging Based ST of the Jemison 1/2 in. Sample-Trial 1

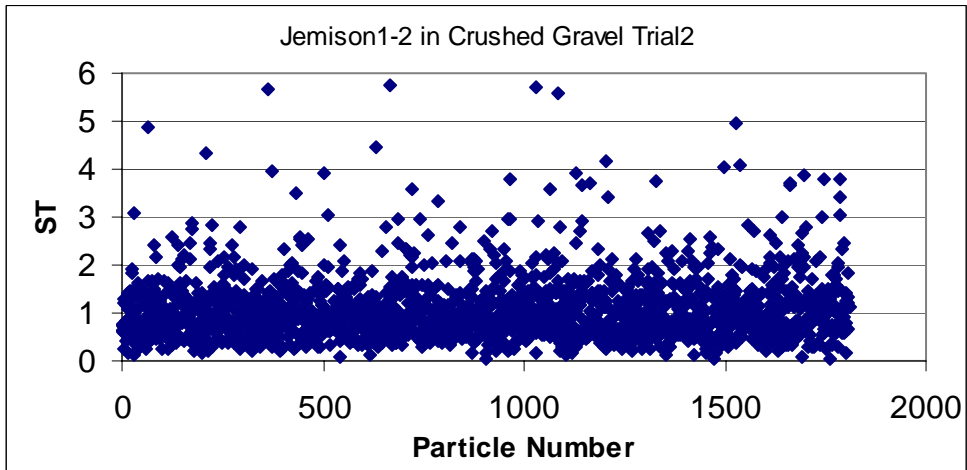


Figure AII-48 (b) Imaging Based ST of the Jemison 1/2 in. Sample-Trial 2

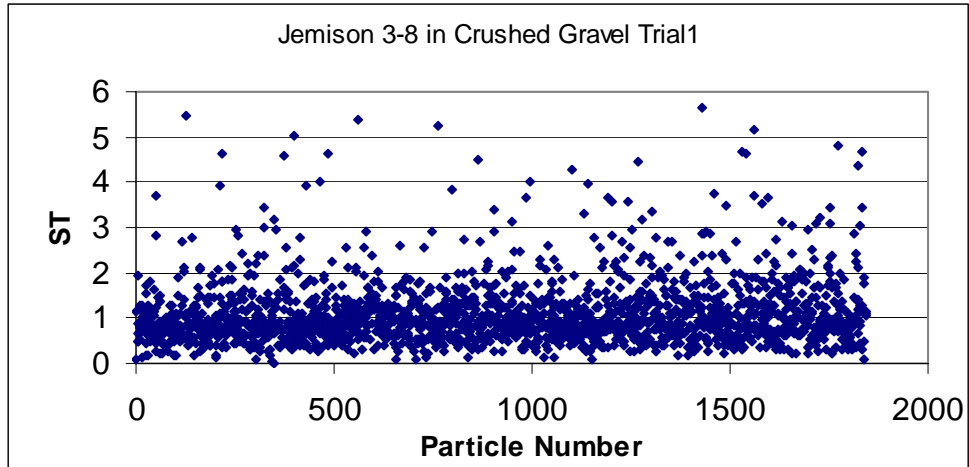


Figure AII-49 (a) Imaging Based ST of the Jemison 3/4 in. Sample-Trial 1

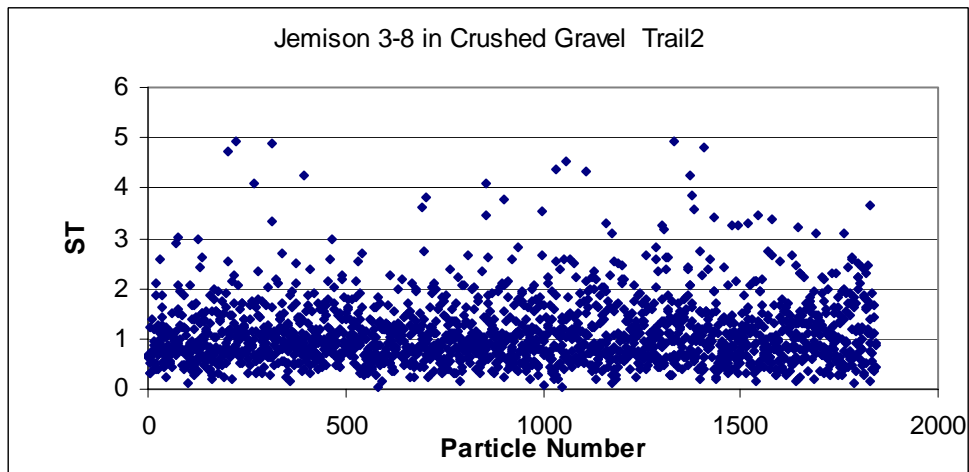


Figure AII-49 (b) Imaging Based ST of the Jemison 3/4 in. Sample-Trial 2

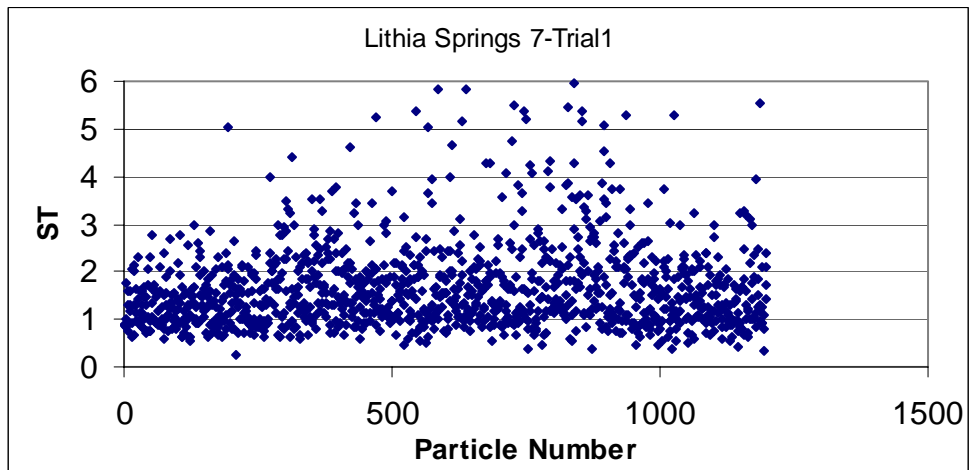


Figure AII-50 (a) Imaging Based ST of the Lithia Spring 7 Sample-Trial 1

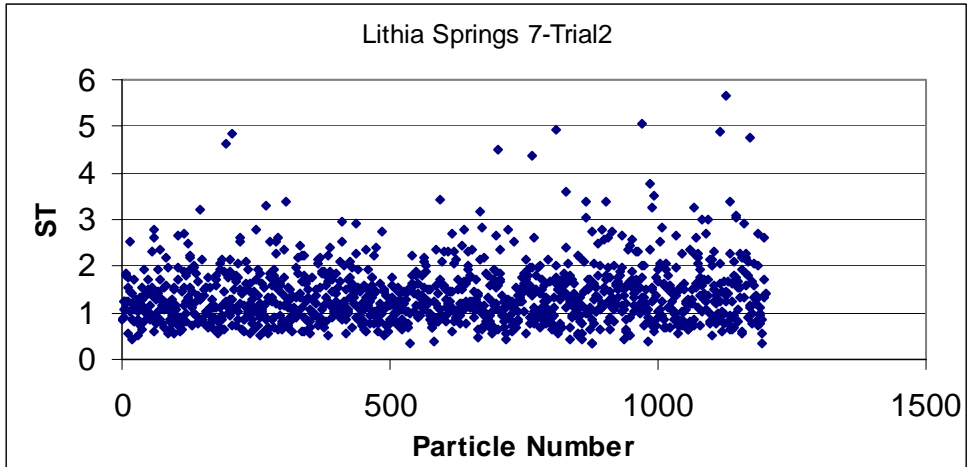


Figure AII-50 (b) Imaging Based ST of the Lithia Spring 7 Sample-Trial 2

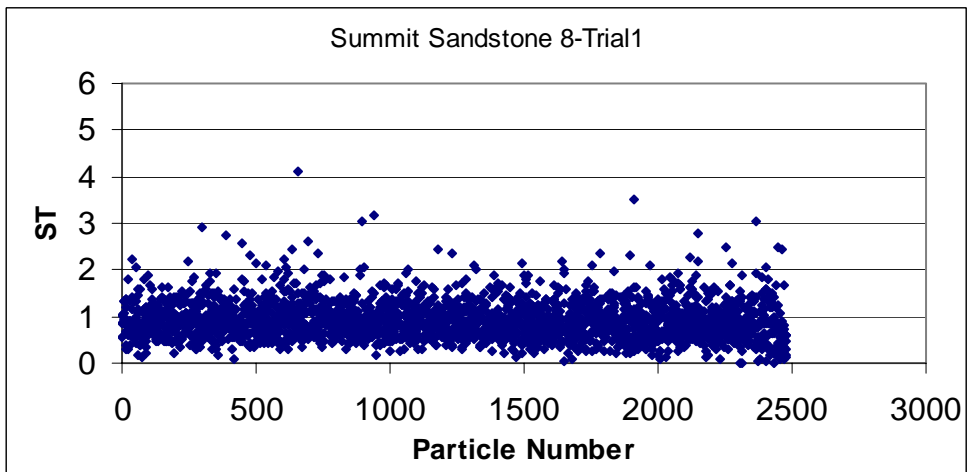


Figure AII-51 (a) Imaging Based ST of the Summit Sandstone 8 Sample-Trial 1

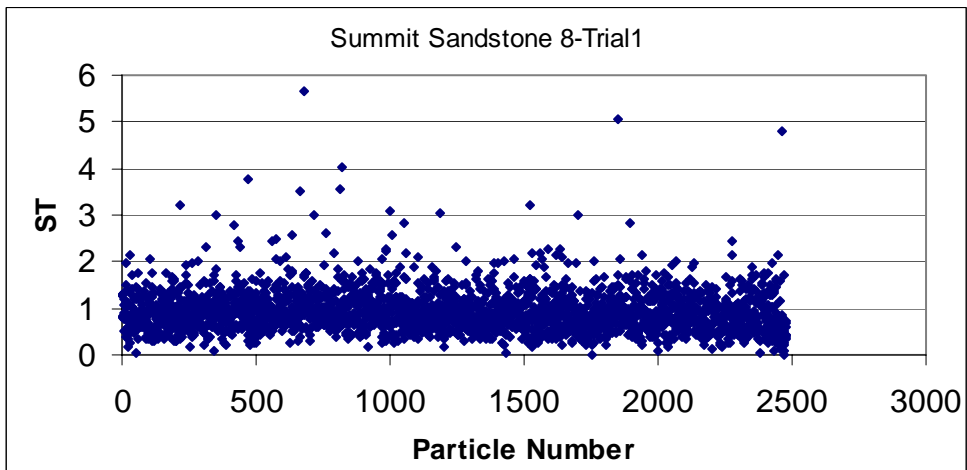


Figure AII-51 (b) Imaging Based ST of the Summit Sandstone 8 Sample-Trial 2

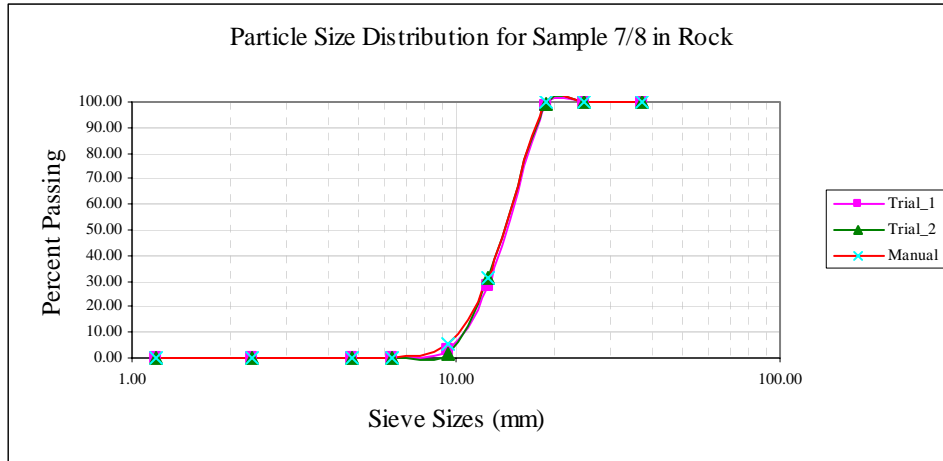


Figure AII-52 Imaging Based Particle Size Distributions of the 7/8 in. Sample

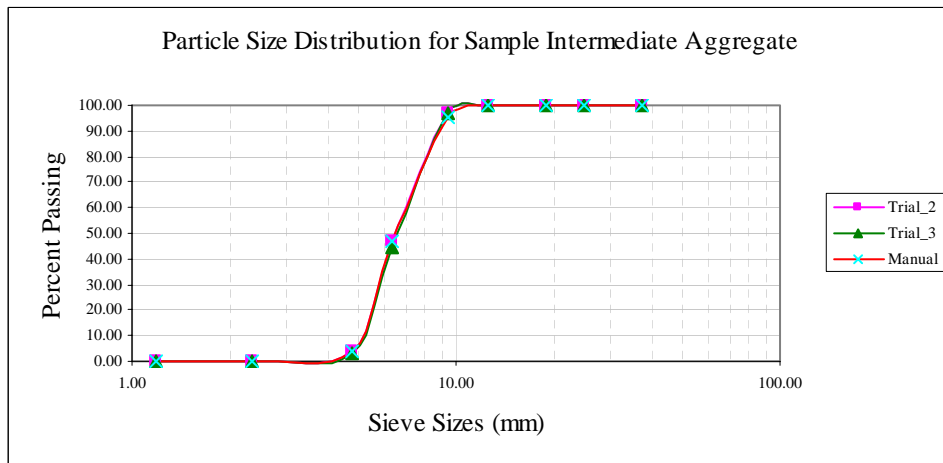


Figure AII-53 Imaging Based Particle Size Distributions of the Intermediate Aggregate Sample

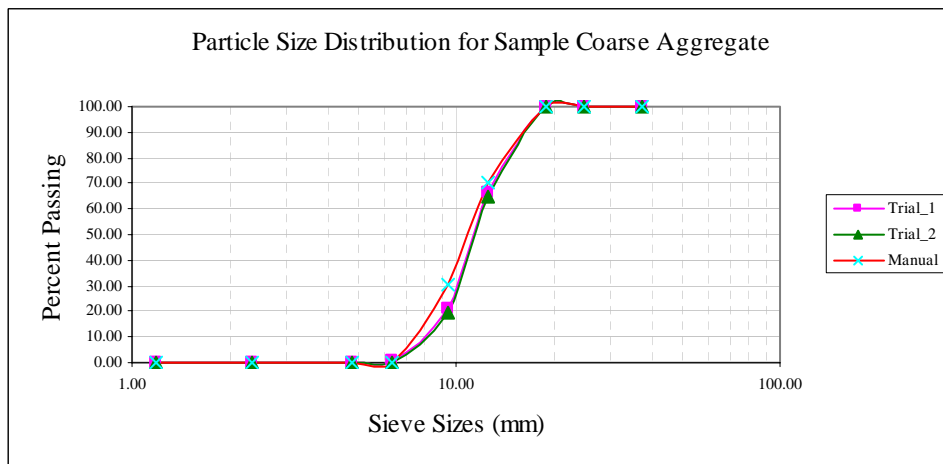


Figure AII-54 Imaging Based Particle Size Distributions of the Coarse Aggregate Sample

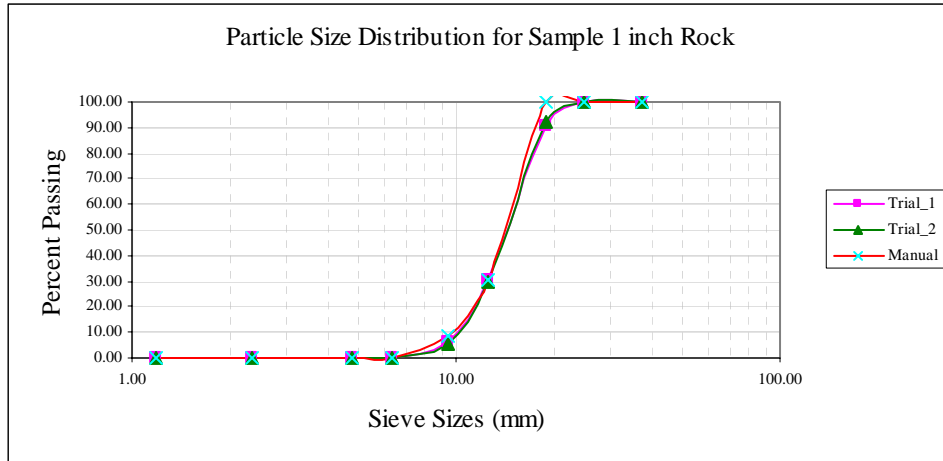


Figure AII-55 Imaging Based Particle Size Distributions of the 1 in. Rock Sample

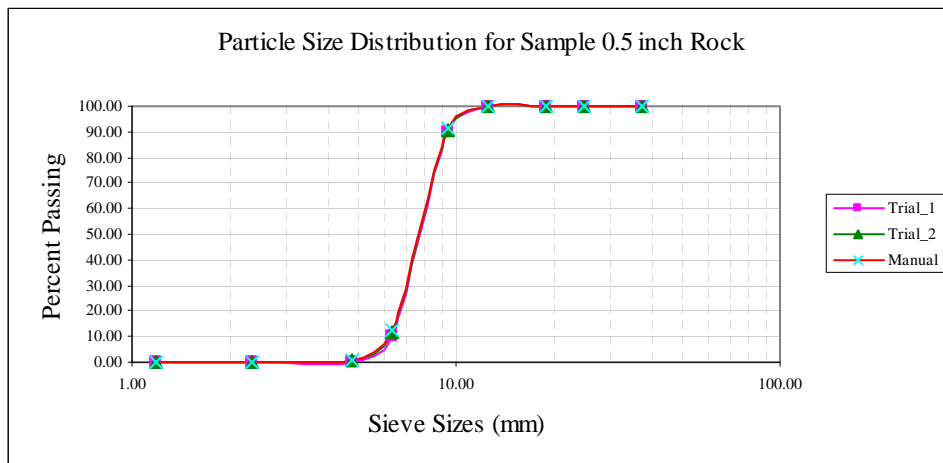


Figure AII-56 Imaging Based Particle Size Distributions of the 0.5 in. Rock Sample

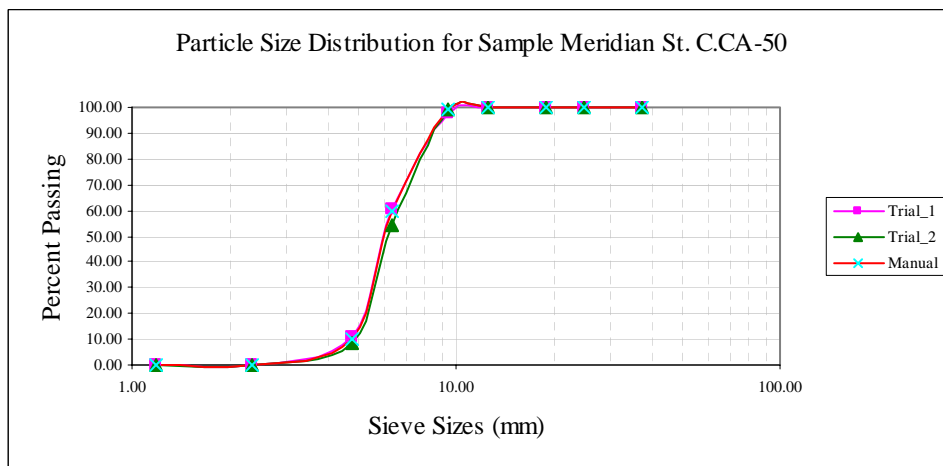


Figure AII-57 Imaging Based Particle Size Distributions of the Meridian St. C. CA-50 Sample

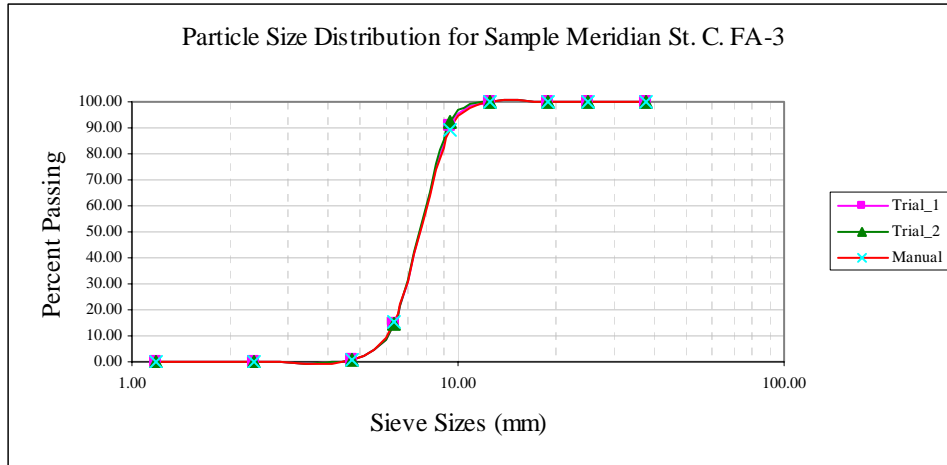


Figure AII-58 Imaging Based Particle Size Distributions of the Meridian St. C. FA-3 Sample

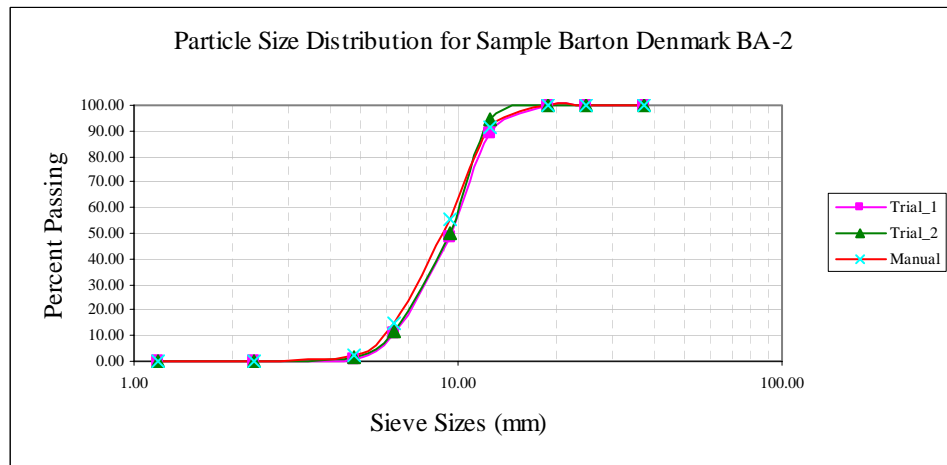


Figure AII-59 Imaging Based Particle Size Distributions of the Barton Denmark BA-2 Sample

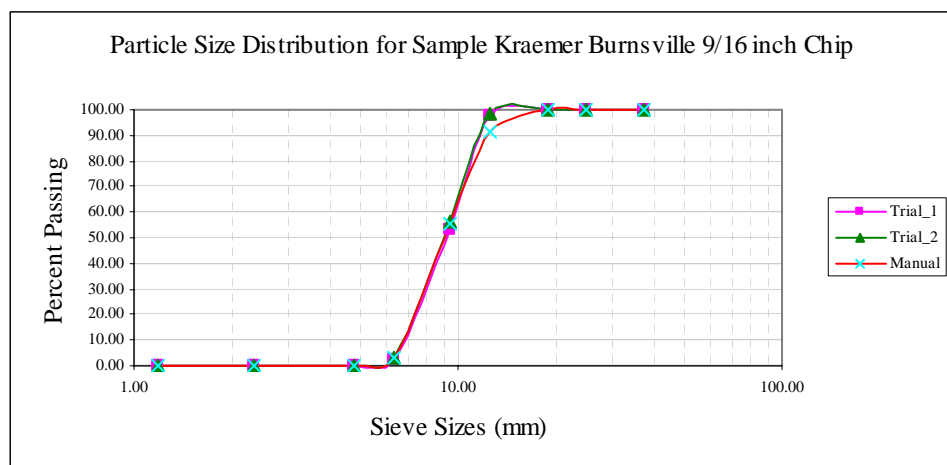


Figure AII-60 Imaging Based Particle Size Distributions of the Burnsville 9/16 in. Sample

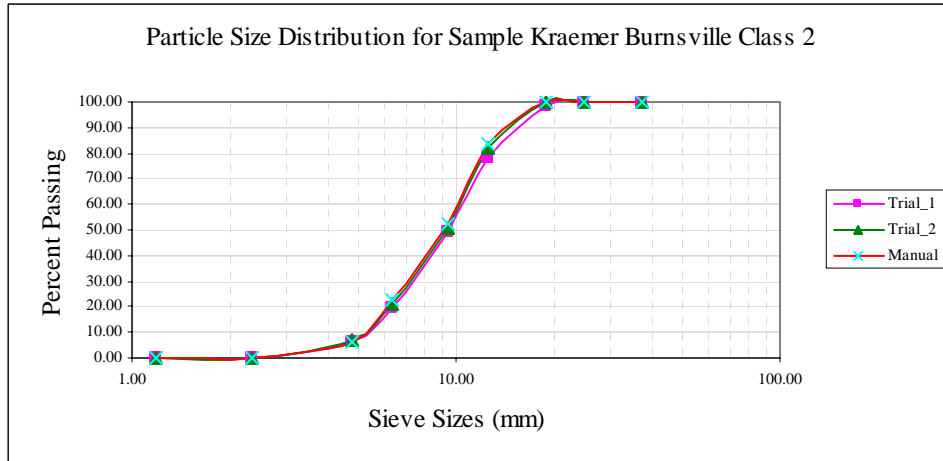


Figure AII-61 Imaging Based Particle Size Distributions of the Kraemer Burnsville Class 2 Sample

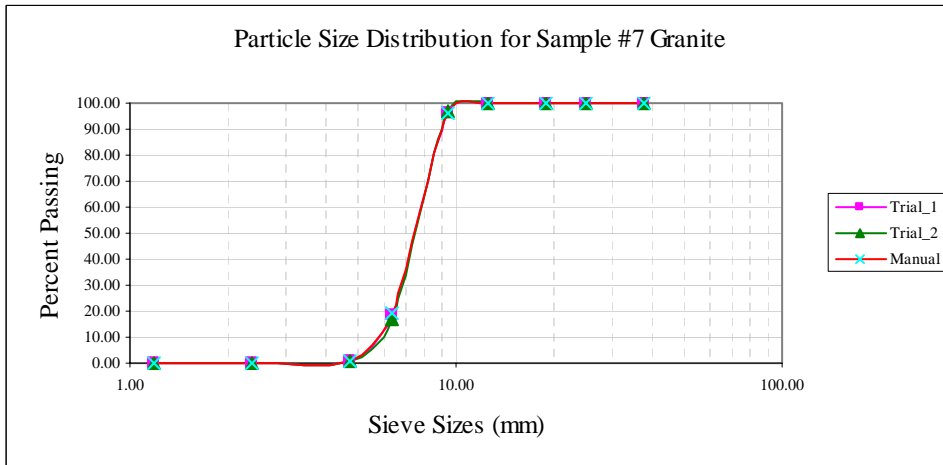


Figure AII-62 Imaging Based Particle Size Distributions of the #7 Granite Sample

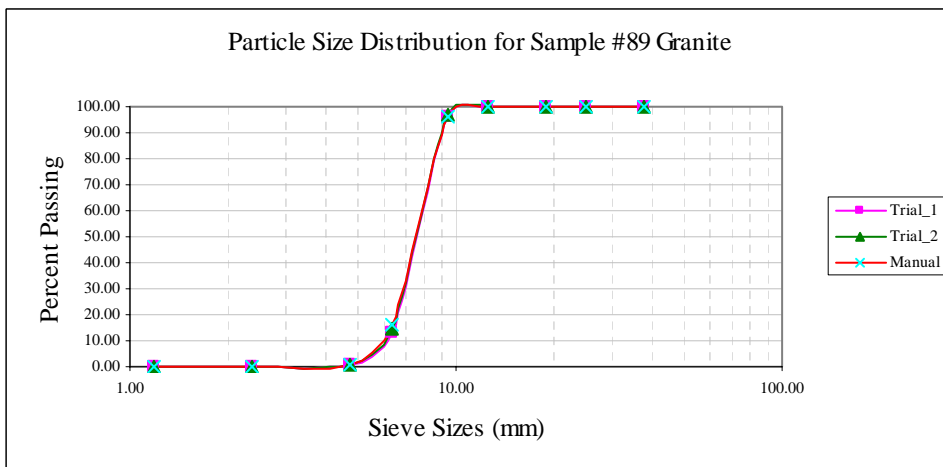


Figure AII-63 Imaging Based Particle Size Distributions of the #89 Granite Sample

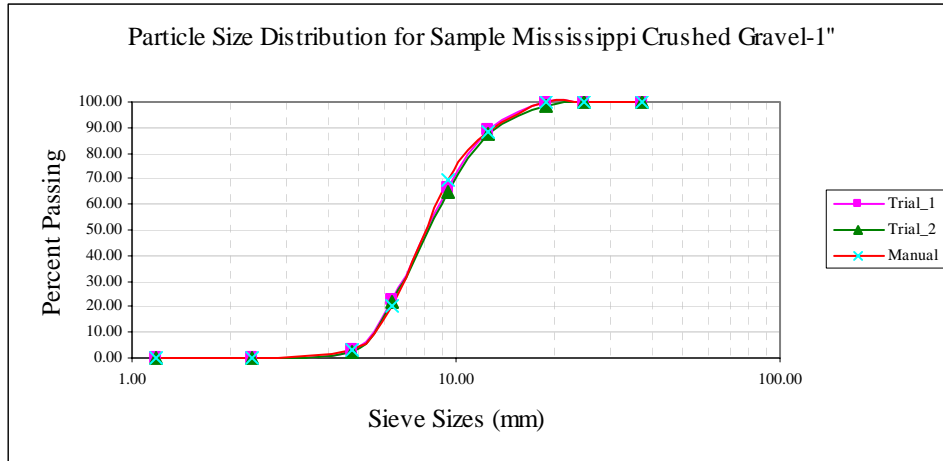


Figure AII-64 Imaging Based Particle Size Distributions of the 1" Crushed Gravel Sample

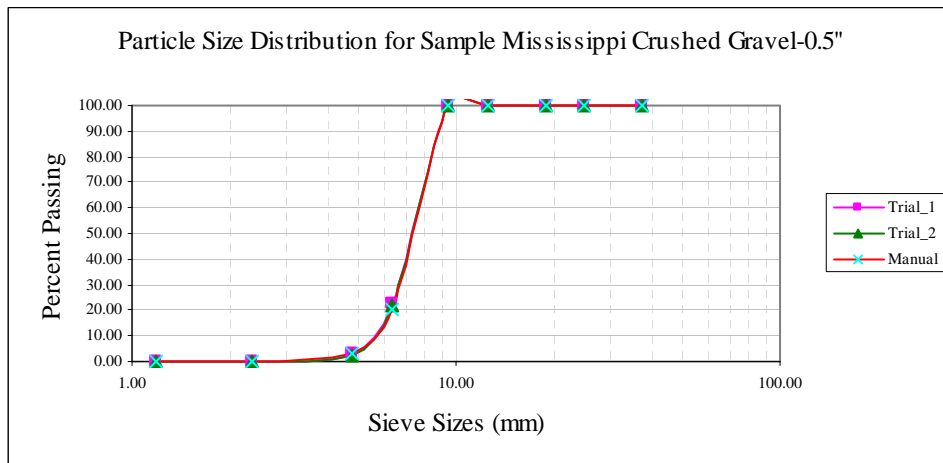


Figure AII-65 Imaging Based Particle Size Distributions of the 0.5" Crushed Gravel Sample

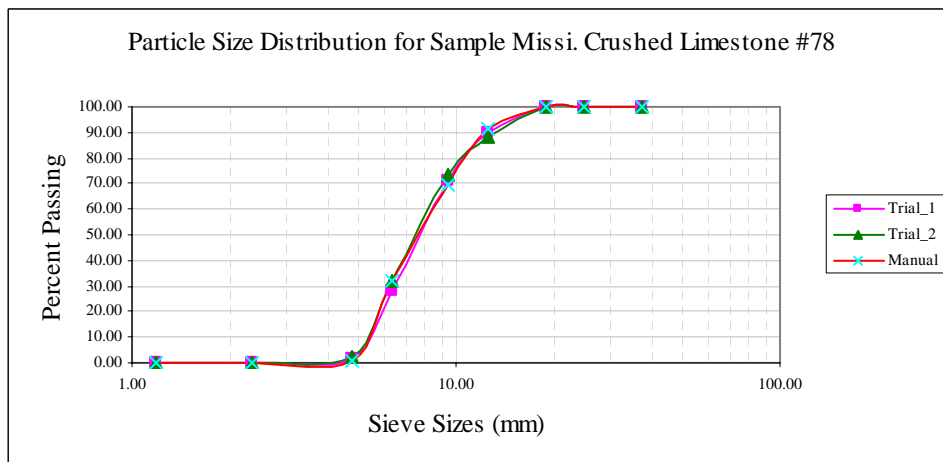


Figure AII-66 Imaging Based Particle Size Distributions of the #78 Crushed Limestone Sample

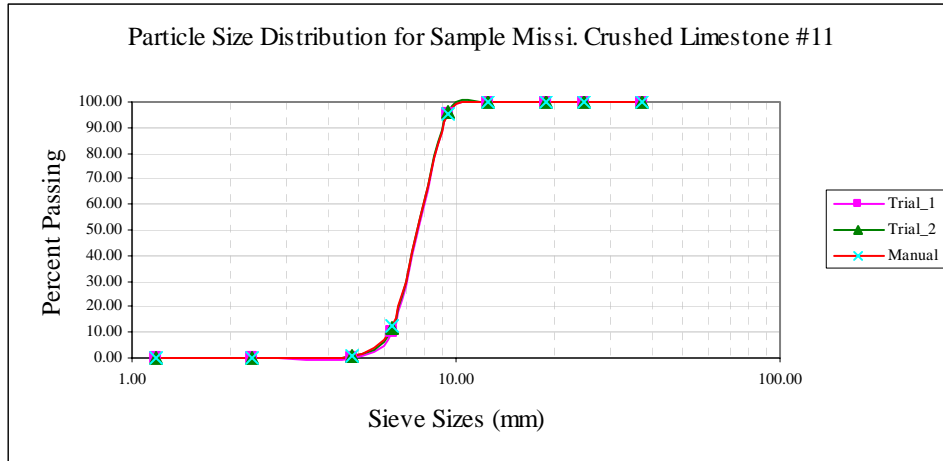


Figure AII-67 Imaging Based Particle Size Distributions of the #11 Crushed Limestone Sample

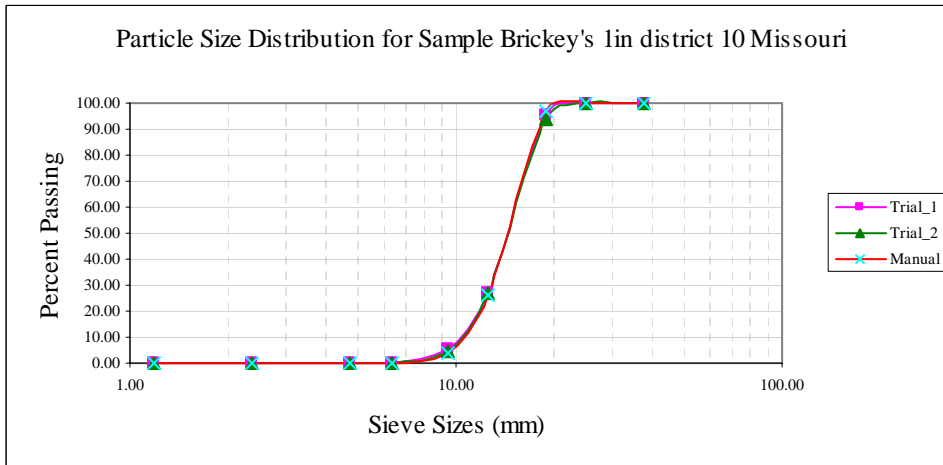


Figure AII-68 Imaging Based Particle Size Distributions of the Brickey's 1" Sample

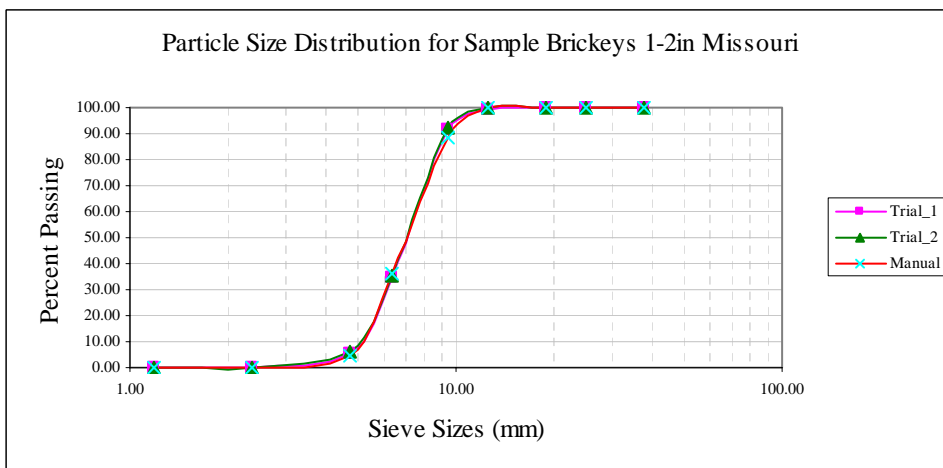


Figure AII-69 Imaging Based Particle Size Distributions of the Brickey's 1/2" Sample

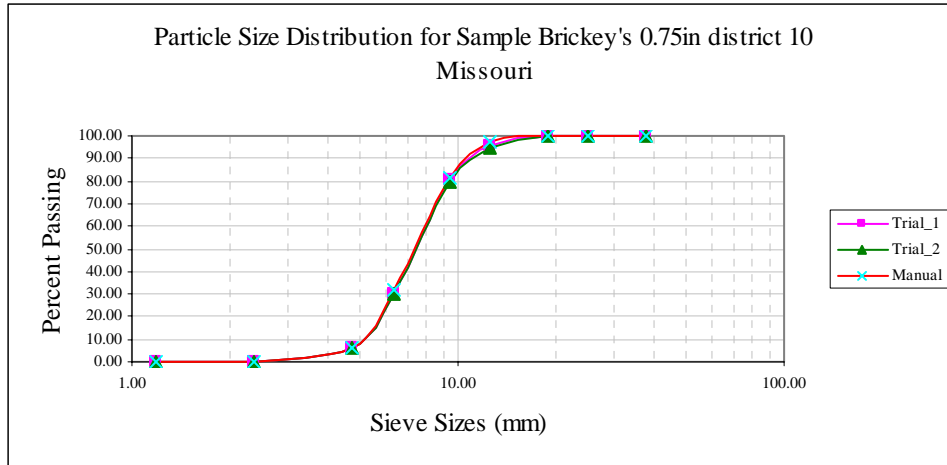


Figure AII-70 Imaging Based Particle Size Distributions of the Brickey's 3/4" Sample

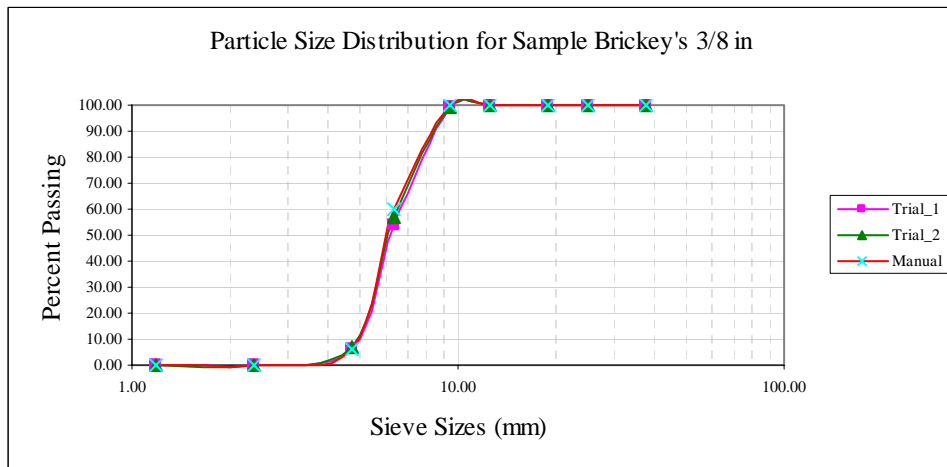


Figure AII-71 Imaging Based Particle Size Distributions of the Brickey's 3/8" Sample

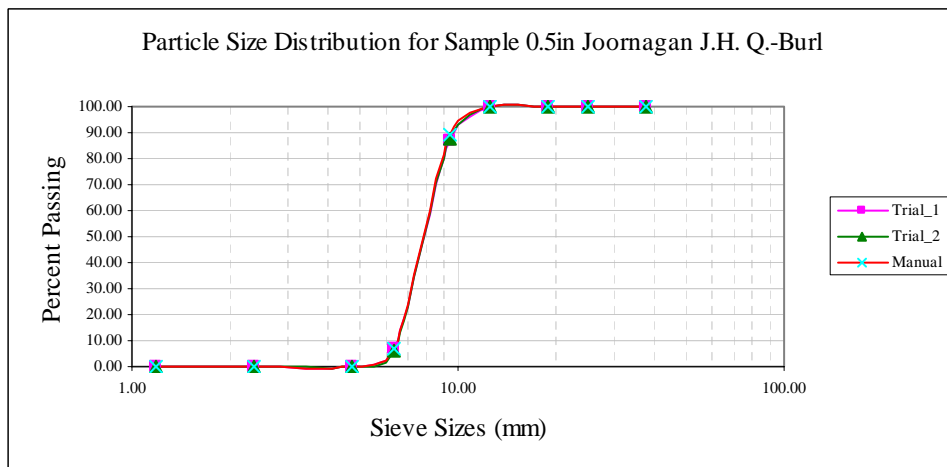


Figure AII-72 Imaging Based Particle Size Distributions of the 1/2 in. Joornagan J.H. Q.-Burl Sample

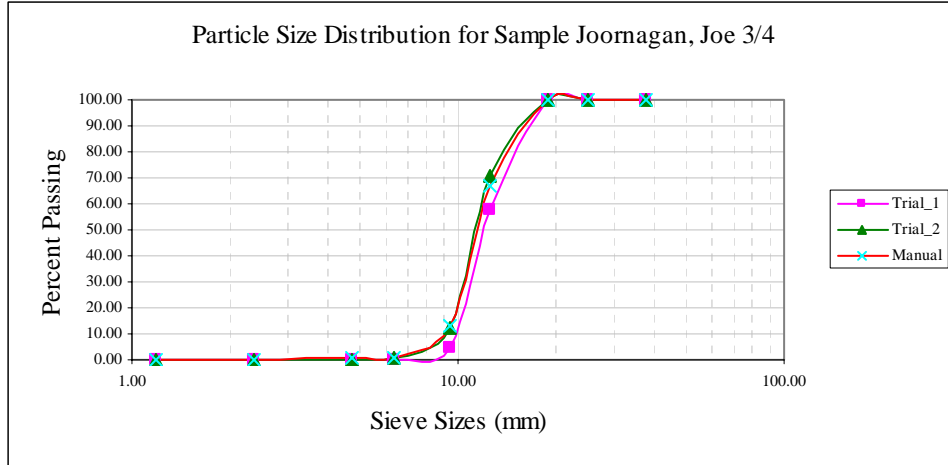


Figure AII-73 Imaging Based Particle Size Distributions of the 3/4 in. Joornagan J.H. Q. Sample

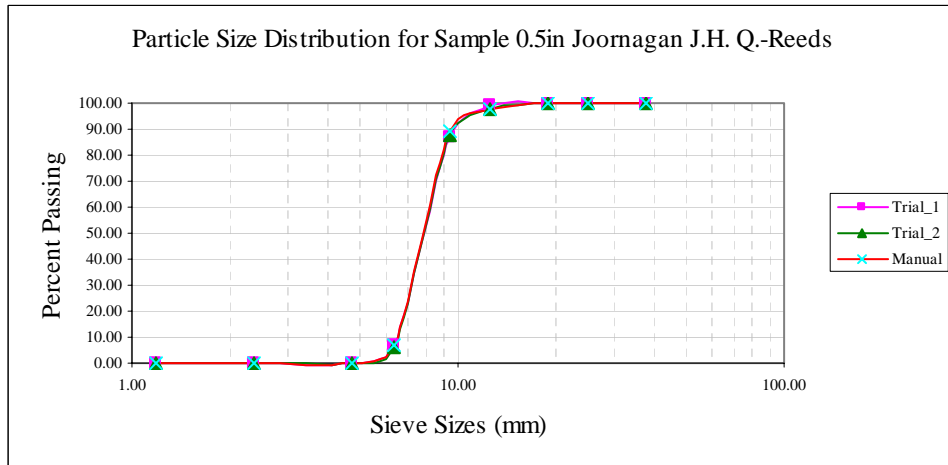


Figure AII-74 Imaging Based Particle Size Distributions of the 1/2 in. Joornagan J.H. R. Sample

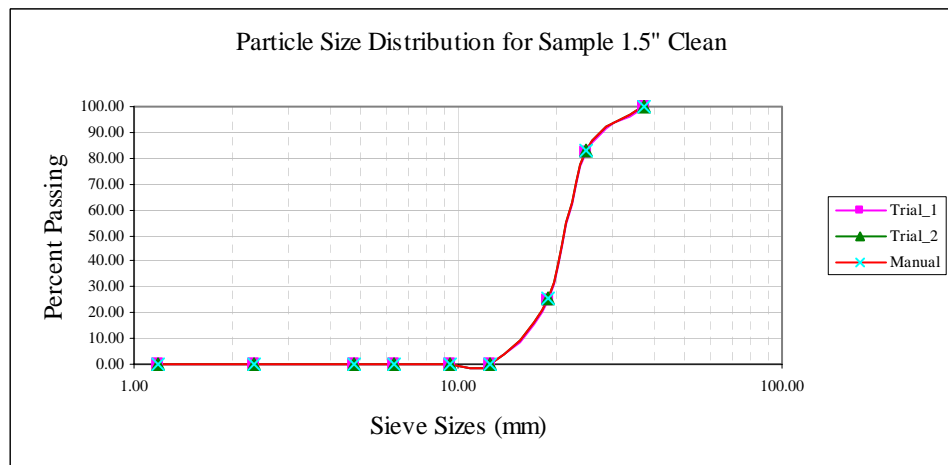


Figure AII-75 Imaging Based Particle Size Distributions of the 1.5 in. Clean Sample

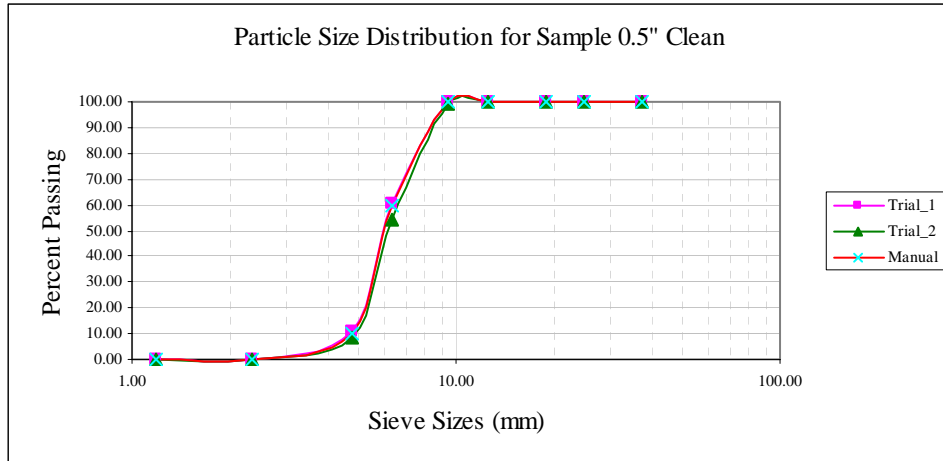


Figure AII-76 Imaging Based Particle Size Distributions of the 0.5 in. Clean Sample

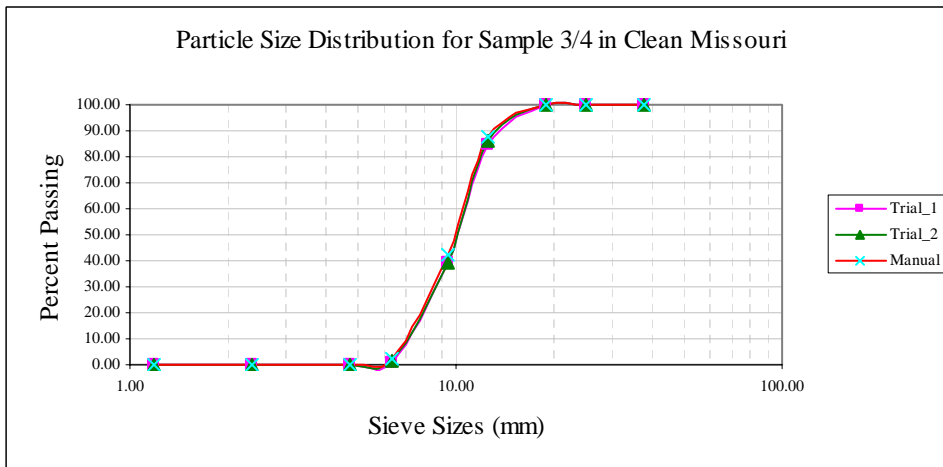


Figure AII-77 Imaging Based Particle Size Distributions of the 3/4 in. Clean Sample

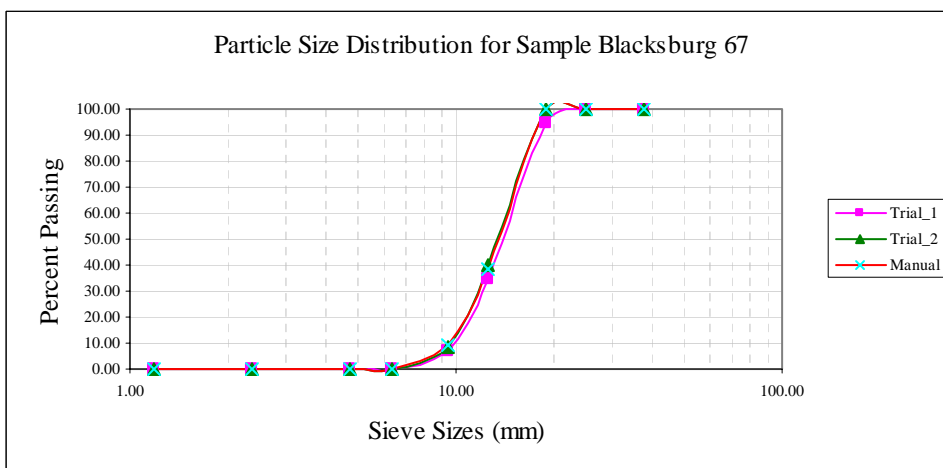


Figure AII-78 Imaging Based Particle Size Distributions of the Blacksburg 67 Sample

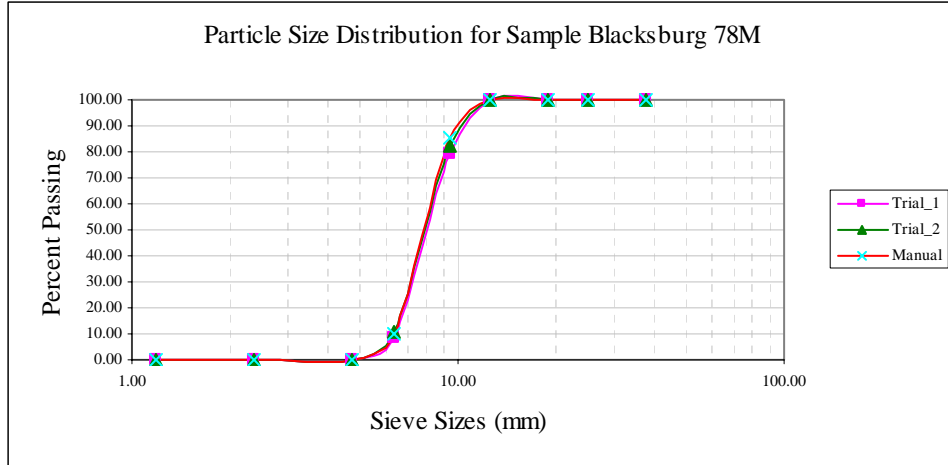


Figure AII-79 Imaging Based Particle Size Distributions of the Blacksburg 78M Sample

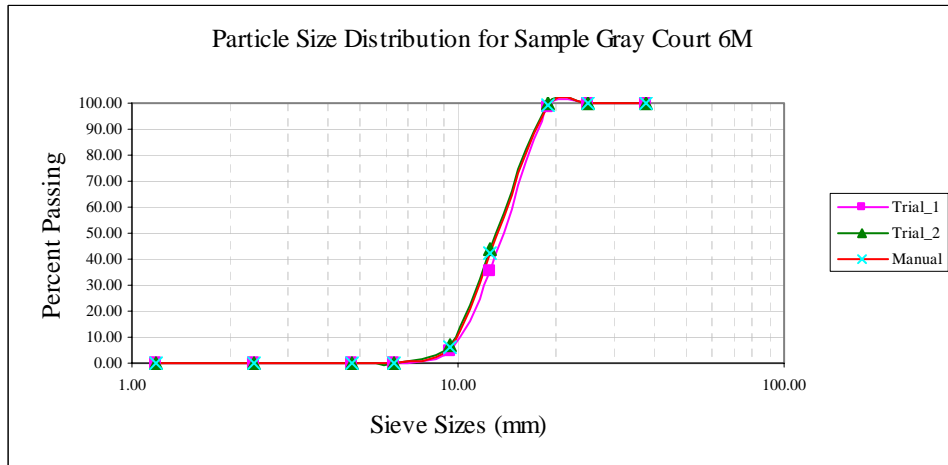


Figure AII-80 Imaging Based Particle Size Distributions of the Gray Court 6M Sample

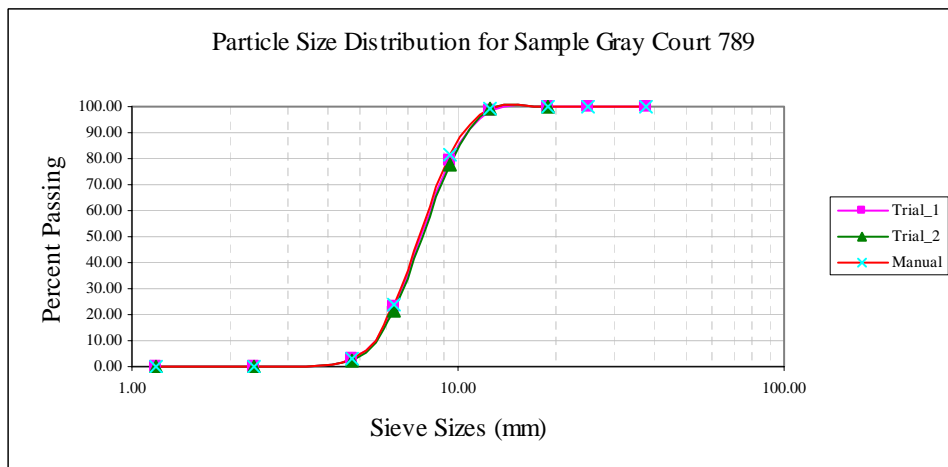


Figure AII-81 Imaging Based Particle Size Distributions of the Gray Court 789 Sample

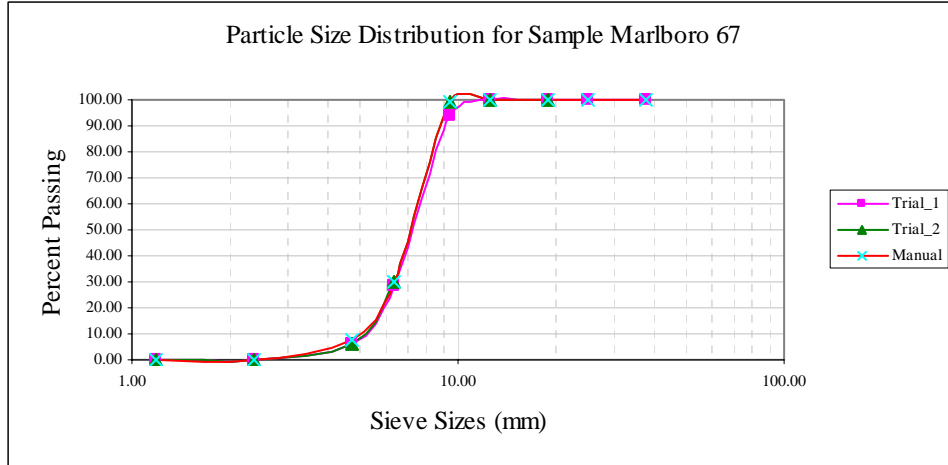


Figure AII-82 Imaging Based Particle Size Distributions of the Marlboro 67 Sample

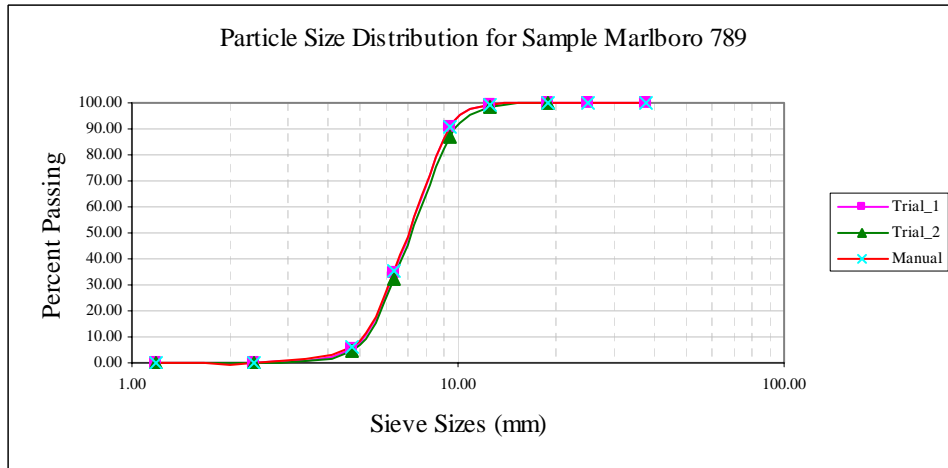


Figure AII-83 Imaging Based Particle Size Distributions of the Marlboro 789 Sample

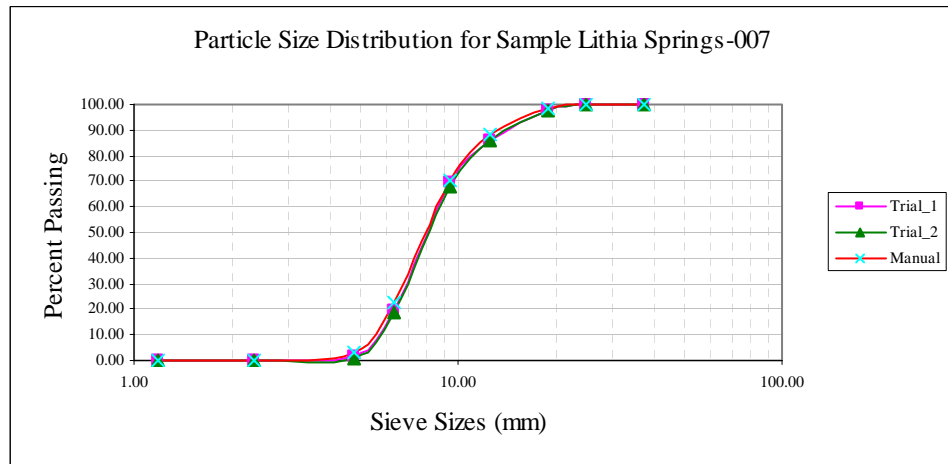


Figure AII-84 Imaging Based Particle Size Distributions of the Lithia Springs-007 Sample

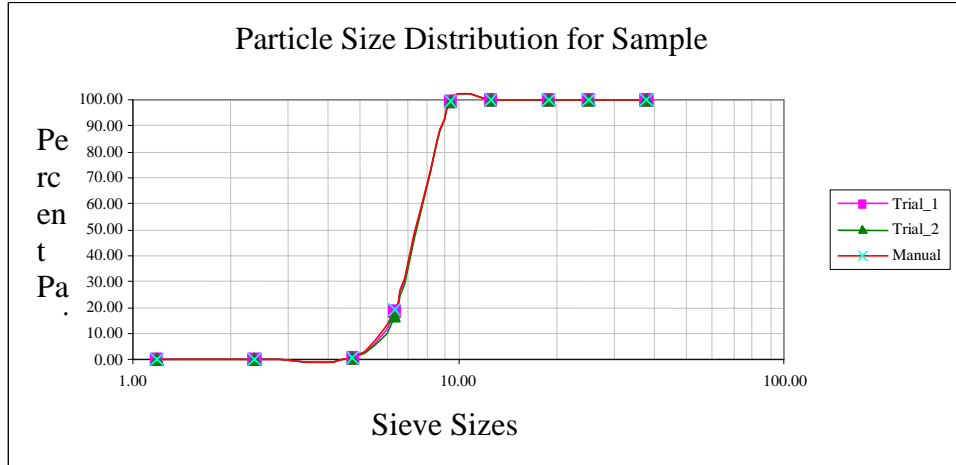


Figure AII-85 Imaging Based Particle Size Distributions of the Georgia 89 Sample

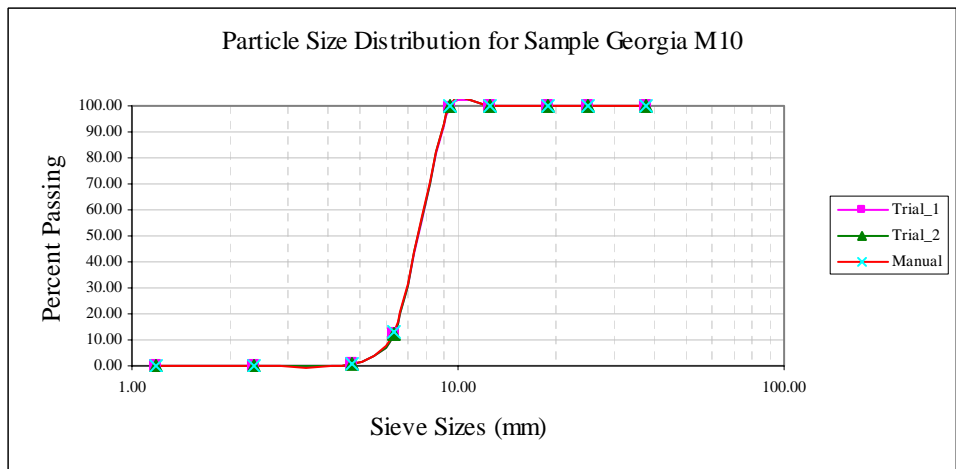


Figure AII-86 Imaging Based Particle Size Distributions of the Georgia M10 Sample

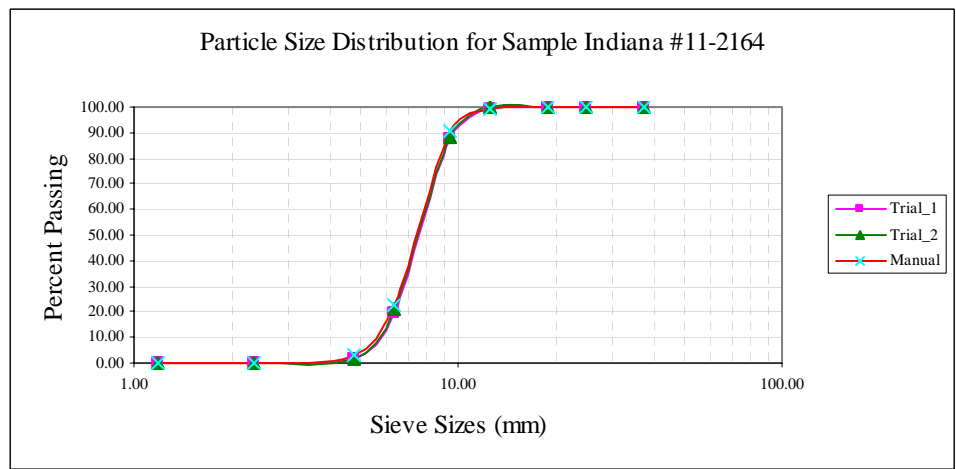


Figure AII-87 Imaging Based Particle Size Distributions of the Indiana #11-2164 Sample

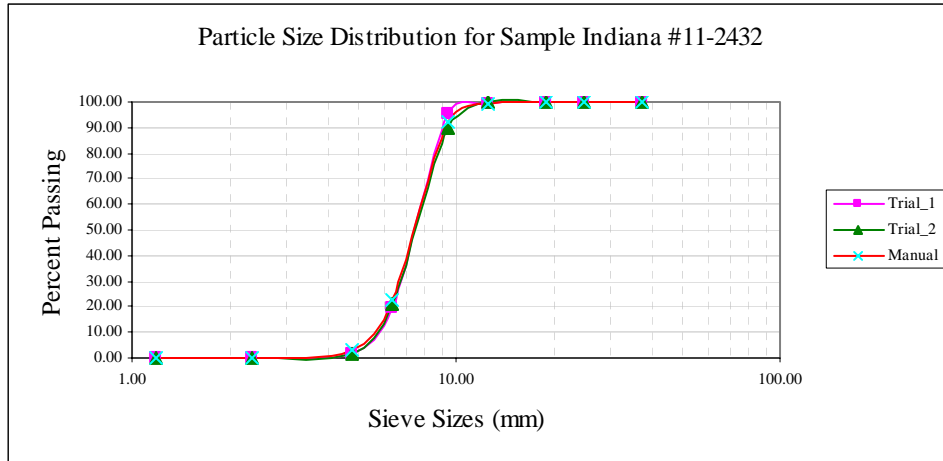


Figure AII-88 Imaging Based Particle Size Distributions of the Indiana #11-2432 Sample

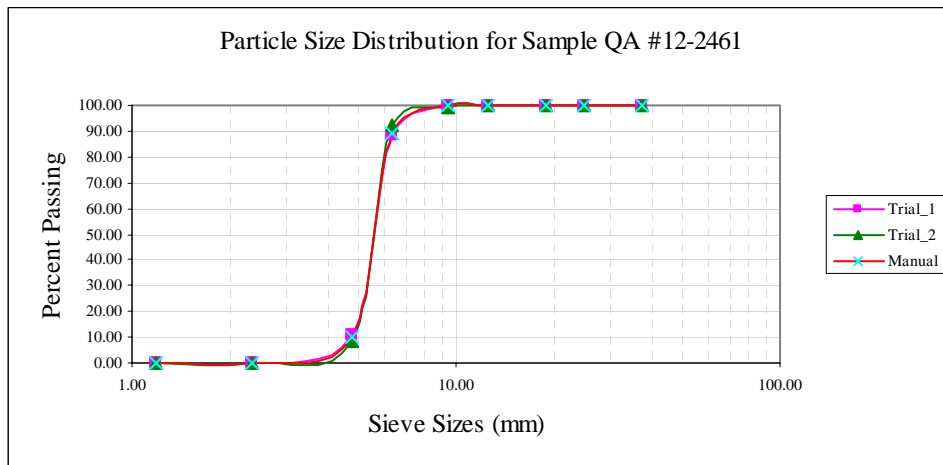


Figure AII-89 Imaging Based Particle Size Distributions of the QA #12-2461 Sample

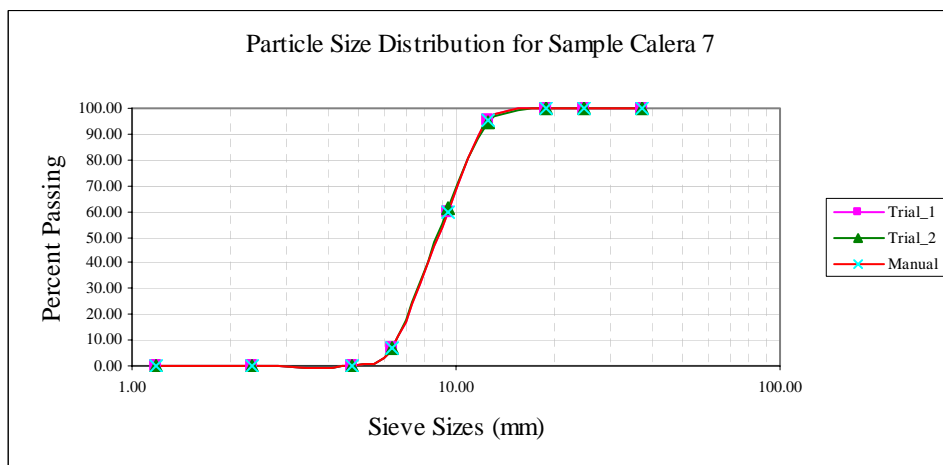


Figure AII-90 Imaging Based Particle Size Distributions of the Calera 7 Sample

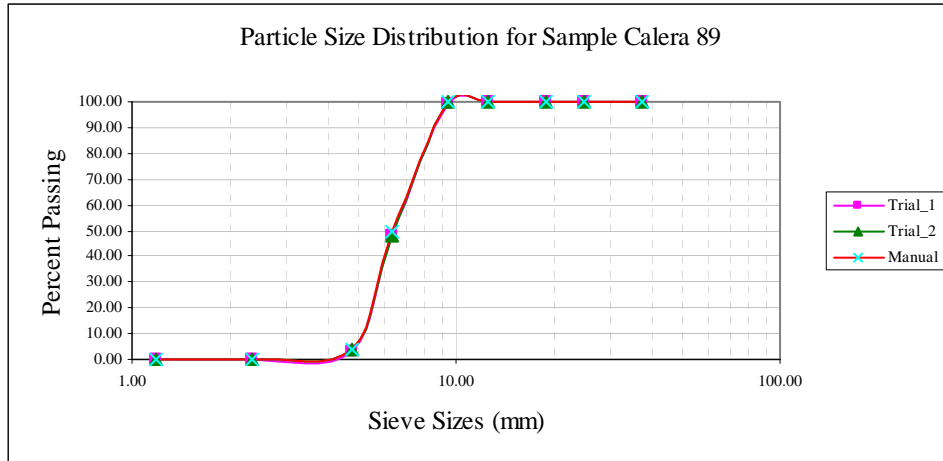


Figure AII-91 Imaging Based Particle Size Distributions of the Calera 89 Sample

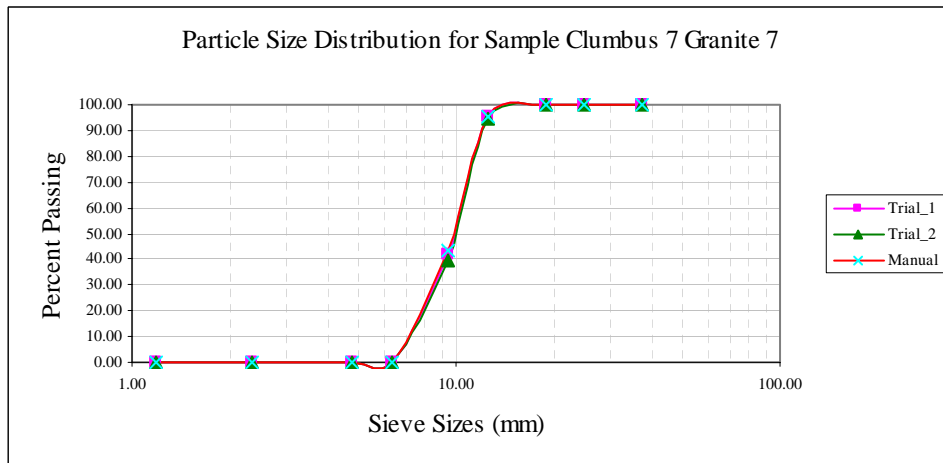


Figure AII-92 Imaging Based Particle Size Distributions of the Columbus 7 Granite 7 ample

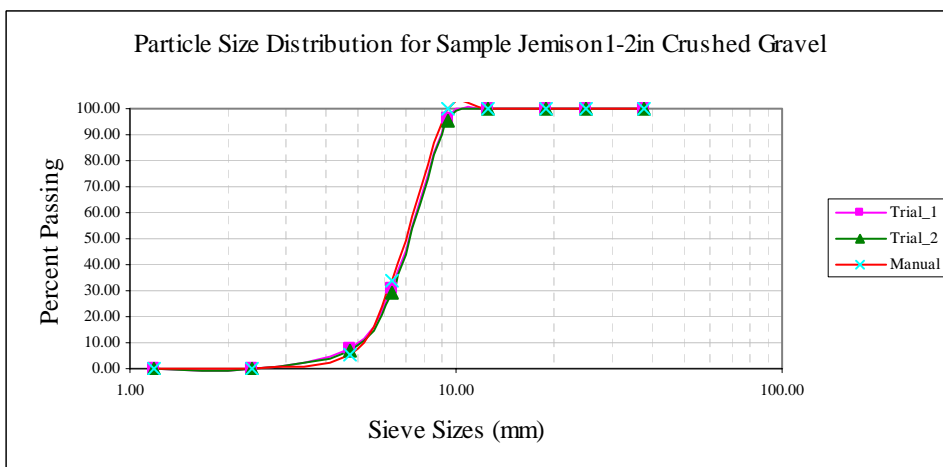


Figure AII-93 Imaging Based Particle Size Distributions of the Jemison 1/2 in. Sample

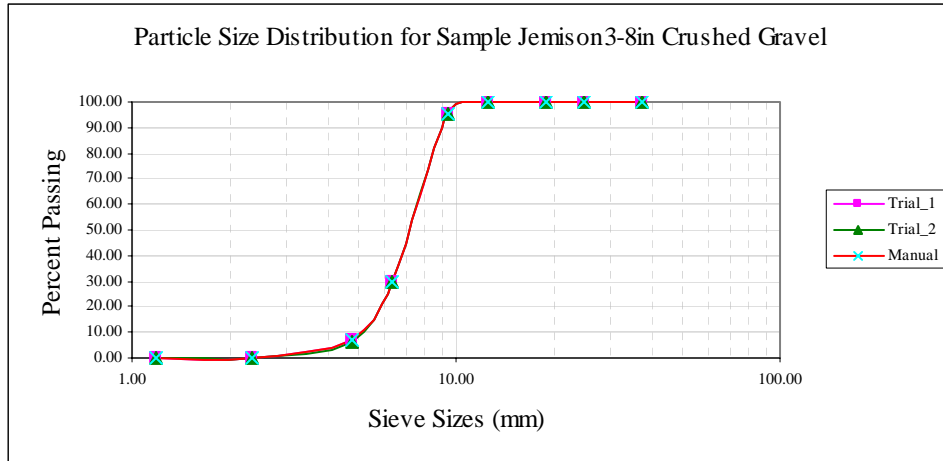


Figure AII-94 Imaging Based Particle Size Distributions of the Jemison 3/8 in. Sample

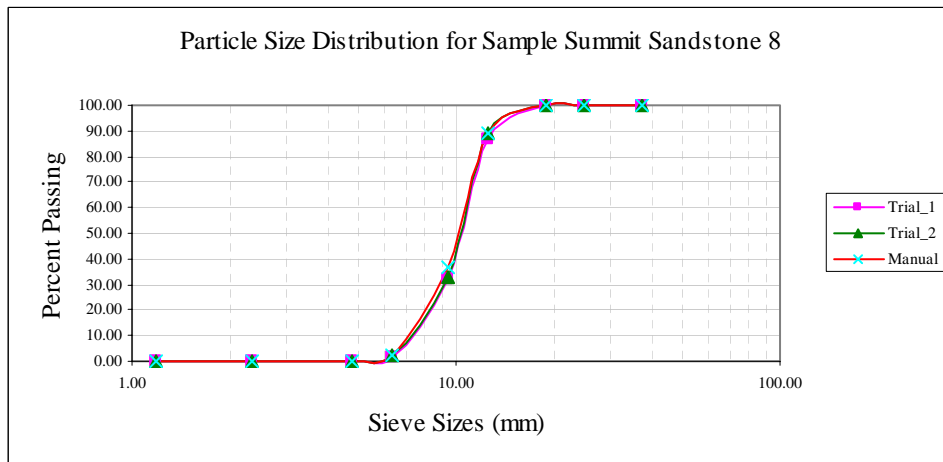


Figure AII-95 Imaging Based Particle Size Distributions of the Summit Sandstone 8 Sample

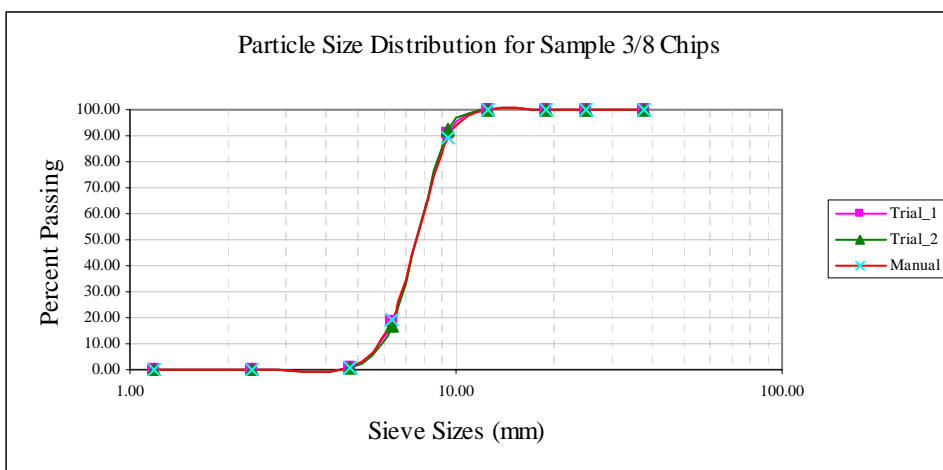


Figure AII-96 Imaging Based Particle Size Distributions of the 3/8 in. Chips Sample

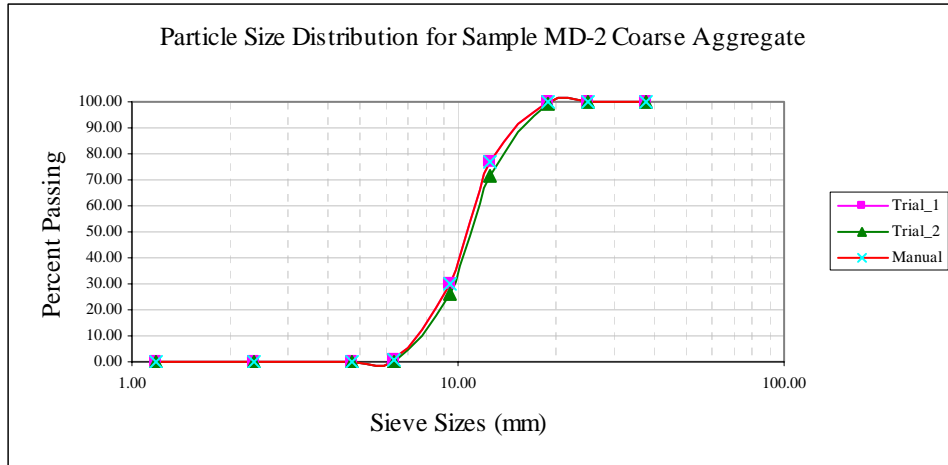


Figure AII-97 Imaging Based Particle Size Distributions of the Coarse Aggregate MD-2 Sample

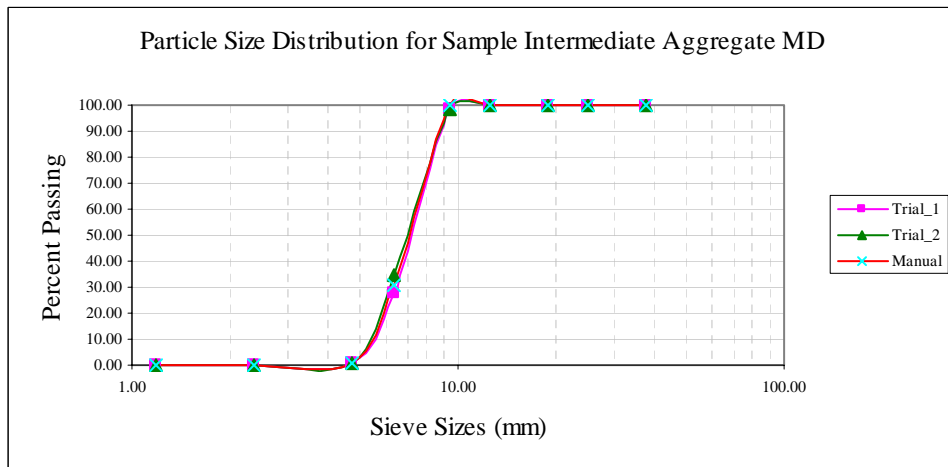


Figure AII-98 Imaging Based Particle Size Distributions of the Intermediate Aggregate-MD Sample

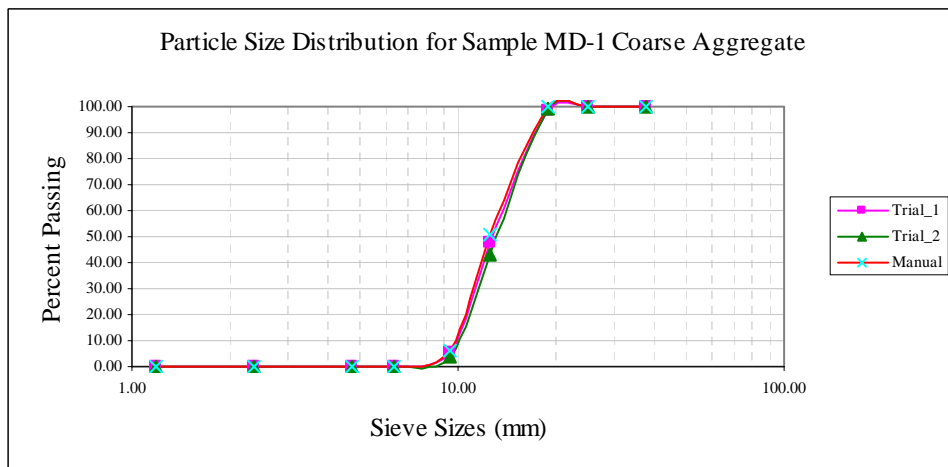


Figure AII-99 Imaging Based Particle Size Distributions of the Coarse Aggregate MD-1 Sample

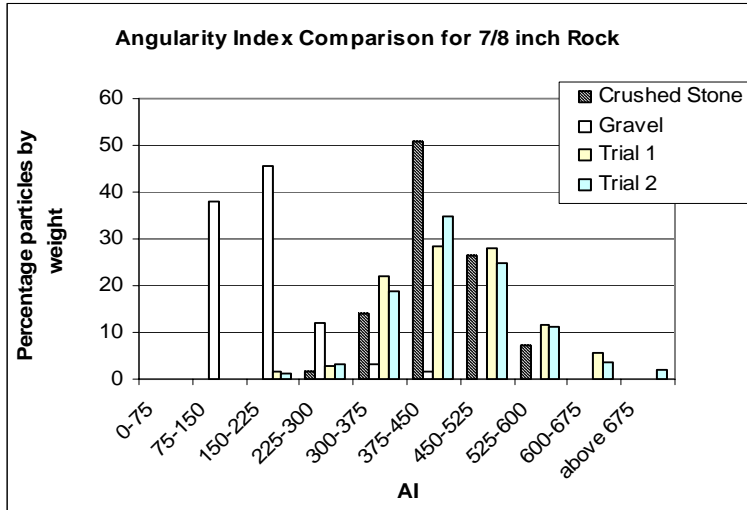


Figure AII-100 Imaging Based AI of the 7/8 in. Rock Sample

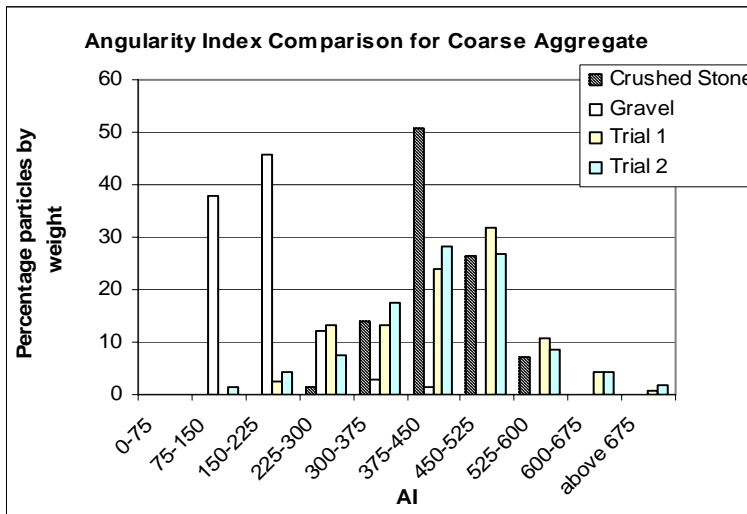


Figure AII-101 Imaging Based AI of the Coarse Aggregate Sample

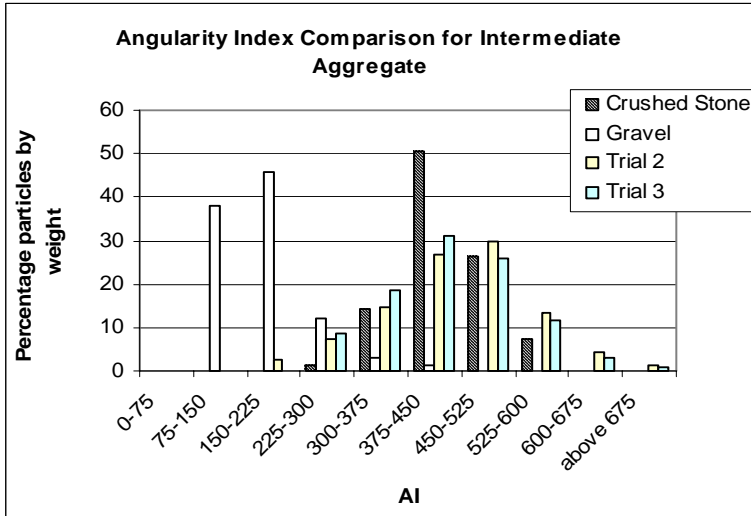


Figure AII-102 Imaging Based AI of the Intermediate Aggregate Sample

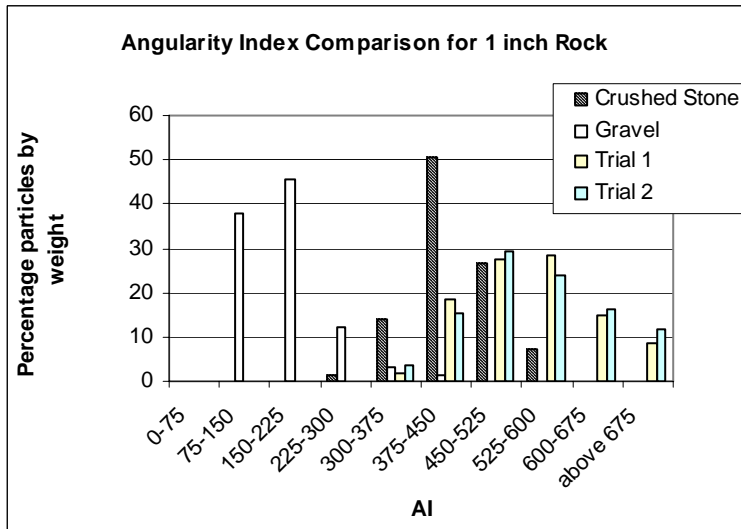


Figure AII-103 Imaging Based AI of the 1" Rock Sample

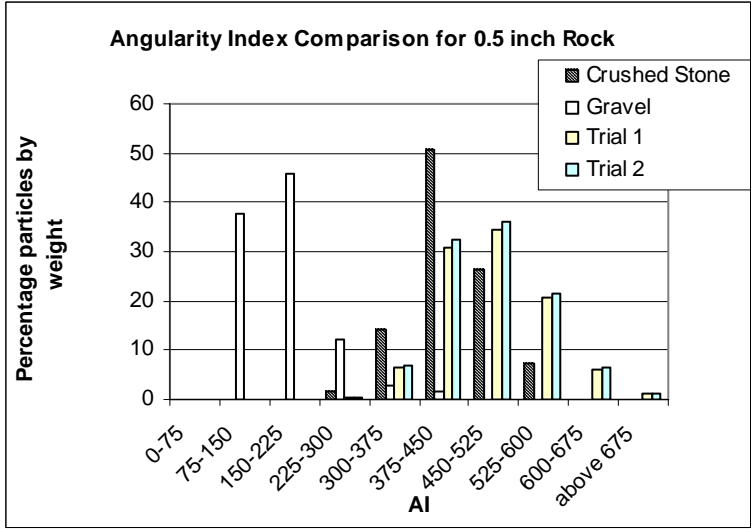


Figure AII-104 Imaging Based AI of the 0.5" Rock Sample

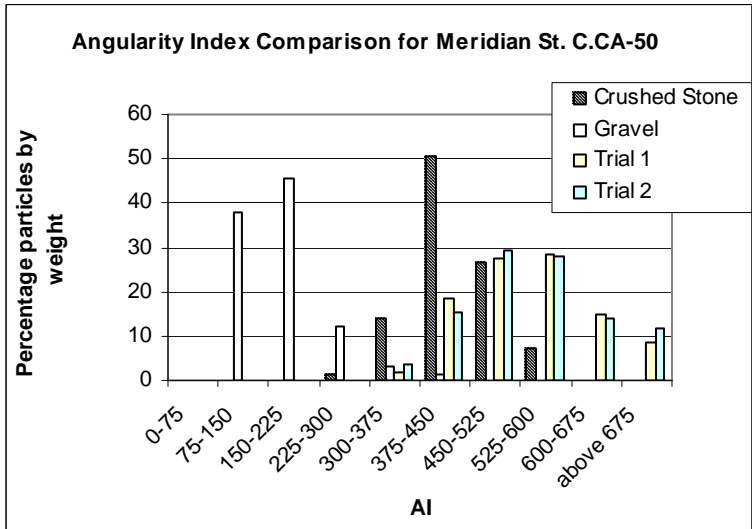


Figure AII-105 Imaging Based AI of the Meridian St. C. CA-50 Sample

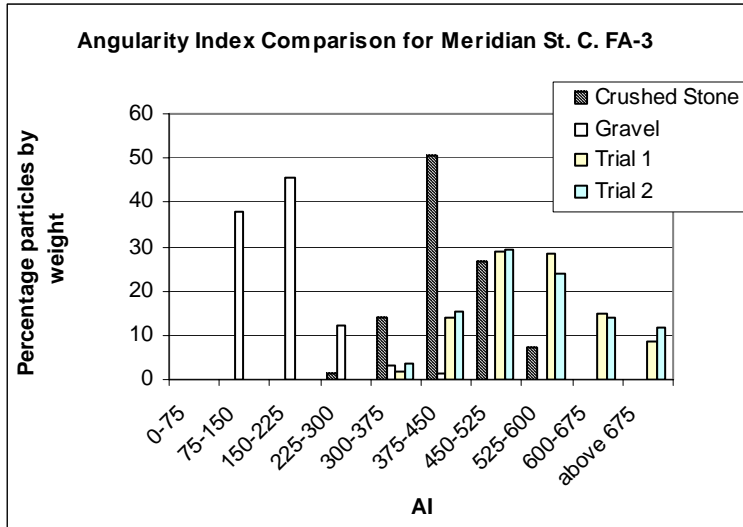


Figure AII-106 Imaging Based AI of the Meridian St. C. FA-3 Sample

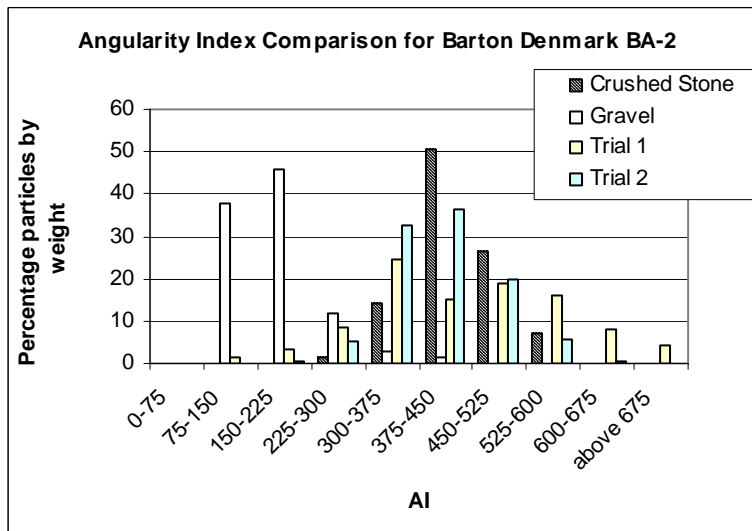


Figure AII-107 Imaging Based AI of the Barton Denmark BA-2 Sample

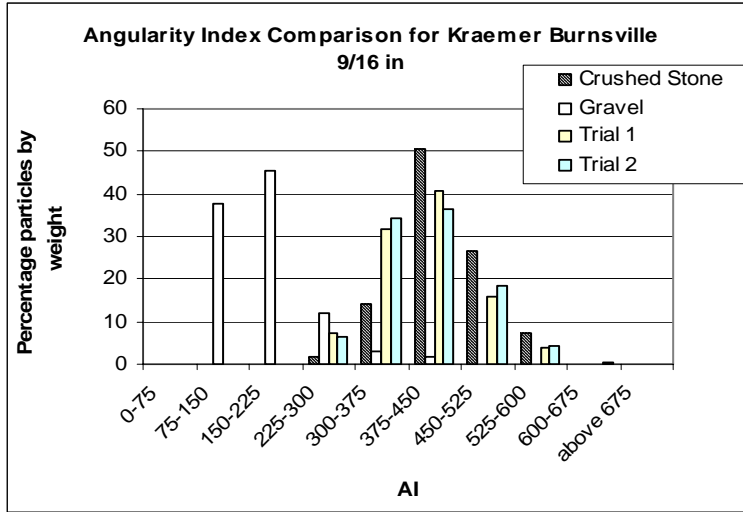


Figure AII-108 Imaging Based AI of the Kraemer Burnsville 9/16 in. Sample

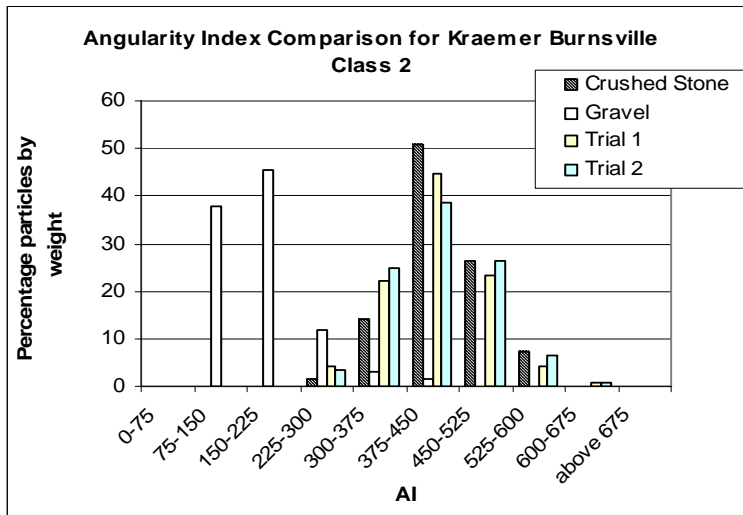


Figure AII-109 Imaging Based AI of the Kraemer Burnsville Class 2 Sample

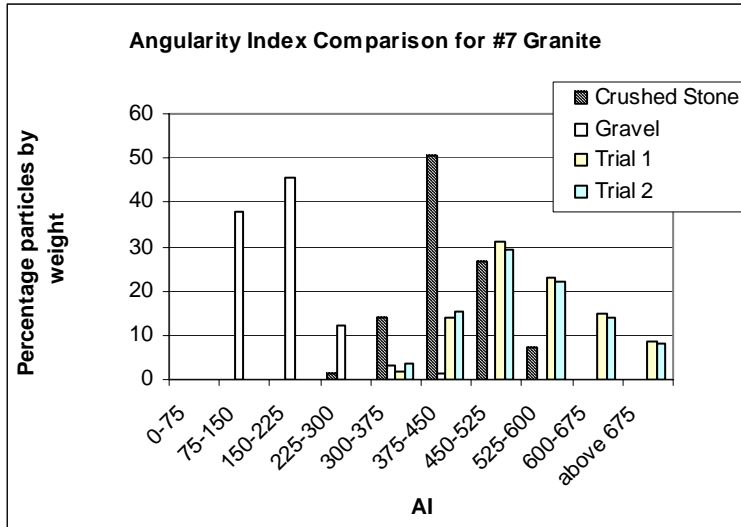


Figure AII-110 Imaging Based AI of the #7 Granite Sample

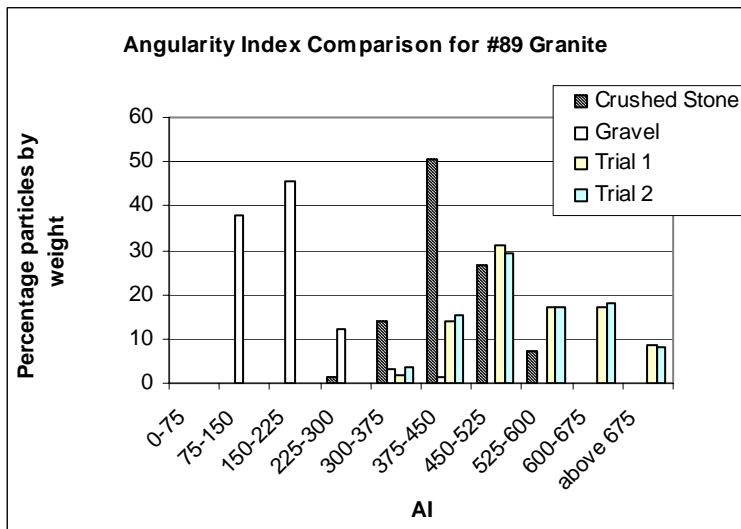


Figure AII-111 Imaging Based AI of the #89 Granite Sample

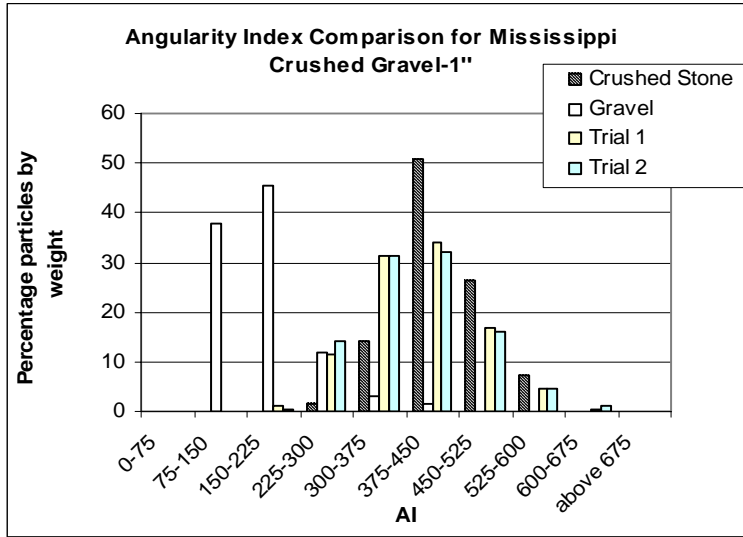


Figure AII-112 Imaging Based AI of the 1" Crushed Gravel Sample

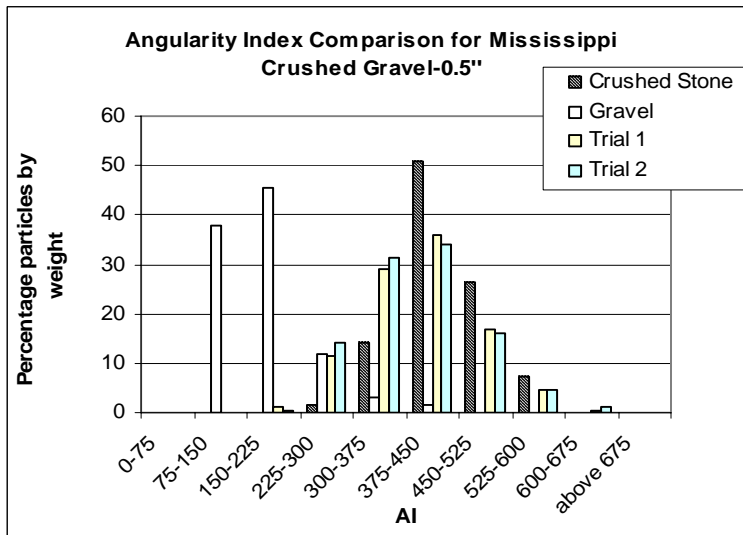


Figure AII-113 Imaging Based AI of the 0.5" Crushed Gravel Sample

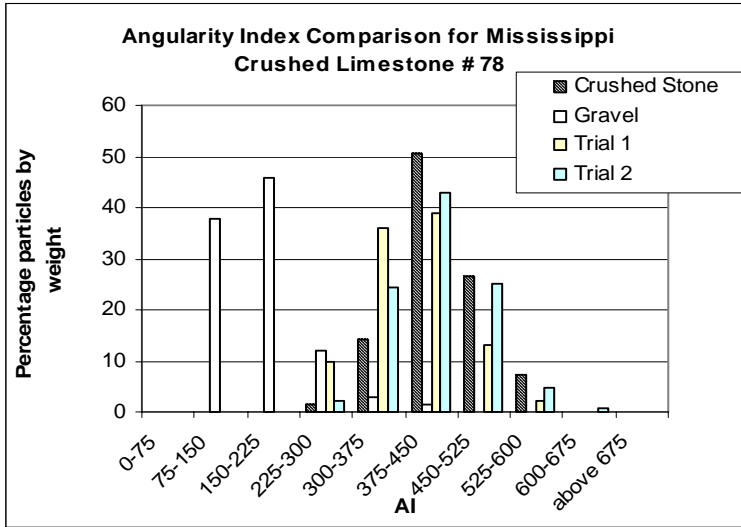


Figure AII-114 Imaging Based AI of the #78 Crushed Limestone Sample

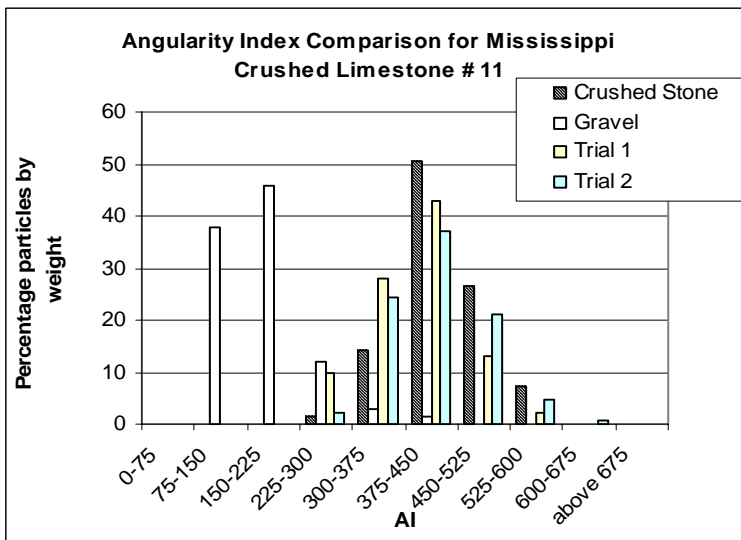


Figure AII-115 Imaging Based AI of the #11 Crushed Limestone Sample

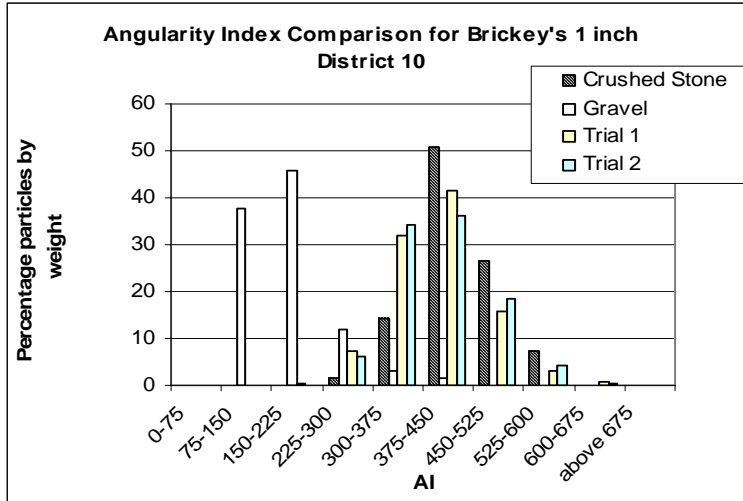


Figure AII-116 Imaging Based AI of the #78 Crushed Limestone Sample

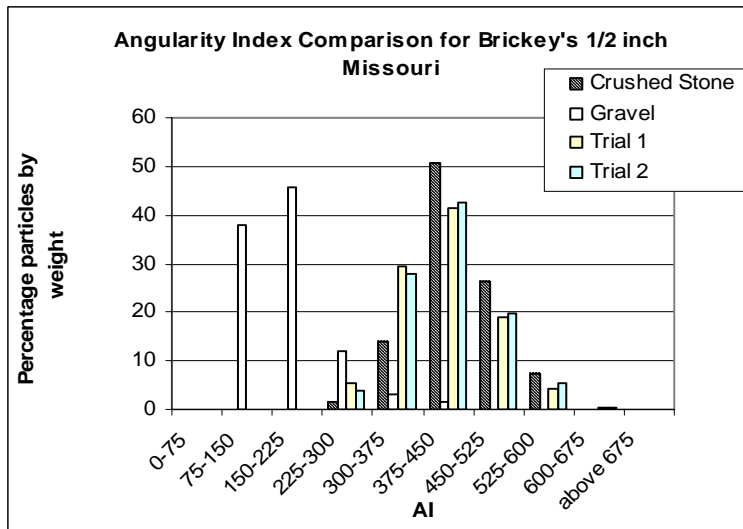


Figure AII-117 Imaging Based AI of Brickey's 1/2 in. Sample

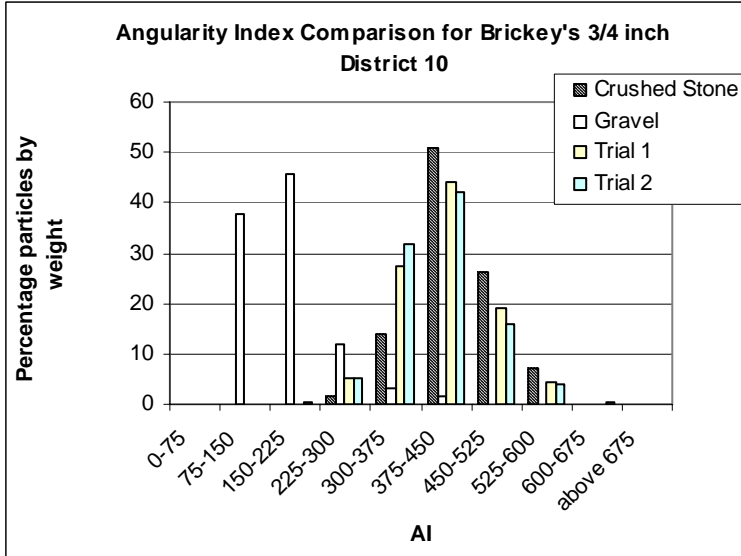


Figure AII-118 Imaging Based AI of Brickey's 3/4 in. Sample

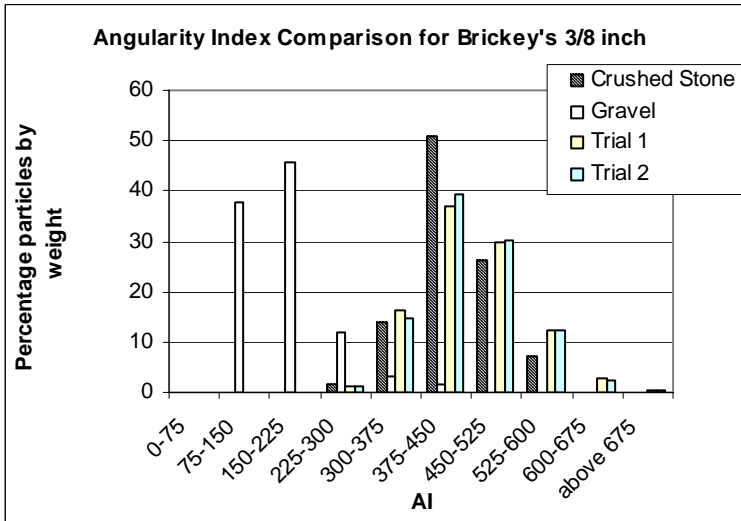


Figure AII-119 Imaging Based AI of Brickey's 3/8 in. Sample

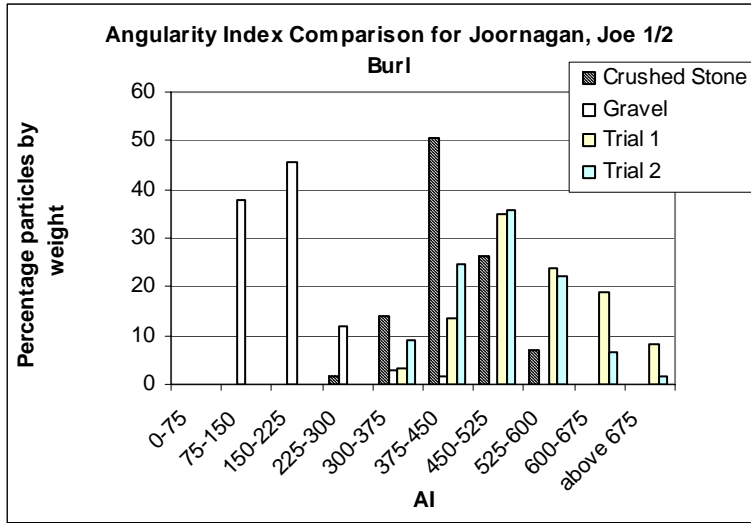


Figure AII-120 Imaging Based AI of 1/2 in. Joornagan, J.H.Q. Burl Sample

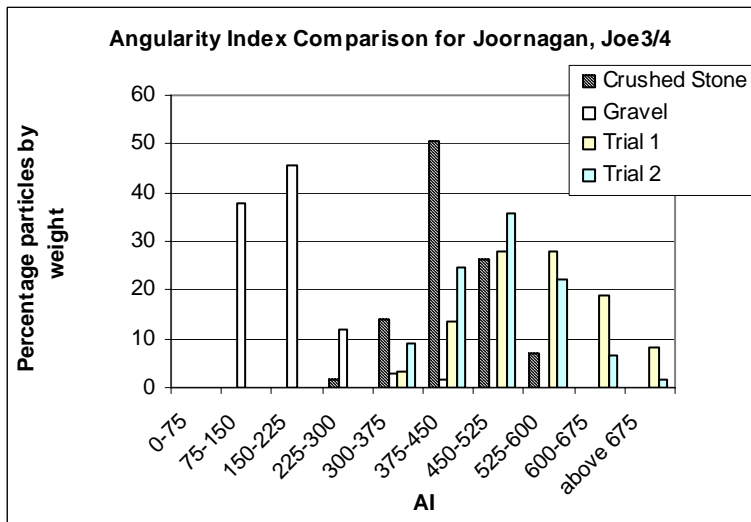


Figure AII-121 Imaging Based AI of 3/4 in. Joornagan, J.H.Q. Sample

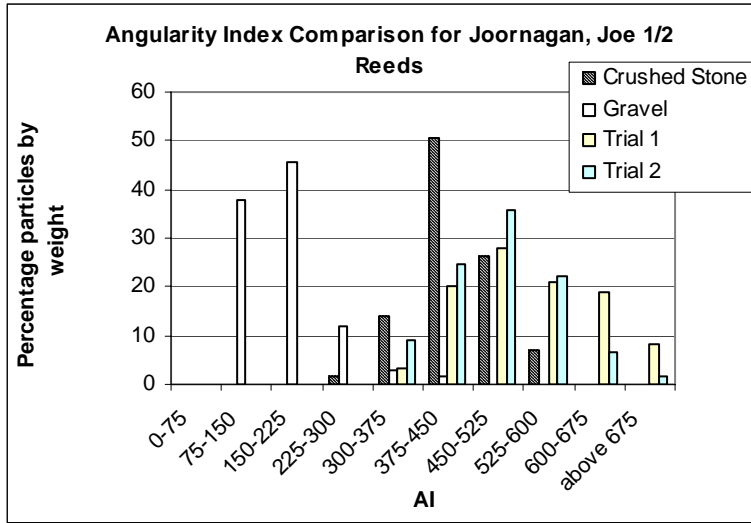


Figure AII-122 Imaging Based AI of 1/2 in. Joornagan, J.H.Q. R Sample

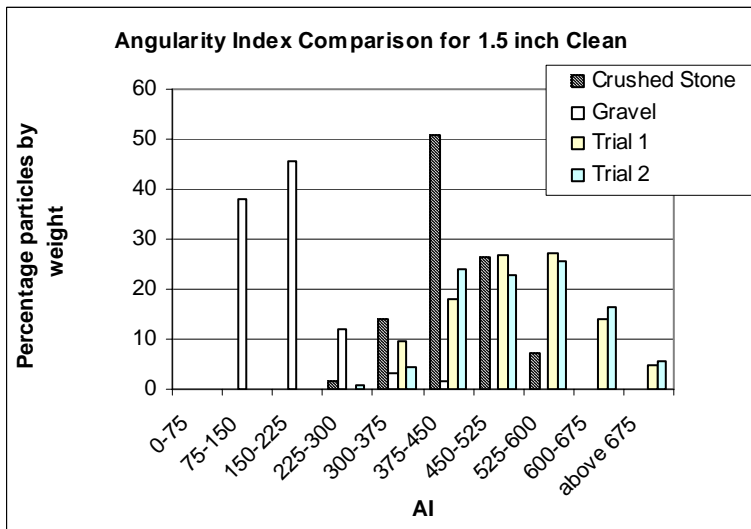


Figure AII-123 Imaging Based AI of 1.5 in. Clean Sample

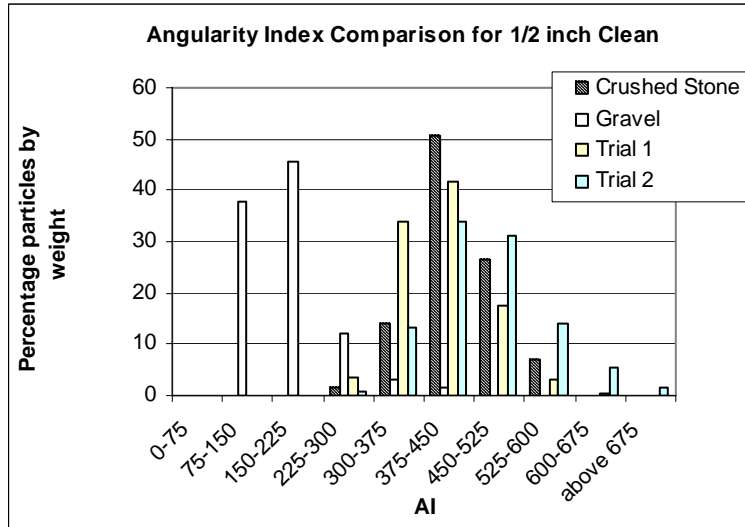


Figure AII-124 Imaging Based AI of 0.5 in. Clean Sample

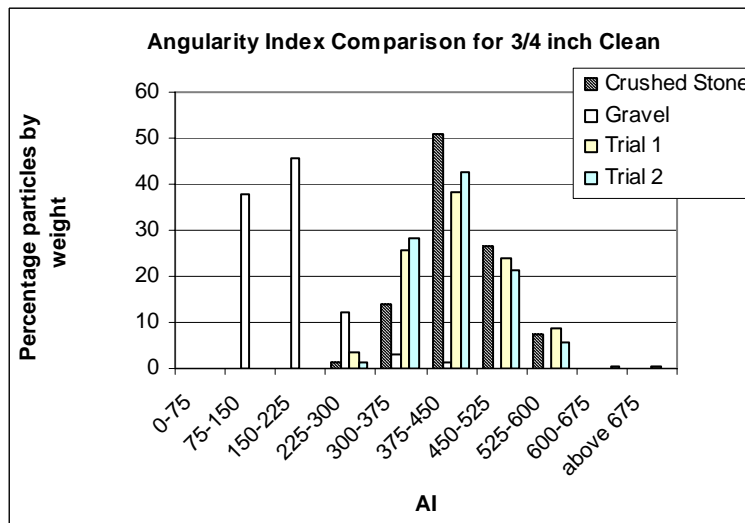


Figure AII-125 Imaging Based AI of 3/4 in. Clean Sample

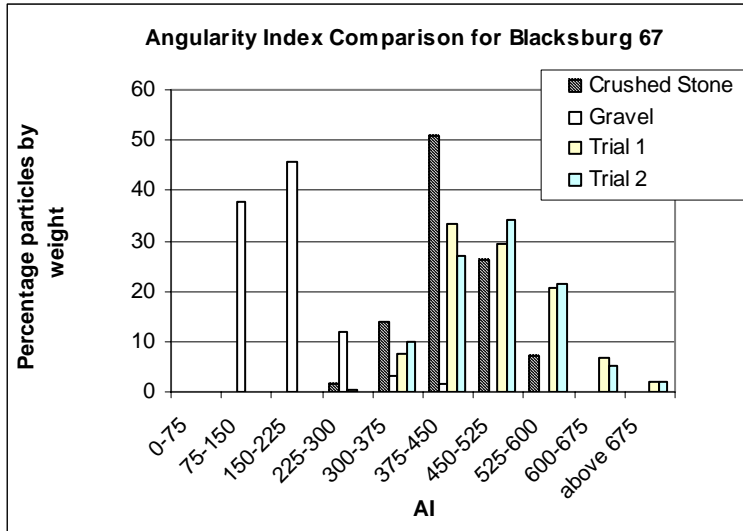


Figure AII-126 Imaging Based AI of the Blacksburg 67 Sample

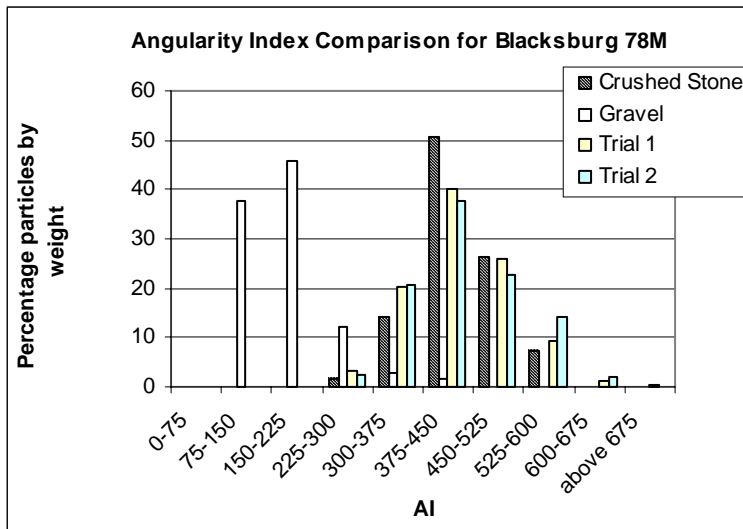


Figure AII-127 Imaging Based AI of the Blacksburg 78M Sample

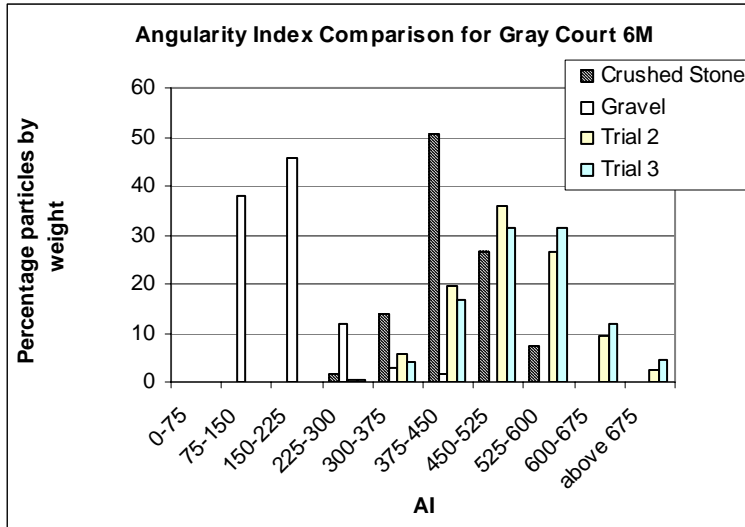


Figure AII-128 Imaging Based AI of the Gray Court 6M Sample

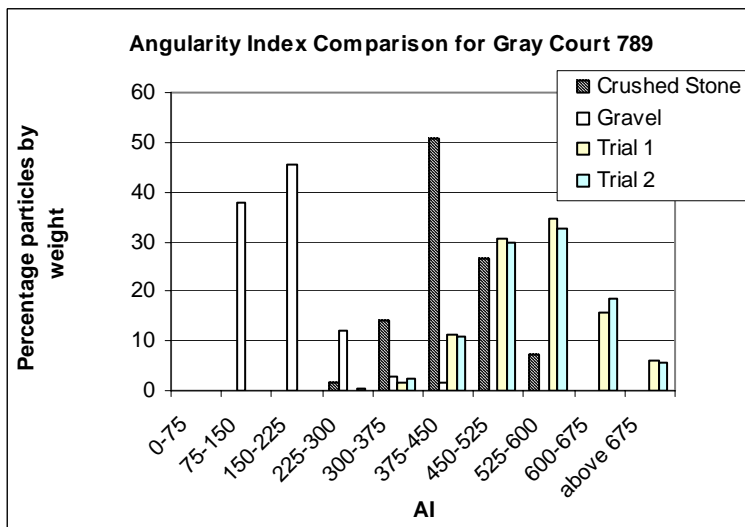


Figure AII-129 Imaging Based AI of the Gray Court 789 Sample

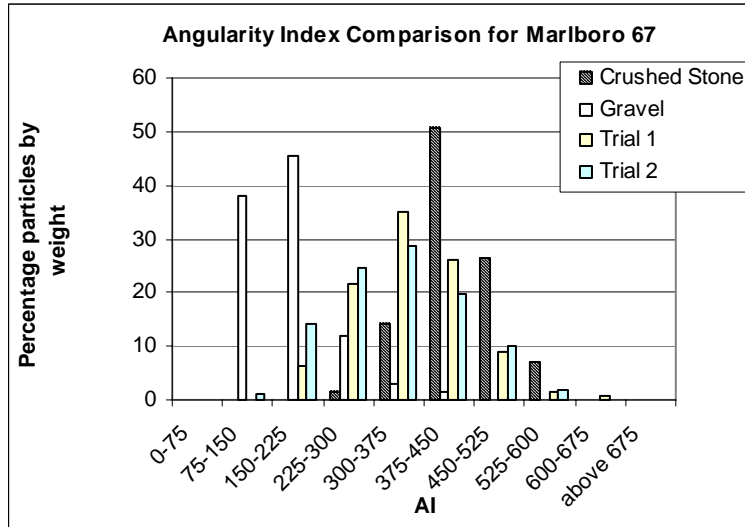


Figure AII-130 Imaging Based AI of the Marlboro 67 Sample

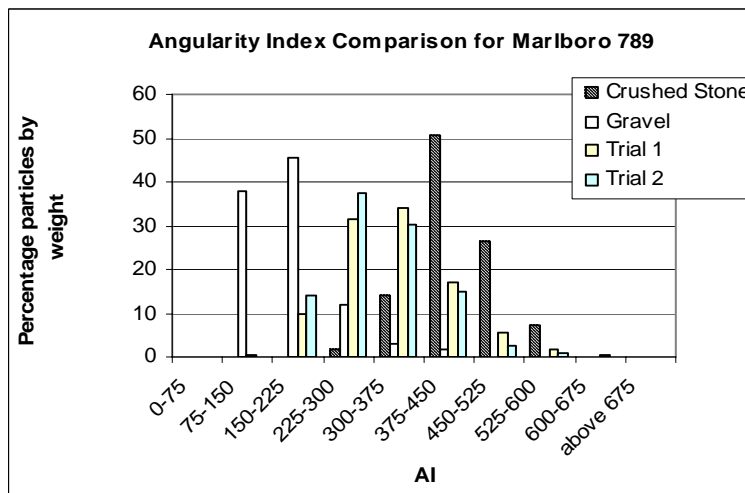


Figure AII-131 Imaging Based AI of the Marlboro 789 Sample

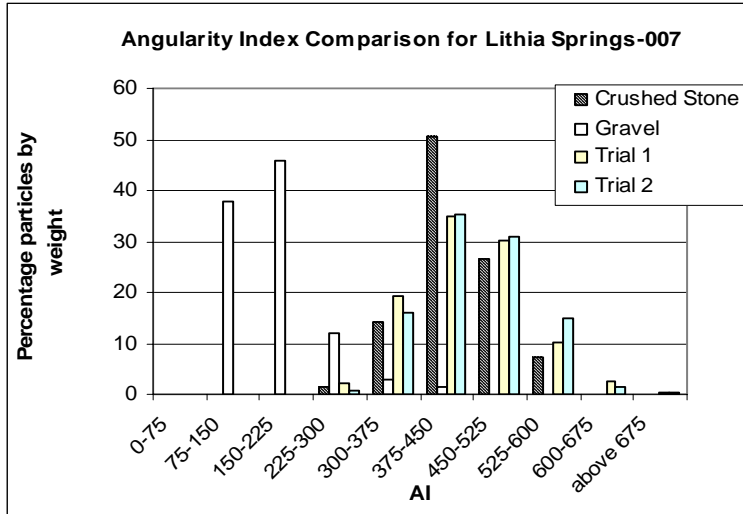


Figure AII-132 Imaging Based AI of the Lithia Springs-007 Sample

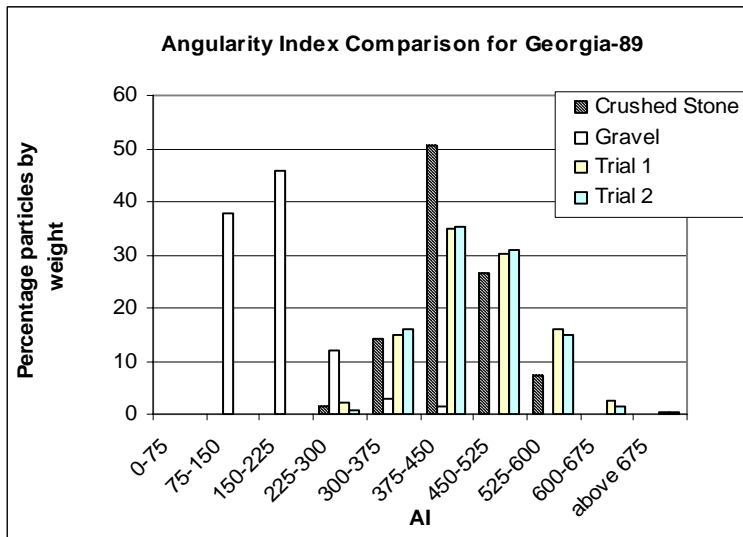


Figure AII-133 Imaging Based AI of the Georgia 89 Sample

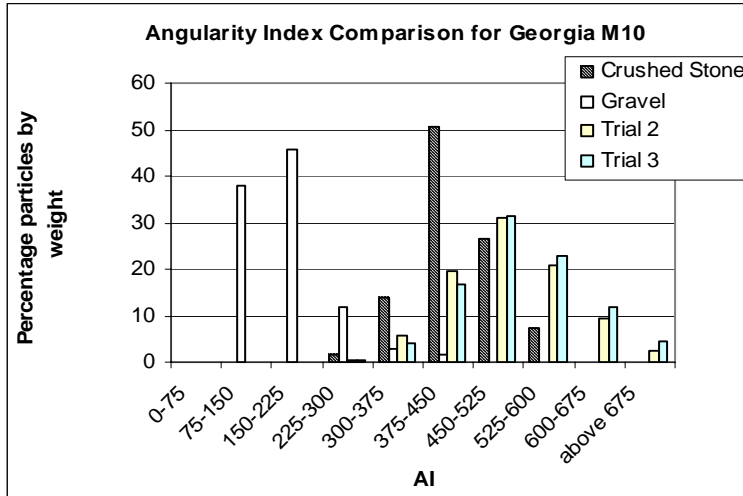


Figure AII-134 Imaging Based AI of the Georgia M10 Sample

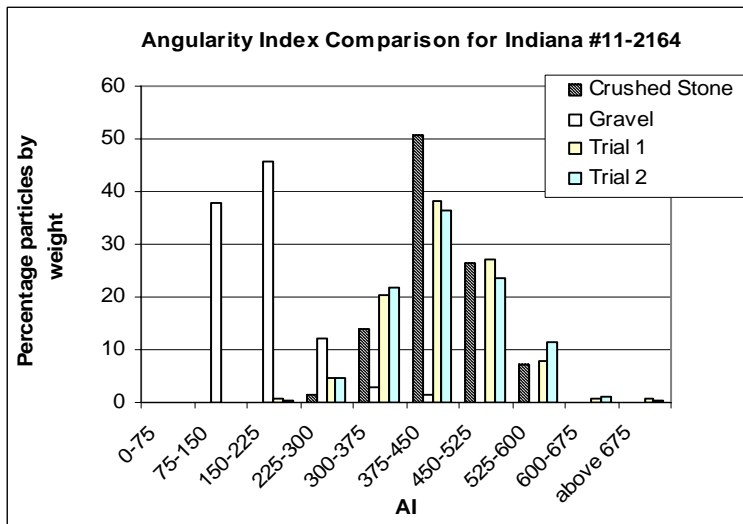


Figure AII-135 Imaging Based AI of the Indiana #11-2164 Sample

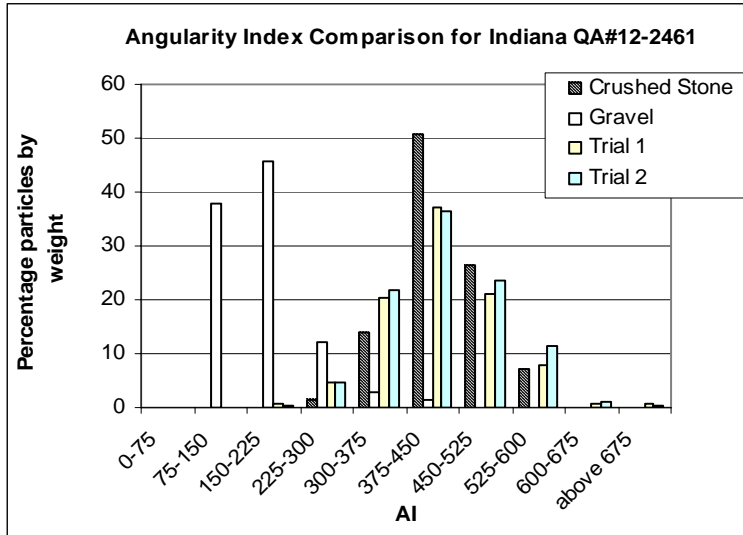


Figure AII-136 Imaging Based AI of the QA #12-2461 Sample

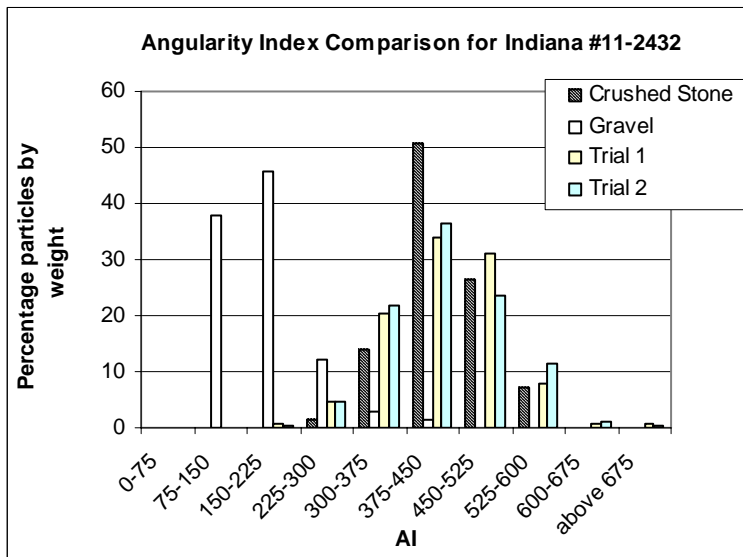


Figure AII-137 Imaging Based AI of the Indiana #11-2432 Sample

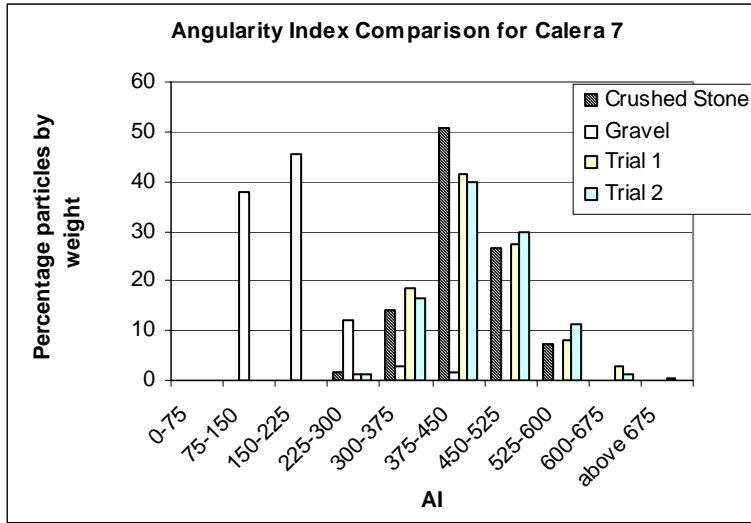


Figure AII-138 Imaging Based AI of the Calera 7 Sample

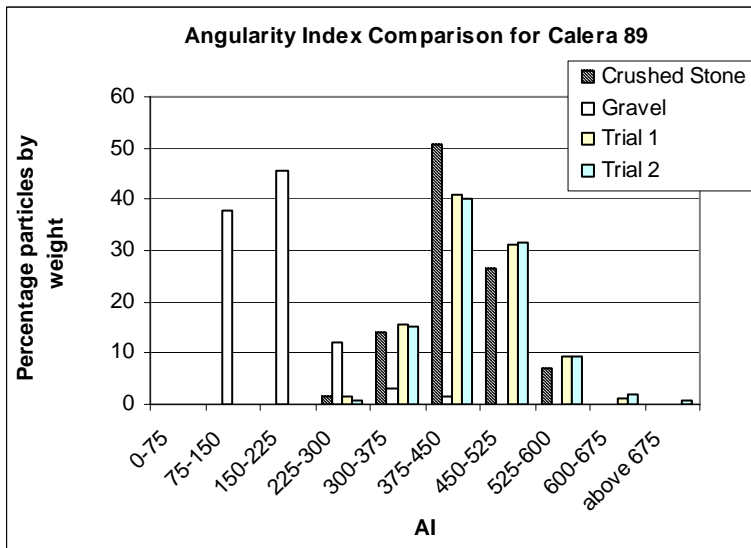


Figure AII-139 Imaging Based AI of the Calera 89 Sample

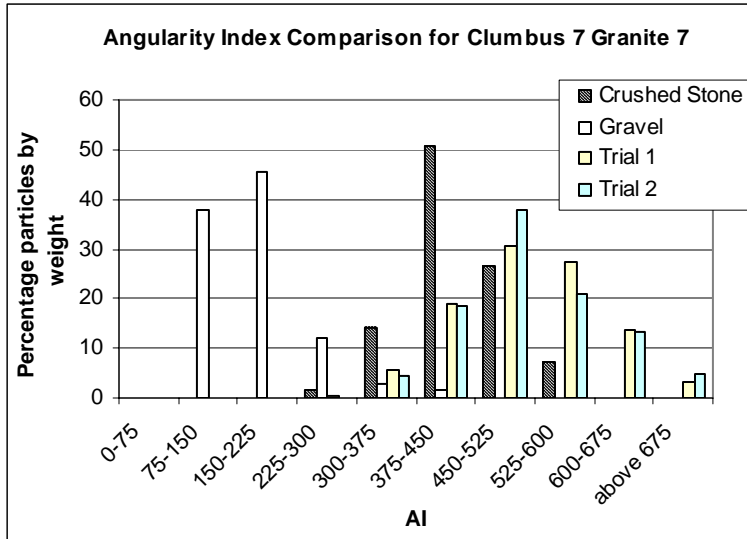


Figure AII-140 Imaging Based AI of the Columbus 7 Granite 7 Sample

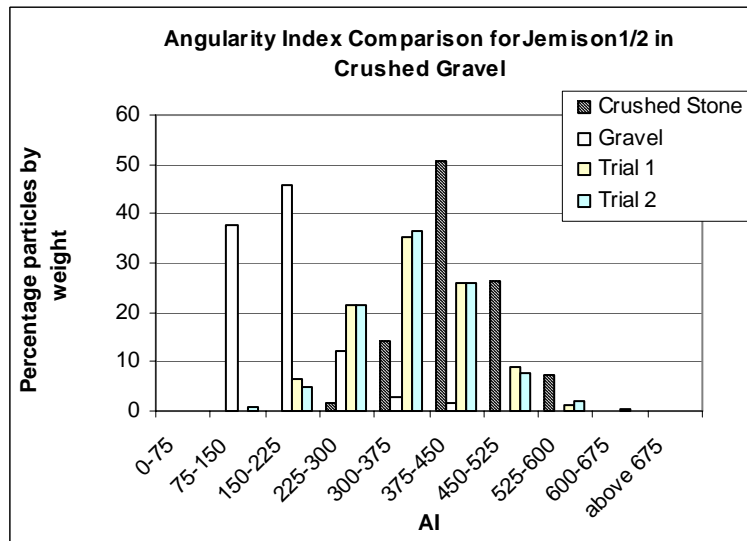


Figure AII-141 Imaging Based AI of the Jemison 1/2 in. Sample

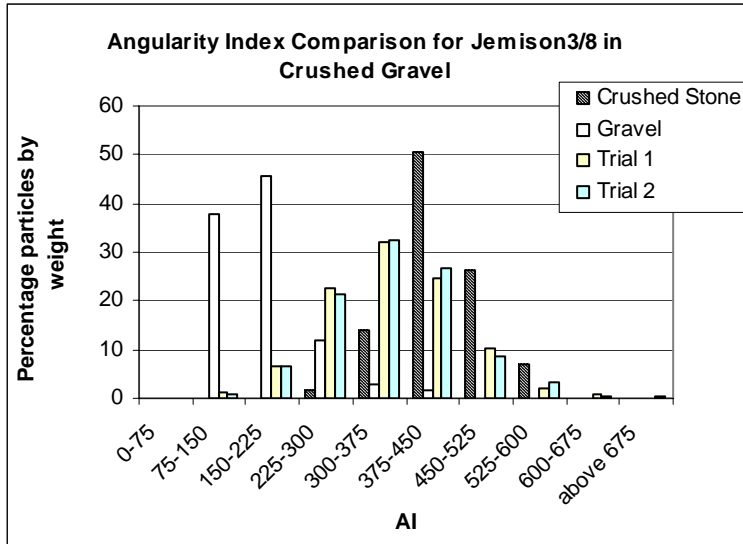


Figure AII-142 Imaging Based AI of the Jemison 3/8 in. Sample

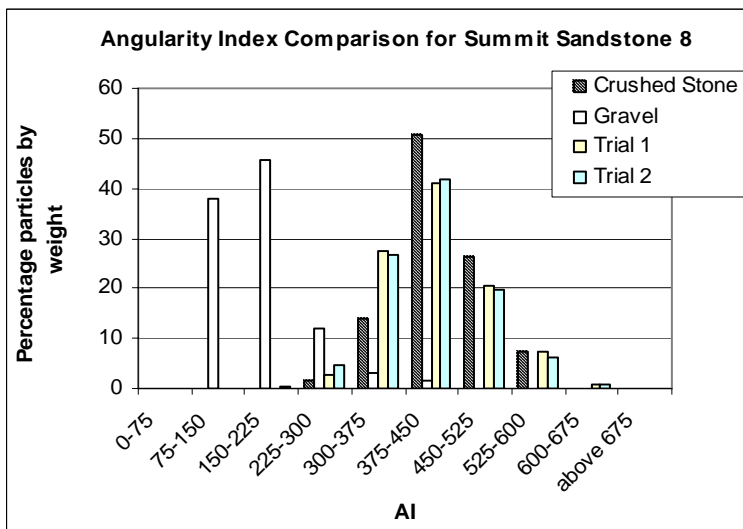


Figure AII-143 Imaging Based AI of the Summit Sandstone 8 Sample

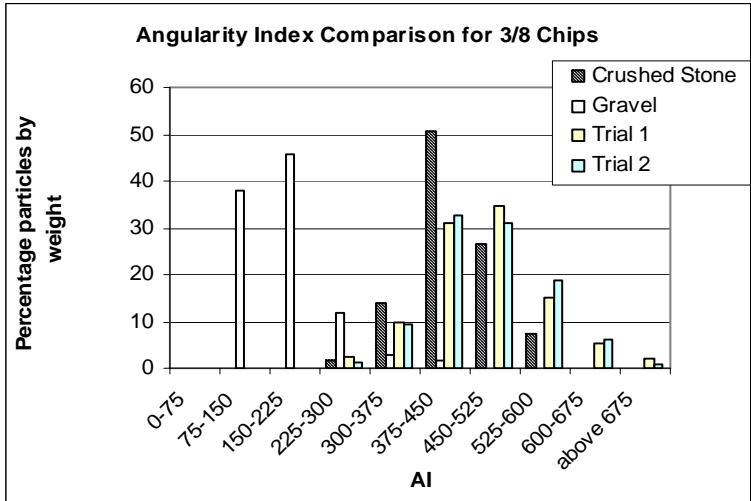


Figure AII-144 Imaging Based AI of the 3/8 in. Chips Sample

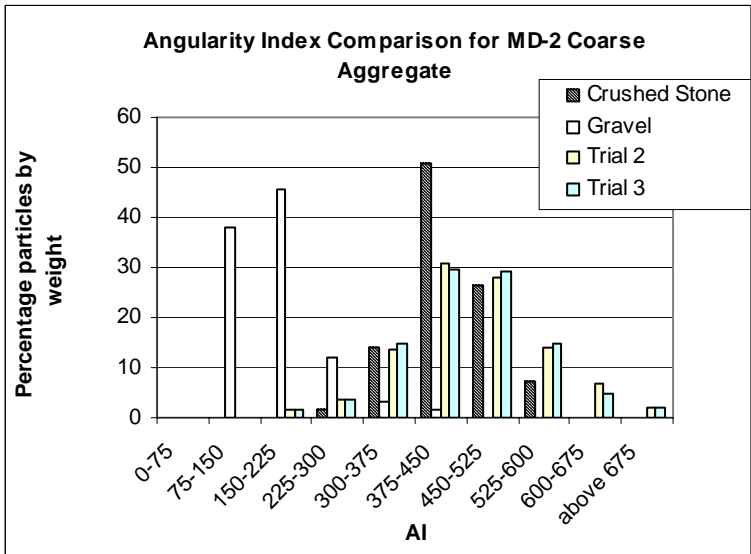


Figure AII-145 Imaging Based AI of the Coarse Aggregate MD-2 Sample

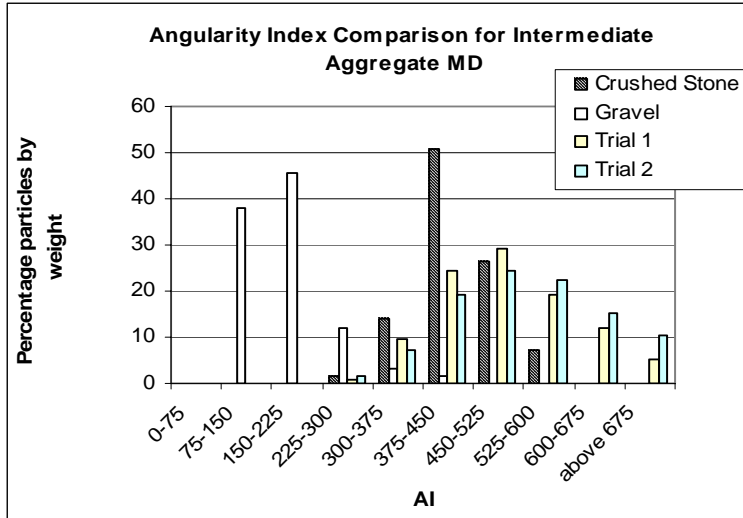


Figure AII-146 Imaging Based AI of the Intermediate Aggregate Sample

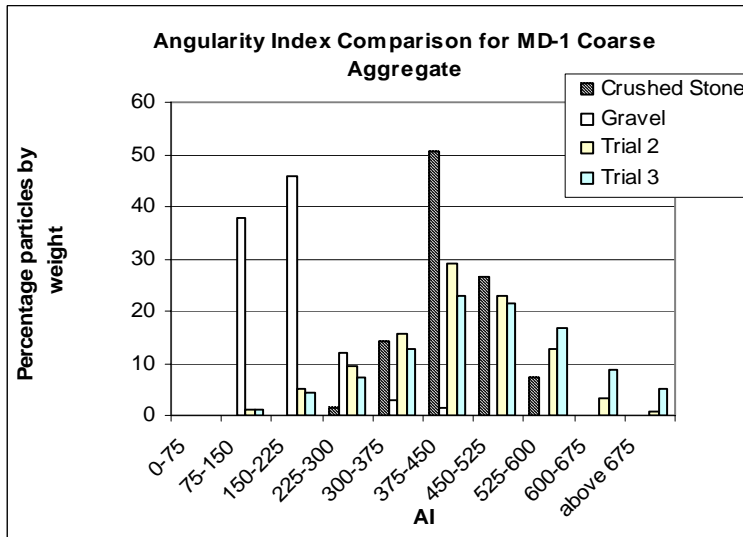


Figure AII-147 Imaging Based AI of the Coarse Aggregate MD-1 Sample

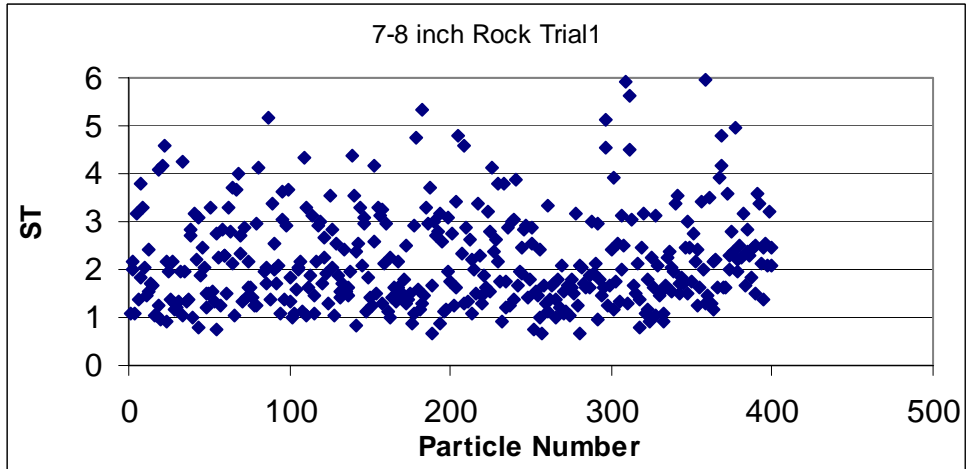


Figure AII-148 (a) Imaging Based ST of the 7/8" Rock Sample-Trial 1

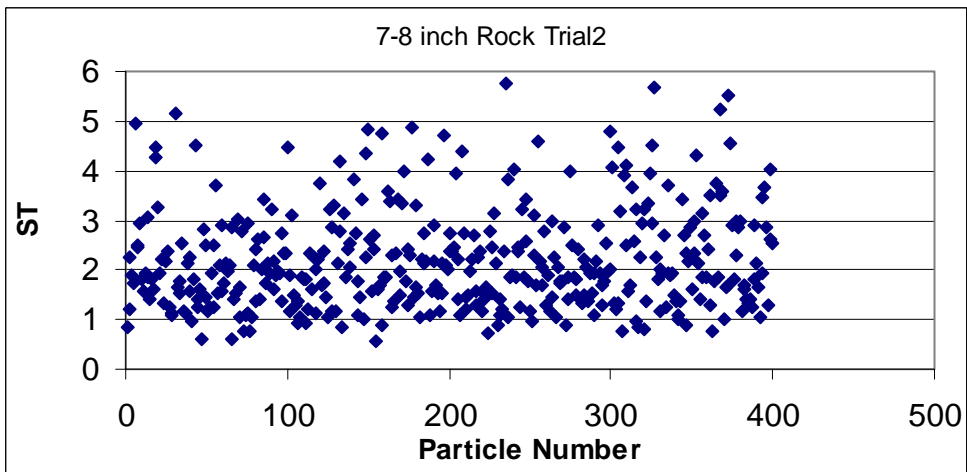


Figure AII-148 (b) Imaging Based ST of the 7/8" Rock Sample-Trial 2

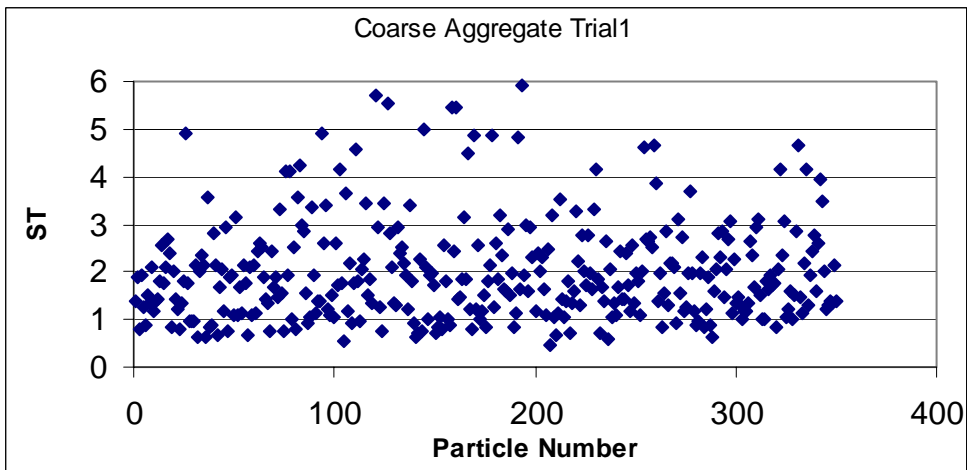


Figure AII-149 (a) Imaging Based ST of the Coarse Aggregate Sample-Trial 1

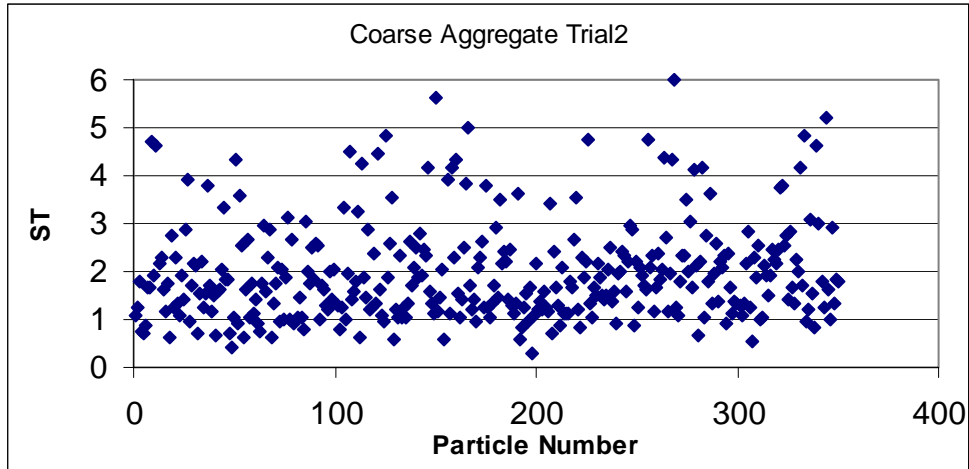


Figure AII-149 (b) Imaging Based ST of the Coarse Aggregate Sample-Trial 2

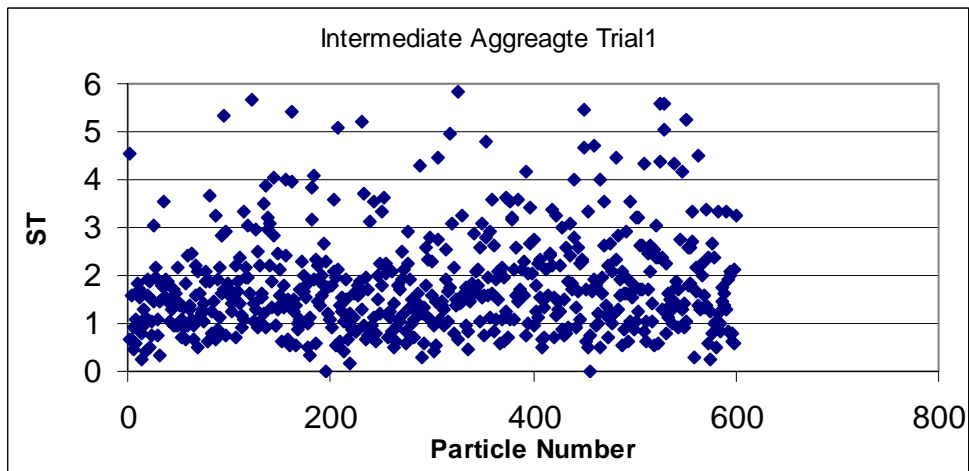


Figure AII-150 (a) Imaging Based ST of the Intermediate Aggregate Sample-Trial 1

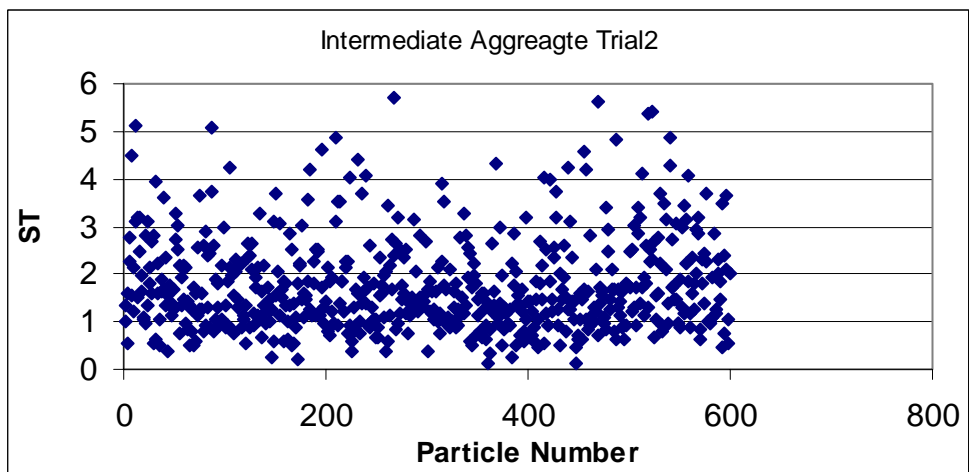


Figure AII-150 (b) Imaging Based ST of the Intermediate Aggregate Sample-Trial 2

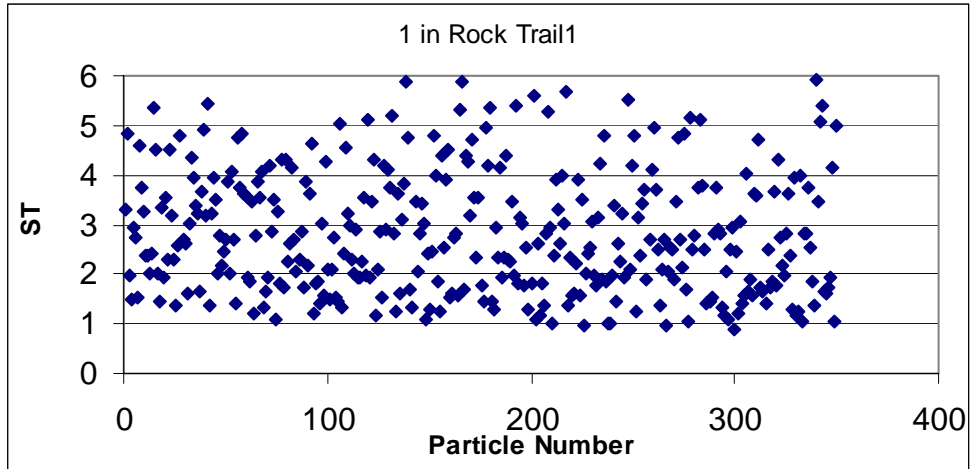


Figure AII-151 (a) Imaging Based ST of the 1" Rock Sample-Trial 1

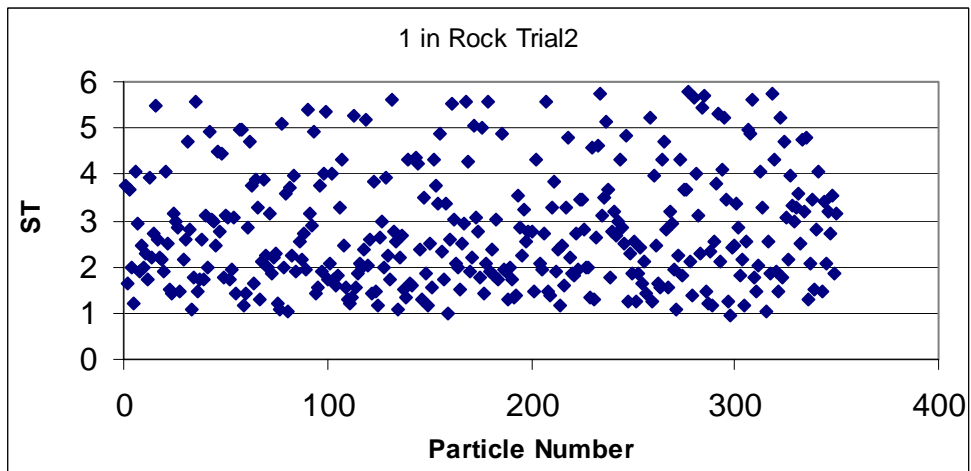


Figure AII-151 (b) Imaging Based ST of the 1" Rock Sample-Trial 2

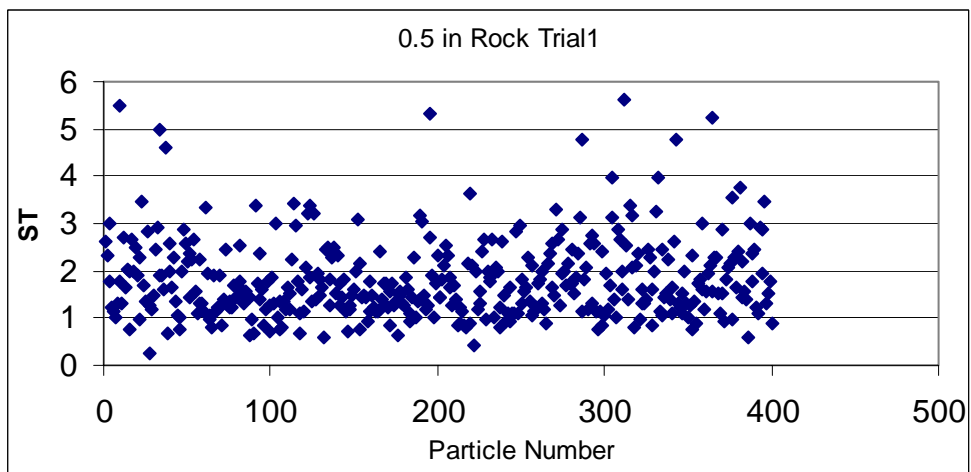


Figure AII-152 (a) Imaging Based ST of the 0.5" Rock Sample-Trial 1

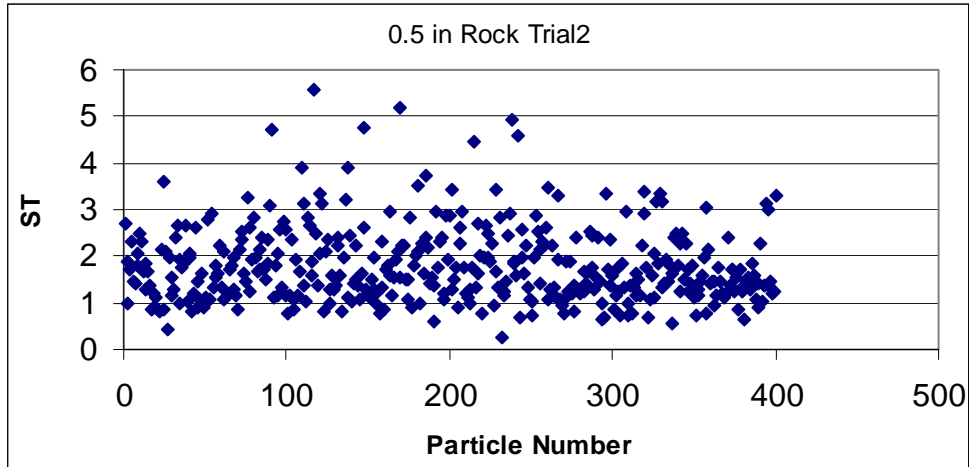


Figure AII-152 (b) Imaging Based ST of the 0.5" Rock Sample-Trial 2

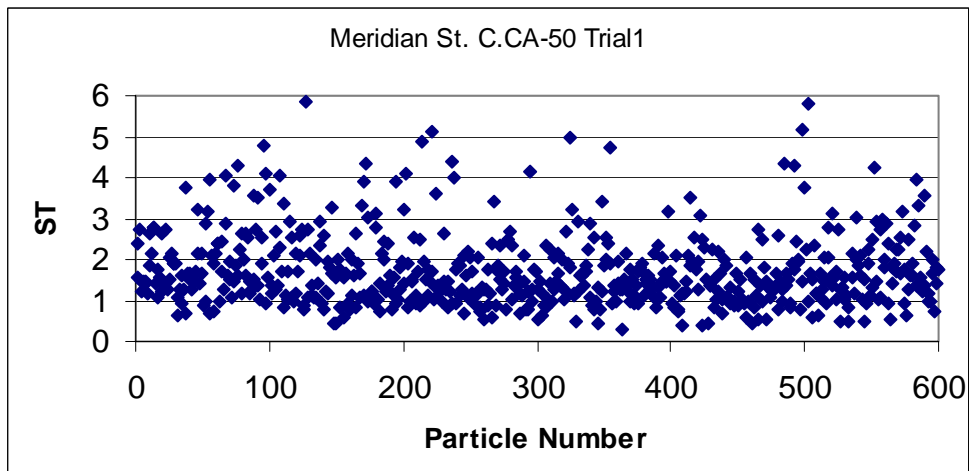


Figure AII-153 (a) Imaging Based ST of the Meridian St.C.CA-50 Sample-Trial 1

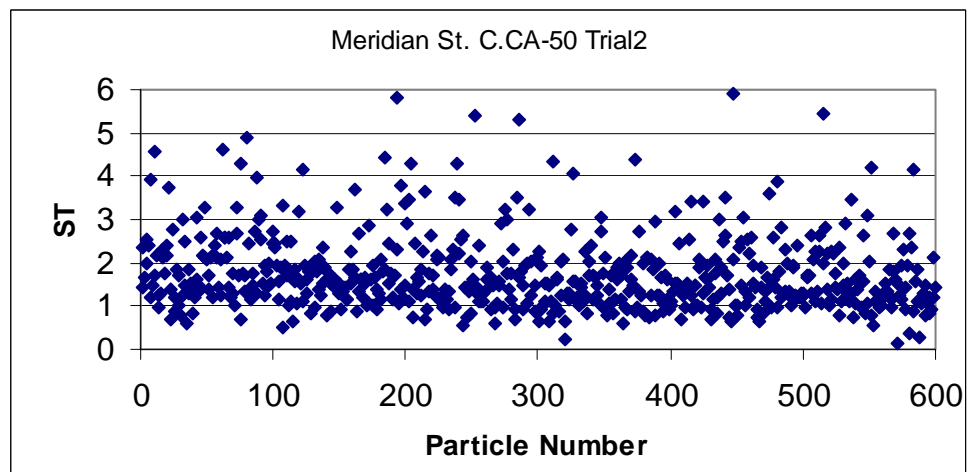


Figure AII-153 (b) Imaging Based ST of the Meridian St.C.CA-50 Sample-Trial 2

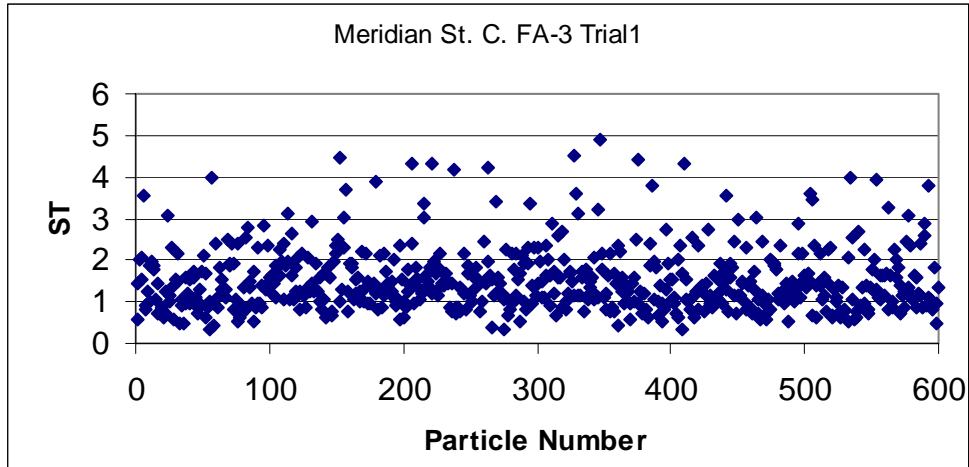


Figure AII-154 (a) Imaging Based ST of the Meridian St.C.FA-3 Sample-Trial 1

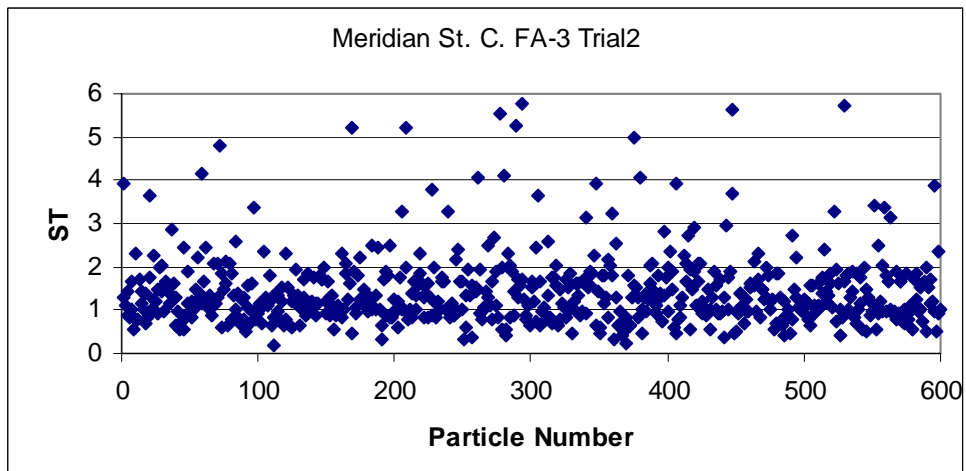


Figure AII-154 (b) Imaging Based ST of the Meridian St.C.FA-3 Sample-Trial 2

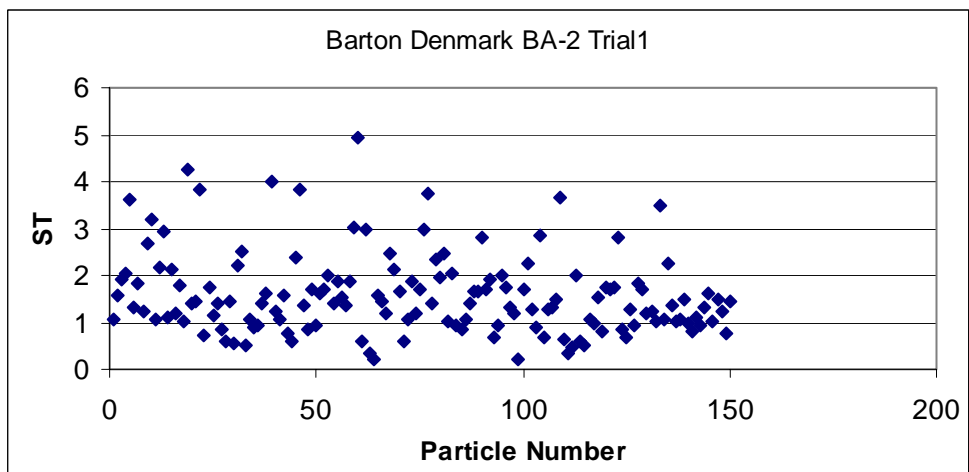


Figure AII-155 (a) Imaging Based ST of the Barton Denmark BA-2 Sample-Trial 1

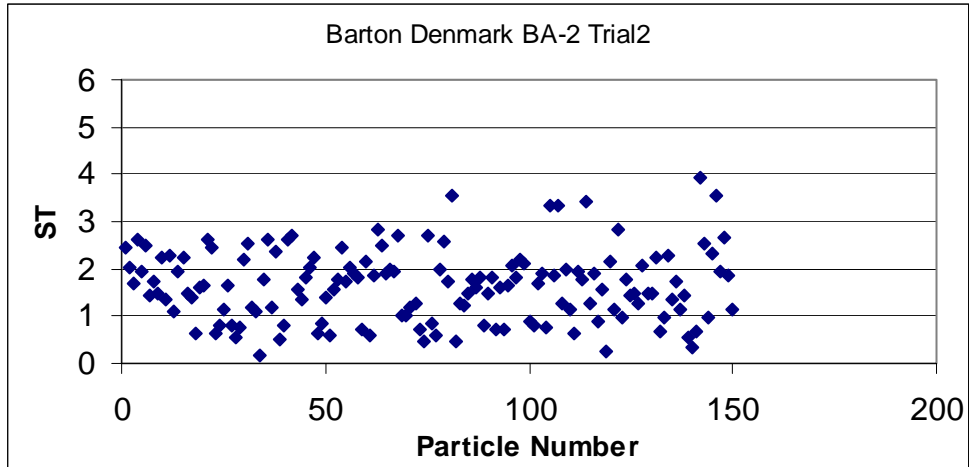


Figure AII-155 (b) Imaging Based ST of the Barton Denmark BA-2 Sample-Trial 2

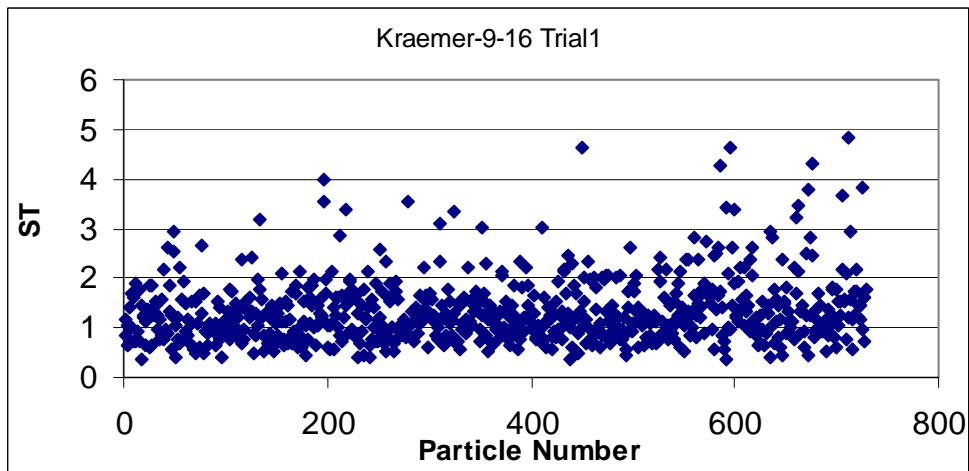


Figure AII-156 (a) Imaging Based ST of the Kraemer Burnsville 9/16" Sample-Trial 1

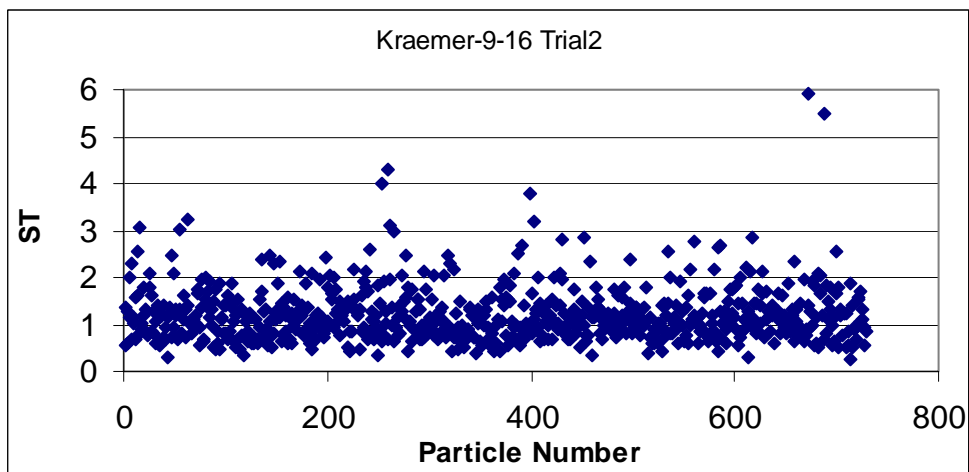


Figure AII-156 (b) Imaging Based ST of the Kraemer Burnsville 9/16" Sample-Trial 2

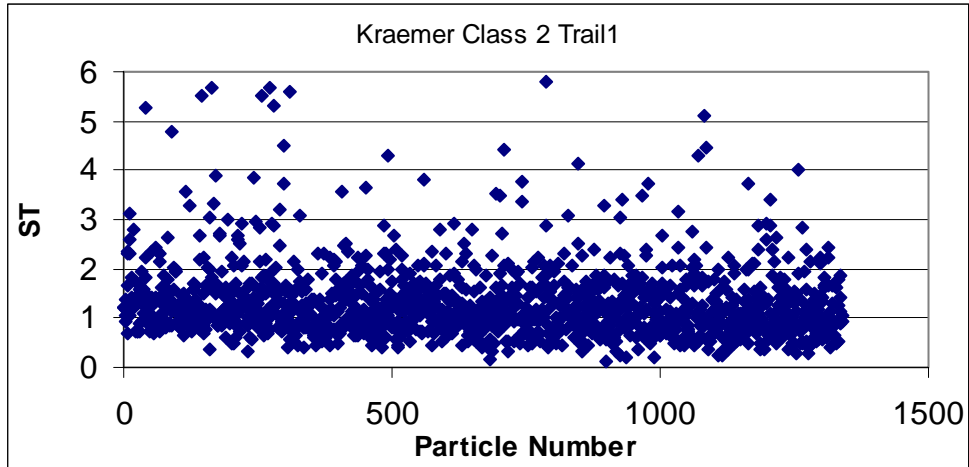


Figure AII-157 (a) Imaging Based ST of the Kraemer Burnsville Class 2 Sample-Trial 1

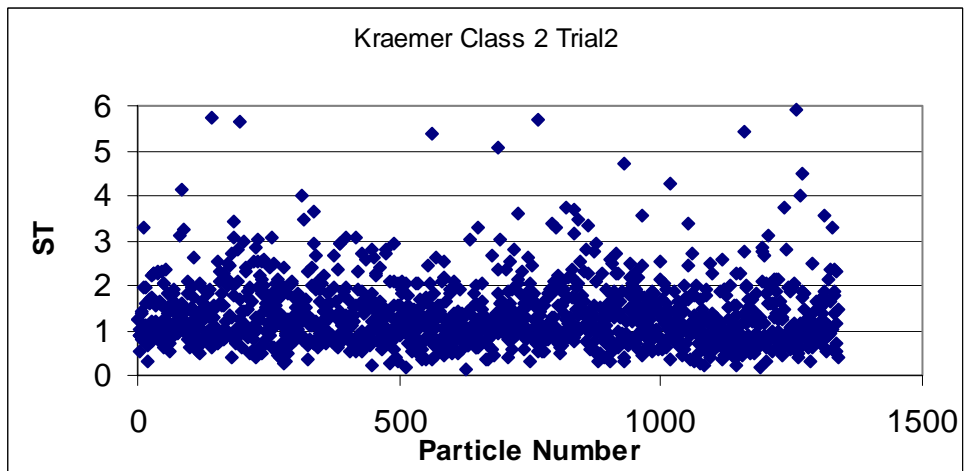


Figure AII-157 (b) Imaging Based ST of the Kraemer Burnsville Class 2 Sample-Trial 2

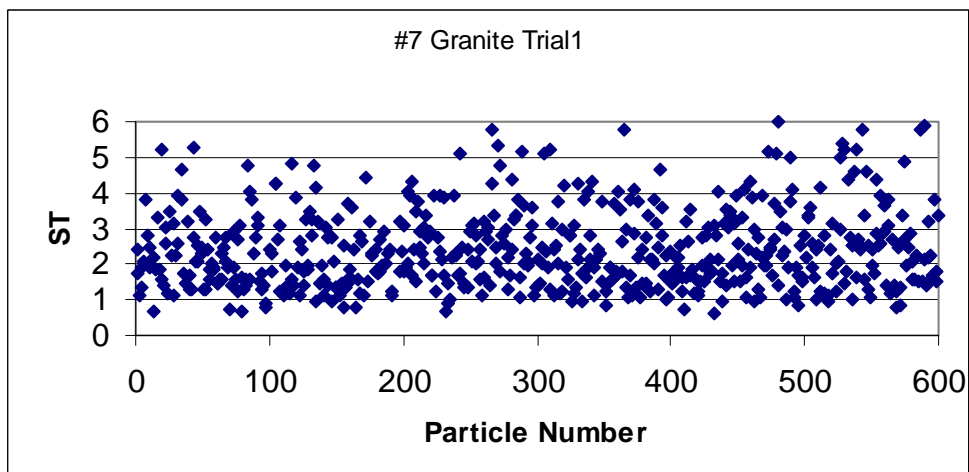


Figure AII-158 (a) Imaging Based ST of the #7 Granite Sample -Trial 1

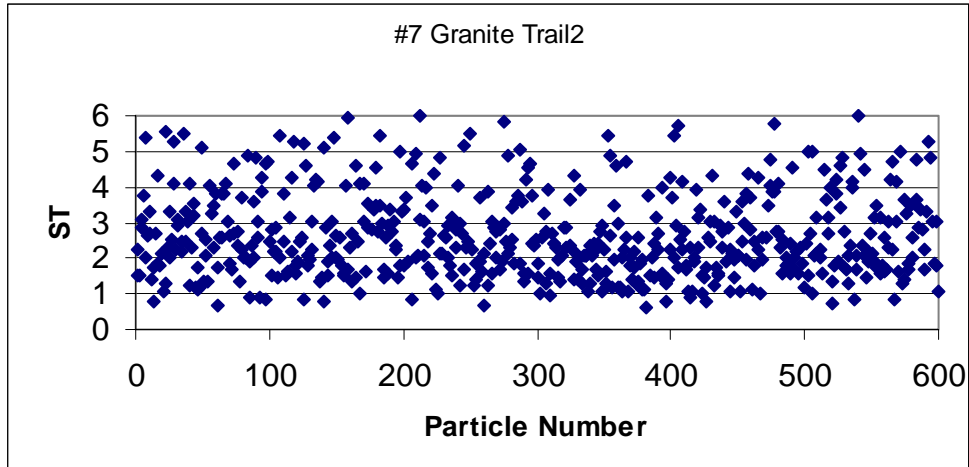


Figure AII-158 (b) Imaging Based ST of the #7 Granite Sample - Trial 2

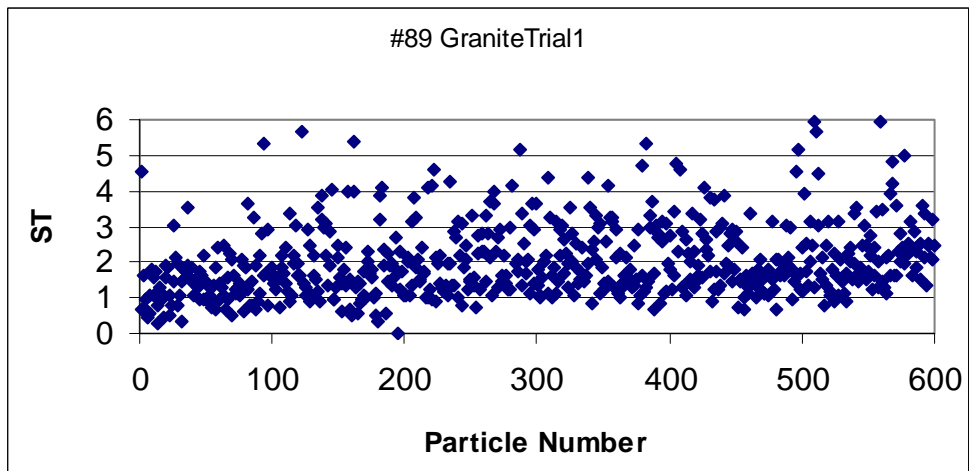


Figure AII-159 (a) Imaging Based ST of the #89 Granite Sample - Trial 1

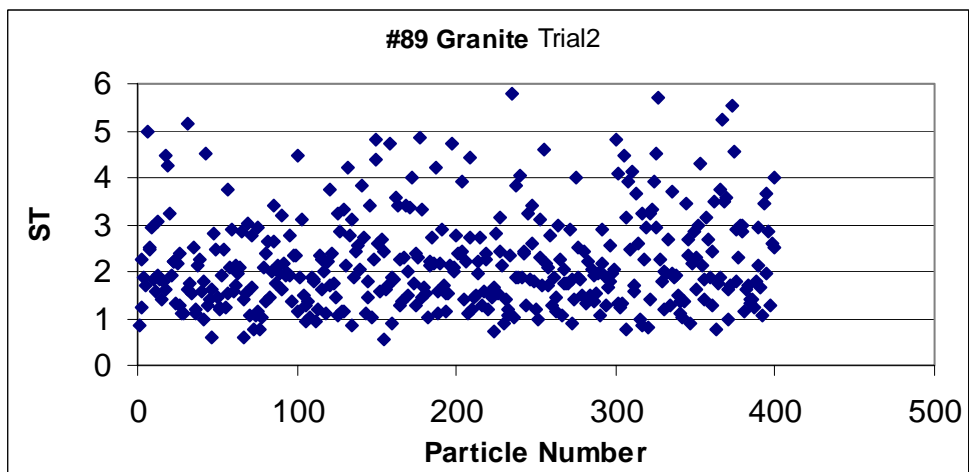


Figure AII-159 (b) Imaging Based ST of the #89 Granite Sample - Trial 2

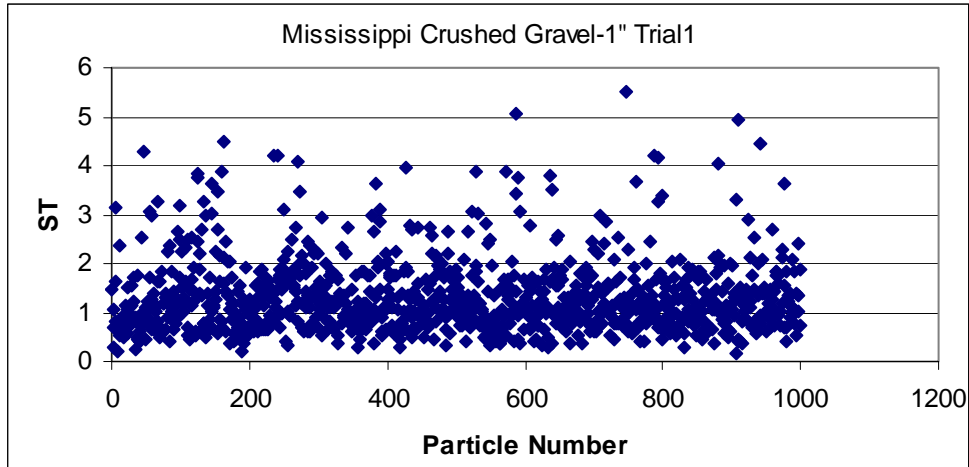


Figure AII-160 (a) Imaging Based ST of the 1" Crushed Gravel Sample - Trial 1

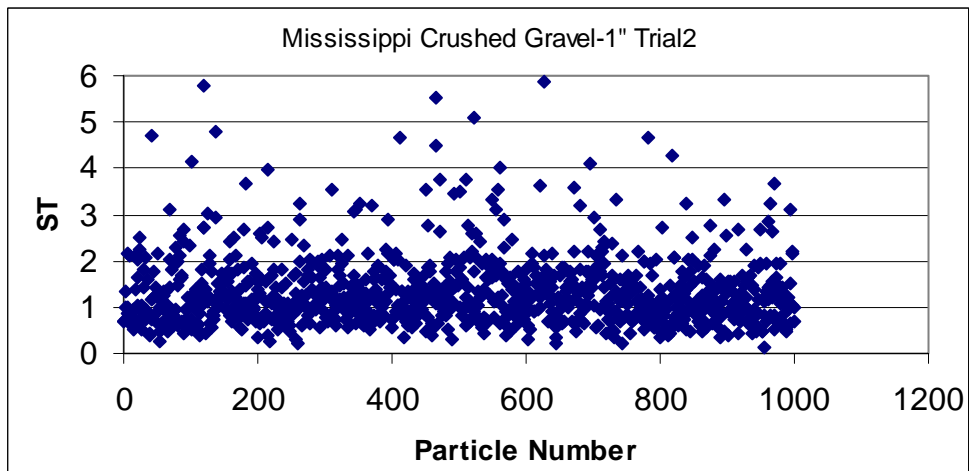


Figure AII-160 (b) Imaging Based ST of the 1" Crushed Gravel Sample - Trial 2

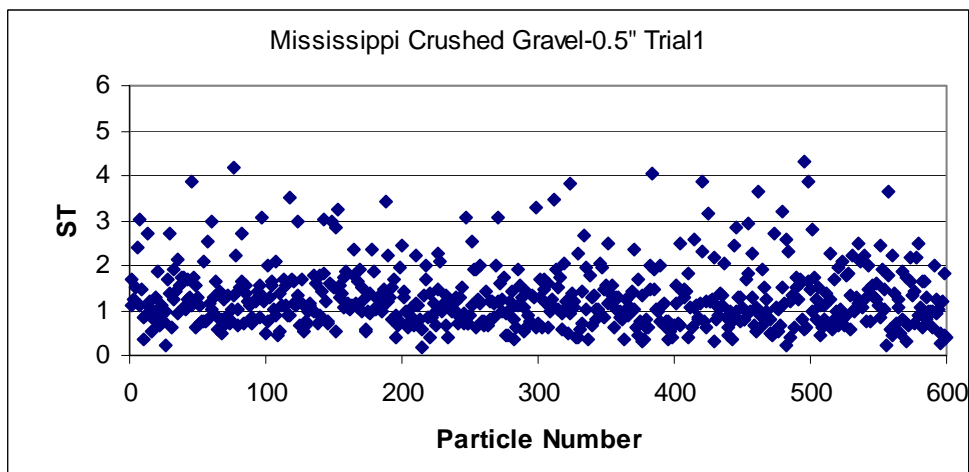


Figure AII-161 (a) Imaging Based ST of the 0.5" Crushed Gravel Sample - Trial 1

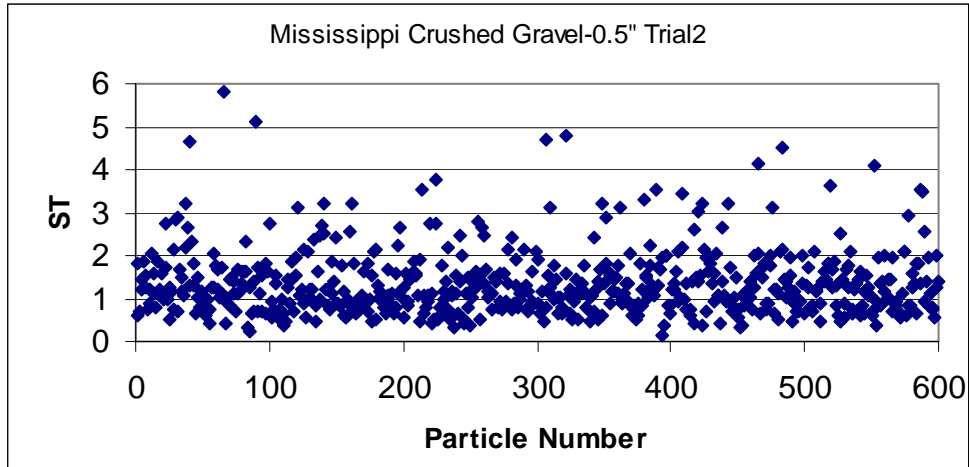


Figure AII-161 (b) Imaging Based ST of the 0.5" Crushed Gravel Sample - Trial 2

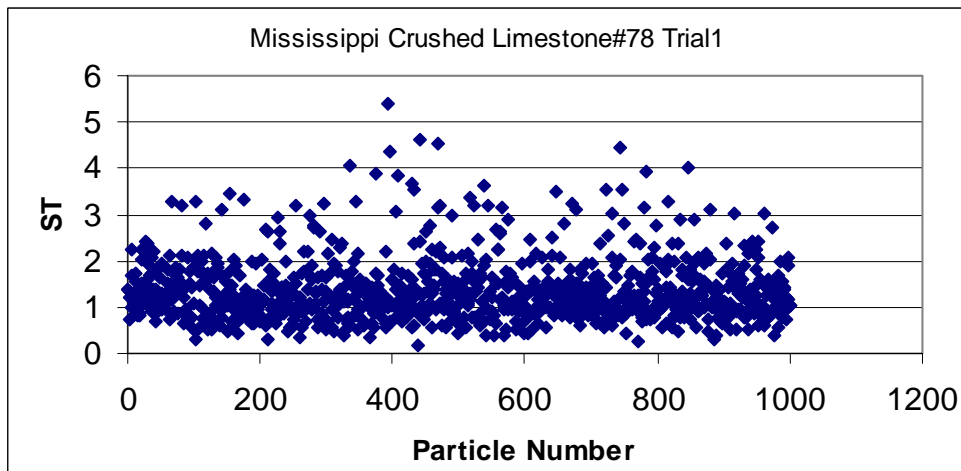


Figure AII-162 (a) Imaging Based ST of the #78 Crushed Limestone Sample - Trial 1

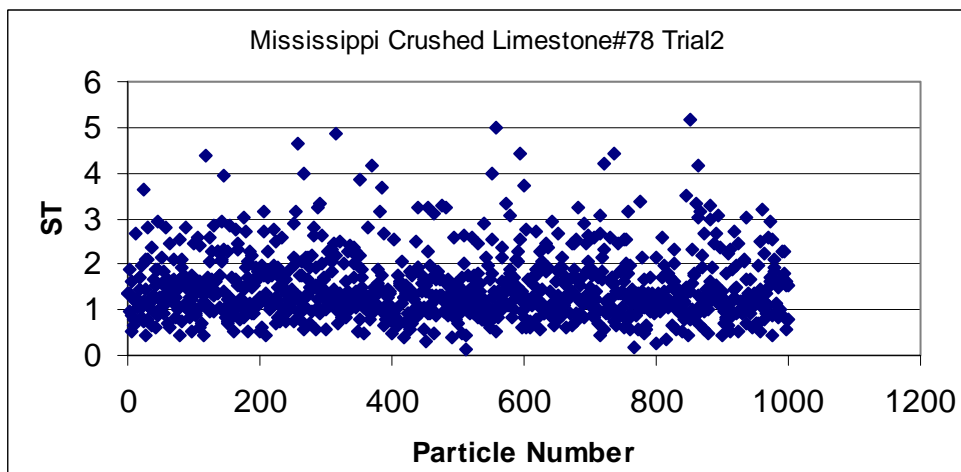


Figure AII-162 (b) Imaging Based ST of the #78 Crushed Limestone Sample - Trial 2

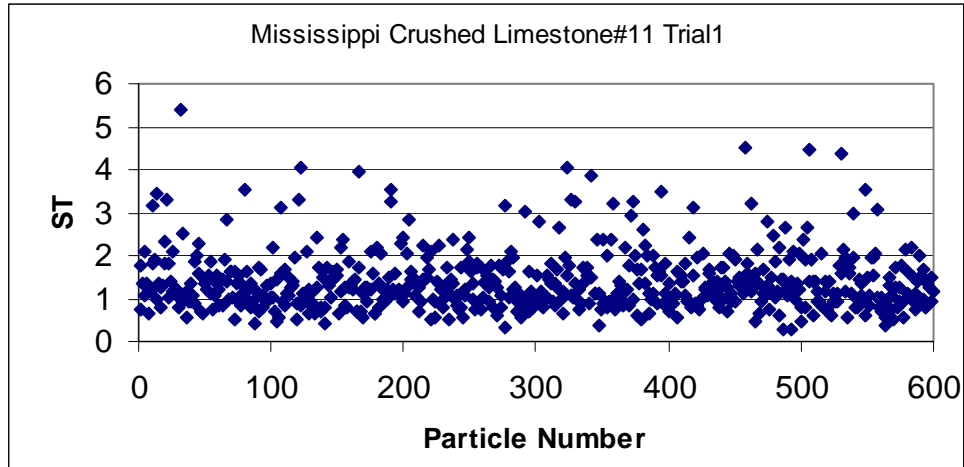


Figure AII-163 (a) Imaging Based ST of the #11 Crushed Limestone Sample - Trial 1

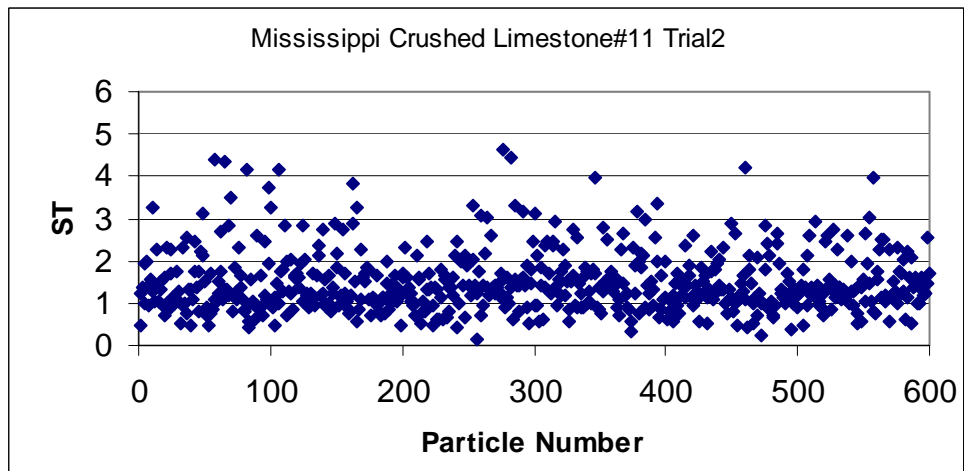


Figure AII-163 (b) Imaging Based ST of the #11 Crushed Limestone Sample - Trial 2

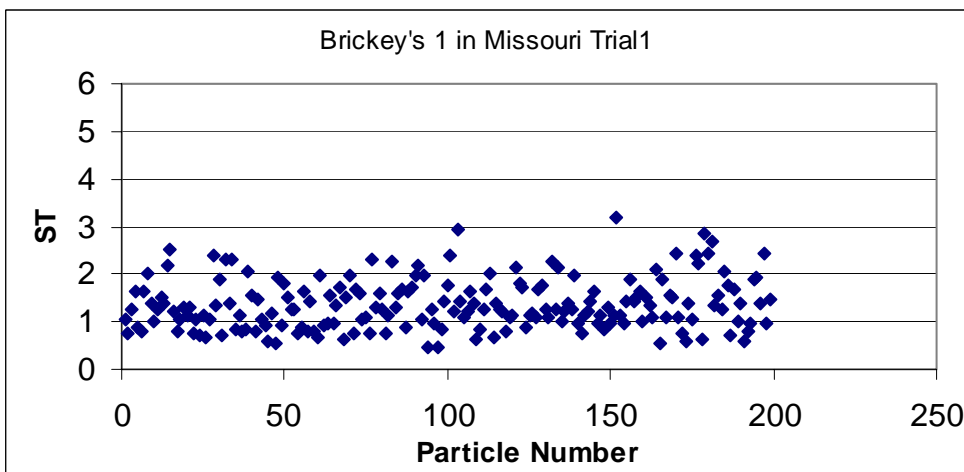


Figure AII-164 (a) Imaging Based ST of the Brickey's 1 in. Sample - Trial 1

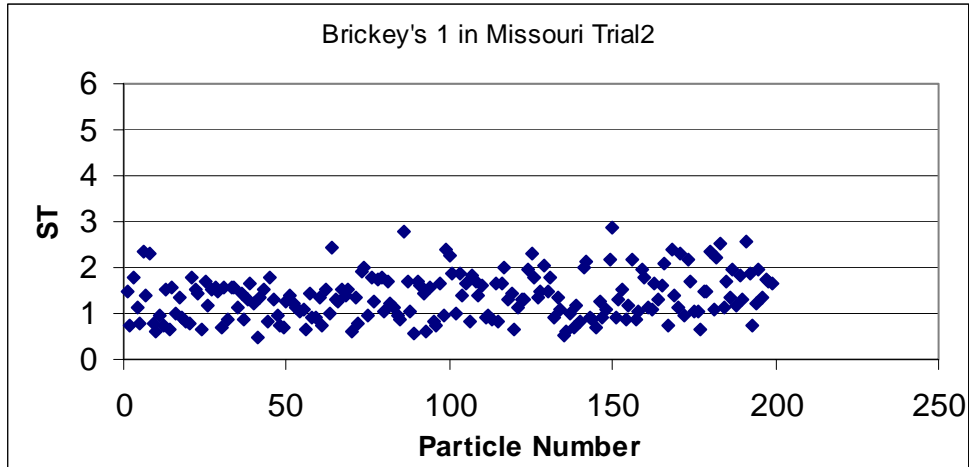


Figure AII-164 (b) Imaging Based ST of the Brickey's 1 in. Sample - Trial 2

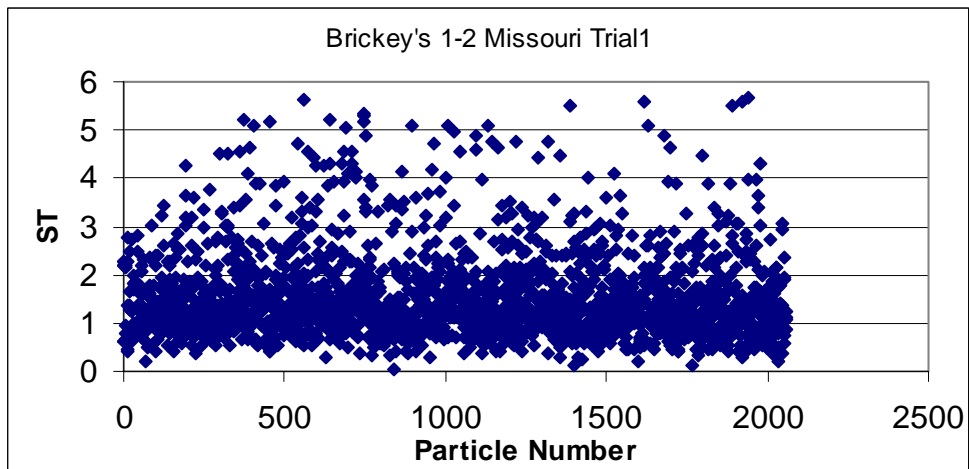


Figure AII-165 (a) Imaging Based ST of the Brickey's 1/2 in. Sample - Trial 1

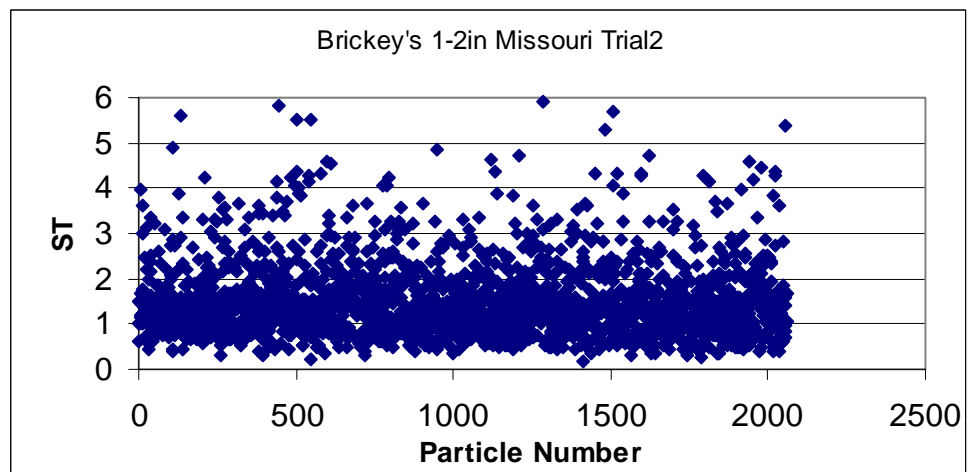


Figure AII-165 (b) Imaging Based ST of the Brickey's 1/2 in. Sample - Trial 2

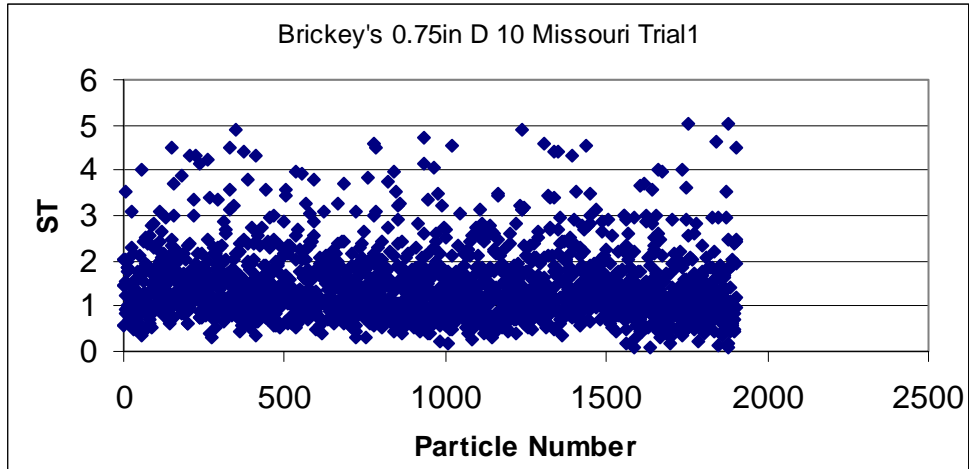


Figure AII-166 (a) Imaging Based ST of the Brickey's 3/4 in. Sample - Trial 1

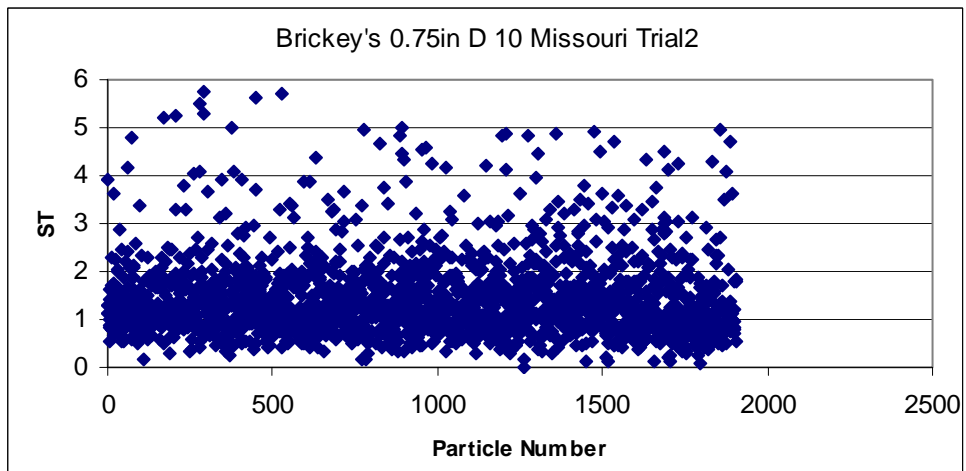


Figure AII-166 (b) Imaging Based ST of the Brickey's 3/4 in. Sample - Trial 2

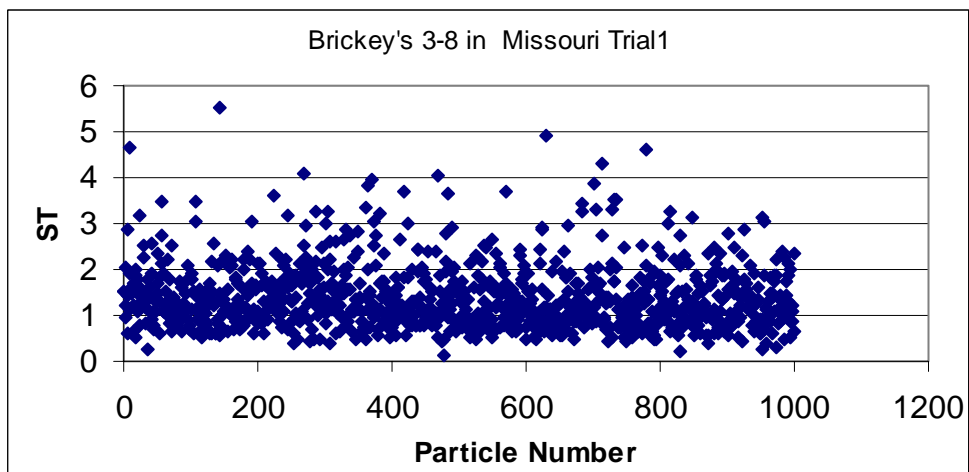


Figure AII-167 (a) Imaging Based ST of the Brickey's 3/8 in. Sample - Trial 1

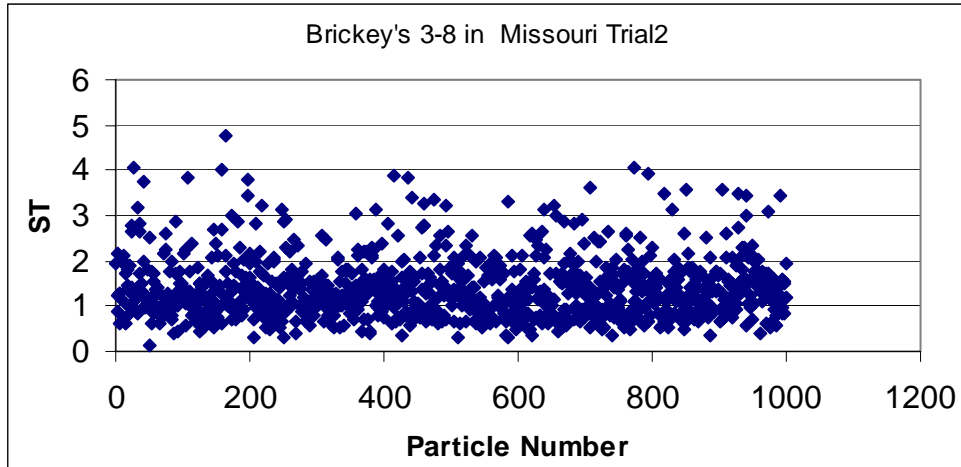


Figure AII-167 (b) Imaging Based ST of the Brickey's 3/8 in. Sample - Trial 2

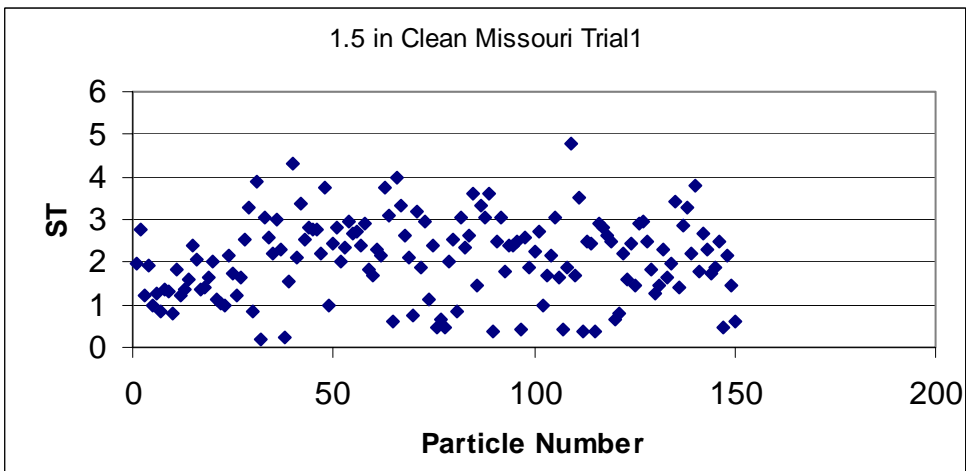


Figure AII-168 (a) Imaging Based ST of the 1.5 in. Clean Sample - Trial 1

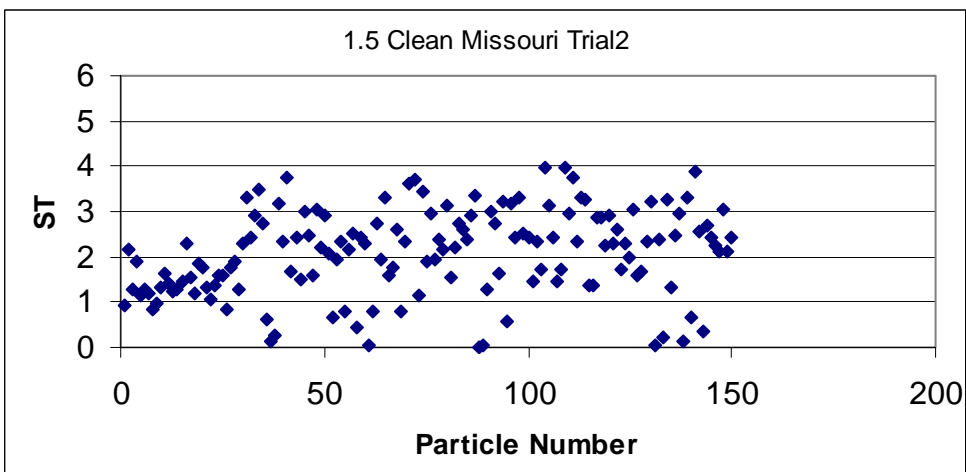


Figure AII-168 (b) Imaging Based ST of the 1.5 in. Clean Sample - Trial 2

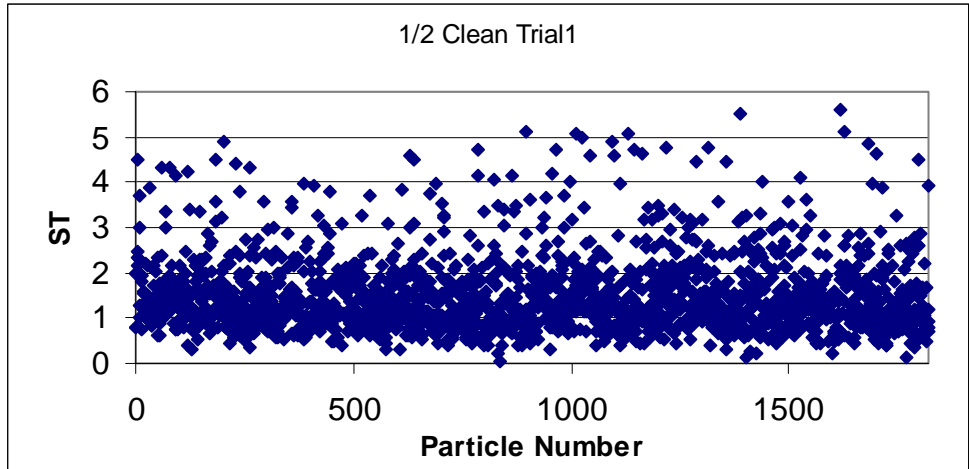


Figure AII-169 (a) Imaging Based ST of the 0.5 in. Clean Sample - Trial 1

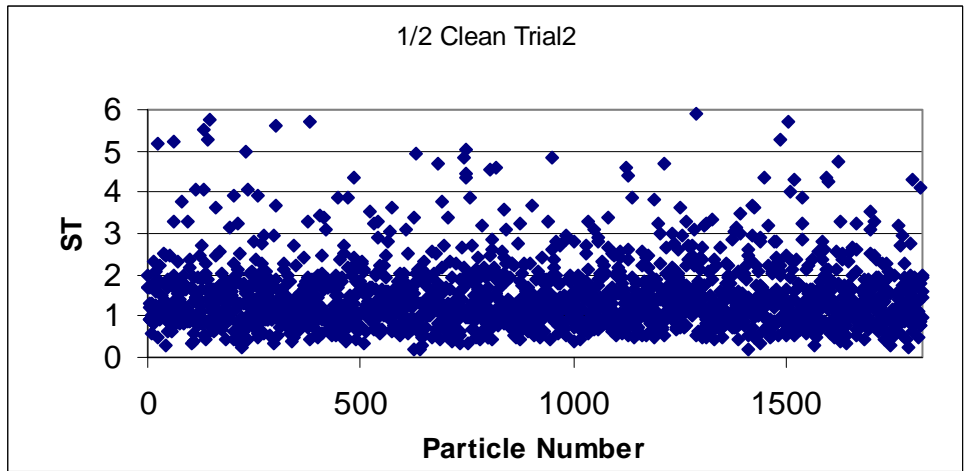


Figure AII-169 (b) Imaging Based ST of the 0.5 in. Clean Sample - Trial 2

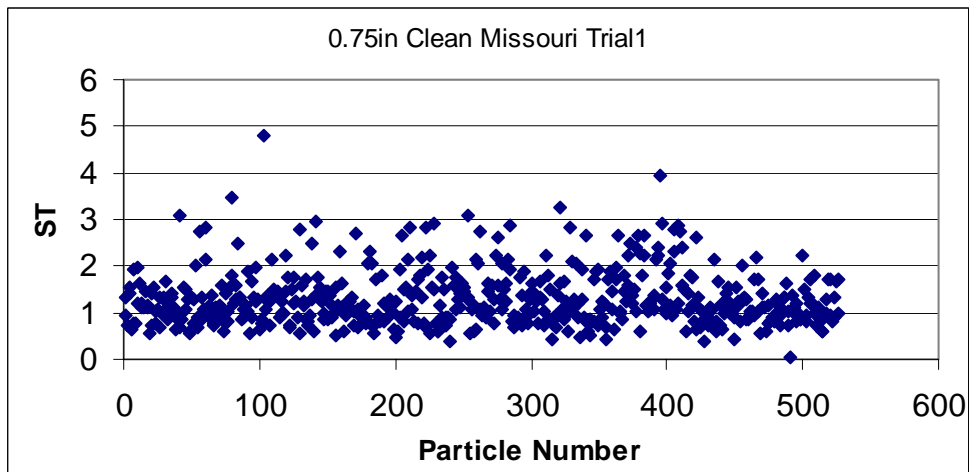


Figure AII-170 (a) Imaging Based ST of the 3/4 in. Clean Sample - Trial 1

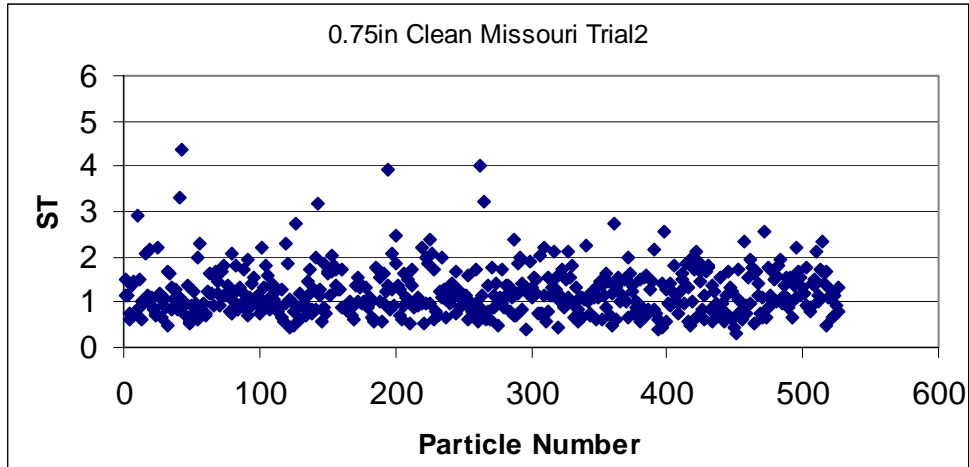


Figure AII-170 (b) Imaging Based ST of the 3/4 in. Clean Sample - Trial 2

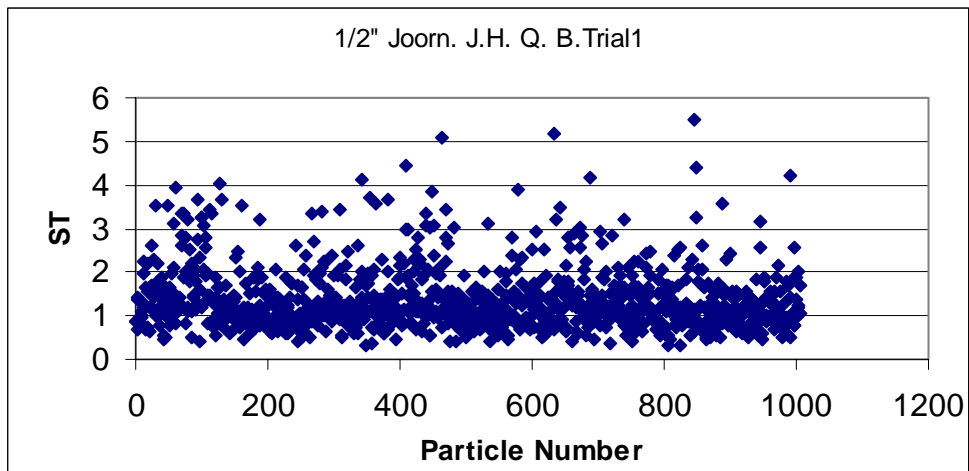


Figure AII-171 (a) Imaging Based ST of the 1/2 in. Joornagan J.H.Q. Burl Sample - Trial 1

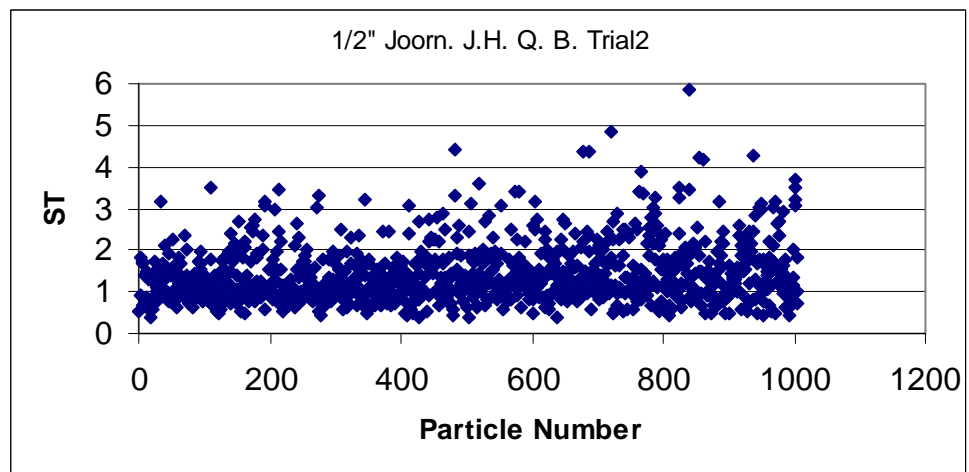


Figure AII-171 (b) Imaging Based ST of the 1/2 in. Joornagan J.H.Q. Burl Sample - Trial 2

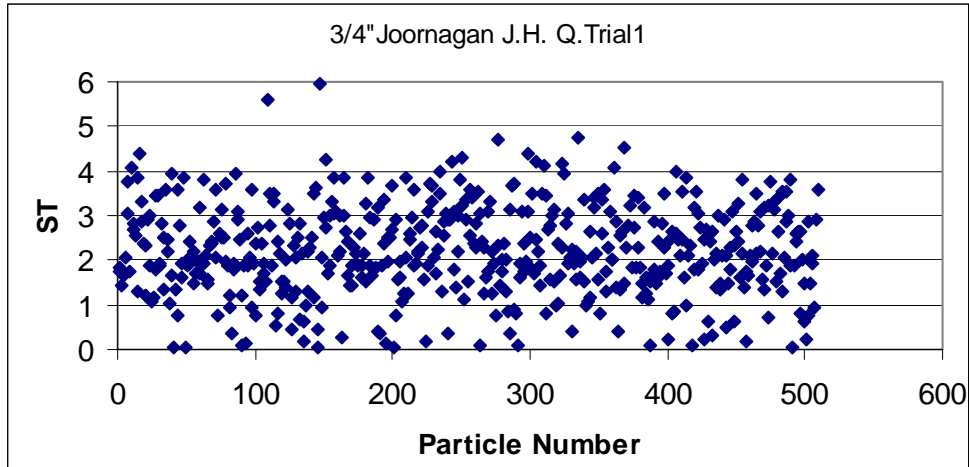


Figure AII-172 (a) Imaging Based ST of the 3/4 in. Joornagan J.H.Q. Sample - Trial 1

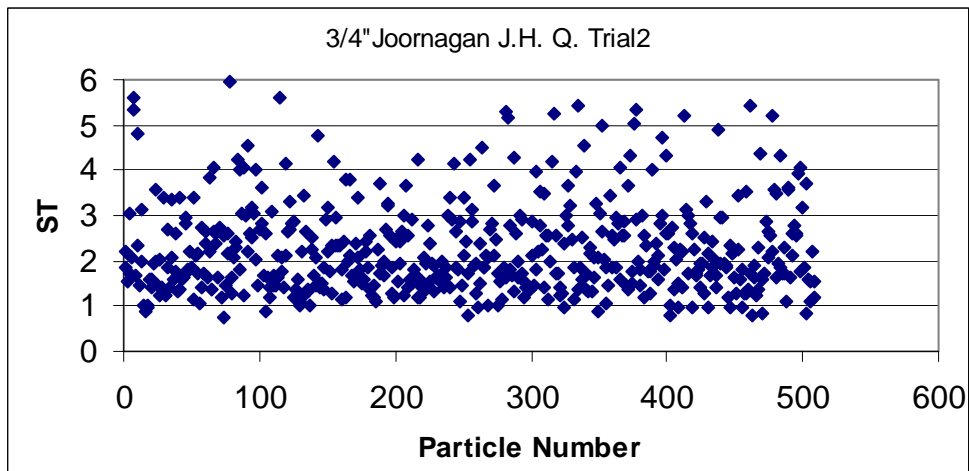


Figure AII-172 (b) Imaging Based ST of the 3/4 in. Joornagan J.H.Q. Sample - Trial 2

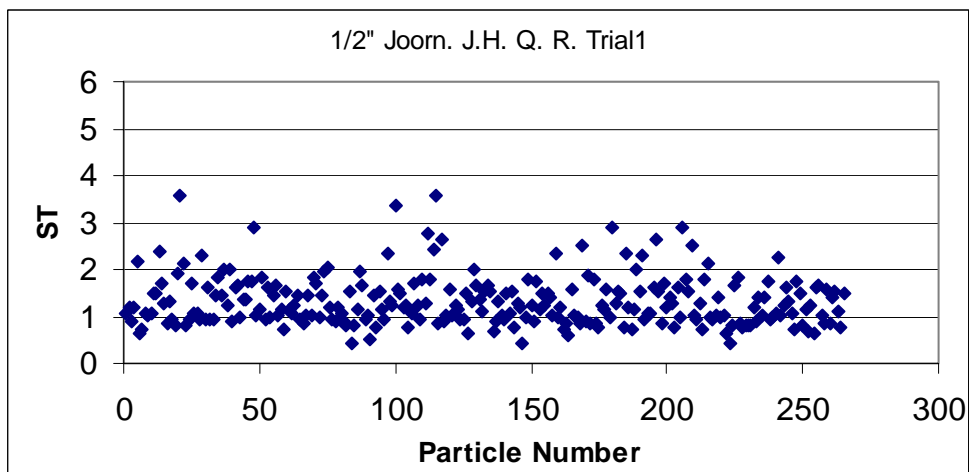


Figure AII-173 (a) Imaging Based ST of the 1/2 in. Joornagan J.H.Q. R. Sample - Trial 1

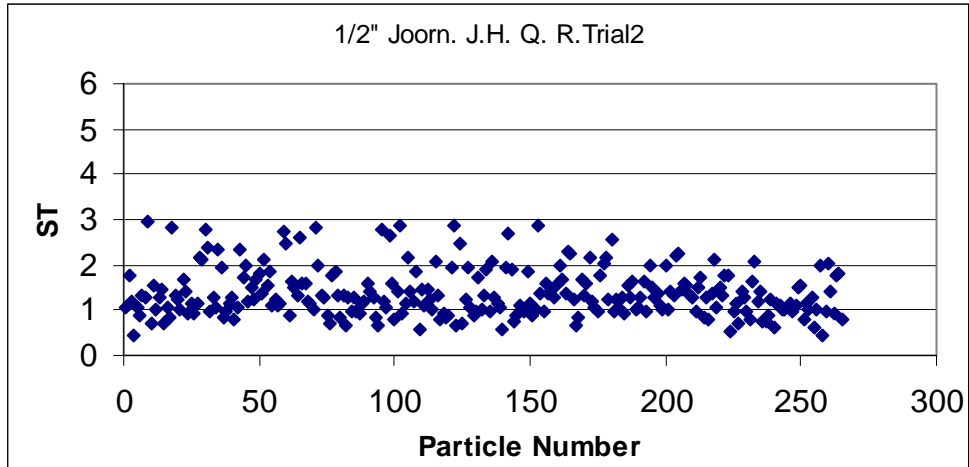


Figure AII-173 (b) Imaging Based ST of the 1/2 in. Joonagan J.H.Q. R. Sample - Trial 2

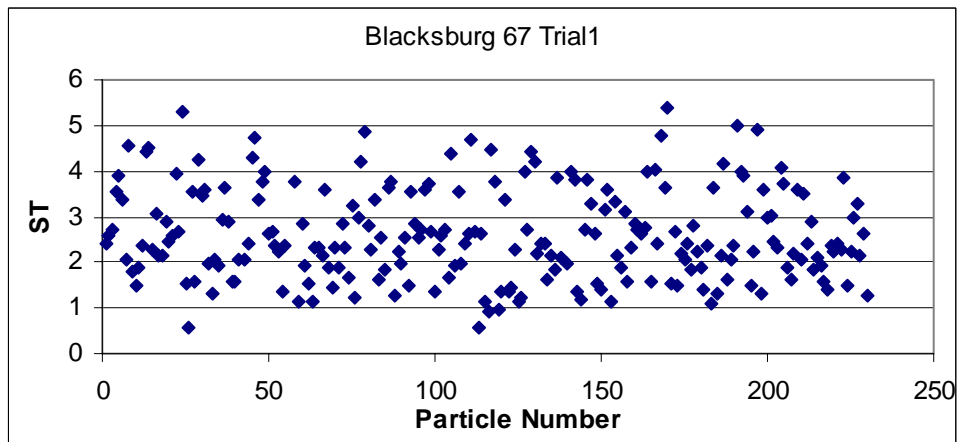


Figure AII-174 (a) Imaging Based ST of the Blacksburg 67 Sample - Trial 1

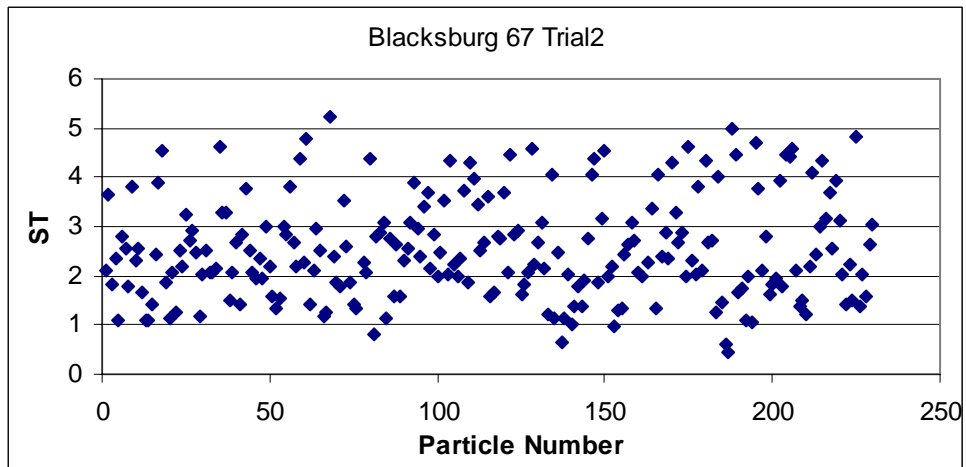


Figure AII-174 (b) Imaging Based ST of the Blacksburg 67 Sample - Trial 2

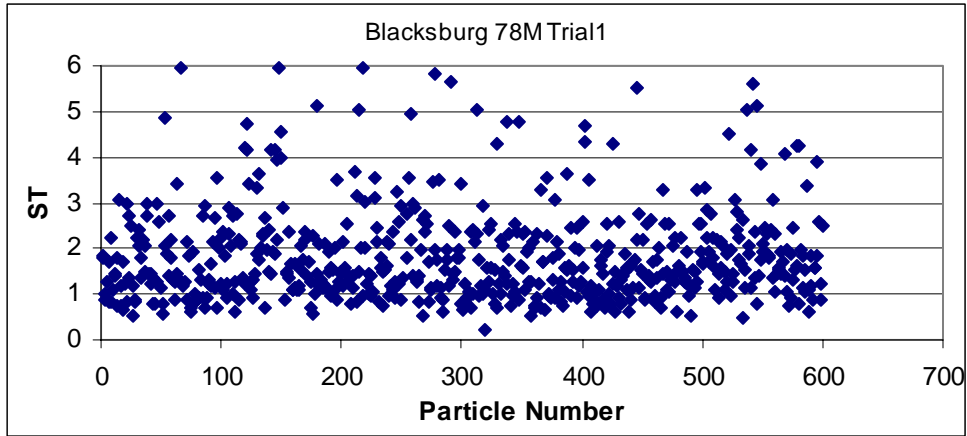


Figure AII-175 (a) Imaging Based ST of the Blacksburg 78M Sample - Trial 1

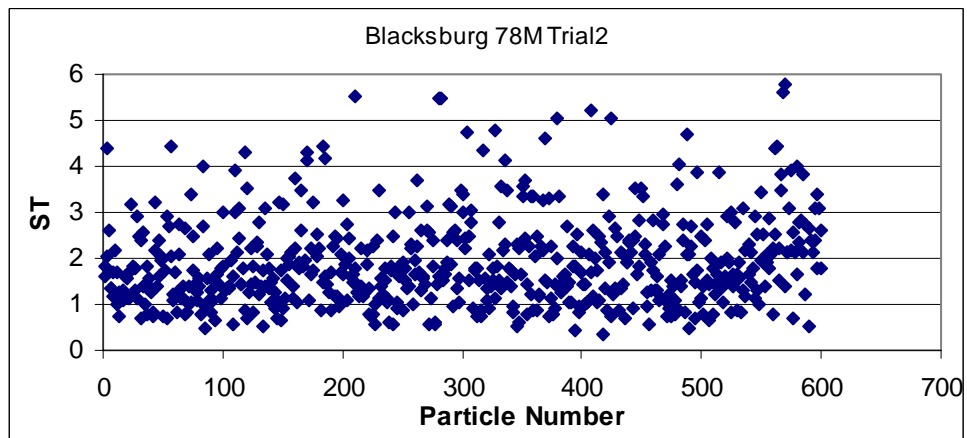


Figure AII-175 (b) Imaging Based ST of the Blacksburg 78M Sample - Trial 2

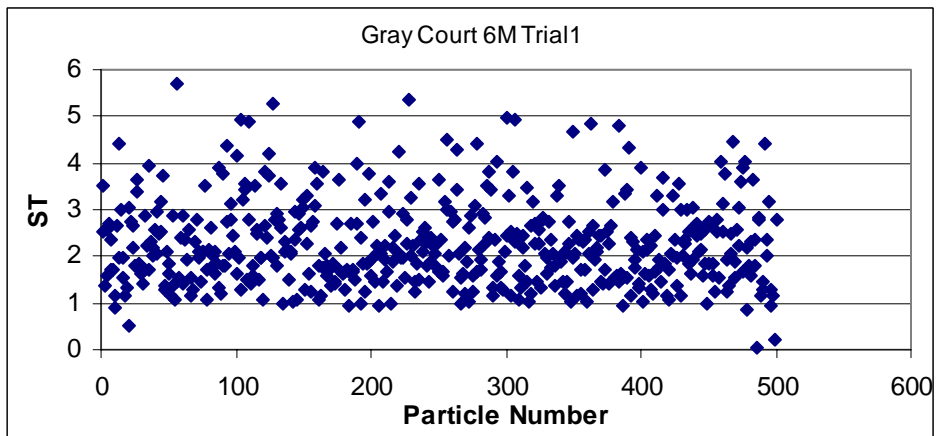


Figure AII-176 (a) Imaging Based ST of the Gray Court 6M Sample - Trial 1

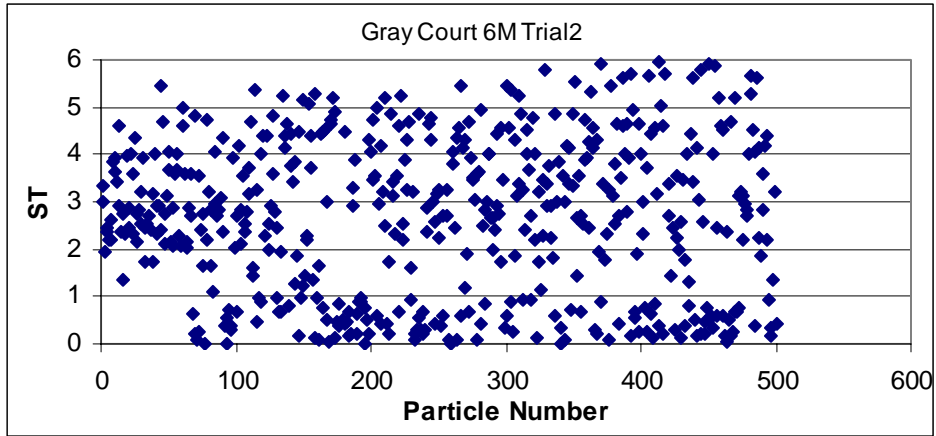


Figure AII-176 (b) Imaging Based ST of the Gray Court 6M Sample - Trial 2

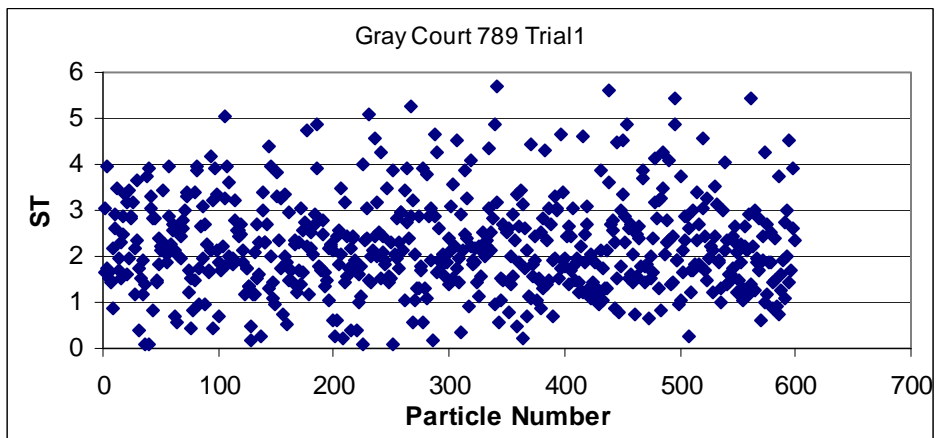


Figure AII-177 (a) Imaging Based ST of the Gray Court 789 Sample - Trial 1

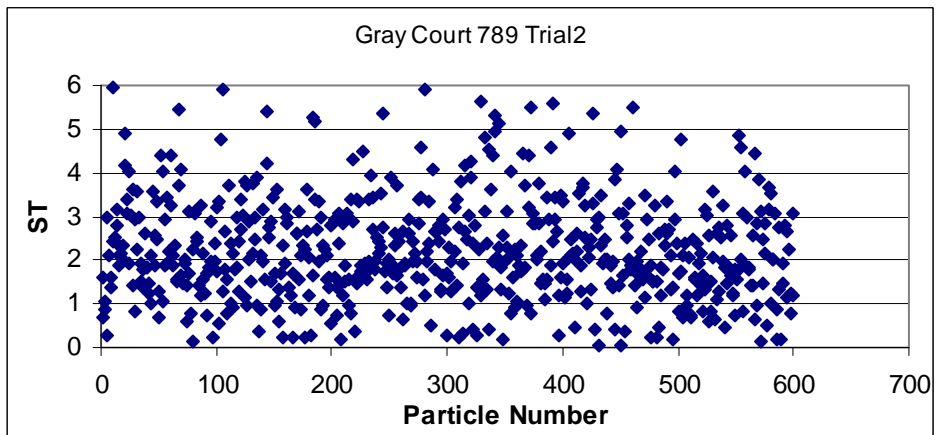


Figure AII-177 (b) Imaging Based ST of the Gray Court 789 Sample - Trial 2

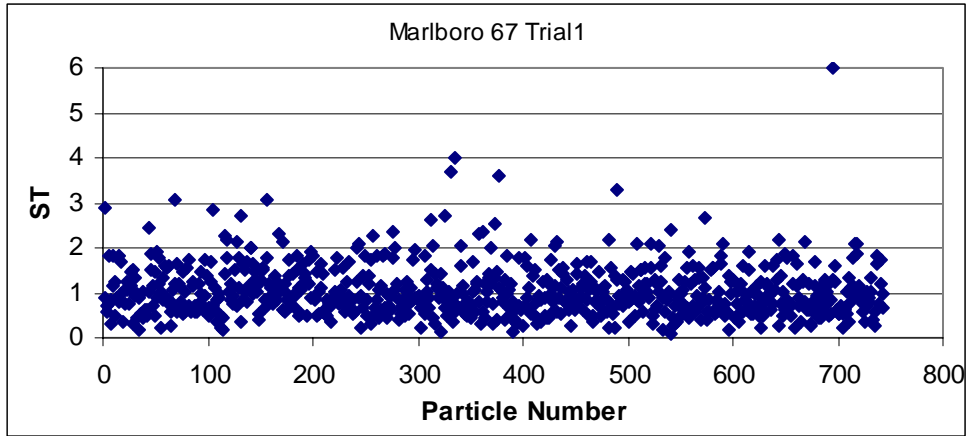


Figure AII-178 (a) Imaging Based ST of the Marlboro 67 Sample - Trial 1

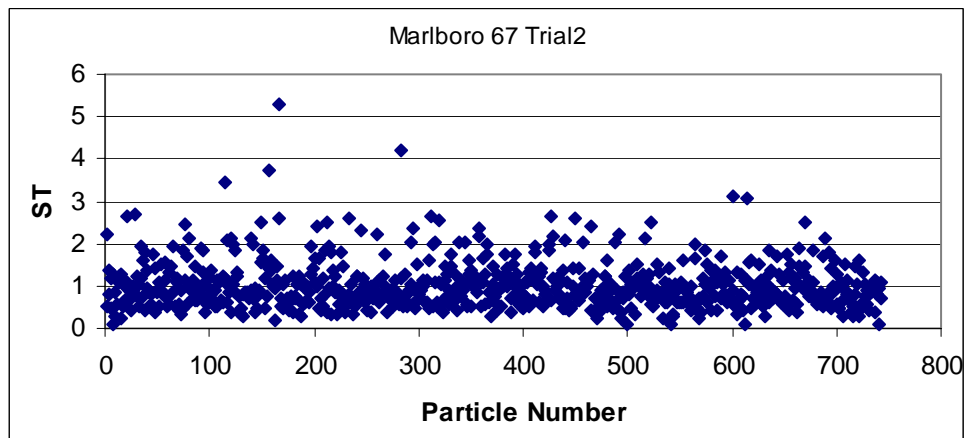


Figure AII-178 (b) Imaging Based ST of the Marlboro 67 Sample - Trial 2

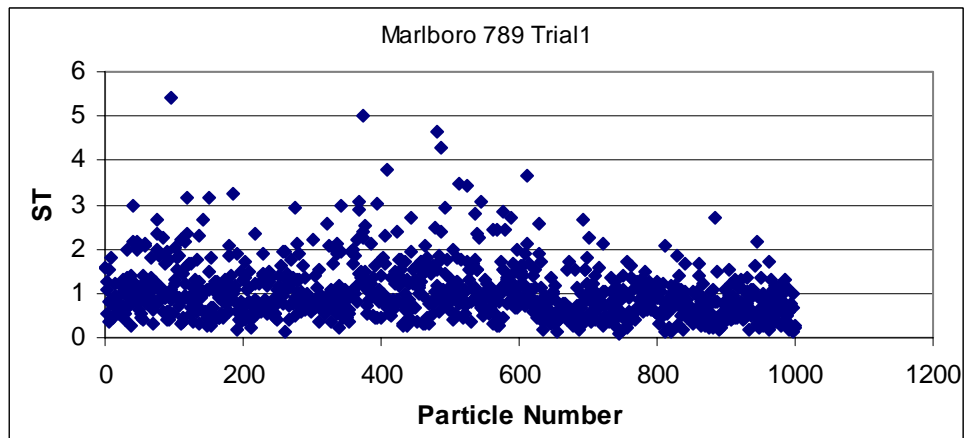


Figure AII-179 (a) Imaging Based ST of the Marlboro 789 Sample - Trial 1

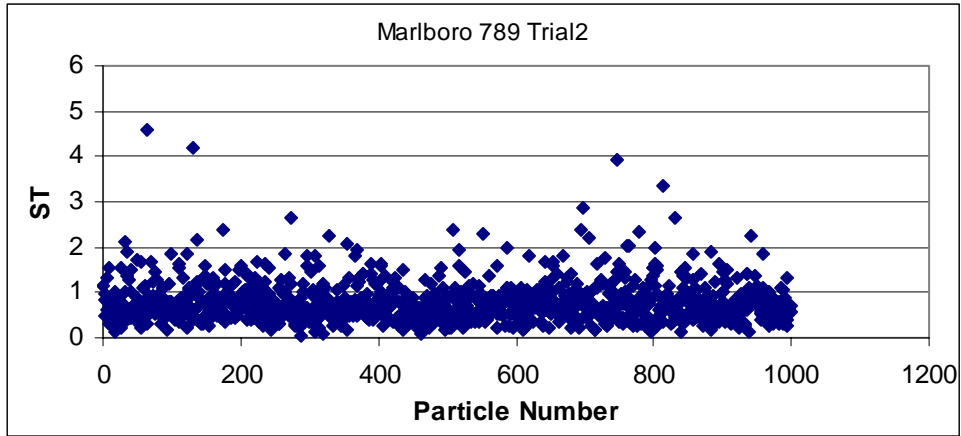


Figure AII-179 (b) Imaging Based ST of the Marlboro 789 Sample - Trial 2

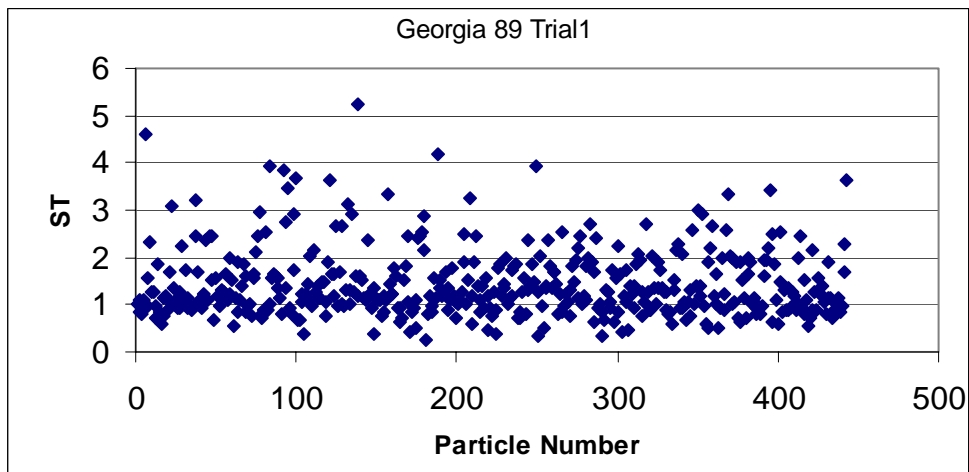


Figure AII-180 (a) Imaging Based ST of the Georgia 89 Sample - Trial 1

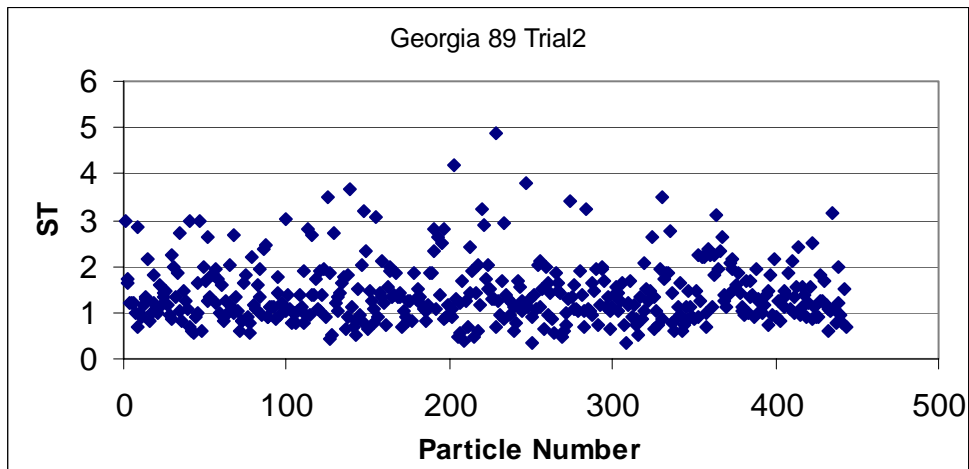


Figure AII-180 (b) Imaging Based ST of the Georgia 89 Sample - Trial 2

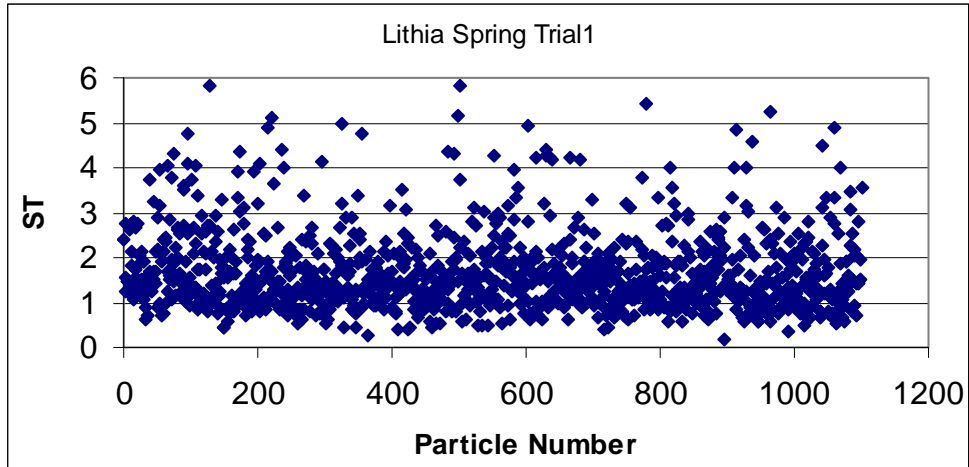


Figure AII-181 (a) Imaging Based ST of the Lithia Springs Sample - Trial 1

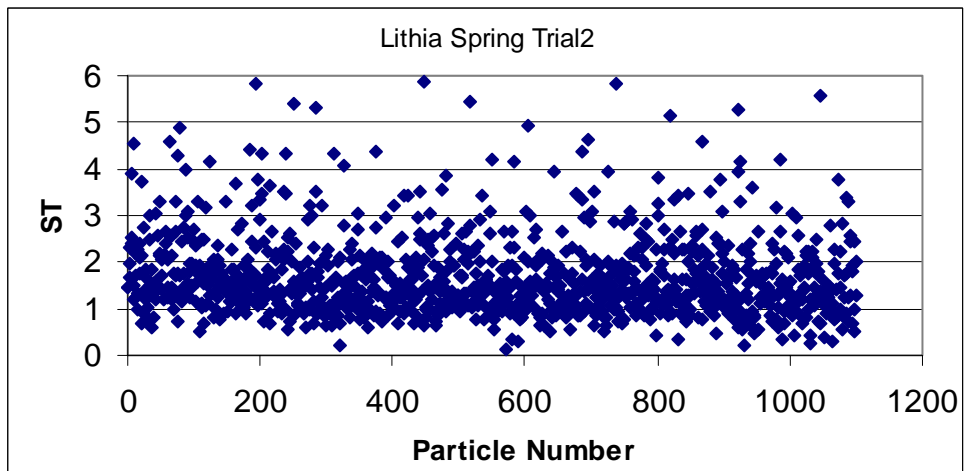


Figure AII-181 (b) Imaging Based ST of the Lithia Springs Sample - Trial 2

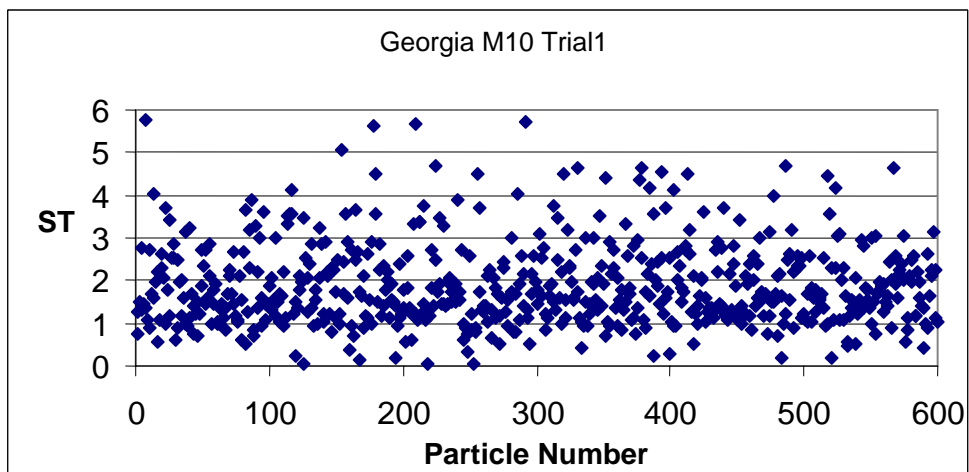


Figure AII-182 (a) Imaging Based ST of the Georgia M10 Sample - Trial 1

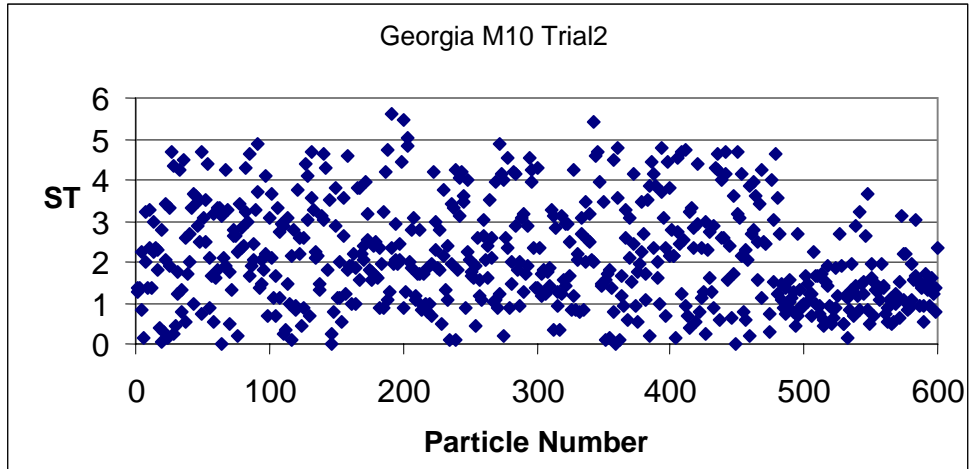


Figure AII-182 (b) Imaging Based ST of the Georgia M10 Sample - Trial 2

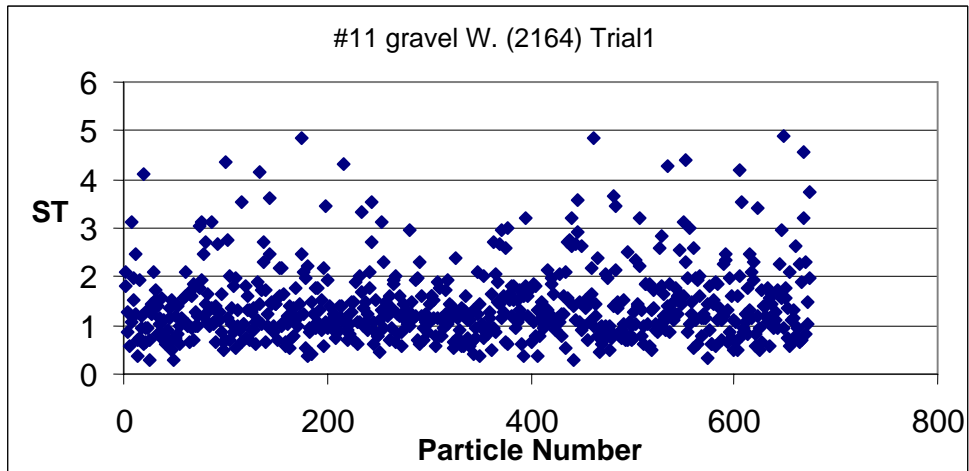


Figure AII-183 (a) Imaging Based ST of the Indiana #11 Gravel 2164 Sample - Trial 1

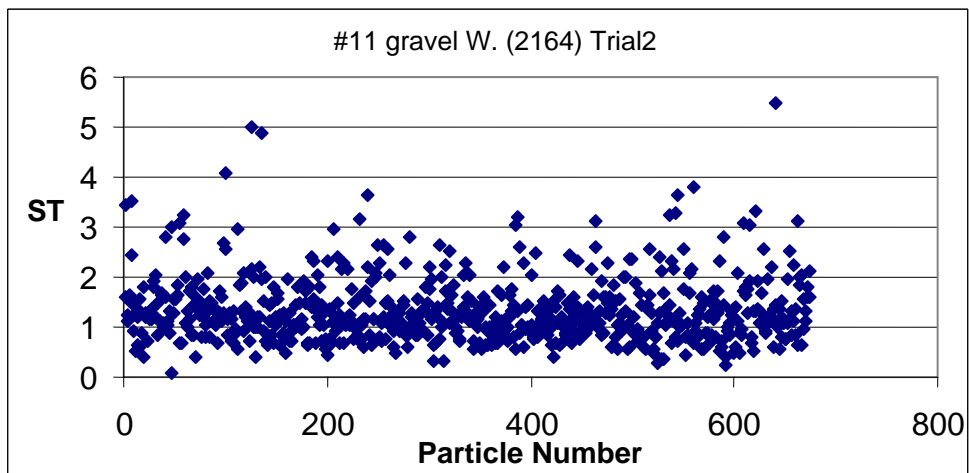


Figure AII-183 (b) Imaging Based ST of the Indiana #11 Gravel 2164 Sample - Trial 2

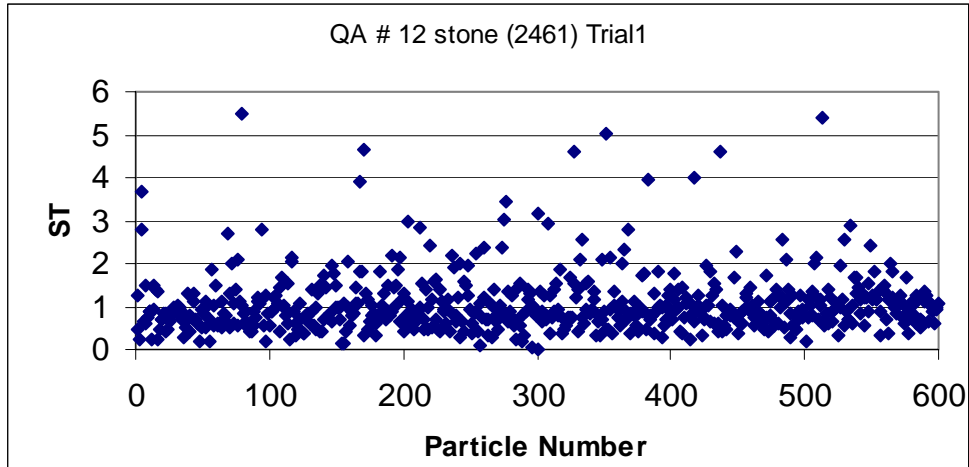


Figure AII-184 (a) Imaging Based ST of the QA #12 Stone 2461 Sample - Trial 1

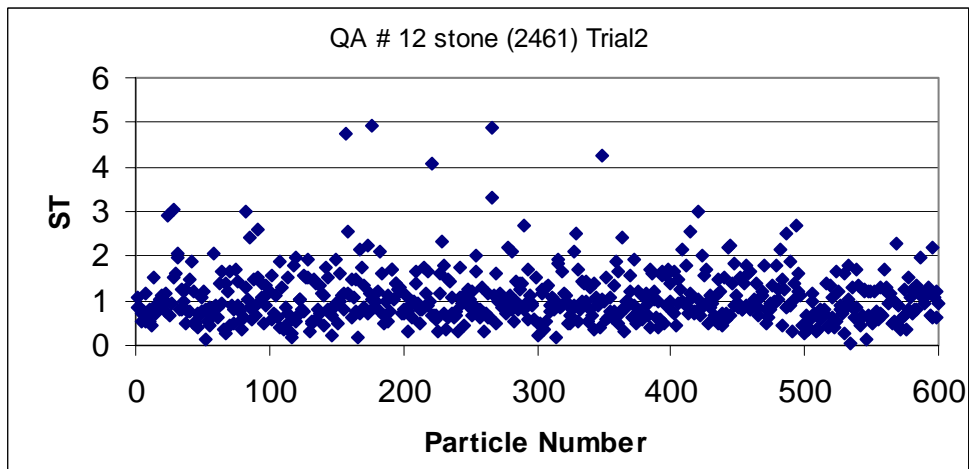


Figure AII-184 (b) Imaging Based ST of the QA #12 Stone 2461 Sample - Trial 2

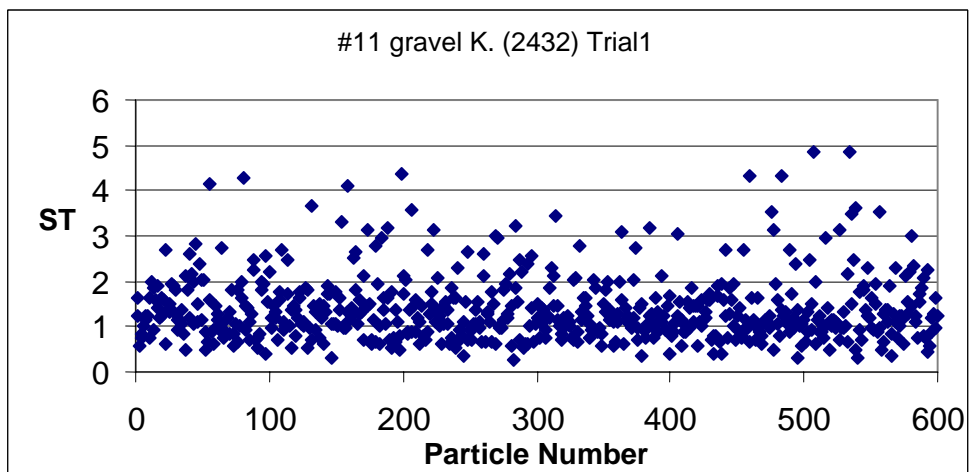


Figure AII-185 (a) Imaging Based ST of the Indiana #11 Gravel 2432 Sample - Trial 1

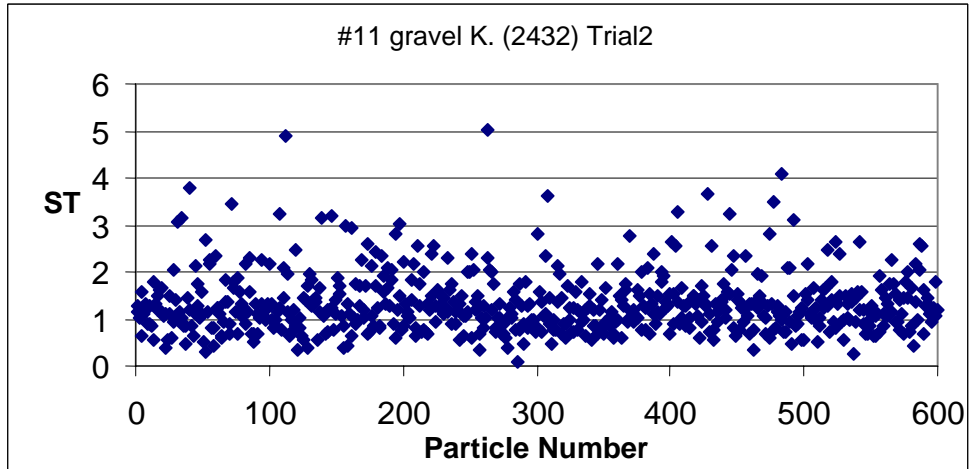


Figure AII-185 (b) Imaging Based ST of the Indiana #11 Gravel 2432 Sample - Trial 2

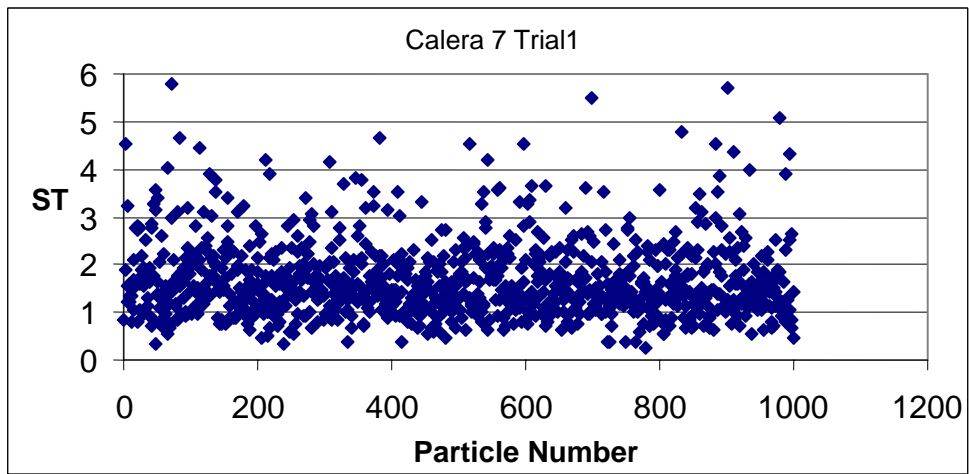


Figure AII-186 (a) Imaging Based ST of the Calera 7 Sample - Trial 1

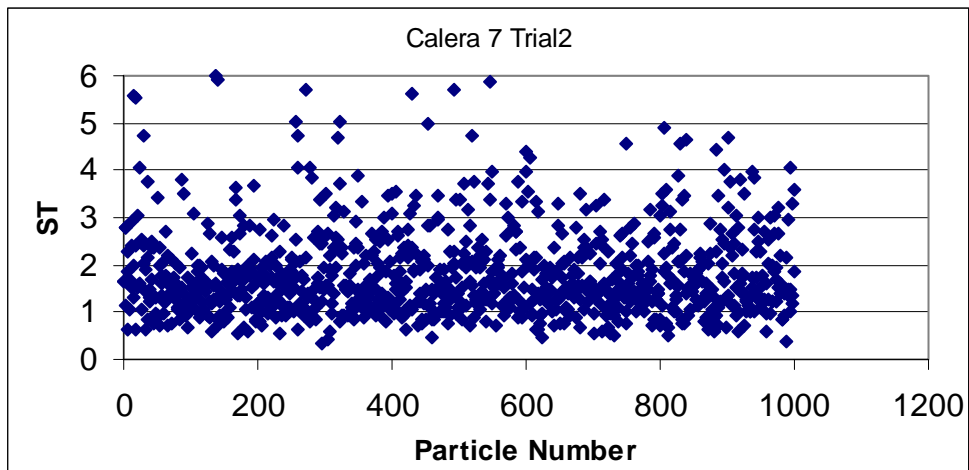


Figure AII-186 (b) Imaging Based ST of the Calera 7 Sample - Trial 2

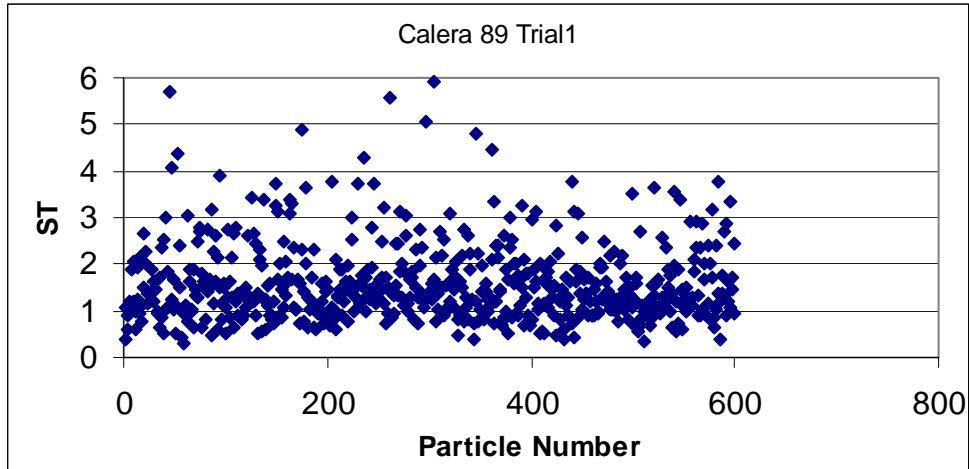


Figure AII-187 (a) Imaging Based ST of the Calera 89 Sample - Trial 1

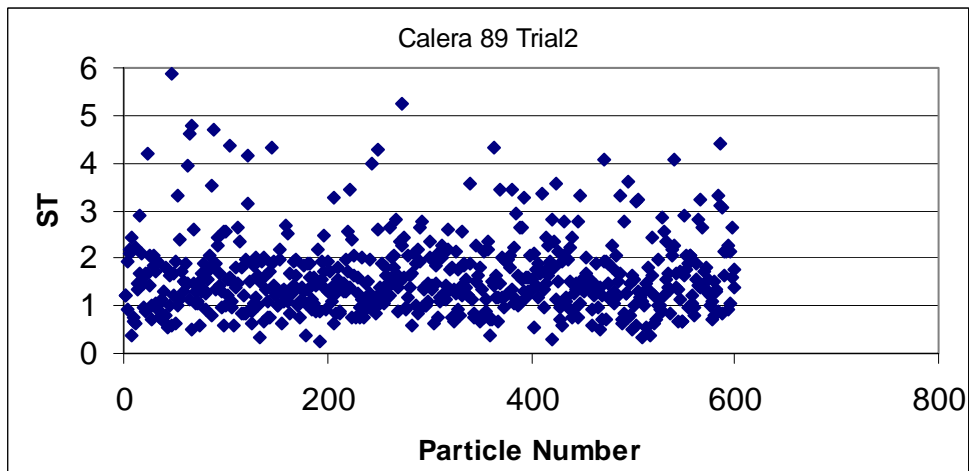


Figure AII-187 (b) Imaging Based ST of the Calera 89 Sample - Trial 2

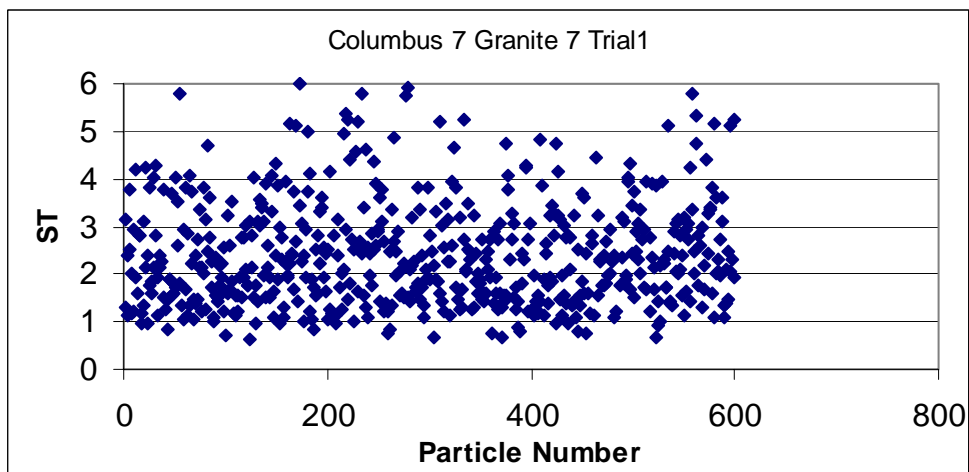


Figure AII-188 (a) Imaging Based ST of the Columbus 7 Granite 7 Sample - Trial 1

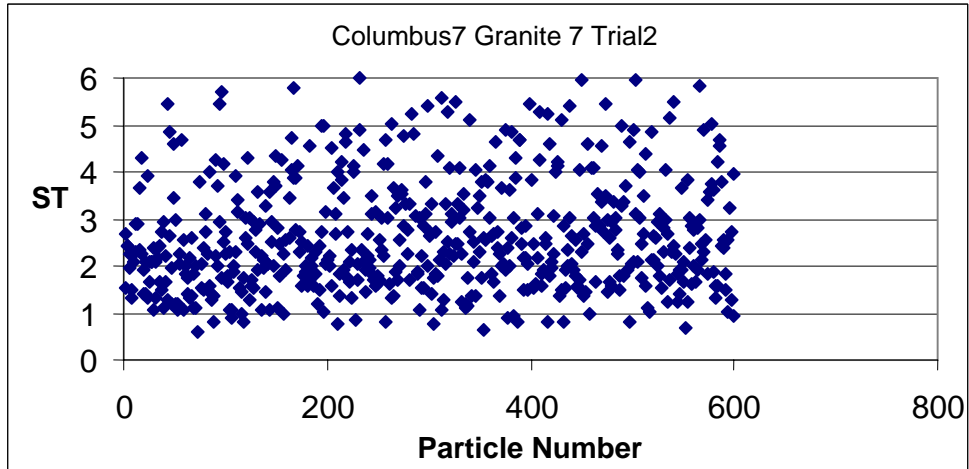


Figure AII-188 (b) Imaging Based ST of the Columbus 7 Granite 7 Sample - Trial 2

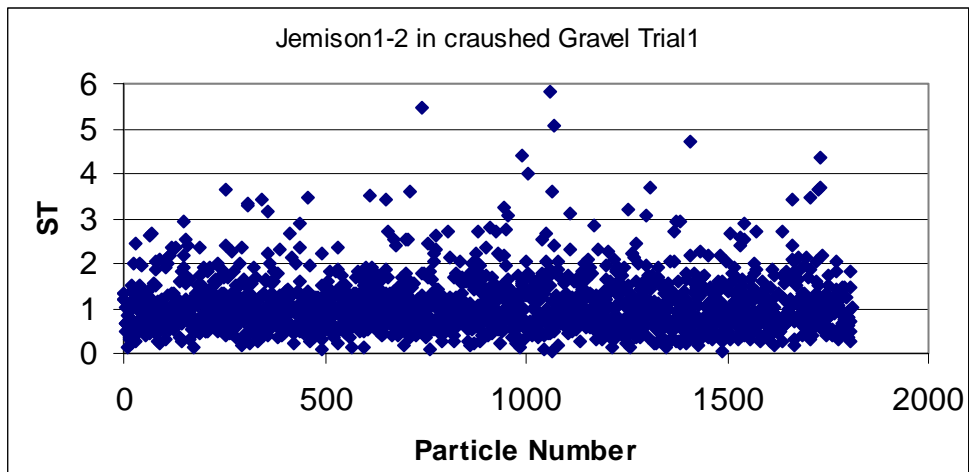


Figure AII-189 (a) Imaging Based ST of the Jemison 1/2 in. Crushed Gravel Sample - Trial 1

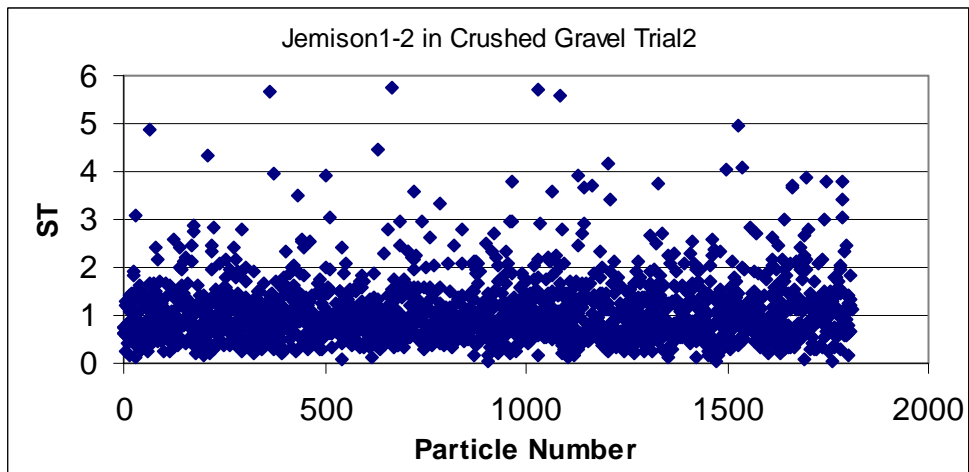


Figure AII-189 (b) Imaging Based ST of the Jemison 1/2 in. Crushed Gravel Sample - Trial 2

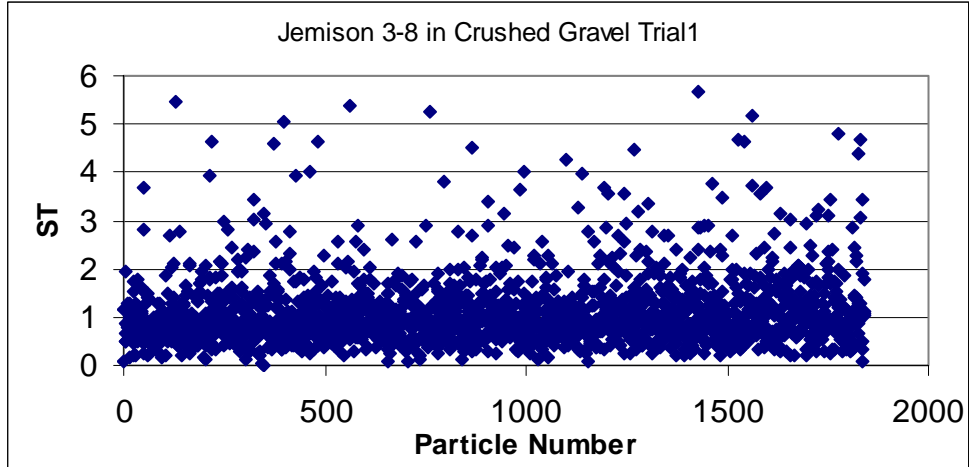


Figure AII-190 (a) Imaging Based ST of the Jemison 3/8 in. Crushed Gravel Sample - Trial 1

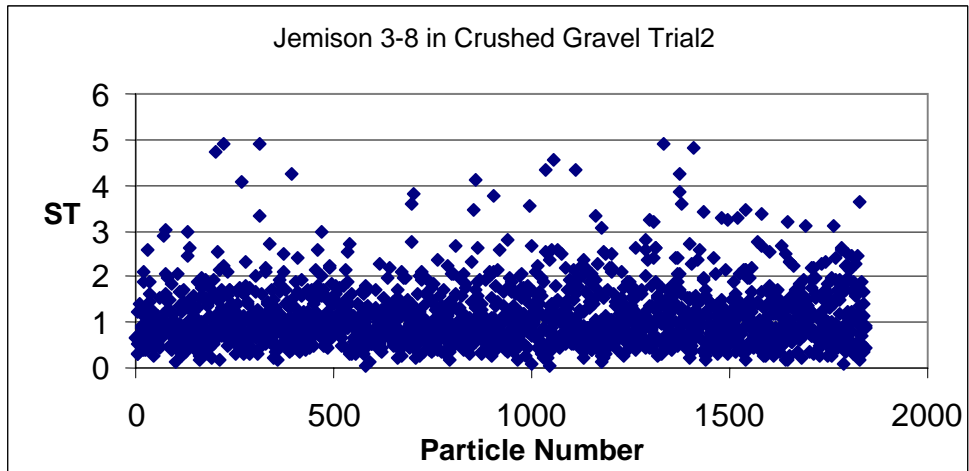


Figure AII-190 (b) Imaging Based ST of the Jemison 3/8 in. Crushed Gravel Sample - Trial 2

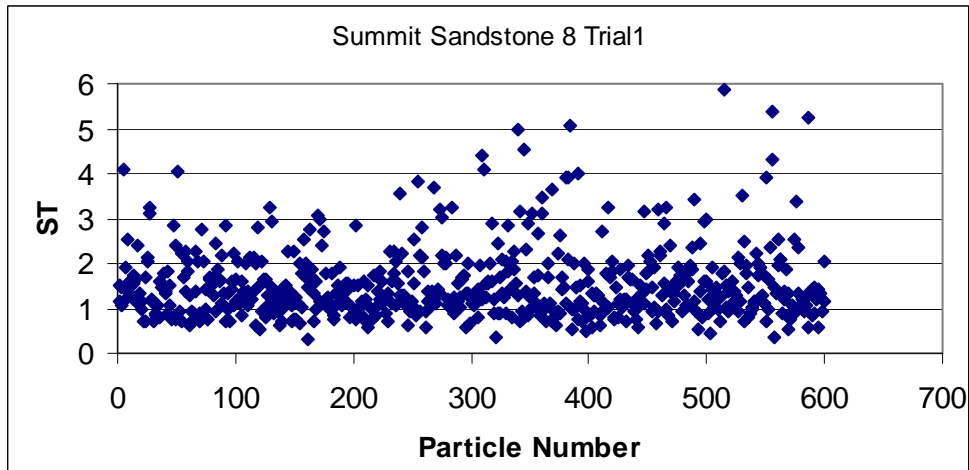


Figure AII-191 (a) Imaging Based ST of the Summit Sandstone 8 Sample - Trial 1

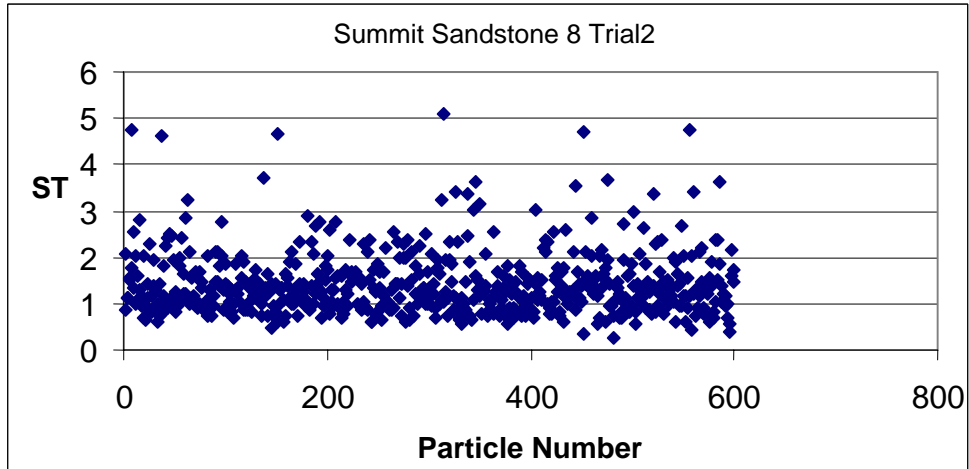


Figure AII-191 (b) Imaging Based ST of the Summit Sandstone 8 Sample - Trial 2

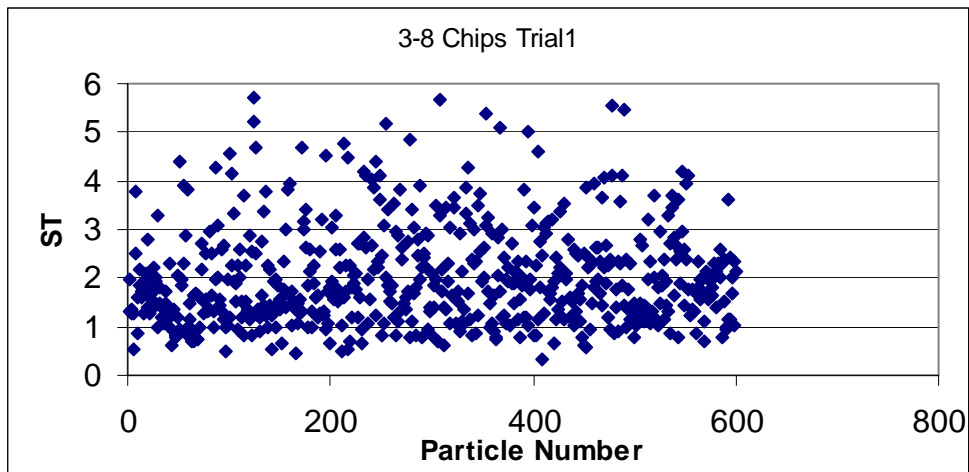


Figure AII-192 (a) Imaging Based ST of the 3/8 in. Chips Sample - Trial 1

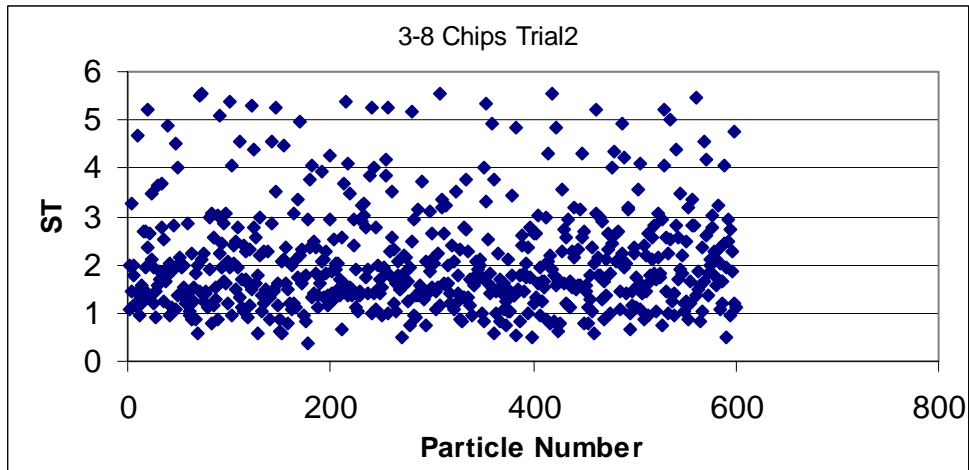


Figure AII-192 (b) Imaging Based ST of the 3/8 in. Chips Sample - Trial 2

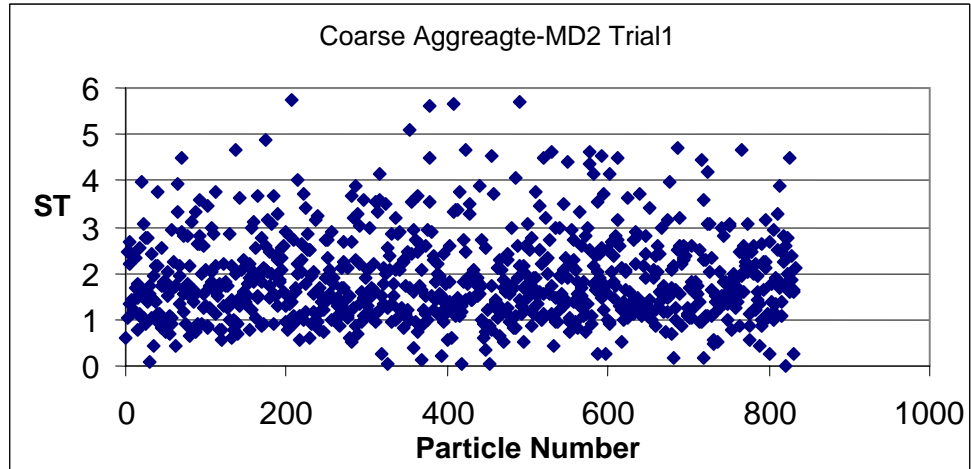


Figure AII-193 (a) Imaging Based ST of the Coarse Aggregate MD-2 Sample - Trial 1

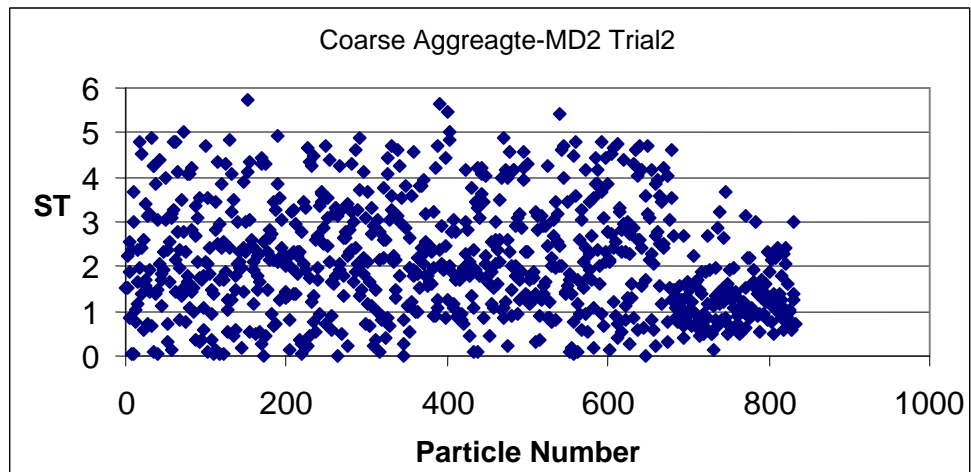


Figure AII-193 (b) Imaging Based ST of the Coarse Aggregate MD-2 Sample - Trial 2

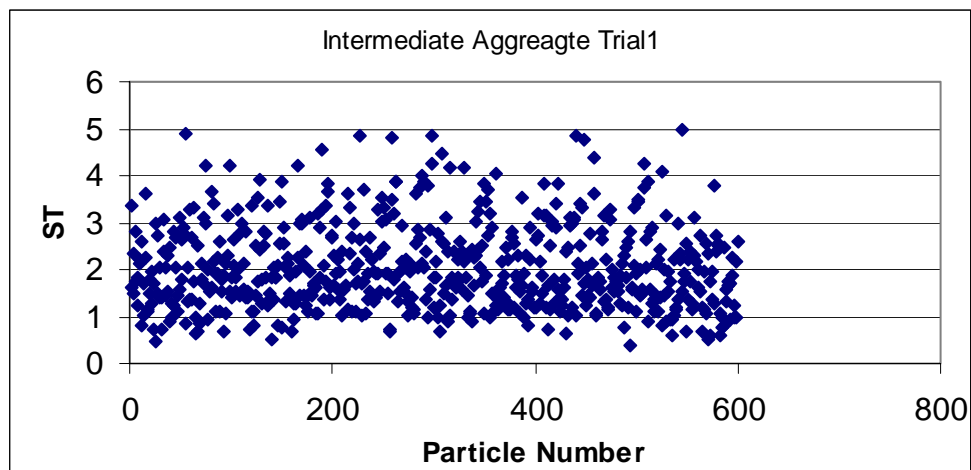


Figure AII-194 (a) Imaging Based ST of the Intermediate Aggregate Sample - Trial 1

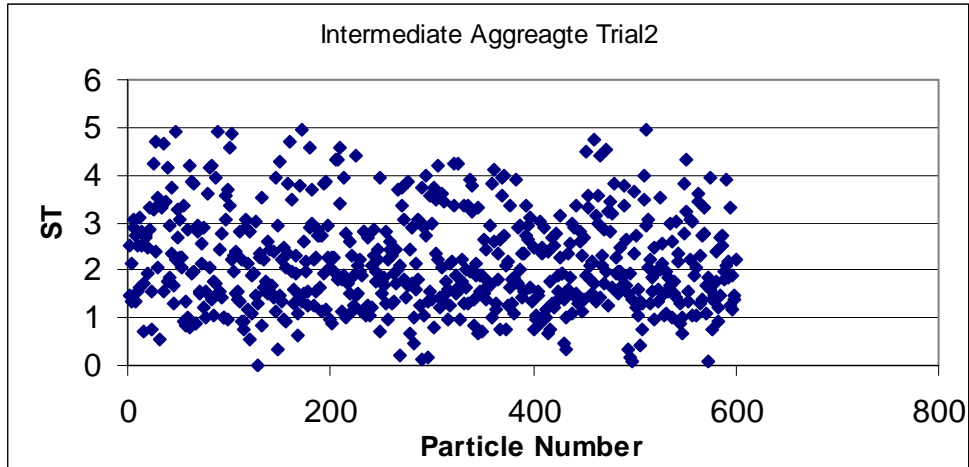


Figure AII-194 (b) Imaging Based ST of the Intermediate Aggregate Sample - Trial 2

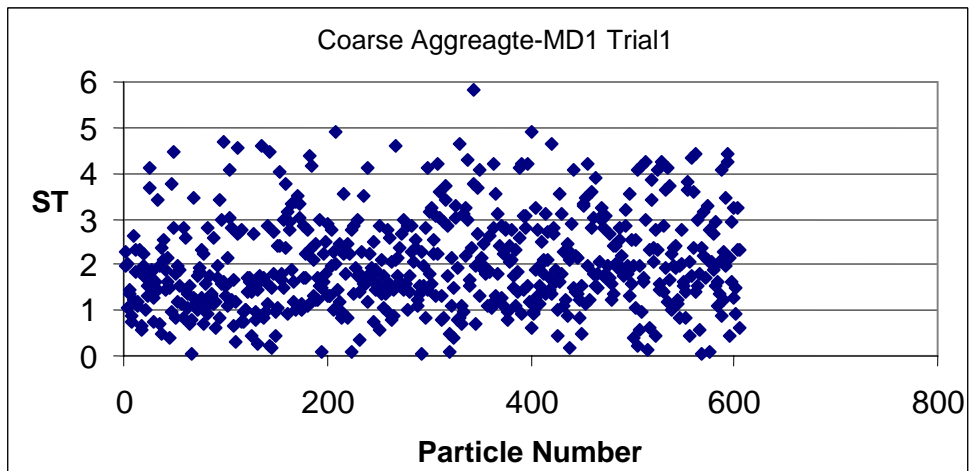


Figure AII-195 (a) Imaging Based ST of the Coarse Aggregate MD-1 Sample - Trial 1

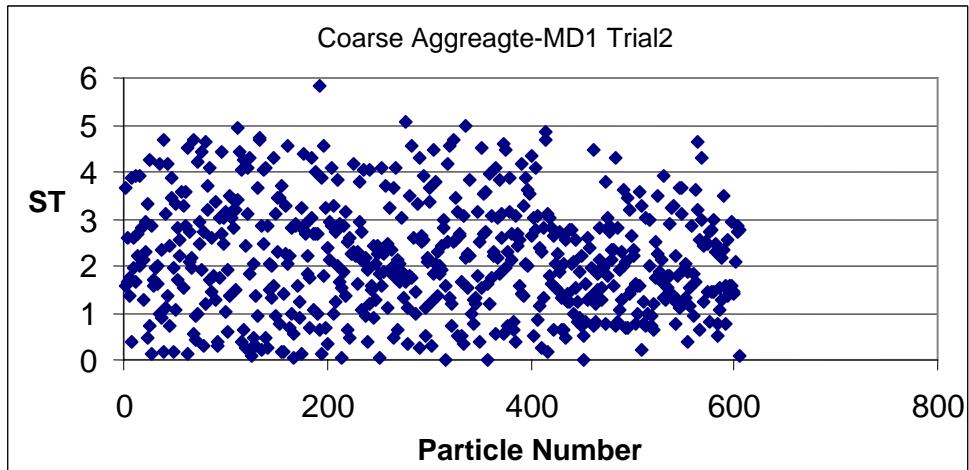


Figure AII-195 (b) Imaging Based ST of the Coarse Aggregate MD-1 Sample - Trial 2